



Dendritic surface modification of photocatalytic nanoparticles for tumour therapy

Susanne Julia Koch

► To cite this version:

Susanne Julia Koch. Dendritic surface modification of photocatalytic nanoparticles for tumour therapy. Organic chemistry. Université de Bordeaux, 2017. English. NNT: 2017BORD0687 . tel-02319439

HAL Id: tel-02319439

<https://theses.hal.science/tel-02319439>

Submitted on 18 Oct 2019

HAL is a multi-disciplinary open access archive for the deposit and dissemination of scientific research documents, whether they are published or not. The documents may come from teaching and research institutions in France or abroad, or from public or private research centers.

L'archive ouverte pluridisciplinaire **HAL**, est destinée au dépôt et à la diffusion de documents scientifiques de niveau recherche, publiés ou non, émanant des établissements d'enseignement et de recherche français ou étrangers, des laboratoires publics ou privés.

THÈSE PRÉSENTÉE
POUR OBTENIR LE GRADE DE
DOCTEUR DE
L'UNIVERSITÉ DE BORDEAUX

ÉCOLE DOCTORALE DES SCIENCES CHIMIQUES

SPÉCIALITÉ : Chimie Organique

Par Susanne Julia KOCH

**Dendritic surface modification of photocatalytic
nanoparticles for tumour therapy**

Sous la direction de : Karine HEUZÉ

Soutenue le 12 Octobre 2017

Membres du jury :

M. TOUPANCE, Thierry	Professeur, Université de Bordeaux	Président
Mme. GLINEL, Karine	Professeur, Université catholique de Louvain (Belgique)	Rapporteur
M. SEXTL, Gerhard	Professeur, University of Würzburg (Allemagne)	Rapporteur
Mme. DEMBSKI, Sofia	Chercheur, Fraunhofer Institute for Silicate Research (Allemagne)	Invitée
M. HACKENBERG, Stephan	Professeur associé, University Clinic Würzburg (Allemagne)	Invité
Mme. HEUZÉ, Karine	Chargée de Recherche, CNRS, Université de Bordeaux	Directrice

Modification dendritique de surface des nanoparticules photocatalytiques pour le traitement des tumeurs

Résumé : L'apparition d'un développement cancérigène est souvent caractéristique des tumeurs de la région de la tête et du cou. En raison des altérations prémaligènes et malignes fréquentes, il n'est souvent pas possible de supprimer complètement la tumeur par chirurgie. Il en résulte un risque élevé de récurrence tumorale. Par conséquent, cette recherche de doctorat vise à développer des nanoparticules photocatalytiques (NPs) qui seront utilisées localement en complément de la thérapie tumorale traditionnelle. Ces NPs, une fois absorbées par les cellules tumorales induiront la mort des cellules photocatalytiques par activation de lumière UV. Des NPs de TiO_2 ayant des propriétés photocatalytiques et une taille moyenne inférieure à 20 nm étaient donc synthétisées. La biocompatibilité des NPs, leur absorption dans les cellules et un ciblage tumoral efficace devraient être garantis par une modification de surface des particules avec des molécules organiques dendritiques permettant un contrôle précis de la charge de surface des particules ainsi que la possibilité de couplage avec des anticorps. Un autre objectif était la combinaison de propriétés thérapeutiques et diagnostiques dans le système de NPs par exemple réalisé par incorporation d'agent luminescent. Cette recherche était menée à l'Université de Bordeaux (synthèse des molécules organiques pour la fonctionnalisation des particules) en coopération avec l'Institut Fraunhofer de recherche en silicate ISC à Würzburg, Allemagne (synthèse des nanoparticules).

Mots clés : Nanoparticules, TiO_2 , photocatalyse, traitement des tumeurs, dendrons, fonctionnalisation de surface

Dendritic surface modification of photocatalytic nanoparticles for tumour therapy

Abstract : The occurrence of field cancerization is characteristic for tumours of the head and neck region. Due to these widespread premalignant and malignant alterations, it is frequently not possible to entirely remove the tumour by surgery. This results in a high risk of tumour recurrence. Therefore, this PhD research aimed to develop photocatalytic nanoparticles (NPs) as completion of the traditional tumour therapy. These NPs are supposed to be incorporated by tumour cells and to induce photocatalytic cell death by UV light activation. TiO_2 with convincing photocatalytic properties and an average size smaller than 20 nm should therefore be synthesized. NP biocompatibility, their uptake into cells and an efficient tumour targeting should be guaranteed by surface modification of the particles with dendritic organic molecules that allow a precise control of the surface charge of the particles as well as antibody coupling. A further objective was the combination of therapeutic and diagnostic properties within the NP system realized for example via introduction of a luminescent dye. This research was carried out at the University of Bordeaux (synthesis of organic molecules for particle functionalization) in cooperation with the Fraunhofer Institute for Silicate Research ISC in Würzburg, Germany (nanoparticle synthesis).

Keywords : Nanoparticles, TiO_2 , photocatalysis, tumour therapy, dendrons, surface functionalization

Acknowledgements

“Theranostic nanoagents possess the potential to greatly enhance the diagnosis and treatment of disease, as they provide for the incorporation of multiple functionalities, including those utilized for targeting, imaging and therapy, within one nanoscaffold. Yet, a number of questions must be answered before the field can move beyond its infancy [...]. Most importantly, there is a need for the scientists formulating the nanoparticle preparations to reconcile their synthetic methodologies with the ultimate clinical utility of the nanoagents. This can only be achieved through the development of fruitful collaborations with scientists and clinicians outside of their chosen fields. Given these challenges, the field of theranostics is rapidly growing, and, like a child, is bound to experience a number of bumps and bruises as it finds its way.”*

When I read this text during my literature study, I felt it was an apt description of my PhD project. Undertaking it has been both an academically and personally challenging experience for me and it would not have been possible without the support and guidance that I received from many people.

First, I would like to thank my supervisor Dr. Karine Heuzé (C2M, University Bordeaux) for giving me the chance to carry out this research project even though I was not an organic chemist but “something else”. Thanks to Dr. Sofia Dembski who supervised my work carried out at Fraunhofer ISC, Würzburg and who worked hard to ensure this international collaboration. Thanks also to Dr. Stefan Hackenberg (University Hospital Würzburg) for his guidance with the biomedical part of my research work. He always took the time to carefully answer my emails and to accompany me at the ICONAN in Paris. I am grateful for the support I received from the above mentioned scientists and for the interest they showed in my PhD project.

I gratefully acknowledge the funding received towards my PhD from Ministère de l'Enseignement Supérieur et de la Recherche (MESR), Fraunhofer “TALENTA start” and EU COST action MP1202.

Many thanks go to Dr. Karl Mandel (ISC) for helping me to publish my scientific work and teaching me so much about writing, while always being open for a vivid discussion. I really admire his scientific enthusiasm, self-confidence and presentation skills. I also greatly appreciated the support I received from Dr. Emilie Genin (C2M), answering my endless questions and filling several gaps in my organic chemistry knowledge. I would like to thank her for believing in me when I was not able to do it myself. For me as a woman, she is a model scientist combining family and work life without ever losing the dedication for both. I also would like to acknowledge my gratitude to Dr. Luc Vellutini (C2M) for taking time to participate in the meetings regarding the organic chemistry of my PhD and to Dr. Thierry Toupance (C2M) for the discussions concerning XRD and photocatalysis results.

I would like to further thank Michael Kessler (University Hospital Würzburg) for all his fast and reliable cell culture work. Thanks to Dr. Aleksey Shmeliov (Trinity College Dublin) for HRTEM studies, Dr. Wojciech Szczerba (BAM, Berlin) for XANES analysis and Shun Kashiwaya (C2M, TU Darmstadt) for XPS measurements. Thanks also to Dr. Gwénaëlle Le Bourdon for her

*J. R. McCarthy, *Nanomed.*, 2009, 4, 693–695.

guidance with IR measurements. I really appreciated the long discussions, amazing results and the great collaborations. I am equally grateful for the experiments conducted by several students (Rebecca Weidner, Stephan Späth, Lena Mungenast, Medine Eyili, Sébastien Zeballos) as well as for the analyses carried out by many colleagues at ISC and C2M (Odile Babot, Benedikt Schug, Peter Löschke, Sabine Rupp, Katalin Pápai and Dr. Alexander Reinhold).

During more than 1.5 years in Bordeaux, all permanent and non-permanent staff at C2M helped me to learn French, get to know the French culture and enjoy France. A special thanks to Yannick Mousli, not only for sharing the office and lab with me but also all the 2nd and 3rd year frustrations and a lot of Haribo. Thank you for also sharing your knowledge in organic chemistry with me! I will certainly miss my international family of C2M and CiVi, including Juan-Angel Moreno, Imane Barbara, Camille Bertrand, Martin Palazzolo, Jessie Ringo, Dieuwertje Schrijvers, Sheavon Lee, Yannick Hermans and many others. I really have to send a special thanks to Caroline Ball; without meeting her and becoming her friend, I may have not survived the first months in France. I am grateful for our great friendship and for her proof-readings of many of my scientific texts. She really helped me to improve my English.

Especially, being far from the ISC, I realized how much this research institute became my home over the last years. Thanks to all my awesome colleagues, making it a special place and creating a perfect research environment. I would like to acknowledge my gratitude to the entire OE290, OE280 and the former AWZ group but also to Johanna Fischer, Luisa Kuhn, Manuel Röder and many others. I have to thank my dear comrades-in-arms Benedikt Schug, Michael Schneider, Marion Straßer and all other OE290/280 PhD students for endless scientific discussions and emotional support. Undertaking this PhD only seemed to be half as hard, having you on my side. Thanks to my office colleagues Kirsten Langguth, Silke Gholami-Toll and Gabriele Ulm; it was a pleasure to spend time with you.

I would like to thank all my friends from my home town, school and university in Germany, for not forgetting me while I was “far away”. I am deeply grateful for the help and support my family (especially my parents Gabriele and Dieter Koch as well as my sister Judith Koch) gave me throughout my PhD thesis, living abroad and organizing my wedding in the meantime. Thanks for understanding when I missed yet another anniversary, wedding or funeral because of being abroad.

Finally, I really would like to thank my husband Andreas Wintzheimer who is always there for me in good and bad times, brightening every single day of my life!

Résumé

En 2016, plus de 48 000 nouveaux cas de cancers des voies aérodigestives supérieures (VADS) ont été diagnostiqués aux États-Unis, ce qui représente 3% de tous les nouveaux cas de cancer.¹ Il est l'un des dix cancers les plus courants au niveau mondial.² Les régions du corps humain qui peuvent être affectées sont la cavité buccale, y compris les lèvres, les parties de la langue ou le plancher de la bouche, et le pharynx qui est un tube musculaire entre le nez et l'œsophage. En outre, il peut également apparaître dans le larynx (boîte vocale), les glandes salivaires, la cavité nasale et les sinus paranasaux qui sont des espaces creux dans les os entourant le nez. Le plus couramment, la lésion ou la tumeur maligne qui se développe dans les cellules de la peau ou des muqueuses est un carcinome épidermoïde.² Les principaux facteurs de risque pour ce type de cancer sont le tabagisme, la consommation d'alcool, le tabac à mâcher et les infections par le virus du papillome humain (VPH). En outre, la combinaison du tabagisme et de la consommation excessive d'alcool a un effet synergique.^{3,4} La chirurgie et la radiothérapie sont les traitements standards pour les patients atteints de cette maladie aux premiers stades avec des taux de réussite de 60% à 90% selon la localisation et l'étendue de la tumeur. Néanmoins, ces patients ont un risque élevé de développer une récurrence locale ou un second cancer en raison du caractère cancéreux des tissus.² Un cancer étendu se produit lorsque la tumeur n'est pas située dans un endroit bien défini mais largement répandue dans les tissus. Habituellement, ces formations sont un mélange de manifestations superficielles pré-malignes et malignes avec certaines régions ayant des fractions tumorales profondément invasives. Cette étendue mal définie de la tumeur rend une élimination chirurgicale très difficile. La chimiothérapie est utilisée dans des cas avancés ou récurrents en association avec la radiothérapie comme traitement curatif ou seul comme traitement palliatif. Les chimiothérapies couramment utilisées sont des analogues du platine comme le cis-platine qui peuvent se coordonner avec l'ADN ou bien les taxanes comme le paclitaxel et le docétaxel qui favorisent l'assemblage microtubulaire.² Ces deux actions conduisent à la mort cellulaire. Néanmoins, les traitements de chimiothérapies sont limités en durée et en intensité en raison de leur toxicité non spécifique.² Au cours des dernières années, des agents ciblés ont été étudiés, comme des anticorps monoclonaux tels que le cetuximab ayant une activité extracellulaire ou des inhibiteurs de la tyrosine kinase ayant une action intracellulaire.² Ils promettent un traitement tumoral plus spécifique réduisant ainsi les effets secondaires indésirables des médicaments. Au cours de la dernière décennie, malgré les progrès dans les procédures thérapeutiques et une amélioration significative du taux de survie à 5 ans, ce taux reste de 66% (aux États-Unis¹), y compris avec un risque élevé de récurrence tumorale ainsi que l'apparition de problèmes de cancers étendus difficiles à traiter.² Ainsi, de nouvelles stratégies thérapeutiques doivent être développées pour améliorer les traitements standard actuels.

Les nanoparticules (NPs) sont des matériaux de taille inférieure à 100 nm qui présentent des propriétés physiques et chimiques uniques par rapport aux matériaux massifs en raison de leurs dimensions. Leur petite taille leur permet traverser les barrières des cellules ou des tissus tout en étant assez grands pour être conjugués à des anticorps ou des médicaments. C'est pourquoi ces nanoparticules ont un grand potentiel en tant qu'outils pour l'imagerie cellulaire ou l'analyse biologique et comme supports de médicaments ou agents thérapeutiques.⁵ Concernant les carcinomes à cellules épithéliales, les NPs photocatalytiques (PC) peuvent fournir une nouvelle approche thérapeutique complémentaire.⁶ La thérapie photodynamique utilisant des molécules photosensibles telles que les porphyrines ou les chlorines sont une alternative non invasive bien connue et établie dans le traitement des malignités cutanées.⁷⁻⁹ Grâce à leurs propriétés uniques, l'utilisation de NPs PC pour le traitement de la tumeur photodynamique est de plus en plus reconnue comme une stratégie prometteuse et les études initiales ont déjà été mis en avant en soulignant leur potentiel.^{5,9,10} Dans cette approche, les NPs PC sont appliquées sur un tissu cancéreux et sont absorbées par des cellules malignes. L'application de lumière ultraviolette (UV) excite les particules PC (Figure Résumé - 1) en raison de leurs propriétés semi-conductrices et de l'écart de bande approprié dans la gamme d'énergie de la lumière UV.

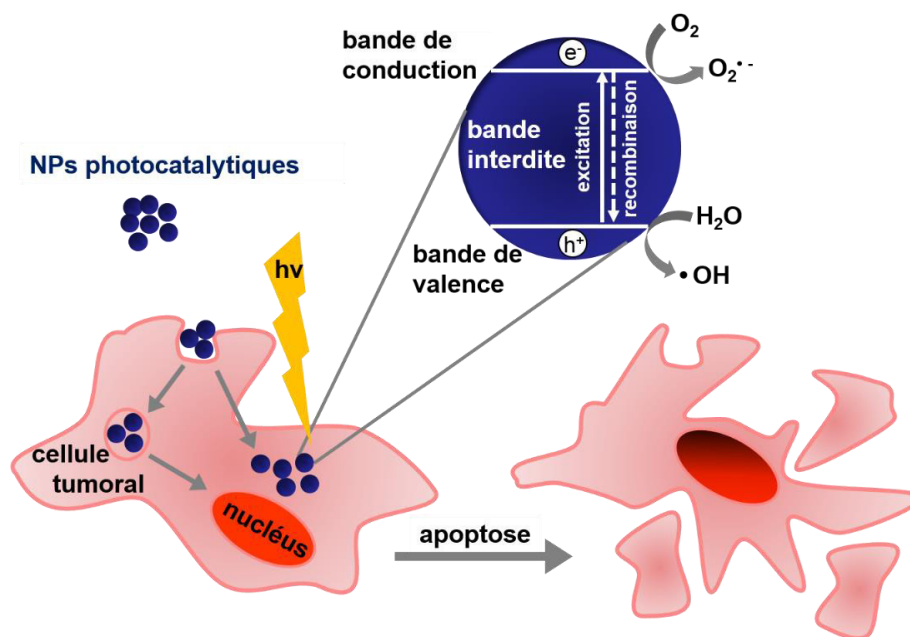


Figure Résumé - 1. La destruction des cellules tumorales par photocatalyse induite par la lumière par des nanoparticules semi-conductrices.

Ainsi, des paires électron-trous sont créées qui vont ou bien se recombiner ou bien migrer vers la surface de la particule, pour réagir avec l'oxygène et l'eau environnants et créer des radicaux hautement réactifs. Ces radicaux sont alors responsables de la destruction cellulaires conduisant à l'apoptose.^{6,11-13} Par rapport aux chimiothérapies, les particules appliquées sont

normalement non toxiques dans l'état non activé et donc moins toxiques pour les organes non-affectés, ou les tissus non-traités aux rayons UV.¹³ Comme la transmission de la lumière dans les tissus est limitée, l'application de la lumière UV et la photocatalyse initiée n'influent que sur le tissu superficiel qui est la région d'intérêt lors du traitement des cancers diffus.

En raison de leur activité PC élevée, les NPs de dioxyde de titane (TiO₂) semblent être un choix approprié pour la thérapie photodynamique. Bien que la destruction des cellules cancéreuses par les UV ait été démontrée, le traitement est en général dépourvu de spécificité vis-à-vis de ces cellules.⁵ En outre, les particules commerciales utilisées sont souvent mal caractérisées et ne présentent pas toutes les propriétés requises. Les propriétés des particules telles que la charge superficielle sur l'absorption cellulaire et les mécanismes menant à l'apoptose cellulaire n'ont pas été étudiés suffisamment. Il est par conséquent indispensable de préparer des systèmes de nanoparticules TiO₂ bien caractérisés et d'affiner leurs propriétés de surface, par exemple par une fonctionnalisation spécifique. Si les particules possèdent des propriétés de luminescence, alors l'absorption cellulaire peut être étudiée ou, dans des applications comme agent antitumoral, leur position exacte dans le tissu peut être déterminée avant l'application de lumière UV. En outre, la charge de surface de ces particules peut être modulée par une fonctionnalisation organique pouvant améliorer l'absorption cellulaire. Si ces particules sont également bioconjuguées, fournissant des ligands spécifiques pour le ciblage de tumeur, un diagnostic de cancer ou une chirurgie guidée par luminescence peut être envisageable. L'application d'un tel système optimisé de particules luminescentes et PC dans le traitement du cancer buccal est représenté ci-dessous (Figure Résumé - 2).

Dans ce contexte, le premier objectif de cette thèse était la synthèse et la caractérisation des NPs photocatalytiques de TiO₂, plus précisément des NPs d'anatases. Deux systèmes de particules avec différents types d'agents complexants et des paramètres d'autoclavage variés devaient être synthétisés par un procédé hydrothermique sol-gel. Parmi ces échantillons, il fallait sélectionner le plus approprié et le plus prometteur pour le traitement PC de la tumeur. Leur application pour les tests de culture cellulaire était l'objectif principal, y compris la stabilisation dans les milieux de culture cellulaire et la réalisation de tests de cytotoxicité. Par la suite, les surfaces des particules ont été modifiées par des molécules organiques appropriées afin de faciliter leur absorption cellulaire et éventuellement fournir un meilleur état de dispersion dans les milieux de culture cellulaire. Des molécules organiques linéaires et dendritiques avec des fonctions amines terminales ont été synthétisées afin d'induire une charge positive favorable à une interaction des particules avec les membranes cellulaires. Les structures dendritiques ont été choisies pour augmenter la quantité de fonctionnalités terminales sans augmenter le nombre d'ancrages de surface. Ceci était crucial car l'activité PC des particules inorganiques doit être préservée malgré l'ancrage de molécules à la surface.

Le greffage des molécules organiques a été réalisé par une fonction alcoxysilane. Un objectif supplémentaire a été l'introduction de propriétés de luminescence des particules afin de combiner les applications thérapeutiques et diagnostiques. La luminescence des particules est un atout supplémentaire pour l'étude de l'absorption des particules par les cellules dans les tests de culture cellulaire. Cet objectif devait être atteint soit par la modification des particules inorganiques, par exemple par dopage ou par intégration d'un chromophore dans les agents de surface organiques. Enfin, l'objectif final a été alors de prouver que l'activité PC des systèmes de particules fonctionnelles développés est maintenue, ainsi que d'examiner leur cytotoxicité et leur potentiel comme agents antitumoraux.

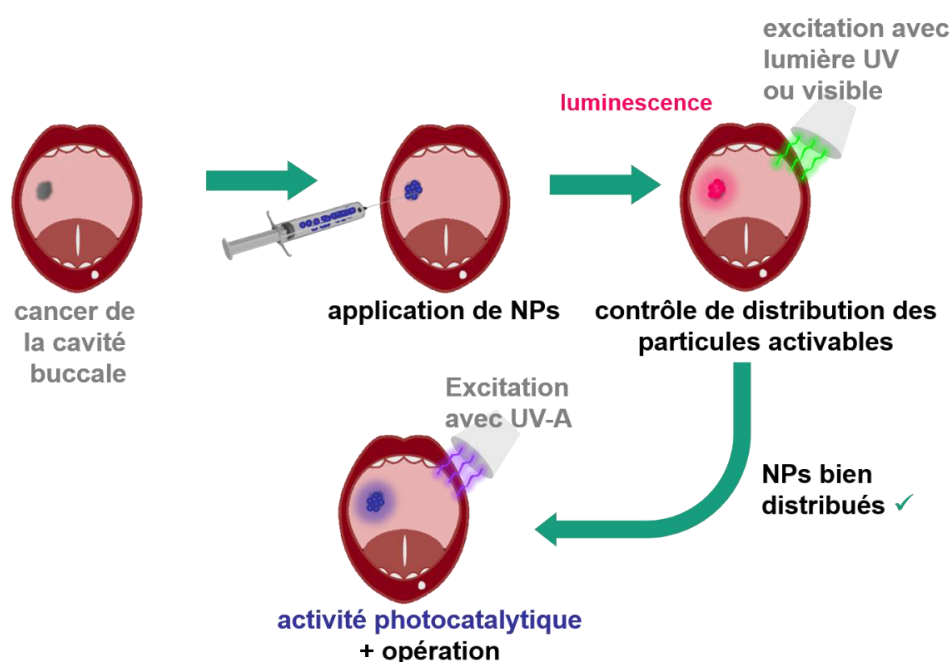


Figure Résumé - 2. Application de nanoparticules photocatalytiques et luminescentes complétant la thérapie du cancer buccal.

En ce qui concerne les synthèses inorganiques des NPs réalisées dans ce travail, deux types différents des NPs d'anatase ont été synthétisés avec succès. Elles ont été soigneusement analysées par DRX, MET, mesures du potentiel zêta, DLS, ATG, sorption d'azote et spectroscopie infrarouge (IR). Alors que la morphologie (forme ovale) et la taille (entre 5 nm et 6 nm) des deux types de cristaux d'anatase semblent être très similaires, elles diffèrent principalement dans les fonctions de surface introduites lors de la synthèse. Alors que le AA-TiO₂ porte des groupes acétate d'acétyle et acide paratoluènesulfonique, le MEEAA-TiO₂ comporte des fonctions acide 2-[2-(2-méthoxyéthoxy)éthoxy]acétique à sa surface. L'activité PC plus élevée du MEEAA-TiO₂ par rapport au AA-TiO₂ est donc principalement liée aux différents groupes de surface ou plus précisément à la plus grande quantité de groupes fonctionnels sur le AA-TiO₂. Dans la Figure Résumé - 3, les groupes de surface des deux systèmes de particules AA-TiO₂ et MEEAA-TiO₂ sont représentés, ainsi que l'activité PC des

deux systèmes par rapport aux NPs P25 TiO₂ commerciales présentées comme matériau de référence.

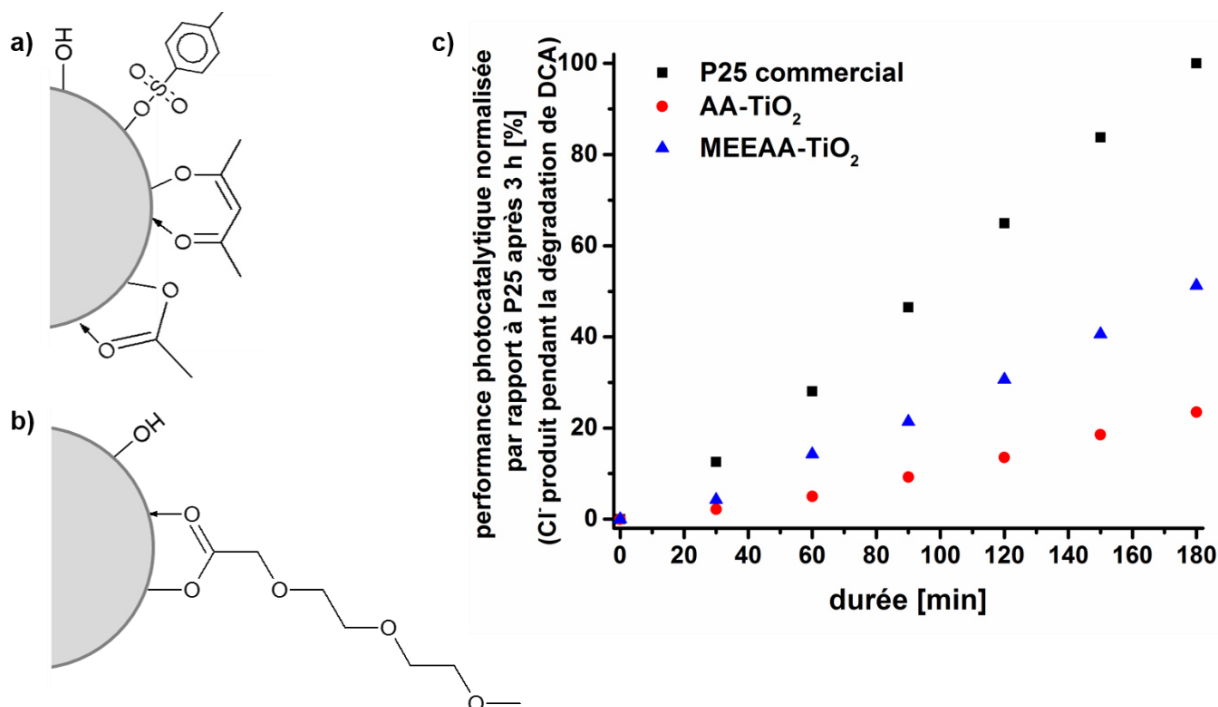


Figure Résumé - 3. Les groupes de surface des deux systèmes de particules a) AA-TiO₂ et b) MEEAA-TiO₂ et leur activité photocatalytique par rapport aux NPs commerciales P25. (DCA = acide dichloracétique)

A la vue de ces résultats, l'étude de l'influence des conditions de traitement hydrothermique sur les propriétés des NPs a été réalisée avec le système MEEAA-TiO₂ le plus prometteur. Ainsi, si le temps ou la température de l'autoclave augmente lors de la synthèse, alors la taille des cristallites augmente de 4,8 nm à 7,7 nm (1h, 160 ° C à 4h, 200 ° C). Ceci a été vérifié par RDX, MET, DLS et des mesures de sorption d'azote. Alors que les propriétés des groupes de surface ne sont que marginalement influencées par des changements dans le temps et / ou la durée du traitement (comme le montrent les mesures IR, ATG et potentiel zêta), l'activité PC de l'échantillon est significativement améliorée avec l'augmentation de la taille des particules. Cela contrastait avec l'attente initiale qui était que l'activité des échantillons aurait dû diminuer avec la taille croissante des particules du fait de l'accroissement de leur surface spécifique. Les performances accrues en photocatalyse avec une surface spécifique décroissante est le résultat d'une modification de la morphologie des cristaux (Figure Résumé - 4). Alors que les petites cristallites montrent la morphologie bipyramidale tétragonale tronquée à l'état d'équilibre typique, la croissance des cristaux conduit à la formation de cristaux en forme de tige avec des vacances d'oxygène provoquées par une fixation orientée de particules simples (comme le montrent les analyses XAFS, RDX et HR-MET). Le caractère plus anisotrope des cristaux et l'augmentation des vacances en oxygène améliorent l'activité PC des échantillons

- probablement en raison d'une séparation plus efficace du support de charge. La croissance des cristaux par l'émergence des facettes {011} est vraisemblablement causée par les conditions aqueuses de traitement hydrothermique et l'adsorption préférentielle de l'acide carboxylique utilisé (MEEAA) sur les facettes {001} de haute énergie.

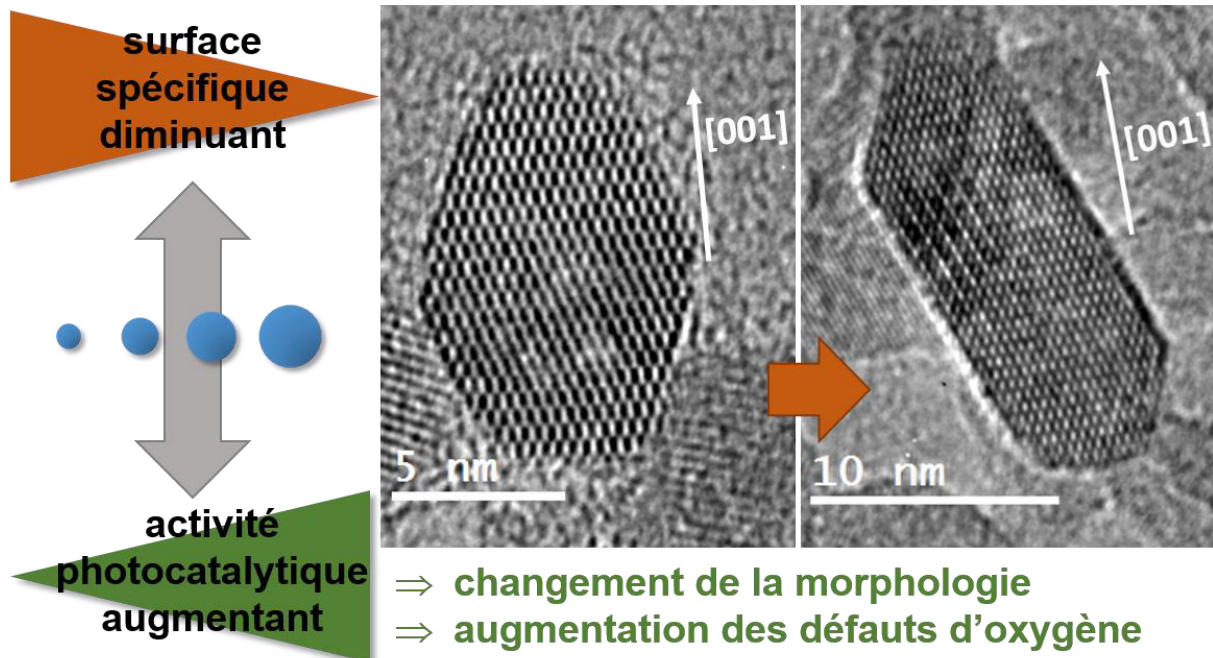


Figure Résumé - 4. L'activité photocatalytique croissante conjointement avec la diminution de la surface spécifique est expliquée par un changement de morphologie des nanoparticules et une augmentation de défauts en oxygène.

Après avoir synthétisé et caractérisé avec succès les NPs PC de TiO_2 , l'incorporation de propriétés lumineuses a ensuite été étudiée. Pour introduire les propriétés de luminescence dans les particules de TiO_2 , la synthèse de NPs de type cœur-coquille $\text{TiO}_2@\text{SiO}_2$ dopées Rhodamine B luminescente a été réalisée avec succès. La formation homogène d'une coquille de silice autour du TiO_2 a été prouvée par des mesures de MET, DLS et zêta potentiel. L'incorporation de Rhodamine B dans la coquille de silice était une méthode de choix en raison de la luminescence résultante des particules finales. Malheureusement, on a montré que l'activité PC des particules diminuait progressivement avec l'augmentation de l'épaisseur de la coquille de silice. Aussi, en raison de l'auto-extinction du colorant dans la coquille, le dopage de la coquille de silice par la Rhodamine B est limité par la concentration de colorant. Cela signifie que, plus la photoluminescence souhaitée est élevée, plus la coquille de silice doit être épaisse et moins l'activité PC du système de particules $\text{TiO}_2@\text{SiO}_2$ est importante. La synthèse d'un système ZnO-TiO_2 reste encore difficile. Nous avons synthétisé avec succès des NPs ZnO luminescentes, cependant, leur stabilité dans l'eau acide n'était pas suffisante pour la synthèse d'une coque TiO_2 . Néanmoins, il a été possible de prouver la faisabilité d'une formation de coque TiO_2 autour des NPs inorganiques telles que les NP d'oxyde de fer. Cela

signifie que, si l'on trouve un système de particules inorganiques luminescentes suffisamment stable à l'acide, on pourrait envisager la formation de coquille TiO_2 à leurs surfaces. Pour cela, il faut tenir compte du fait que l'excitation du matériau du cœur doit être supérieure aux longueurs d'onde d'absorption de l'enveloppe de TiO_2 pour assurer l'arrivée de la longueur d'onde d'excitation au noyau. En outre, il faut garder à l'esprit que l'activité PC de l'enveloppe pourrait être aussi influencée négativement par le noyau. Pour conclure sur les tentatives de synthèse des particules de cœur/coquille luminescentes, on peut affirmer que les deux systèmes n'ont pas été jugés suffisamment actifs pour être utilisés en photocatalyse. C'est la raison pour laquelle il fallait trouver une autre façon d'intégrer les propriétés de luminescence dans le système NPs.

L'intégration d'un colorant organique dans les agents de couplage a été identifiée comme la voie la plus prometteuse. Elle est décrite dans la partie suivante de ce travail, dans laquelle des agents de couplage organiques ont été synthétisés et ensuite greffés sur les NPs TiO_2 . En ce qui concerne les synthèses organiques, quatre structures dendritiques ou linéaires luminescentes ou non luminescentes ont été conçues comme indiqué dans le Schéma Résumé - 1. Les trois premiers agents de couplage contiennent tous le colorant rhodamine. L'**agent de couplage I**, molécule linéaire sans groupe aminé terminal, a été obtenu avec succès et a prouvé la stabilité de l'agent de luminescence pendant toutes les étapes de synthèse et de lavage. L'**agent de couplage II** est une molécule linéaire portant un groupe amine terminal et une fonction Rhodamine. Plusieurs étapes de synthèse ont été menées avec succès jusqu'au couplage des composants non luminescents de l'agent de couplage au colorant par la formation d'une liaison thiourée. Cependant, cette liaison thiourée sur la position alpha de la lysine a donné lieu à un réarrangement de la molécule dans des conditions acides. La labilité de la liaison amide à côté du thiourée n'a jamais été rapportée dans la littérature dans le cas de la lysine dans les conditions réactionnelles utilisées (acides forts, température ambiante). Dans ce contexte, le clivage du groupe de protection Boc et Z n'a pas été possible et la voie synthétique n'a pas été poursuivie.

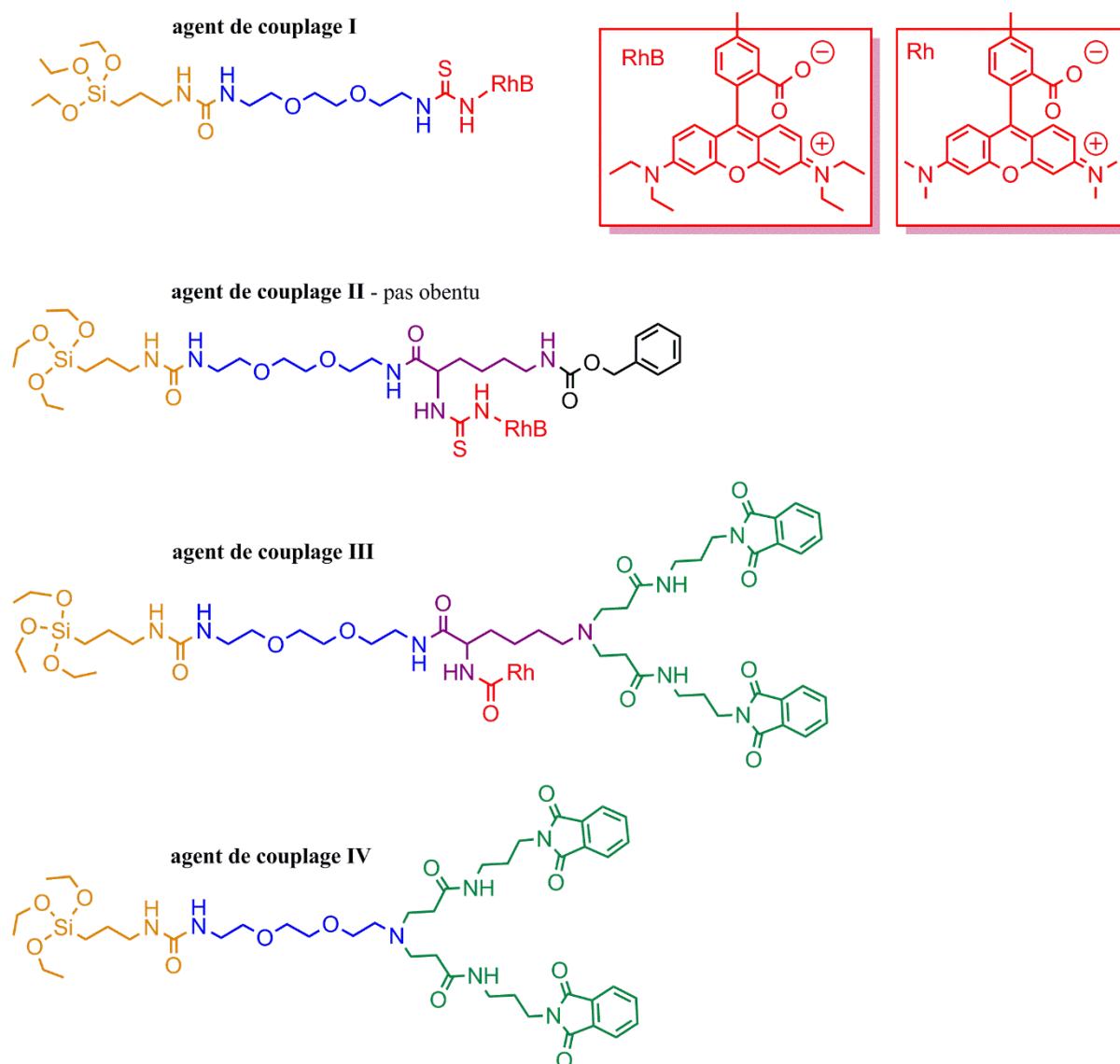


Schéma Résumé - 1. Des agents de couplage organiques synthétisés dans ce travail.

Néanmoins, les connaissances acquises lors des étapes de synthèse de l'**agent de couplage II** ont contribué à synthétiser l'**agent de couplage III** (molécule dendritique de 1^{ère} génération lumineuse et porteuse de fonctions amines). Ce travail de synthèse a été le plus complexe car nous avons rencontré plusieurs obstacles à surmonter. Par exemple, nous avons dû faire face à la formation de dipeptides lors de la protection Fmoc de la Z-lysine. Ce problème a été contourné par l'utilisation de DMF comme solvant organique (au lieu de THF ou dioxane). L'instabilité de la liaison ester due à des réactions de trans-estérification (en présence d'un alcool) a également été inattendue et a initié d'autres études de la stabilité de cette liaison. Ceci qui nous a permis d'établir que ces liaisons ester sont sensibles aux réactions de transestérification en milieu aqueux-alcoolique basique. L'utilisation d'un amide au lieu d'un ester, a fourni une structure moléculaire plus stable jusqu'à l'étape de réaction finale. Ainsi, du NHS-rhodamine a été utilisé dans l'étape finale de formation de l'agent de **couplage III** à la place de l'isothiocyanate de rhodamine (qui avait été utilisé dans le cas de l'agent de couplage

II). Nous avons ainsi garanti la stabilité de la structure moléculaire pour les étapes de réaction ultérieures. L'**agent de couplage III** a donc été obtenu avec succès. L'**agent de couplage IV** (molécule dendritique analogue non luminescent de l'**agent de couplage III**). Ce composé a également été obtenu avec succès. Alors que la quantité d'**agent de couplage III** était trop faible pour procéder à la réaction de greffage, **les agents de couplage I et IV** ont pu être synthétisés en quantité suffisante pour procéder à leur greffage sur les NPs TiO₂.

Dans l'étape de greffage, la procédure a été mise au point avec des silanes commerciaux ([3-(2-aminoethylamino)propyl]-trimethoxysilane, *N'*-(3-trimethoxysilylpropyl)diethylenetriamine). Les conditions basiques de greffage hydroalcoolique semblent être plus efficaces que dans un milieu acide, même si les deux procédures ont conduit à une modification des particules. La charge de surface des particules a été effectivement modifiée comme indiqué par les mesures du potentiel zêta, tandis que l'activité PC des particules de TiO₂ a été légèrement réduite (une réduction de 20 à 40 % a été généralement enregistrée). Dans le cas de MEEAA-TiO₂ (4 h, 200 °C), une quantité de 1 à 4 µmol de silane ajouté par mg de NPs a donné des résultats similaires concernant la charge de surface et l'activité de PC. Une quantité minimale de silane de 1 µmol/mg est nécessaire pour obtenir une monocouche sur les particules. Ceci est en accord avec la quantité théorique calculée de 1,09 µmol/mg (pour MEEAA-TiO₂). L'ajout de quantités de silane considérablement plus élevées (testé avec AA-TiO₂) conduit vraisemblablement à la croissance de couches moléculaires supplémentaires autour des NPs.

La quantité optimale pour le greffage des **agents de couplage** synthétisés **I et IV** sur MEEAA-TiO₂ (4h, 200 °C) a été fixée 2 µmol de silane par mg de NPs. Le greffage de l'**agent de couplage I** a été confirmé par plusieurs les méthodes d'analyse utilisées (IR, DLS, potentiel zêta). Le potentiel de surface des NPs a été significativement modifié, ce qui a conduit à une charge superficielle considérablement plus négative, à pH physiologique. Dans le contexte des applications de tests de culture cellulaire, une charge de surface positive est souhaitée et, par conséquent, ces NPs ne sont pas adéquates en l'état pour de telles applications. Egalement, l'état de dispersion des particules modifiées dans l'eau était relativement mauvais, ce qui n'est pas surprenant, car on sait que la rhodamine a une faible solubilité. Ainsi, l'introduction de groupements amine à la surface des NPs devrait améliorer la dispersibilité de celles-ci en milieu aqueux. Les NPs modifiées ont montré également une photoluminescence très élevée (Figure Résumé - 5 a) et une excellente activité PC (Figure Résumé - 5 b), allant même au-delà des propriétés des NPs non modifiées. Ce phénomène inattendu est sans doute dû à la charge superficielle significativement modifiée qui favorise l'adsorption des molécules prenant part aux réactions PCs.

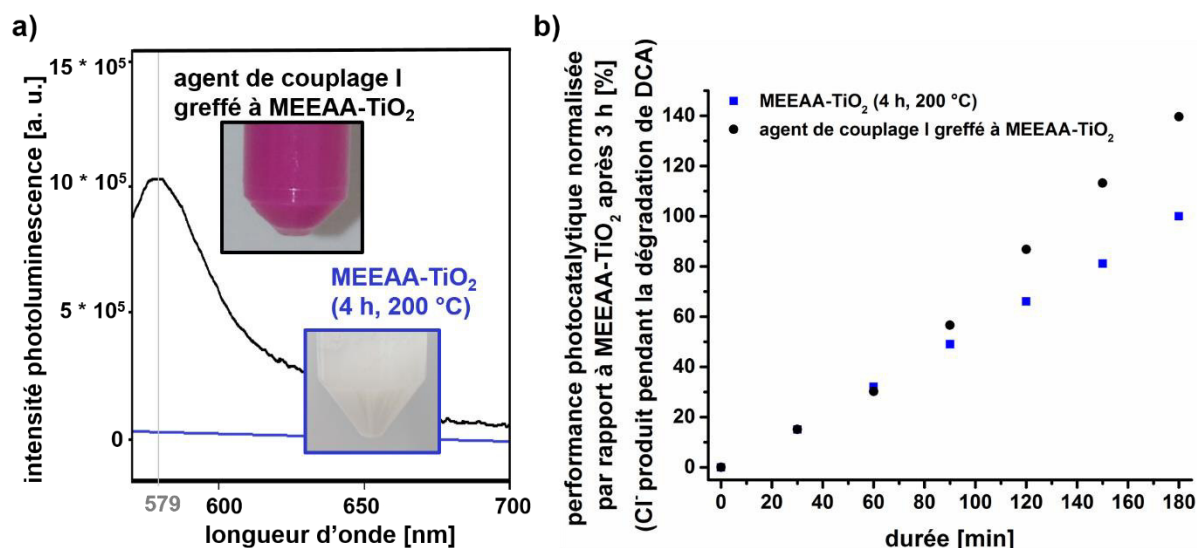


Figure Résumé - 5. A) Spectre de photoluminescence de MEEAA-TiO₂ pur (bleu) et fonctionnalisé (noir) (avec l'**agent de couplage I**); Excité à 556 nm (c'est-à-dire au maximum d'absorption du système de particules fonctionnalisées). En outre, des photos des deux échantillons de particules comme dispersion dans l'eau à pH = 10 sont représentées. b) Activité photocatalytique de MEEAA-TiO₂ fonctionnalisé avec l'**agent de couplage I** (noir) par rapport au MEEAA-TiO₂ non modifié (bleu). (DCA = acide dichloracétique)

Le greffage réussi de l'**agent de couplage IV** a été confirmé par IR même si les bandes d'absorption caractéristiques détectées étaient de faible intensité. L'IEP de l'échantillon n'a pas été modifié de manière significative, ce qui peut être dû à l'absence de groupes ioniques dans l'agent de couplage. Les tentatives qui ont été réalisées pour cliver le groupement protecteur phthalimide des **agents de couplage IV** greffés n'ont pas été concluantes à ce jour.

En résumé, la synthèse des agents de couplage dendritiques luminescents et non luminescents ainsi que leur greffage sur les TiO₂ NPs précédemment synthétisés ont été démontrés avec succès. Les avancées ainsi que les obstacles rencontrés lors des synthèses organiques et les procédures de greffage de ces agents de couplage ont été clairement montrés. Pour les études futures, la synthèse des agents de couplage luminescents (en particulier) devrait être étudiée et optimisée. En outre, le clivage du groupe protecteur du phthalimide des agents de couplage greffés doit encore être développé.

Avant les premiers essais de culture cellulaire sur les NPs synthétisés, les échantillons doivent être transférés dans des milieux de culture cellulaire. Pour éviter l'agglomération et la sédimentation, un agent de stabilisation approprié pour les NPs TiO₂ doit être recherché. La stabilisation des NPs TiO₂ avec du sérum fœtal de veau (FBS) et des éthers de polycarboxylate Melpers® V4343 ou Sika® ViscoCrete®-10110178 a amélioré la dispersion des NPs dans divers milieux de culture cellulaire. L'éther de polycarboxylate Melflux® 4930 F (Melflux) semble être l'agent stabilisant le plus approprié dans cette étude car on observe une absence d'agglomération et de sédimentation jusqu'à 24 h dans les trois milieux de culture

cellulaire testés. La stabilisation assure un dosage précis des particules pour les tests de culture cellulaire et des études fiables de l'absorption de particules par les cellules en fonction de la concentration car les particules ne sédimentent pas. Dans la Figure Résumé - 6, la sédimentation d'un échantillon stabilisé avec Melflux est comparée à un échantillon non stabilisé et à un échantillon stabilisé par FBS.

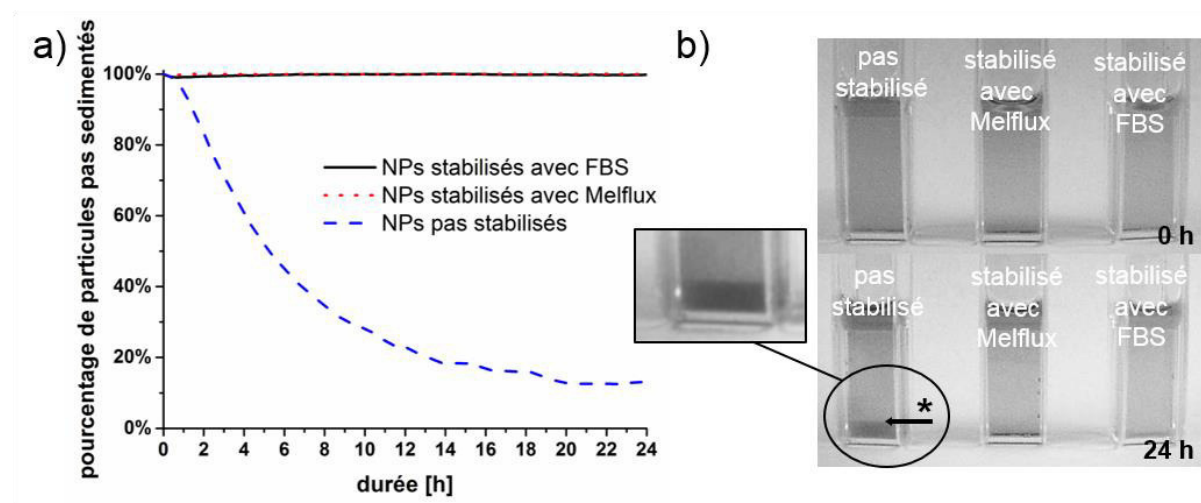


Figure Résumé - 6. Etude de la sédimentation de AA-TiO₂ (0,5 mg/ml) stabilisé avec FBS (1 mg NP: 100 mg FBS) ou Melflux (1 mg NP: 0,4 mg Melflux) et non stabilisé: a) pourcentage de particules non-sédimentées déterminées par mesure d'absorbance et b) photographies des échantillons à 0 h et 24 h après l'addition du stabilisateur à la dispersion des NPs (* particules sédimentées).

Contrairement au FBS, qui est couramment utilisé comme stabilisant dans la littérature, Melflux n'a pas d'influence sur la cytotoxicité des particules. Par conséquent, il est approprié en tant qu'agent stabilisant de NPs TiO₂ et peut être d'un intérêt particulier pour les études sur la toxicité ou le potentiel thérapeutique de ces NPs. De plus, ce travail de recherche a mis en évidence que les systèmes testés AA-TiO₂ et MEEAA-TiO₂ se sont tous deux révélés non toxiques contre les cellules malignes et non malignes dans leur état non activé - à la fois particules bien stabilisées et agglomérats non stabilisés. Cela ouvre une voie prometteuse pour leur application en tant qu'agent de traitement tumoral car leur non-toxicité peut permettre un traitement spécifique de la tumeur spécifique à la lumière UV.

L'activité antitumorale détectée des échantillons de MEEAA-TiO₂ pré-activés pendant 24h par lumière UV est probablement causée par la dégradation par PC du MEEAA en composés toxiques pour les cellules. Ce travail, d'une part, a fourni des résultats impressionnants concernant un traitement spécifique de la tumeur, et d'autre part, il a souligné que le transfert de composés commerciaux et chimiques dans des applications biomédicales peut provoquer des obstacles inattendus concernant la toxicité des impuretés non identifiées. Cependant, pour

les NPs modifiées par les agents de couplage synthétisés dans ce travail, cette toxicité n'est pas pertinente car les particules sont purifiées pendant la procédure de fonctionnalisation.

A terme, ce travail devrait inclure l'évaluation de la cytotoxicité des échantillons fonctionnalisés de MEEAA-TiO₂ ainsi que le développement du traitement tumoral par PC par l'application de lumière UV sur des cellules traitées avec les échantillons de NPs PC.

Une avancée majeure de ce travail de recherche a été le développement de systèmes de NPs fonctionnalisées pour les applications biomédicales à partir de particules fonctionnalisées par des agents de couplage organiques. Ainsi, ce travail a abouti au greffage des particules, à leur test en culture cellulaire et à l'étude de cytotoxicité. Bien que la plupart des recherches se concentrent uniquement sur une seule de ces étapes, nous avons mené à bien toutes ces étapes au sein d'un même projet. Ceci a permis de mieux comprendre l'influence de chaque étape entre elles et la possibilité de résoudre les problèmes antérieurs qui se produisent. Des travaux récents ont montré que la morphologie des cristaux influence la performance PC des NPs anatase. Il est donc possible d'optimiser les croissances cristallines lors des synthèses sol-gel hydrothermales des TiO₂ NPs pour les rendre hautement actifs en photocatalyse. La stabilisation de ces NPs dans les milieux de culture cellulaire avec Melflux® 4930 F peut être transposée aux autres systèmes de particules et peut donc être particulièrement intéressante pour les études sur la toxicité ou le potentiel thérapeutique des NPs en général. La preuve de la faisabilité du greffage des organo-silanes sur les particules de TiO₂ synthétisées ouvre la voie à leur utilisation dans une large gamme d'applications, du fait de leurs propriétés de surface modulables. Elles pourraient éventuellement être utilisés comme additifs, par exemple dans des revêtements plastiques ou fonctionnels, comme supports de médicaments ou dans des cellules solaires. Le développement de nouveaux agents de couplage dendritiques luminescents n'est pas seulement d'une grande importance pour la fonctionnalisation des NPs PC utilisées pour le traitement des tumeurs, mais aussi pour la modification de surfaces de drug-carriers, par exemple. En outre, la caractérisation de l'internalisation des particules par les cellules pourrait être facilitée par la fonctionnalisation des NPs avec ces agents de couplage luminescents, car ils pourraient permettre la détection des NPs par luminescence.

En conclusion, les systèmes de NPs TiO₂ PC fonctionnalisés ou non modifiés qui ont été développés dans ce travail sont d'un grand intérêt pour la thérapie tumorale photodynamique. Mise en pratique, cette approche thérapeutique consisterait en l'application de particules sur le tissu d'intérêt puis elles seraient internalisées par les cellules. Par la suite, une irradiation UV serait appliquée sur la zone à traiter pour activer les NPs et induire la photocatalyse des composants cellulaires conduisant à l'apoptose cellulaire et à la destruction de la tumeur. En raison de la non toxicité des NPs, les zones qui ne sont pas traitées avec de la lumière UV ne

seront pas endommagées et la photocatalyse du TiO_2 . Nous visons donc à détruire spécifiquement les cellules tumorales. En plus du traitement photodynamique de la tumeur, les systèmes de NPs développés pourraient être appliqués à la purification photocatalytique de l'eau ou pour le développement de dispositifs photoniques et optoélectroniques. Dans le cas de la purification de l'eau, les échantillons NPs dispersées pourraient être utilisés pour décomposer les contaminants organiques dans les eaux usées comme les pesticides ou les médicaments. Pour le développement de dispositifs photoniques et optoélectroniques, les NPs d'anatase semi-conductrices à larges bandes interdites sont idéales pour la conversion d'énergie lumineuse. Ainsi, la possibilité de fonctionnaliser leur surface donne la possibilité de coupler des sensibilisateurs tels que par exemple des colorants pour construire des cellules solaires à colorant.

References :

- 1 R. L. Siegel, K. D. Miller and A. Jemal, *CA. Cancer J. Clin.*, 2016, **66**, 7–30.
- 2 S. Purohit, R. Bhise, D. Lokanatha and K. Govindbabu, *Indian J. Surg. Oncol.*, 2013, **4**, 19–26.
- 3 L. A. Torre, F. Bray, R. L. Siegel, J. Ferlay, J. Lortet-Tieulent and A. Jemal, *CA. Cancer J. Clin.*, 2015, **65**, 87–108.
- 4 M. Marron, P. Boffetta, Z.-F. Zhang, D. Zaridze, V. Wunsch-Filho, D. M. Winn, Q. Wei, R. Talamini, N. Szeszenia-Dabrowska, E. M. Sturgis, E. Smith, S. M. Schwartz, P. Rudnai, M. P. Purdue, A. F. Olshan, J. Eluf-Neto, J. Muscat, H. Morgenstern, A. Menezes, M. McClean, E. Matos, I. N. Mates, J. Lissowska, F. Levi, P. Lazarus, C. L. Vecchia, S. Koifman, K. Kelsey, R. Herrero, R. B. Hayes, S. Franceschi, L. Fernandez, E. Fabianova, A. W. Daudt, L. D. Maso, M. P. Curado, G. Cadoni, C. Chen, X. Castellsague, S. Boccia, S. Benhamou, G. Ferro, J. Berthiller, P. Brennan, H. Moller and M. Hashibe, *Int. J. Epidemiol.*, 2010, **39**, 182–196.
- 5 Z. Fei Yin, L. Wu, H. Gui Yang and Y. Hua Su, *Phys. Chem. Chem. Phys.*, 2013, **15**, 4844.
- 6 S. Hackenberg, A. Scherzed, W. Harnisch, K. Froelich, C. Ginzkey, C. Koehler, R. Hagen and N. Kleinsasser, *J. Photochem. Photobiol. B*, 2012, **114**, 87–93.
- 7 T. Hasan, B. Ortel, N. Solban and B. Pogue, *Cancer Med.*, 2003, **7**, 537–48.
- 8 S. B. Brown, E. A. Brown and I. Walker, *Lancet Oncol.*, 2004, **5**, 497–508.
- 9 P. Agostinis, K. Berg, K. A. Cengel, T. H. Foster, A. W. Girotti, S. O. Gollnick, S. M. Hahn, M. R. Hamblin, A. Juzeniene, D. Kessel, M. Korbelik, J. Moan, P. Mroz, D. Nowis, J. Piette, B. C. Wilson and J. Golab, *CA. Cancer J. Clin.*, 2011, **61**, 250–281.
- 10 F. U. Rehman, C. Zhao, H. Jiang and X. Wang, *Biomater. Sci.*, 2015, **4**, 40–54.
- 11 S. Hackenberg, A. Scherzed, A. Gohla, A. Technau, K. Froelich, C. Ginzkey, C. Koehler, M. Burghartz, R. Hagen and N. Kleinsasser, *Nanomed.*, 2014, **9**, 21–33.
- 12 S. Hackenberg, F.-Z. Zimmermann, A. Scherzed, G. Friehs, K. Froelich, C. Ginzkey, C. Koehler, M. Burghartz, R. Hagen and N. Kleinsasser, *Environ. Mol. Mutagen.*, 2011, **52**, 582–589.
- 13 Kleinsasser, *Int. J. Oncol.*, 2010, **37**, 1538–1590.

Contents

General Introduction.....	1 -
I. Bibliographic study.....	9 -
I.1. Titanium dioxide particles.....	11 -
I.1.1. TiO ₂ nanoparticle synthesis.....	12 -
I.1.2. Photocatalytic activity.....	15 -
I.1.3. Photocatalytic tumour therapy with TiO ₂ particles.....	19 -
I.1.4. Luminescent TiO ₂ nanoparticles.....	21 -
I.2. Surface modification of nanoparticles for biotechnological applications.....	24 -
I.2.1. Surface modification of TiO ₂ particles.....	26 -
I.2.2. Surface modification of particles with dendrons.....	28 -
I.3. Conclusion.....	33 -
II. Inorganic syntheses: Titanium dioxide nanoparticles.....	43 -
II.1. Influence of the coordinating agent on TiO ₂ nanoparticles.....	45 -
II.1.1. Size and morphology.....	45 -
II.1.2. Surface moieties.....	48 -
II.1.3. Photocatalytic activity.....	53 -
II.2. Influence of hydrothermal processing parameters on MEEAA-TiO ₂ particles.....	56 -
II.2.1. Size and morphology.....	56 -
II.2.2. Surface moieties.....	62 -
II.2.3. Photocatalytic activity.....	65 -
II.3. Luminescent TiO ₂ based core/shell structured nanoparticles.....	71 -
II.3.1. Luminescent TiO ₂ /SiO ₂ core/shell nanoparticles.....	71 -
II.3.2. ZnO/TiO ₂ core/shell nanoparticles.....	76 -
II.4. Conclusion.....	83 -
III. Synthesis of organic coupling agents and their grafting onto TiO₂ nanoparticles.....	89 -
III.1. Synthesis of functional coupling agents.....	91 -
III.1.1. Synthesis of linear and dendritic fluorescent coupling agents.....	94 -
III.1.2. Synthesis of dendritic non-fluorescent coupling agents.....	111 -
III.2. Grafting of organic molecules onto particles.....	115 -
III.2.1. Optimization of grafting protocols with commercial silanes.....	116 -
III.2.2. Grafting of synthesized coupling agents onto MEEAA-TiO ₂ (200 °C, 4 h).....	123 -
III.3. Conclusion.....	133 -

IV. Cell culture examinations of synthesized TiO₂ particle systems.....	141 -
IV.1. Stabilization of TiO ₂ nanoparticles in cell culture media.....	144 -
IV.2. Cytotoxicity of TiO ₂ nanoparticles.....	151 -
IV.3. Tumor treatment effect of MEEAA particles.....	154 -
IV.4. Conclusion.....	164 -
General Conclusion.....	167 -
Experimental part.....	173 -
1. Materials, equipment and experimental set-ups.....	175 -
1.1. Solvents, reagents and materials for cell culture experiments.....	175 -
1.2. Equipment and experimental set-ups.....	175 -
2. Inorganic nanoparticle synthesis protocols.....	179 -
2.1. Synthesis of TiO ₂ nanoparticles.....	179 -
2.2. Synthesis of luminescent TiO ₂ based core/shell nanoparticles.....	180 -
3. Organic coupling agent synthesis protocols.....	182 -
4. Grafting protocols.....	206 -
4.1. Optimization of grafting protocols with commercial silanes.....	206 -
4.2. Grafting of synthesized coupling agents onto MEEAA-TiO ₂ (200 °C, 4 h).....	206 -
5. Cell culture tests.....	208 -
Appendices.....	213 -
Appendix I Influence of hydrothermal processing parameters on AA-TiO ₂ particle.....	214 -
Appendix II Cleavage of the phthalimide protecting group of the coupling agent IV grafted onto MEEAA-TiO ₂ (200 °C, 4 h).....	218 -
Appendix III Stabilization of MEEAA-TiO ₂ in cell culture media with FBS, BSA, Melflux, Melpers or Sika ViscoCrete.....	219 -
List of appreviations.....	221 -

General introduction

In 2016, over 48,000 new cases of head and neck cancer were estimated in the USA which represents 3% of all new cancer cases.¹ This cancer counts as one of the ten most common cancers globally.² Regions of the human body that can be affected by head and neck cancer are the oral cavity, including the lips, parts of the tongue or the floor of the mouth, and the pharynx which is a muscular tube between the nose and oesophagus. In addition, it can also occur in the larynx (voicebox), salivary glands, nasal cavity and paranasal sinuses which are hollow spaces in the bones surrounding the nose. The most common entity of head and neck cancer is the squamous cell carcinoma.² Major risk factors for this type of cancer are smoking, alcohol consumption, smokeless tobacco use and human papillomavirus infections. Furthermore the combination of smoking and excessive alcohol consumption has a synergistic effect.^{3,4} Surgery and radiotherapy are the standard treatments for patients with this disease in the early stages with success rates of 60 % to 90 % depending on the tumour localization and extent. Nevertheless, these patients have a high risk of developing a local recurrence or a second primary due to field cancerization.² Field cancerization occurs when the tumour is not situated in a well-defined location but widely spread over the tissue. Usually these formations are a mixture of pre-malignant and malignant superficial manifestations with some regions having deeply invasive tumour fractions. This unclear extent of the tumour makes a surgical removal very difficult. Chemotherapy is used in advanced or recurrent cases in combination with radiotherapy as a curative regime or alone as a palliative treatment. Common chemotherapeutics are platinum analogues like cisplatin that act by forming covalent bonds with the DNA or taxanes like paclitaxel and docetaxel that promote microtubular assembly.² Both of these actions lead to cell death. Nevertheless, the chemotherapeutic treatments are limited in duration and intensity due to their non-specific toxicity.² In recent years, targeted agents have come to the research fore, including monoclonal antibodies such as cetuximab possessing an extracellular domain activity and small tyrosine kinase inhibitors acting intracellularly.² They promise a more specific tumour treatment thereby reducing unwanted side-effects of drugs. Despite the advances in therapy procedures and a significant improvement in the 5-year survival rate during the last decade, the rate remains at 66 % (in the USA¹) including a high risk of tumour recurrence as well as the appearance of difficult-to-treat field cancerization.² Thus, novel therapy strategies need to be developed to enhance the current standard treatments.

Nanoparticles (NPs), materials smaller than 100 nm in size, exhibit unique physical and chemical properties compared to bulk material due to their dimensions. Their small size makes them ideal to cross cell or tissue barriers while being large enough to be conjugated to antibodies or drugs. This is why they have a great potential as tools for cell imaging or biological analysis and as drug carriers or therapeutic agents.⁵ Concerning squamous cell carcinomas,

photocatalytic NPs can provide a novel, complementary therapy approach.⁶ The photodynamic therapy using photosensitive molecules such as porphyrins or chlorins is a well-known and established non-invasive alternative in the treatment of dermal malignancies.^{7–9} Thanks to their unique properties, the use of photocatalytic NPs for photodynamic tumour treatment is increasingly recognized as a promising strategy and initial studies have already been carried out stressing their potentials.^{5,9,10} For this approach, photocatalytic NPs are applied onto carcinogenic tissue to be taken up by malignant cells. Ultraviolet (UV) light application excites the photocatalytic particles (Figure Intro - 1) because of their semiconductor properties, including an appropriate band-gap within the energy-range of UV light. Thus, electron-hole pairs are created which either recombine or migrate to the particle surface, react with surrounding oxygen and water and create highly reactive radicals. These radicals are then responsible for the destruction of cell components leading to apoptosis.^{6,11–13} Compared to chemotherapeutics, the applied particles are normally non-toxic in the non-activated state and therefore less toxic towards non-affected organs or non-UV light treated tissue.¹³ As the transmission of light within tissue is limited, the UV light application and the initiated photocatalysis will only affect superficial tissue which is the region of interest when treating field cancerization.

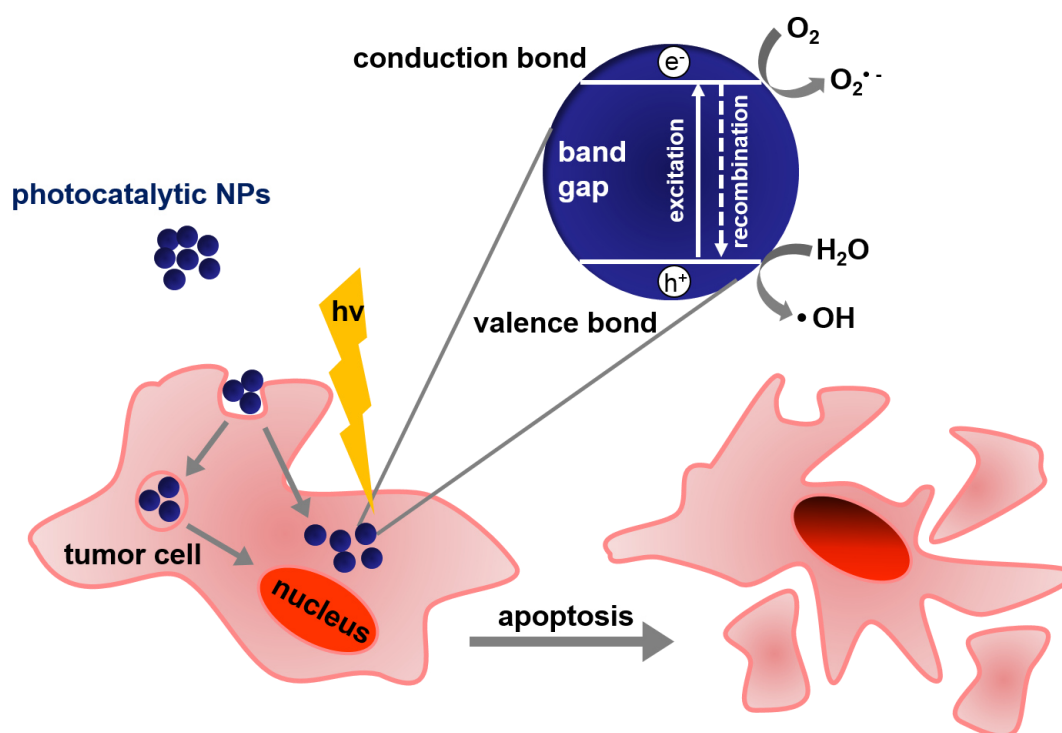


Figure Intro - 1. Tumour cell destruction via light-induced photocatalysis by semiconductor nanoparticles.

Due to their high photocatalytic activity, titanium dioxide (TiO_2) NPs seem to be an appropriate choice for the photodynamic therapy. Though the killing of cancer cells by UV light activated

TiO₂ NPs has been demonstrated, the treatment is in general lacking specificity towards these cells.⁵ Furthermore, the particles used are often not well characterized and do not show well-tailored properties as they were commercially obtained. In addition, the dependency of particle properties such as surface charge on the cellular uptake and mechanisms leading to cell apoptosis have not been studied thoroughly. Hence, in order to make advances in this research area, it is indispensable to prepare well-characterized TiO₂ nanoparticle systems and to be able to finely tune their surface properties, for example by functionalization. If the particles additionally possess luminescence properties, cellular uptake can be studied or, in later applications as an anti-tumour agent, their exact position in the tissue can be confirmed prior to UV light application. Additionally, a fine manipulation of the surface charge of these particles by organic functionalization may enhance the cellular uptake. If these particles are also bioconjugated, providing specific ligands for tumour targeting, even cancer diagnosis or luminescence guided surgery can be possible. The hypothetical application of an optimized, luminescent and photocatalytic particle system in oral cancer therapy is depicted below (Figure Intro - 2).

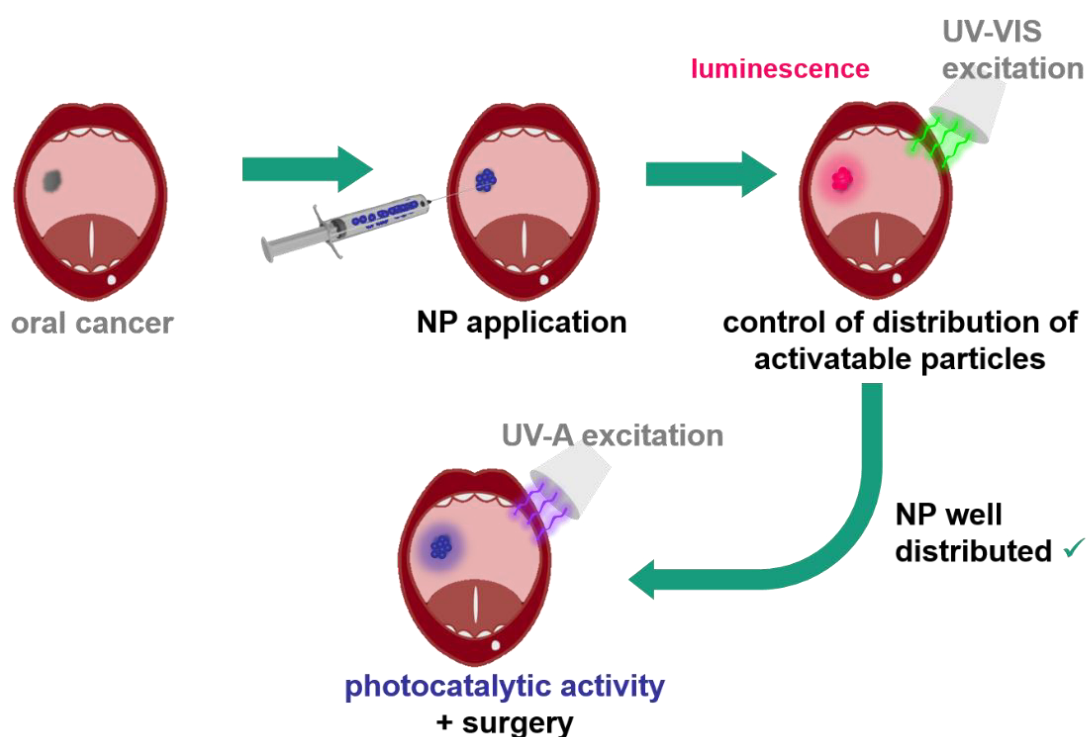


Figure Intro - 2. Application of photocatalytic, luminescent nanoparticles complementing the therapy of oral cancer.

In order to realize this approach, the first goal was the synthesis and characterization of photocatalytic TiO₂ NPs, more precisely anatase NPs. Two particle systems with different types of complexing agents and varied autoclaving parameters were to be synthesized via a hydrothermal sol-gel process. Out of these samples, the most suitable and promising

candidate for photocatalytic tumour treatment had to be selected. Furthermore, their transfer to cell culture tests was a main objective, including their stabilisation in cell culture media and the realization of cytotoxicity tests. Subsequently, the particle surfaces were then to be modified with suitable organic molecules to facilitate their cellular uptake and possibly provide a better dispersion state in cell culture media. The task was to synthesize linear and dendritic organic molecules with terminal amine functions as their positive charge is favourable for an interaction of the particles with cell membranes. Dendritic structures were chosen to increase the amount of terminal functionalities while not increasing the number of surface anchors. This was crucial as the photocatalytic activity of the inorganic particles should be inhibited as little as possible by the molecules anchored to the surface. For the grafting of the organic molecule with an alkoxysilane serving as an anchor group, suitable grafting procedures were to be developed. This also includes proving the feasibility of grafting onto the developed TiO₂ NPs. An additional goal was the introduction of luminescence properties into the particle system in order to combine the therapeutic with diagnostic applications. Luminescence would also facilitate cell culture studies on the particle behaviour such as the particle uptake by cells. This objective was meant to be achieved either by the modification of the inorganic particles e.g. via doping or by the integration of a chromophore into the organic surface agents. The final objective was then to prove the maintained photocatalytic activity of the developed functional particle systems, as well as to examine their cytotoxicity and potential as possible anti-tumour agents.

The following work is structured into four main chapters:

The first chapter comprises a bibliographic study, which includes an introduction to TiO₂ NPs, their synthesis, photocatalytic activity and potential as tumour treatment agents. Additionally, different approaches to obtain luminescent TiO₂ NPs are presented. For the surface-modification of TiO₂ NPs, possible anchoring moieties are first introduced, followed by the description of dendritic surface agents for NP functionalization. Subsequently, a short overview of the introduction of luminescent moieties into dendritic structures is given.

The second chapter deals with the synthesis and characterisation of anatase NPs. First, two particle systems synthesized with different coordinating agents are compared in their size and morphology, their surface moieties and their photocatalytic activity. Next, the influence of processing parameters, such as hydrothermal treatment time and temperature, on the particle characteristics (including size, morphology, surface moieties and photocatalytic activity) are

described. The last part of the chapter presents two approaches in order to obtain luminescent inorganic particle systems via core-shell strategies.

In the third chapter, the synthesis of organic coupling agents for the particle functionalization is described, including the development of dendritic non-luminescent molecules and the synthesis approach of linear and dendritic structures incorporating the dye rhodamine. Subsequently, the grafting of coupling agents is treated. After optimizing the grafting procedure with the help of commercial silanes, the grafting of synthesized molecules is described. These steps also include the analytical characterization of the functionalized NPs.

The fourth chapter reports the transfer of the synthesized particle systems into cell culture tests. The stabilisation of the as-synthesized TiO₂ NPs in cell culture media with the help of stabilising agents is presented. Furthermore, cytotoxicity tests of these particles are discussed. Finally, a detected anti-tumour activity of one of the synthesized particle systems is investigated.

References:

- 1 R. L. Siegel, K. D. Miller and A. Jemal, *CA. Cancer J. Clin.*, 2016, **66**, 7–30.
- 2 S. Purohit, R. Bhise, D. Lokanatha and K. Govindbabu, *Indian J. Surg. Oncol.*, 2013, **4**, 19–26.
- 3 L. A. Torre, F. Bray, R. L. Siegel, J. Ferlay, J. Lortet-Tieulent and A. Jemal, *CA. Cancer J. Clin.*, 2015, **65**, 87–108.
- 4 M. Marron, P. Boffetta, Z.-F. Zhang, D. Zaridze, V. Wunsch-Filho, D. M. Winn, Q. Wei, R. Talamini, N. Szeszenia-Dabrowska, E. M. Sturgis, E. Smith, S. M. Schwartz, P. Rudnai, M. P. Purdue, A. F. Olshan, J. Eluf-Neto, J. Muscat, H. Morgenstern, A. Menezes, M. McClean, E. Matos, I. N. Mates, J. Lissowska, F. Levi, P. Lazarus, C. L. Vecchia, S. Koifman, K. Kelsey, R. Herrero, R. B. Hayes, S. Franceschi, L. Fernandez, E. Fabianova, A. W. Daudt, L. D. Maso, M. P. Curado, G. Cadoni, C. Chen, X. Castellsague, S. Boccia, S. Benhamou, G. Ferro, J. Berthiller, P. Brennan, H. Moller and M. Hashibe, *Int. J. Epidemiol.*, 2010, **39**, 182–196.
- 5 Z. Fei Yin, L. Wu, H. Gui Yang and Y. Hua Su, *Phys. Chem. Chem. Phys.*, 2013, **15**, 4844.
- 6 S. Hackenberg, A. Scherzed, W. Harnisch, K. Froelich, C. Ginzkey, C. Koehler, R. Hagen and N. Kleinsasser, *J. Photochem. Photobiol. B*, 2012, **114**, 87–93.
- 7 T. Hasan, B. Ortel, N. Solban and B. Pogue, *Cancer Med.*, 2003, **7**, 537–48.
- 8 S. B. Brown, E. A. Brown and I. Walker, *Lancet Oncol.*, 2004, **5**, 497–508.
- 9 P. Agostinis, K. Berg, K. A. Cengel, T. H. Foster, A. W. Girotti, S. O. Gollnick, S. M. Hahn, M. R. Hamblin, A. Juzeniene, D. Kessel, M. Korblick, J. Moan, P. Mroz, D. Nowis, J. Piette, B. C. Wilson and J. Golab, *CA. Cancer J. Clin.*, 2011, **61**, 250–281.
- 10 F. U. Rehman, C. Zhao, H. Jiang and X. Wang, *Biomater. Sci.*, 2015, **4**, 40–54.
- 11 S. Hackenberg, A. Scherzed, A. Gohla, A. Technau, K. Froelich, C. Ginzkey, C. Koehler, M. Burghartz, R. Hagen and N. Kleinsasser, *Nanomed.*, 2014, **9**, 21–33.
- 12 S. Hackenberg, F.-Z. Zimmermann, A. Scherzed, G. Friehs, K. Froelich, C. Ginzkey, C. Koehler, M. Burghartz, R. Hagen and N. Kleinsasser, *Environ. Mol. Mutagen.*, 2011, **52**, 582–589.
- 13 Kleinsasser, *Int. J. Oncol.*, 2010, **37**, 1538–1590.

I. Bibliographic study

Contents

I.	Bibliographic study	- 11 -
I.1.	Titanium dioxide particles	- 11 -
I.1.1.	TiO ₂ nanoparticle synthesis	- 12 -
I.1.2.	Photocatalytic activity	- 15 -
I.1.3.	Photocatalytic tumour therapy with TiO ₂ particles	- 19 -
I.1.4.	Luminescent TiO ₂ nanoparticles	- 21 -
I.2.	Surface modification of nanoparticles for biotechnological applications	- 24 -
I.2.1.	Surface modification of TiO ₂ particles	- 26 -
I.2.2.	Surface modification of particles with dendrons	- 28 -
I.3.	Conclusion	- 33 -

I. Bibliographic study

I.1. Titanium dioxide particles

Since its first commercial production in the beginning of the twentieth century,¹ titanium dioxide (TiO_2) has been widely used in sunscreens^{2,3} or as a pigment,⁴⁻⁶ for example in paints.^{7,8} Nowadays it is utilized for a variety of applications including: hydrogen sensing, storage and separation; lithium batteries and photovoltaic technologies, as an additive in food, and cosmetic; and as a catalyst or coating for medical implants.⁹⁻¹² The wide range of applications is thanks to the fact that TiO_2 not only provides semiconductor properties but also has an excellent chemical stability.^{9,13} Its four natural crystal structures are rutile (tetragonal), anatase (tetragonal), brookite (rhombohedral) and TiO_2 (B) (monoclinic).¹⁴ The two photocatalytically active polymorphs, rutile and anatase, are the most intensively studied. Their crystal structures are shown in Figure I - 1 and can be described as an assemblage of TiO_6 octahedrons; each Ti^{4+} ion at the centre of the octahedron is coordinated by six O^{2-} ions. The two crystal lattices only differ in the distortion of each octahedron and in the octahedron arrangement structure.^{1,15} These differences in lattice structure cause slight differences in their mass densities and electron band structures while their physical properties remain very similar.^{1,11} Nevertheless, the anatase form is commonly most preferred because of its high photocatalytic (PC) activity and its more negative conduction band edge potential giving a higher potential energy of photogenerated electrons. Furthermore, it offers non-toxicity, photochemical stability and a relatively low price.^{13,16}

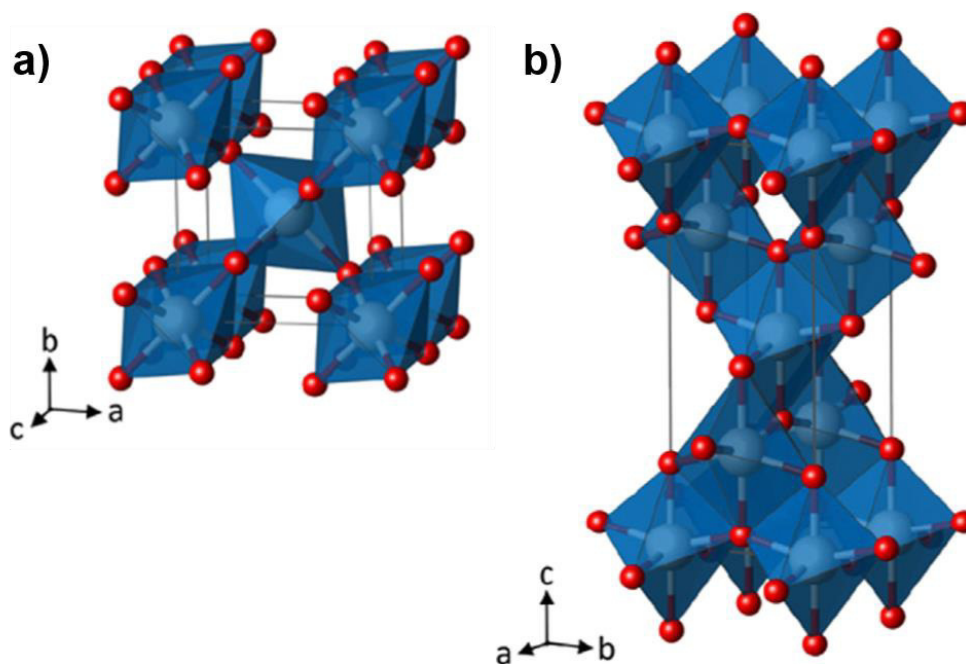


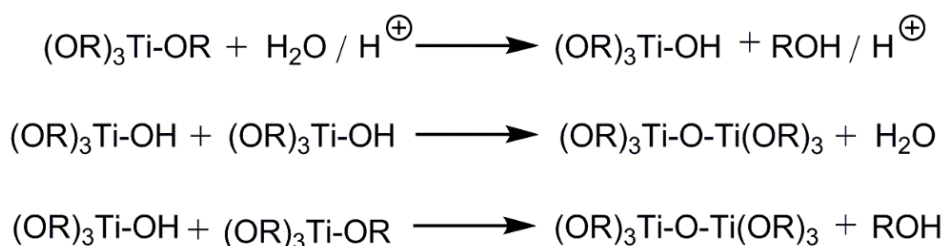
Figure I - 1. Crystallographic structure of a) rutile and b) anatase consisting of octahedrons containing titanium atoms (white) in their centre and oxygen atoms (red) at their corners.¹¹

In recent decades the synthesis of TiO_2 nanostructures, which are structures possessing between one and three dimensions smaller than 100 nm, has become an important field of research. As TiO_2 is a semiconductor material, in its nano form (1 to 25 nm) its electronic and optical properties deviate substantially from those of bulk materials due to the quantum confinement effect.^{17–19} This effect describes the fact that if the diameter of a particle is smaller than the exciton Bohr radius, its energy levels are discrete instead of continuous. As the particle size is varied, the energy levels shift, with an increasing separation of valence and conduction bands with decreasing radius. As the confining dimension decreases and reaches a certain limit, typically in nanoscale, the energy spectrum becomes discrete. As a result, the bandgap becomes size-dependent which results for example in a blue shift in light emission with decreasing particle size.¹⁷ Nanomaterials also possess a very high surface area and surface-to-volume ratio which increases the efficiency in applications that are based on surface or interface interactions between the TiO_2 device and an interacting medium.¹

I.1.1. TiO_2 nanoparticle synthesis

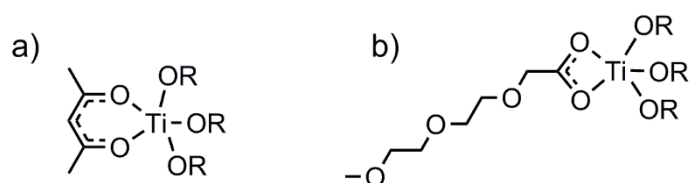
Titanium dioxide nanostructures can be synthesized via a vast variety of reactions^{1,16} such as sol-gel reactions,^{20,21} micelle and reverse micelle methods^{22–24} and solvo- and hydrothermal processing,^{25,26} as well as chemical and physical vapour deposition.^{27,28} Further synthesis methods are flame hydrolysis (commercial Degussa P25),¹⁶ sonochemical^{29,30} and microwave-assisted^{31,32} reactions or a combination of various methods.³³ A combined sol-gel and hydrothermal processing is frequently chosen^{34–37} as it unites the advantages of sol-gel reactions with hydrothermal treatments. Typical characteristics due to the sol-gel process are a controlled stoichiometry and excellent reproducibility,³⁴ while a high density of the particles, high crystallinity with a minimum of defects and controlled morphology are due to the hydrothermal treatment.^{1,34,35} The resulting nanostructures are of high purity, with narrow size distributions and can carry organic surface moieties of the synthesis, hence ensuring a high reactivity for further treatments.

Sol-gel reactions are characterized by the hydrolysis and condensation of metal alkoxide precursors (Scheme I - 1) resulting in colloidal suspensions or sols. In the case of titanium dioxide synthesis, the hydrolysis is often acid-catalysed.^{1,35,38–40}



Scheme I - 1. Hydrolysis and condensation reactions of a titanium alkoxide precursor.

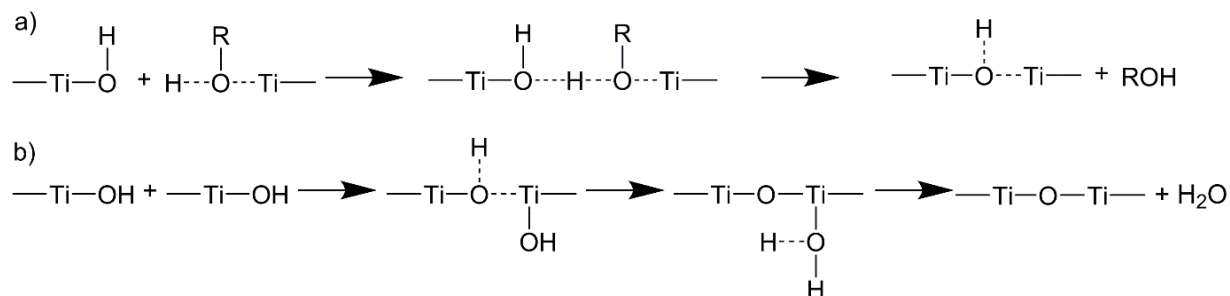
Transition metals like titanium are commonly not fully coordinated in the molecular precursor state for example in metal alkoxides. This is why a chemical modification with chelating ligands is needed to retard hydrolysis and condensation rates preventing uncontrolled precipitation and mediating the formation of smaller titanium-oxo species.⁴¹⁻⁴³ Possible chelating agents can be alkoxy- and aminoalcohols, beta-diketons, beta-ketoester, carboxylic and phosphonic acids.⁴¹⁻⁴³ Furthermore these ligands can have positive effects on the formation of non-aggregated nanoparticles (NPs), as well as their growth behavior.^{44,45} Examples for the complex formed by titanium alkoxide and beta-diketon⁴⁶ or carboxylic acid⁴⁷ are shown in Scheme I - 2.



Scheme I - 2. Titanium alkoxide complexed with chelating agents: a) acetyl acetone and b) 2-[2-(2-methoxyethoxy)ethoxy]acetic acid.

Hydrolysis (Scheme I - 1, 1st reaction equation) of the alkoxy ligands (Ti-OR) of these precursors, leading to hydroxyl groups (Ti-OH), is achieved by the addition of water while the hydrolytically stable chelating agents remain unmodified.⁴⁵ Condensation (Scheme I - 1, 2nd and 3rd reaction equation) can start as soon as Ti-OH groups are present. Two competitive mechanisms can occur depending mainly on the experimental conditions: oxolation and ololation. Ololation is the formation of hydroxo bridges between two titanium atoms while water or an alcohol is released (Scheme I - 3 a). For this nucleophilic substitution reaction, the OH ligand represents the nucleophile which only changes its coordination from a terminal to a bridging ligand. The reaction is kinetically controlled by the lability of the M-OHR bond (with a metal M or in this case M = Ti) which is usually rather high. This is why without complexing ligands or steric effects, ololation is fast and diffusion-controlled.^{48,49} In contrast to ololation, oxolation is the formation of “oxo” bridges (M-O-M) between two metals that do not possess aquo ligands (Scheme I - 3 b). It usually proceeds via a 2-step S_N2 associative mechanism; first, a nucleophilic addition forming an “ol” (M-OH-M) bridge takes place, followed by the proton transfer from the “ol” bridge to a terminal OH ligand, which results later on in the removal

of the aquo ligand. The reaction rate is mainly dependent on the acidity of the medium.^{48,49} Continuous polycondensation reactions (either ololation or oxolation) lead first to polymeric chains and rings before the formation of an amorphous Ti-O-Ti network. Depending on the presence and ratio of water and titanium precursors, the resulting TiO₂ appears as a 3D polymeric skeleton or (either loosely or closely packed) first-order particle sols. Complete condensation of the precursor and loss of solvent leads to the conversion of the sol to a solid gel.¹



Scheme I - 3 : Condensation via a) ololation and b) oxolation (with R = H or organic group of alkoxy ligand).

However, to obtain TiO₂ nanocrystals the solution must be heated in order to favour ion diffusion and crystallization rate.^{43,50} In the case of titanium stabilised by complexing ligands, heating also helps to remove the ligands, thus allowing the formation of further Ti-O-Ti bonds.⁴³ The formation of either anatase or rutile crystals (without addition of strong complexing agents) can be explained by taking into account the first stage (of ololation) which is the formation of the dimer [Ti₂(OH)₈(OH)₂]⁰.⁴⁸ This is a structure of two octahedrons sharing an edge as depicted in Figure I - 2. This “embryo” grows by ololation with further monomers forming nuclei and subsequent condensation of these nuclei by oxolation is likely to result in rutile or anatase crystals. Considering that the TiO₆ octahedrons in anatase only share edges while in rutile both edges and corners are shared, it is more likely that anatase is formed. The probability that the “embryo” grows through edge sharing only in the same plane is smaller than in different planes. This is why curved or bent edge sharing chains are formed, inhibiting the sharing of corners between different planes. Nevertheless, rutile as the thermodynamically stable phase is said to be formed based on Ostwald ripening (dissolution/crystallization mechanisms).⁴⁸ For the heating to produce crystal structures, hydrothermal treatment is ideal as the synthesis is conducted in a steel pressure vessel and the reaction temperature can exceed the boiling point of water, reaching the pressure of vapour saturation. The temperature and the filling grade of the autoclave with solution determines the internal pressure produced.^{1,51} In contrast to calcination or thermal annealing,⁵² this method does not lead to unwanted phase transformation, sintering or grain growth of the particles and therefore loss of surface area.⁵⁰ Additionally, it is less energy consumptive and an environmentally friendly process. Moreover,

with hydrothermal treatment the crystallization temperature for anatase phase is below 200 °C.⁴⁴

In conclusion, the properties of the final TiO₂ particles, such as the degree of crystallization, crystal phase composition, size, morphology and surface chemical properties, are controlled by the type and concentration of the precursors, solvent, additives, catalysts, pH and hydrothermal reaction conditions.^{44,50}

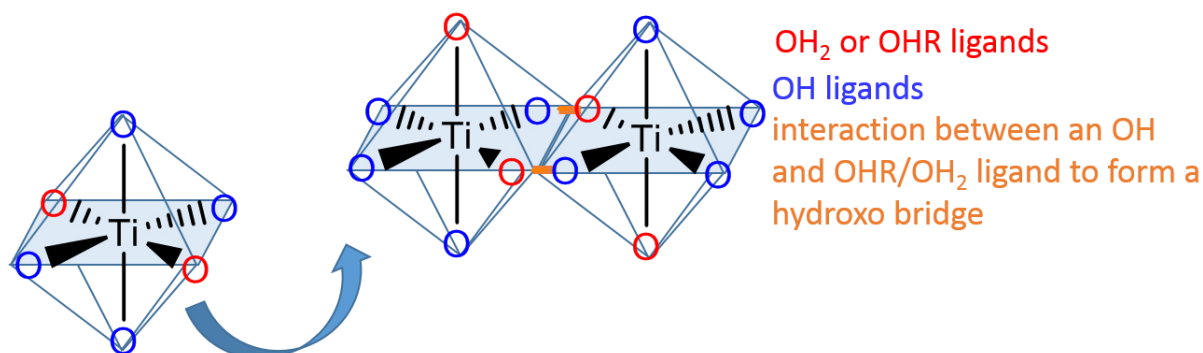
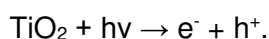


Figure I - 2. Ongoing growth via oligation of the first formed dimer during condensation.⁴⁸

I.1.2. Photocatalytic activity*

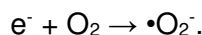
TiO₂, especially in its nano-form, is often used for photocatalysis as it efficiently catalyses a broad variety of reactions if activated by light.⁵³ Applications include waste water treatment,^{53,54} catalysis of chemical reactions,⁵⁵ disinfection⁵⁶ and tumour therapy.⁵⁶ Anatase has an energy band gap of 3.2 eV with an absorption edge at 386 nm, while rutile possesses a band gap of 3.02 eV with an absorption edge at 416 nm.¹¹ Both forms can be activated by light with an energy equal to or greater than the band gap; in general ultraviolet (UV) light with wavelengths from 280 to 400 nm. This provokes the elevation of an electron (e⁻) from the valence band to the conduction band. A hole (h⁺) in the valence band is therefore created resulting in a so-called electron-hole pair:^{11,57,58}



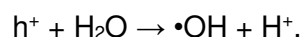
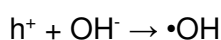
After excitation there are different processes taking place that compete with each other (Figure I - 3); the separated electron-hole pair can either recombine within the volume of the particle

* Parts of this chapter have been submitted to Nanoscale for publication. The submitted title is "Discovering the determining parameters for the photocatalytic activity of TiO₂ colloids based on an anomalous dependence on the specific surface area".

dissipating energy like light or heat or it can migrate onto the particle surface. On the surface, either - once again - a recombination occurs or the electron and the hole react with their surrounding environment (for example adsorbed inorganic or organic species or solvent) by electron transfers.⁵⁷ In this case, the electron can reduce an electron acceptor, typically oxygen in an aerated solution:^{11,57}



Further reactions of superoxide radicals ($\cdot O_2^-$) with holes can also lead to singlet oxygen (1O_2). In the meantime, the hole combines with an electron from a donor species like water or hydroxyl groups, oxidizing it:^{11,57}



Reactions of water and hydroxyl groups and its resulting radicals can also produce hydrogen peroxide (H_2O_2) or protonated superoxide radicals ($HOO\cdot$).⁵⁹

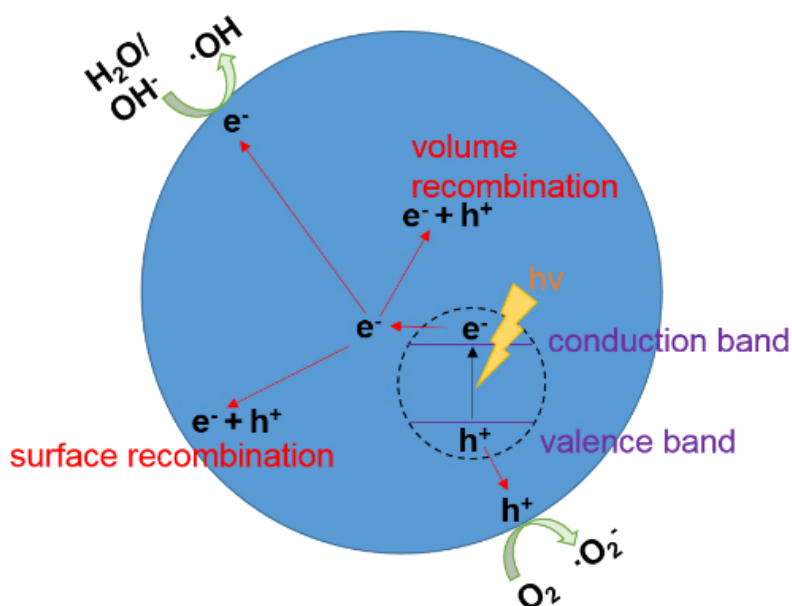


Figure I - 3. Photoexcitation in a semiconductor particle followed by deexcitation events.⁵⁷

These reactive oxidizing species (ROS) react with other surface adsorbed organic, inorganic or biological species, decomposing them.^{11,59} The probability and rate of charge transfer responsible for photocatalysis depends on the band energy positions of the material and the redox potential levels of the adsorbate species. The potential level of the acceptor species has to be thermodynamically lower (more positive) than the conduction band position of TiO_2 to be able to accept the electron. The donor has to show a higher (more negative) potential level than the valence band for the transfer of an electron to the hole.⁵⁷

As recombination and electron transfer processes are competing with each other, it is evident that the efficiency of a photocatalyst increases, when the recombination of the photoexcited electron-hole pair is retarded. This is achieved by charge carrier trapping which suppresses recombination and increases the lifetime of the separated pair. Traps can be provided by (surface) defect sites in the crystal lattice naturally created during the synthesis but also by manipulations like the creation of heterojunctions or doping with ions.^{57–59} The presence of a certain concentration of oxygen vacancies in the TiO₂ crystal lattice can on the one hand improve the PC performance due to enhancement of the charge carrier separation (e⁻ and h⁺). On the other hand, if the amount of oxygen vacancies is too high, they act as recombination centres and therefore decrease the PC activity.^{60–62} The PC performance of TiO₂ NPs not only depends on their defect concentration but also on their crystallite size, surface area, morphology and phase structure.^{16,44} Concerning the phase of TiO₂, the anatase phase is said to be more active than rutile because of its superior mobility of electrons and holes and a higher surface hydroxyl density.^{11,59} Regarding the size, monodispersed particles with small crystallite size are favoured as they benefit from a high surface area and a reduced bulk recombination of electrons and holes. Nevertheless, the particle should not be too small in order to avoid increased surface recombination and low crystallinity. The perfect particle size for a high PC activity cannot be generally identified as it depends on several factors such as the synthesis or the photocatalysis test chosen.^{53,58}

Recently, the type and ratio of exposed facets of anatase crystals was also found to influence the PC performance of TiO₂ NPs.^{61,63–73} Under equilibrium conditions, anatase has the shape of a slightly truncated tetragonal bipyramid enclosed with eight {101} facets (which contribute 94% of the surface area) and two {001} facets (according to the *Wulff* construction).^{64,68,69} This seems logical as the {101} facet is the thermodynamically most stable one with a calculated surface energy (0.44 J m⁻²) lower than that of the {001} (0.90 J m⁻²) and {100} (0.53 J m⁻²) facets.^{70,74} Nevertheless, under certain reaction conditions, the appearance of a “belt” consisting of {100} is also predicted.^{75,76} Both morphologies are depicted in Figure I - 4. The main difference between these facets is their surface atomic structure and therefore their Ti-coordination; both {001} and {100} facets expose 100% 5-fold-coordinated titanium atoms (5c-Ti) as compared to 50% 5c-Ti (and 50% 6-fold-coordinated Ti; 6c-Ti) on the {101} surface (Figure I - 5).^{60,68} Due to their surface structure, the high energy facets with 100% 5c-Ti allow a dissociative adsorption of water molecules while {101} facets only permit a molecular adsorption.^{68,73,77,78} As for PC reactions, the pre-adsorption of molecules on the catalyst surface is a determining step, the increase in 100% Ti5c surface area, *i.e.* the enhancement of pre-adsorption of water molecules, results in a higher PC performance.^{68,73,77,78}

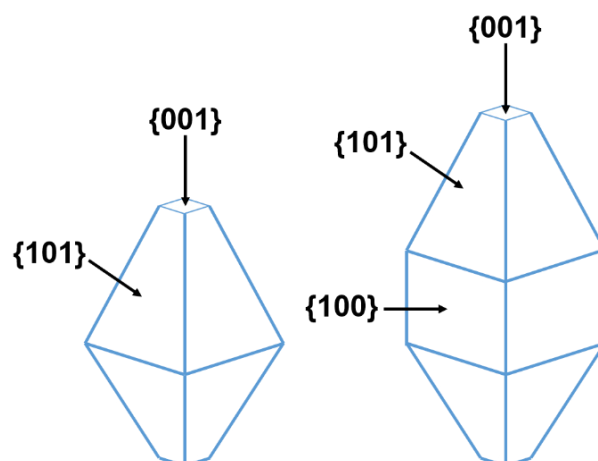


Figure I - 4. Equilibrium shape anatase exposing $\{101\}$ and $\{001\}$ facets and anatase additionally exposing $\{100\}$ facets appearing as a belt around the centre of the crystal.

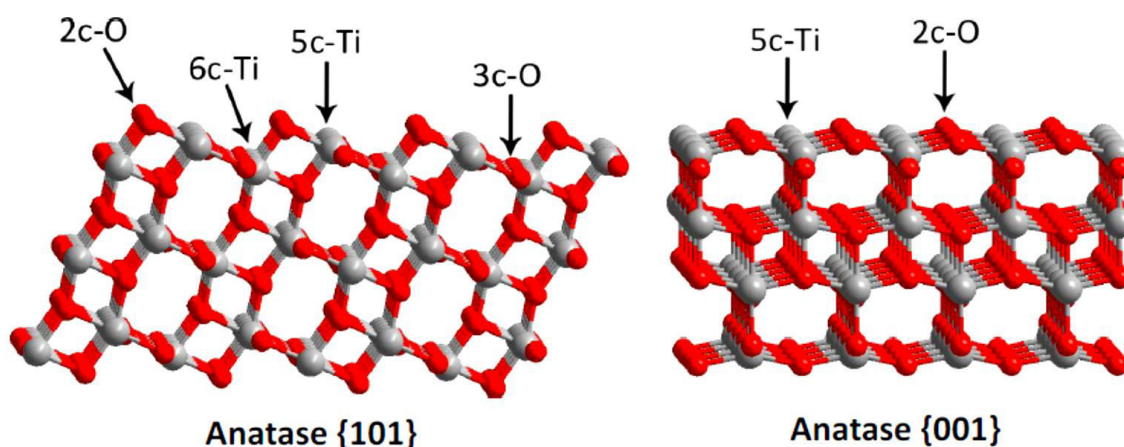


Figure I - 5. Surface atomic structures of anatase $\{101\}$ and $\{001\}$ facets.⁶⁰

Thus, numerous approaches have already been carried out to obtain TiO_2 nanoparticles with well determined exposed facets to increase their PC performance using appropriate solvents or additives.^{65,66,68–73,78–87} The solvent-solute interactions along different orientations of a crystal vary significantly because of the surface atomic arrangements. This results in different surface affinities of the solvent or additive towards each facet. A high affinity of either the solvent or additive to a certain facet results in their stabilisation as it for example lowers the surface energy or changes the surface tension of the bound plane.^{68,76,80}

To determine the PC activity of particle samples, various degradation tests have been developed such as the degradation of organic dyes (e.g. crystal violet, methylene blue, orangeG or methyl orange)^{88,89} or phenols.⁹⁰ Most of these methods follow the degradation process with the help of the absorption or luminescence of these substances and for this, the particles have to be removed from the measurement to avoid errors caused by NP absorption, luminescence or scattering.⁹⁰ This is why the PC decomposition of dichloroacetic acid (DCA) into CO_2 and Cl^- (HCl) has been frequently preferred over other test methods as an in-situ

measurement is possible with the help of a chloride ion sensitive electrode.^{90–93} Furthermore, the DCA does not degrade with UV light application alone, which is a concern when using dyes as this can falsify the measurement results.⁹⁰ The behaviour of DCA and influence of testing parameters on the degradation results have been intensively studied.^{91–93} The main degradation mechanisms of this substance are shown in Figure I - 6. While the interaction of the photogenerated electrons with DCA on the surface of TiO₂ is seen as very unlikely, the reaction of photogenerated holes (h⁺) with the organic molecule (photo-Kolbe reaction, Figure I - 6 bottom; anticlockwise reaction pathway), freeing CO₂ and initiating further degradation steps seems to be the main degradation pathway.^{92,94,95} Additionally, hydroxyl radicals can abstract the proton from the α-carbon in the initial step of the degradation of DCA (Figure I - 6 top; clockwise reaction pathway). These radicals are generated through the trapping of photogenerated holes by surface OH⁻ ions or adsorbed water, or by the reaction of H₂O₂ with photogenerated electrons. The dominant reaction is most likely dependent on the catalyst material (as it is documented in detail for acetate degradation).^{92,94–97}

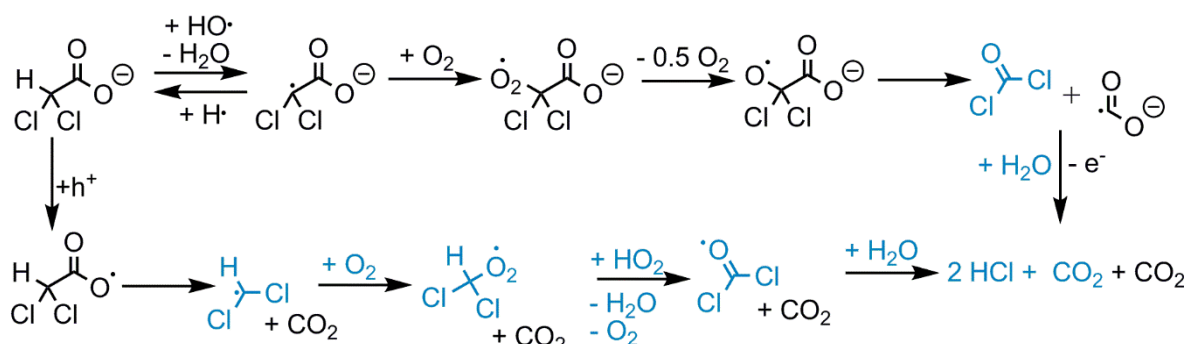


Figure I - 6. Main photocatalytic degradation mechanisms of dichloroacetic acid (DCA): primary H-abstraction leading to the reaction pathway on the top and photo-Kolbe reaction leading to the reaction pathway on the bottom.^{92,98–100}

I.1.3. Photocatalytic tumour therapy with TiO₂ particles

Because of their unique properties NPs are often considered for biomedical applications.¹⁰¹ In particular their small size makes them ideal to cross cell or tissue barriers while being large enough to be conjugated to antibodies or drugs. TiO₂ NPs have already been used as drug delivery systems, carriers for cell imaging, biosensors in biological assays and for genetic engineering. In addition to these uses, PC tumour therapy is also a potential application field.¹⁰² PC tumour therapy with TiO₂ NPs is a form of the so-called photodynamic therapy.^{10,102,103} For this treatment, a photosensitizer, a light source and the presence of oxygen (and/or water) are required. The photosensitizer, i.e. a macromolecule, an organic or an inorganic NP,^{102,104–106} is introduced into living tissue, for example into a tumour. They have to be non-toxic and excitable by photons (of the light source). After excitation they transfer their energy (i.e. electron-hole

pairs) to the surrounding oxygen or water creating highly reactive radicals. Those species readily destroy cell components leading to apoptosis. This therapy form seems to be a promising alternative to conventional cancer therapies thanks to a high safety record, minimal invasiveness, low cost and high localization.^{10,107} Photodynamic therapy is ideal for dermal illnesses and exposed body cavities such as the oral cavity, vagina, rectum or bladder. Small and superficial tumours located above or just below the skin tissue can be easily treated via this method.¹⁰ In contrast, for deeply infiltrating tumours or tumours located inside the body photodynamic therapy is not applicable as most photosensitizers are excited by UV light (≤ 400 nm). This wavelength range lies outside the phototherapeutic window (600-1300 nm)^{108,109} and therefore does not deeply penetrate the tissue. Furthermore, DNA damage by UV light is an unwanted side effect.¹⁰ Up to now the research concerning photodynamic therapy with TiO_2 is still in its early days. This mainly includes in vitro studies to examine the PC killing of cancer cells by UV light activated TiO_2 NPs.^{110–114} One study even indicated the preferential destruction of tumour cells while non-malignant cells were less affected.¹¹⁵ A few in vivo studies were able to confirm the anticancer effect, stressing the potential of TiO_2 as a potential cancer treatment agent.^{13,116}

Nevertheless, future applications of NPs in human bodies always cause concern about the potential toxicity. In the last decade, the toxicity and biodistribution of (non-activated) TiO_2 particles has been controversially discussed.^{10,117–123} In order to understand contradicting outcomes of studies, one has to consider that the toxicity is strongly dependent on the TiO_2 crystal phase, morphology and size, NP number and mass concentration. Also the agglomeration state, charge and added functional groups or impurities influence the NP toxicity. Therefore toxicological results can be different for every synthesized NP system.^{118,124} Additionally, the exposure routes and dose greatly influence the toxicity of the applied particles.^{118,120} This is why, on one hand inhalation of TiO_2 NPs is proven to cause inflammation, lung damage and may cause cancer.^{118,120} This initiated the International Agency for Research on Cancer (IARC) to classify it as possibly carcinogenic to humans (Group 2B).¹¹⁸ On the other hand, TiO_2 NPs in sunscreens and cosmetics have been applied on the skin for years and are considered non-toxic as they cannot penetrate through skin.^{118,120} Moreover, in 1969 the Joint FAO/WHO Expert Committee on Food Additives (JECFA) approved TiO_2 as an ingredient in human food as no significant absorption or tissue storage was found.¹¹⁷ For other organs besides the lungs and skin, toxicological data is still too limited for a reliable assessment of TiO_2 risks.¹¹⁸ Nevertheless, it is assumed that if they enter circulation, they could translocate in organs such as the spleen, liver, and kidney^{117,125} while the rate of such translocation remains undetermined.¹²² This is why the possible toxicity of TiO_2 should be kept

in mind if used for biomedical applications and should be evaluated for every newly developed particle system.

I.1.4. Luminescent TiO₂ nanoparticles

In the last decades, the combination of therapy and diagnosis within one tool (also called theranostics), for example within a NP system, has really come to the fore in research. The clear advantage of theranostics is the simultaneous diagnosis and treatment of a disease. Additionally, the release or efficacy of a therapeutic agent and its biodistribution may be monitored.^{126,127} The theranostic approach is especially promising for tumour diagnosis and therapy¹²⁸: Particle systems targeting malignant cells or cumulating in the pathologic tissue, can indicate the location and degree of the disease. This is visualized via an imaging method including resonance imaging, x-ray computed tomography, ultrasound, bioluminescence or fluorescence imaging, and single photon emission computed or positron emission tomography.¹²⁹ Then, therapy can be conducted thanks to specific particle properties like hyperthermia or photocatalysis but also drug-conjugates on the particle surface or incorporated into the NP system. Typical examples for inorganic theranostic NP systems are gold^{130,131} and superparamagnetic NPs¹³² which can be used for surface plasmon resonance or resonance imaging, while both offer the possibility of hyperthermal cancer therapy. Polymeric particle systems incorporating for example luminescent dyes or paramagnetic complexes and drug-conjugates are promising approaches as well.^{133,134}

In the case of TiO₂ NPs, photoluminescence (PL) properties for imaging in later applications as a treatment agent but also in cell culture studies are widely discussed in literature. While bulk TiO₂ does not exhibit PL, small NPs show band-band PL. This light emission is caused by the electron transition from the conduction band to the valence band, emitting radiation with an energy (in general) equal to the band gap energy (Figure I - 7). Due to the band gap energy of TiO₂, this PL is in the blue wavelength range. Anatase NPs with sizes around 4 to 6 nm synthesized by hydrolysis, nonhydrolytic preparations or hydrothermal synthesis were reported to exhibit under excitation at 300 to 365 nm a blue light emission (400-450 nm) visible by eye, which was in all cases assigned to band-band PL of the anatase NPs.¹³⁵⁻¹³⁹ Because of the band-band transition, the higher the PL intensity, the higher the recombination rate of excited electron-hole pairs and therefore the lower the PC activity of the sample.¹⁴⁰ Another possibility to obtain luminescent TiO₂ materials is the introduction of dopants into the crystal lattice. The doping of TiO₂ crystals has already been widely explored for a large range of elements, mainly to increase the PC activity of the samples. As the excitation of electron-hole pairs depends on the TiO₂ band gap, dopants in the crystal lattice have been used to modify it, for example to

enable photocatalysis under visible light excitation which also increases the efficiency of the catalyst.^{141–143} It is also known that the photoreactivity of TiO_2 is related to its defect disorder which is why introducing new defect sites through doping can be used to increase the PC activity.^{142,144–146} Additionally, the doping of TiO_2 can result in luminescence in the visible wavelength range (as mentioned before).^{147,148} In this case, the radiation is normally caused by surface oxygen vacancies or defects and can be identified as excitonic photoluminescence processes: the excited electrons first transit from the conduction band to a different sub-band or surface state without radiation (Figure I - 7). Subsequently, radiative transition from this state to the valence band occurs.¹⁴⁰ The emitted energy is lower than the band gap energy. The introduction of a dopant impacts all listed properties of the semiconductor material and therefore the properties of the two components can either compete or intensify each other. This means that an increasing luminescence of the doped TiO_2 can result in a higher or lower PC activity of the sample, depending on the dopant species.¹⁴⁰

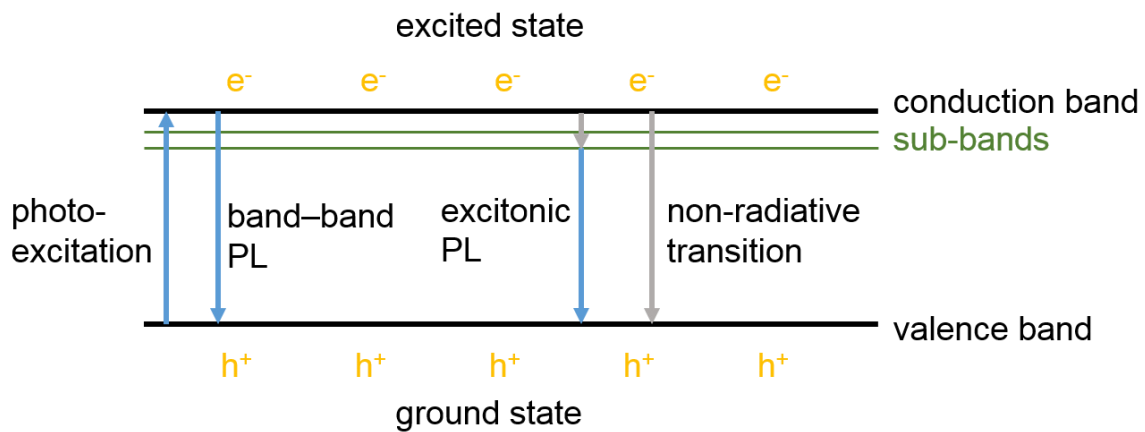


Figure I - 7. Simplified main photophysical processes of a semiconductor excited by light with equal to band gap energy. Photoexcitation results in electron/hole (e^-/h^+) pair formation and is followed by the 3 competing recombination processes of band-band photoluminescence (PL), excitonic PL and non-radiative transition.¹⁴⁰

Elements most often used to create materials with visible luminescence properties are rare earth elements due to their sharp luminescence bands and visible transition of the triply charged ions; examples include erbium, europium, terbium or cerium in the red, green or blue region of the light spectrum.^{149,150} There are already several reports on TiO_2 NPs doped with europium (showing red light emission),^{151–153} with erbium (red and/or green emission)^{154,155} and with lanthanum (blue emission).^{140,156} Nanofibers with visible luminescence have also been shown thanks to praseodymium and cerium doping.¹⁵⁷ In addition, visible light emitting europium-samarium co-doped nanocrystalline TiO_2 microspheres¹⁵⁸ and thin films with luminescence between 400 to 600 nm caused by terbium doping¹⁵⁹ have been developed. For all given examples, calcination or annealing was necessary to induce photoluminescence

properties or to obtain high enough intensities for later applications.^{148,151,153,154,160,161} The only exception was a rutile film prepared with very high amounts of europium which resulted in strong red luminescence without annealing.¹⁴⁷ In general, the particle samples aggregated during calcination which resulted in larger particle sizes and a decrease in specific surface area.^{137,152} An example for calcinated, europium (Eu^{3+}) doped anatase NPs in their aggregated powder form is shown in Figure I - 8.



Figure I - 8. Luminescence of anatase nanoparticles, doped with europium (Eu^{3+} ; 5 mol-%) and calcinated at 200 °C or 400 °C; excited at 365 nm.

Another method to obtain luminescent particle systems, is the functionalization of the inorganic particles with an organic dye. This strategy was so far primarily used for the production of dye-sensitized solar cells^{162–164} which did not focus on the fluorescence of the system but on a more efficient light-activation of the TiO_2 catalyst. Nevertheless, labelling of TiO_2 NPs with dopamine-modified dyes (1-pyrenemethylamine, piperazinyl-4-chloro-7-nitrobenzo-furazane, TexasRed or tetramethylrhodamine) has been realized and examined by confocal laser scanning microscopy.^{165,166} Adsorption of a conjugate of rhodamine B and phenylphosphonic acid onto TiO_2 particles was carried out for stem cell labelling.¹¹⁰ In one study, these semiconductor particles were first functionalized with 3-glycidoxypopyl tri-methoxysilane and then reacted with dyes such as xanthene dye rhodamine B, 4-phenylazo-phenol and 4-phenylazoaniline.¹⁶⁷ Adsorption of a perylene diimide dye onto TiO_2 also resulted in fluorescent samples applicable for finger-mark detection.¹⁶⁸ All the herein cited examples for a functionalization of particle systems with a dye imply their surface modification causing significant changes to their properties. How this enables the fine manipulation and tuning of the particle behaviour depending on the desired application is discussed in the following chapter.

I.2. Surface modification of nanoparticles for biotechnological applications[†]

There are several reasons why the surface of synthesized particles is modified. First, particles in a colloidal dispersion agglomerate and sediment if they are not electrostatically (between equally charged particles)¹⁶⁹ or sterically stabilised (for example by hydrocarbon chains/bulky polymers adsorbed or grafted onto the particles)¹⁷⁰. These two types of particle repulsions are shown in Figure I - 9. Electrostatic stabilisation is always limited to a certain pH range as at a particular concentration of OH^- or H_3O^+ , these ions may neutralize the surface charge of the particles up to their isoelectric point resulting in flocculation.¹⁷¹ In the same way, an increase in ionic strength of the solution, for example caused by dissolved salts, results in destabilisation of the colloidal dispersion, which is well described by the DLVO theory.¹⁷² By contrast, steric stabilisation – in a very simple picture – keeps NPs apart due to the space taken up by the organic molecules that are attached to the NP surfaces. For entropic reasons, distance is maintained between the chains of different particles. In theory this stabilisation mechanism is therefore indifferent to pH changes or varying salt concentrations.^{173,174} However, when particles are used in the biomedical field and applied in a physiological environment, they tend to agglomerate and sediment in physiological solutions because of their pH and salt content.^{175–177} This issue needs to be addressed in order to ensure a consistent assessment of the therapeutic and diagnostic potential of NPs in cell culture experiments or animal testing. Studies concerning particle concentrations are only reliable when carried out with stable dispersions that guarantee an accurate dosing. The effect of different sized particles on cells can only be studied if the particles do not form large agglomerates.^{175,178,179} Furthermore, agglomeration leads to a reduction in accessible surface area. If TiO_2 NPs are applied as therapeutic photosensitizing agents¹³, a decrease in surface results in a lower PC efficiency of the particles.^{175,180}

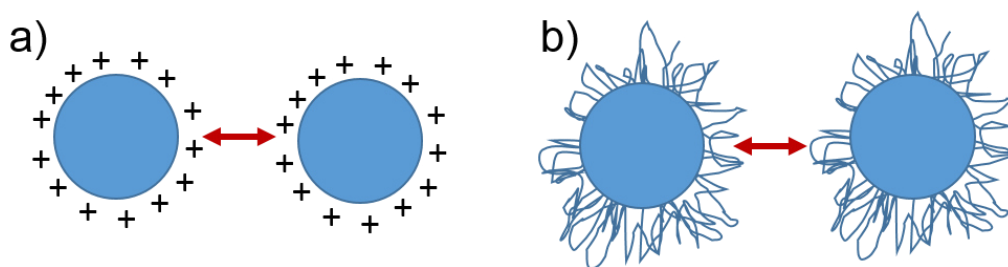


Figure I - 9. a) Electrostatic repulsion between equally charged particles and b) steric repulsion of particles.

[†] Parts of this chapter have been published and are reused in this work by courtesy of Elsevier, original article: S. Koch et al., Colloids Surf., B, 2016, 143, 7–14.

Second, in the last decade studies focused more and more on the influence of particle surface charges on their uptake by cells. Apart from the particle size, shape, dispersion state and composition, the surface charge was determined to be a crucial particle property for this.^{181–184} Numerous studies examined particles with sizes from below 10 nm up to 500 nm consisting of various materials¹⁸⁵ such as chitosan,¹⁸¹ PLGA¹⁸⁶, hydroxyapatite,¹⁸⁷ zinc sulphide,¹⁸⁸ cerium oxide,¹⁸⁹ silica,^{190,191} titanium dioxide,^{192,193} magnetite^{194–198} or gold.¹⁸² The particle surface charge or hydrophilicity was manipulated with the help of surface groups, for example hydroxyls,^{189,190} thiols,^{190,194,196} amines,^{182,187,188,190,192,194} carboxylic acids,^{181,187,188,190,192,194–196} glucans,^{194,196,197} alkanes,^{188,192} as well as polymethylsiloxane,¹⁹³ glycerol,¹⁹³ polyvinyl alcohol^{186,198} or polyethyleneglycol chains.^{188,195} The uptake of these surface modified particles was tested with a variety of non-malignant cells, malignant cells and macrophages. In the first instance the studies indicated that the particle uptake is cell type dependent.^{181,191} It was also stated that the adsorption of components of the cell culture medium onto the particles often makes the analysis challenging as it covers the surface and changes the surface charge and properties.^{182,188,189} Hydrophobic particles and those with very high positive or negative charges or sizes over 150 nm are taken up by macrophages,¹⁸¹ while no or less uptake by other cell types is detected for hydrophobic particles.^{188,192} If the particles provide neutral surface charge, no internalization takes place^{192,194} due to lower particle-cell membrane interaction.¹⁸⁵ Negatively charged particles can be taken up by cells even if their charge is unfavourable for interaction with the negatively charged cell membranes. It is believed that internalization occurs through binding of the particles on scarce cationic sites on the membrane and subsequent endocytosis.¹⁸⁵ Logically, positively charged particles are taken up better than negatively charged ones because of their increased interactions with the cell membrane.^{182,185,187,190,192,194,197}

Third, surfaces can be modified via bioconjugation with agents that fulfil a special purpose like targeting an organ or cell type of interest or mediating the cellular uptake.¹⁸³ Especially for tumour therapies, this is a powerful tool; targeting ligands or antibodies specifically bind to cell-surface antigens or receptors that are, for example, exclusively expressed on tumour cells (Figure I - 10).¹⁹⁹ In this way, the drug or particle conjugated to the targeting moiety is directed to the place of interest and then internalized into the targeted cell by receptor-mediated endocytosis. As a target, the folate receptor is often used as it is expressed in tumour tissue and can bind vitamin folate but also folate-particle or folate-drug conjugates.^{200–206} Transferrins which are non-heme iron-binding glycoproteins and bind to the transferrin receptors, are also considered as targeting agents for tumours as the transferrin receptor is overexpressed by them.²⁰⁷ Similarly, the epidermal growth factor receptor is overexpressed by many types of epithelial tumours and can therefore be targeted by anti-epidermal growth factor receptor

monoclonal antibodies.²⁰⁸ Lectins are proteins which bind to glycans present on the cell membrane. As the glycans expressed by tumour cells are often different to those of their non-malignant counterparts, lectins can be used as cancer targeting agents.²⁰⁹ Furthermore, aptamers which are oligonucleic acids like DNA or RNA with unique 3-D conformations, can bind specifically to target antigens and are therefore interesting as targeting agents bound to particles or drugs.^{210–214}

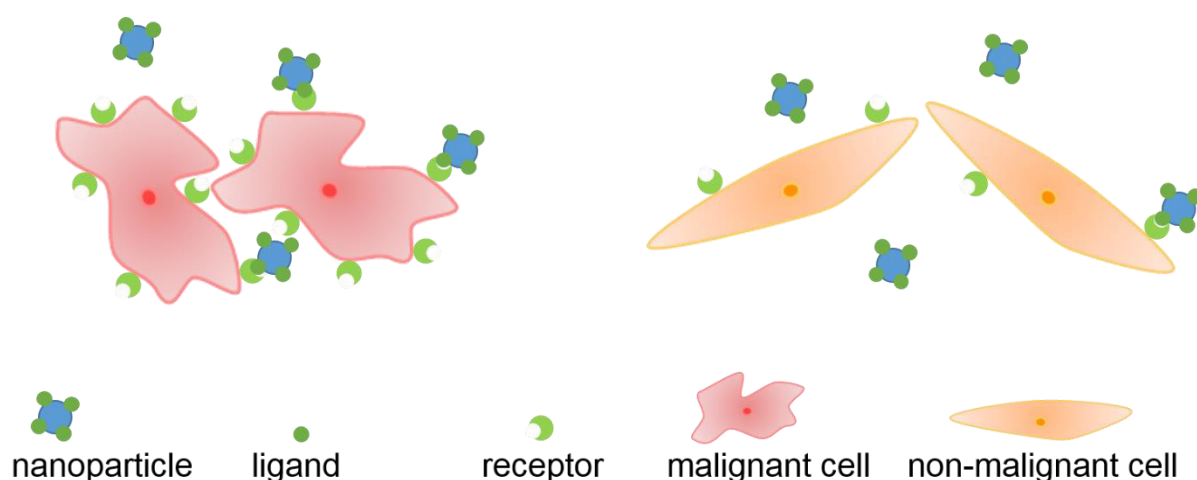


Figure I - 10. Nanoparticles with ligands targeting a receptor which is overexpressed by malignant cells.

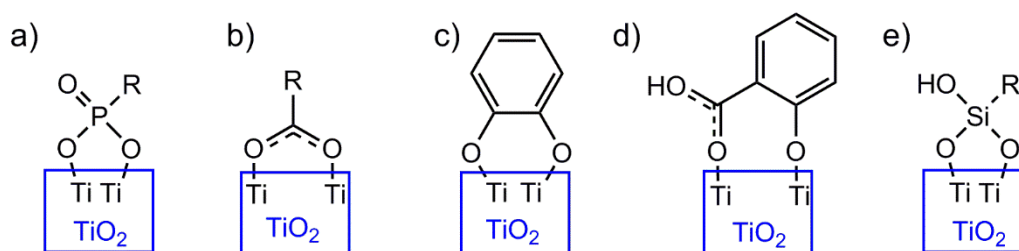
Due to these three above mentioned purposes, particle surfaces usually have to be functionalized for their intended biomedical applications. The modification of the surface for example with targeting agents will always influence the other particle properties such as the dispersion state in physiological media and their cellular uptake. Additionally, the surrounding liquid medium and its composition strongly influences the particle behaviour. This is why the functionalization of NPs is very complex and has to be studied intensively to avoid unwanted side effects caused by the modification.

I.2.1. Surface modification of TiO₂ particles

In literature, the surface of TiO₂ particles has already been modified for several decades. For example as photosensitizers for optoelectronic and photonic devices, the particles (as electron acceptors) were decorated with organic structures serving as electron donors.^{162,215} The particles were functionalized with organic dyes for several biological and non-biological related applications as mentioned in I.1.4. For biomedical uses, TiO₂ was also modified with DNA-oligonucleotides for potential gene therapy²¹⁶ or with PEG-ligands¹¹³ and carboxylic acids²¹⁷ to improve their biocompatibility. Anti-body linked NPs were developed for active tumour targeting¹¹⁵ or polymer-NP conjugates as a versatile toolbox for molecule immobilization.¹⁶⁵

TiO₂ NPs can either be surface modified during particle synthesis (in situ modification) or by grafting of organic groups onto the NPs (post-synthesis modification). The advantage of in situ functionalization lies in the double function of the organic ligand controlling the particle growth and/or morphology and serving as functional surface group.²¹⁸ Post-synthesis modification has the benefit of an easy processing and the organic molecule can be chosen depending on the specific demands of later applications without considering the requirements for particle synthesis.²¹⁹ Most of the examples for the functionalization of TiO₂ particles (mentioned in this chapter) are post-synthesis modifications.^{110,115,163,166–168,216,220–223} However, in the case of sol-gel syntheses a coordinating agent is often used to control the hydrolysis and condensation reactions and after NP synthesis this agent serves always a functional surface molecule as well.^{165,218,224,225} The surface groups obtained by in situ modification can sometimes be transformed by a ligand exchange which still provides a certain flexibility in the modification of the NPs independent of the synthesis procedure.^{112,217}

Irrespective of the aimed application area and the chosen modification procedure, the modification of TiO₂ particles requires an adequate anchoring group that attaches the functional molecule onto the surface via direct linkage of the anchoring group with the hydroxyl groups of the oxide surface.²¹⁵ One possible group are phosphonic acids (P(O)(OH)₂) that can bind via a phosphonate ester linkage (Scheme I - 4 a) onto the TiO₂ surface,^{215,226} examples include phenylphosphonic acid,²²⁶ rhodamine-phosphonic acid¹¹⁰ or 2,2-bipyridine-4-phosphonic acid.²¹⁵ Another commonly used class of ligands are carboxylic acid derivatives that can attach to TiO₂ with both the oxygen and hydroxyl moiety (Scheme I - 4 b). Mercaptosuccinic acid,^{112,217} ascorbic acid,²²⁷ oleic acid,²²⁵ thiolactic acid,²²³ maleic acid,¹¹³ anthracene acetic acids¹⁶⁴ and various others^{215,217} have already been utilized as surface functionalities. Furthermore, enediol ligands such as dopamine,^{163,165,166,216,220} cyanidin 3-glucoside,¹⁶³ catechol,^{221,222} gallic acid²²¹ or pyrogallol²²¹ can also modify TiO₂ surfaces as they covalently link to the surface with both hydroxyl groups (Scheme I - 4 c). A salicylate binding type has been shown for ligands like 2-hydrobenzoic acid and 2,5- or 2,3-dihydrobenzoic acid (Scheme I - 4 d).²²² Finally, silanes have been readily applied onto TiO₂ NPs,²²⁸ for example 3-glycidoxypentyl tri-methoxysilane,¹⁶⁷ N-(Tri-methoxysilylpropyl) ethylene diamine triacetic acid,²²⁹ tetraethoxysilane^{114,230–233} or 4-(trichlorosilylethyl)-4-methyl-2,2-bipyridin.²¹⁵ They react with the surface hydroxyl groups to form a silyl bond (Scheme I - 4 e). The binding of anchoring groups is in general reversible, this is why in aqueous solutions of higher pH values, hydrolysis and de-chelation from the surface can occur.^{162,215} As well as the anchoring group, the structure and properties of functional groups of the ligand are very important as they dictate the later particle behaviour and allow tailoring for specific applications.



Scheme I - 4. Possible binding modes of the anchoring groups onto TiO_2 : a) Phosphonate ester linkage²¹⁵, bidentate binding of a carboxyl group¹⁶², c) binding of enediol ligands shown with catechol as example²²², d) binding of 2-hydrobenzoic acid²²² and e) silyl linkage on TiO_2 ²¹⁵.

I.2.2. Surface modification of particles with dendrons

Whilst linear ligands^{162,215} are most commonly applied, since 2001, the substitution of linear coupling agents by dendrons has been increasingly studied in the field of NP surface modification. The concept of such dendritic molecules compared to a linear one is shown in Figure I - 11.

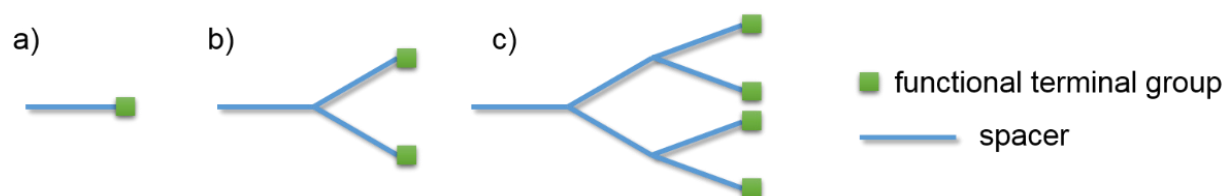


Figure I - 11. Concept of dendritic molecules: a) linear (one branch), b) 1st generation (2 branches) and c) 2nd generation (4 branches).

The amount of functional terminal groups is increased via symmetric branching of the molecule, while one focal point is maintained. Dendrons typically possess a precise architecture and low polydispersity as they are synthesized by increasing the generation of the branches step by step.²³⁴ Additionally, in contrast to polymer synthesis purification during their growth at intermediate steps is in general possible.²³⁴ This allows the control and manipulation of the size, branching points and number or type of terminal functions.²²¹ In comparison to linear molecules or polymers, dendritic structures show very unique physicochemical properties which are due to the so-called “dendritic effect” caused by the multiplicity of functional groups, architectural steric effects and a differing nature in the internal dendritic structure.²³⁵ While the multiplicity of the functional terminal groups is mainly responsible for the solubility or chemical reactivity of these molecules, the first linear and with increasing generations 2D or even 3D architecture results in eminent changes in the shape and flexibility.^{234,235} Because of terminal groups and several branch generations, the inner core of dendritic structures is sterically protected from the outside environment which provides the possibility of hosting other organic, inorganic or metallic compounds and protecting them from solvent effects of the outside.²³⁵

The synthesis of these molecules can be carried out via either a divergent or convergent approach (Figure I - 12).²³⁴

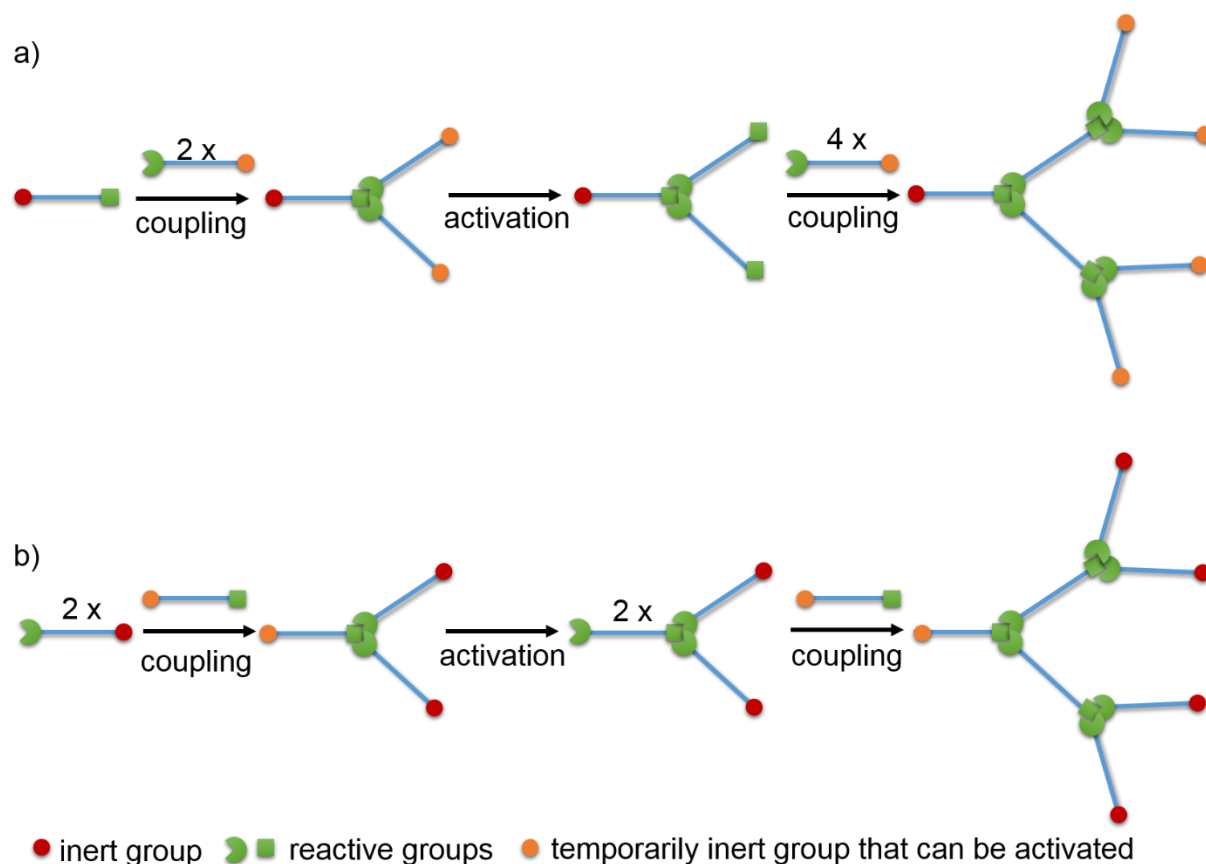


Figure I - 12. a) Divergent and b) convergent synthesis of dendritic molecules.²³⁴

Both procedures consist of coupling and activation steps; during coupling the number of branches is increased while side reactions between other functionalities of the reactants are disabled, then a subsequent activation of either the peripheral points or the focal points of the molecules enables a further coupling step. The divergent synthesis produces growth starting from the focal point and forming the branches stepwise by repeated coupling and activation of the peripheral groups (Figure I - 12 a).²³⁴ For a convergent synthesis the dendritic growth begins from the exterior molecules and proceeds via reactions at the focal point of each branch (Figure I - 12 b).²³⁴

In order to modify NP surfaces with dendrons, the focal points of these molecules also need to represent the anchoring groups. As both anchor and core of the dendron, various ligands have already been studied²³⁶ including siloxanes,^{237–241} thiols,^{242–252} amines,^{253,254} enediols,^{255,256} phosphonates^{257–259} and carboxylates.^{260,261} The nature of the anchor mainly depended on the studied NP type which was most commonly Au^{242–246,248–251} or iron oxide.^{238,253,255–257,259,260,262–264} Additionally, a few other inorganic particle types have been studied: silica,²⁴¹ TiO₂,²⁴⁰ Pd,^{265,266} ZnO,²³⁷ CdSe/ZnS,²⁵⁴ CdSe/CdS^{247,261} and CdSe^{252,258} NPs.

The increase in functionalities by dendritic surface agents (compared to linear molecules) results in a better NP colloidal stability enhanced by their conical structure and allows the coupling of more biofunctions. Additionally, their cone-like structure is appropriate for the functionalization of ultrasmall NPs which possess a high curvature, as the density of radial functional groups decreases to a lesser extent with increasing distance from the surface. This guarantees a dense surface functionalization. Furthermore, the dendritic framework is suitable for the adsorption and encapsulation of small molecules such as drugs or pollutants providing opportunities for applications such as drug release or waste water treatment.²⁶⁷ Even if the synthesis of dendrons is more difficult and time consuming compared to (hyperbranched) polymers,²⁶⁸ the precise control of the molecule architecture allows a better tailoring of the properties, which can be crucial for later uses and reproducibility. These can not only be tailored by the increase of generations and therefore terminal groups, but also by the structure of the spacer itself. The most studied dendritic structure for particle functionalization clearly is poly(amidoamine).^{237,239,241,244,262,265} Although, the functionalization of particles with various other structures has been studied; for example poly(ester amine)s,²³⁸ lysine based structures,^{243,269} poly(benzyl ether)s,²⁶⁶ poly(oxymethylphenylene)s,²⁵⁰ polycarbazoles,²⁴⁵ as well as Newkome-type²⁴⁸ and Fréchet-type dendrons.²⁴²

Particle functionalization with dendrons has been carried out after NP synthesis in most of the before mentioned references. There are only a few exceptions in which the dendritic molecules have already been applied during synthesis.^{240,243,245,264,266} This was mainly to combine later tasks as surface groups with the function as capping agents for size and morphology control during synthesis.^{236,243} Moreover, the dendron has usually been grafted as an entire molecule onto the particle surface which allows the complete characterization of the dendron before grafting. Additionally, the perfect integrity of the applied molecules is ensured as defective structures like incomplete branches can be separated before grafting and the formation of rather polymer-like disordered structures is avoided.²⁷⁰ This functionalization procedure can be called “grafting onto” while “grafting from” means the building of the dendron onto the NP after anchoring of the focal point.²⁶⁰ The latter method was suitable in a few cases to prevent the occurrence of NP clusters since possible reactions of one dendritic molecule with two particles at the same time are avoided.^{238,239,241,260} The disadvantages of both the “grafting onto” and “grafting from” approaches are also depicted in Figure I - 13.

In the last two decades, the unique properties of dendrons have been used for the design of NPs for applications such as catalysis^{239,253,255,265,266} and water purification.²⁴¹ Redox-active dendron-functionalized NPs were synthesized for future nanoelectronics or sensors.^{242,246,250} Systems with switchable solubility in various solvents^{244,248} or temperature induced NP

aggregation²⁵⁶ have been developed. With aims such as improving the solubility of hydrophobic particles in water,^{237,254,261} stabilisation at physiological pH²⁵⁷ and biocompatibility,^{251,254} as well as coupling or incorporating drugs,^{249,269} NP-dendron systems have been designed for a broad variety of biotechnological uses.¹⁰¹ These include cell labelling,²³⁷ biosensors for pathogen detection,²⁵⁴ DNA recovery^{262,271} or delivery,^{249,269} magnet resonance imaging^{255,257,259} and drug delivery.^{260,272}

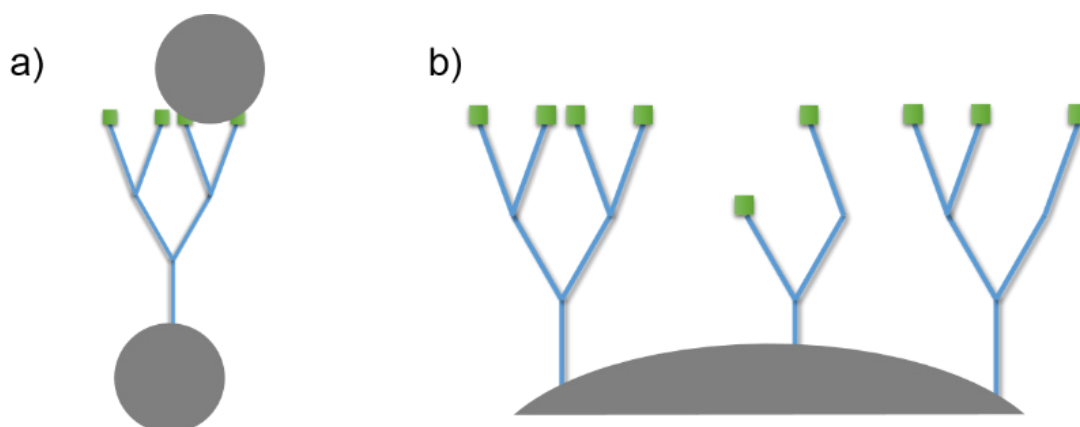


Figure I - 13. Possible problems occurring during grafting procedures: a) reaction of one dendron with two particles resulting in the formation of nanoparticle cluster during “grafting on” and b) formation of defective dendritic structures on the particle during “grafting from”.

Currently, a new form of dendrons is gaining scientific interest; luminescent dendritic structures as luminescence offers the monitoring of basic properties as well as of its surroundings. The combination of dendritic properties and luminescence can therefore lead to novel functions and new applications.^{273,274} While the incorporation of luminescence into dendrimers is already well established, only a few studies have been carried out on luminescent dendrons for the functionalization of NPs.^{275–280} Luminescence properties can be incorporated into a dendron with the help of metal complexes such as $[\text{Ru}(\text{2,2'}\text{-bipyridine})_3]^{2+}$, fullerenes or organic chromophores, including metal complex chromophores such as porphyrins or azo-compounds.²⁷³ There are several possibilities for the location of a luminescence centre; besides dendron structures that consist out of chromophores themselves,²⁷⁵ the luminescence agent can be situated “off-centred” (i. e. not integrated into the dendron, Figure I - 14 a),^{281,282} in its periphery (Figure I - 14 b),^{276–278,283} or at the focal point (i. e. as anchor or between anchor and dendritic branches, Figure I - 14 c).^{279,280,284}

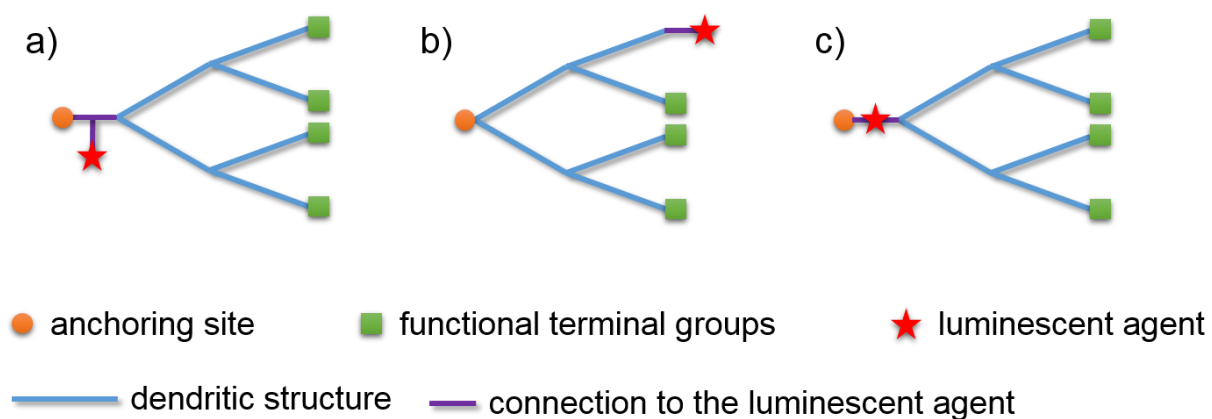


Figure I - 14. Integration of a luminescence centre into the coupling agent, a) “off-centred”, b) in the periphery of the dendritic structure or c) at the focal point.

I.3. Conclusion

In this chapter, titanium dioxide was introduced, including its crystal structures, main physical properties and benefits in its nano form. The hydrothermal sol-gel synthesis was explained, stating its advantages and the mechanisms that are responsible for the nanocrystal formation. After this the PC properties of TiO_2 were described comprising the principles of photocatalysis and factors influencing the PC performance such as defects, exposed facets and surface area. While the synthesis of TiO_2 NPs is already well developed, their PC properties still require further study to understand the basic mechanisms and factors that influence their performance. The connection between its PC properties and applications in tumour therapy were established, giving a short overview of the treatment and its pros and cons. The use of TiO_2 NPs as anti-tumour agents is still in its infancy, giving rise to a lot of controversial discussions debating their potential as nano-medicine against their possible toxicity. As a final point, a possible integration of luminescence properties into TiO_2 nanosystems was discussed including the intrinsic luminescence, excitonic luminescence via doping or the particle functionalization with organic dyes. While several studies on luminescent TiO_2 have been carried out, no general concept for an efficient luminescence incorporation into the crystals without compromises to their PC performance was found. Nevertheless, the particle modification with an organic dye seems to be the most feasible approach.

This led to the next topic, namely the surface modification of NPs for biotechnological applications. First, the main reasons for such a modification were stated: stabilisation in physiological media, enhancement of cellular uptake and bioconjugation. Then surface modifications of TiO_2 for various uses were cited and possible anchoring groups presented. Similar to other NPs, the surface modification of TiO_2 is crucial for their adaption to high application requirements. This is why several approaches have been carried out using a vast variety of anchoring groups and organic molecules. However, the influence of these surface agents on the PC performance of TiO_2 was generally neglected. Finally, the NP functionalization with dendritic structures was introduced, including their basic concept, grafting methods, state of the art applications and luminescent dendritic structures. In contrast to other NPs such as iron oxide or gold, TiO_2 NPs have not readily been functionalized with dendritic structures. Interestingly, the advantages of luminescent dendritic structures are already frequently studied in the case of dendrons but particle functionalization with them is still scarce.

This bibliographic study confirmed prevailing motivations for this work, as many research issues have not been addressed yet and give opportunities for new outcomes as well as controversial discussions.

References:

- 1 X. Chen and S. S. Mao, *Chem. Rev.*, 2007, **107**, 2891–2959.
- 2 A. P. Popov, A. V. Priezzhev, J. Lademann and R. Myllylä, *J. Phys. Appl. Phys.*, 2005, **38**, 2564–2570.
- 3 C. Contado and A. Pagnoni, *Anal. Chem.*, 2008, **80**, 7594–7608.
- 4 O. B. Willcox, US2591988 A, 1952.
- 5 G. M. Sheehan, G. Leathwhite Roberts, P. Montgomery Dupree, US 3769255, 1973.
- 6 G. Wiederhofs, G. Lailach, US5094834 A, 1992.
- 7 A. W. Harrison and M. R. Walton, *Sol. Energy*, 1978, **20**, 185–188.
- 8 S. Guo, Z. Wu and W. Zhao, *Chin. Sci. Bull.*, 2009, **54**, 1137–1142.
- 9 D. V. Bavykin, J. M. Friedrich and F. C. Walsh, *Adv. Mater.*, 2006, **18**, 2807–2824.
- 10 F. U. Rehman, C. Zhao, H. Jiang and X. Wang, *Biomater. Sci.*, 2015, **4**, 40–54.
- 11 Y. Lan, Y. Lu and Z. Ren, *Nano Energy*, 2013, **2**, 1031–1045.
- 12 M. Kulkarni, A. Mazare, E. Gongadze, š. Perutkova, V. Kralj-Iglič, I. Milošev, P. Schmuki, A. Iglič and M. Mozetič, *Nanotechnology*, 2015, **26**, 062002.
- 13 A. Fujishima, T. N. Rao and D. A. Tryk, *J. Photochem. Photobiol. C Photochem. Rev.*, 2000, **1**, 1–21.
- 14 O. Carp, *Prog. Solid State Chem.*, 2004, **32**, 33–177.
- 15 A. Fahmi, C. Minot, B. Silvi and M. Causa, *Phys. Rev. B*, 1993, **47**, 11717.
- 16 D. P. Macwan, P. N. Dave and S. Chaturvedi, *J. Mater. Sci.*, 2011, **46**, 3669–3686.
- 17 X. Xue, W. Ji, Z. Mao, H. Mao, Y. Wang, X. Wang, W. Ruan, B. Zhao and J. R. Lombardi, *J. Phys. Chem. C*, 2012, **116**, 8792–8797.
- 18 H. Peng, J. Li, S.-S. Li and J.-B. Xia, *J. Phys. Chem. C*, 2008, **112**, 13964–13969.
- 19 W. F. Zhang, M. S. Zhang, Z. Yin and Q. Chen, *Appl. Phys. B*, 2000, **70**, 261–265.
- 20 J. Yu, X. Zhao, J. Du and W. Chen, *J. Sol-Gel Sci. Technol.*, 2000, **17**, 163–171.
- 21 M. Zhang, Y. Bando and K. Wada, *J. Mater. Sci. Lett.*, 2001, **20**, 167–170.
- 22 K. T. Lim, H. S. Hwang, W. Ryoo and K. P. Johnston, *Langmuir*, 2004, **20**, 2466–2471.
- 23 E. Stathatos, P. Lianos, D. Levy, D. Tsiourvas and F. Del Monte, *Langmuir*.
- 24 P. D. Moran, J. R. Bartlett, G. A. Bowmaker, J. L. Woolfrey and R. P. Cooney, *J. Sol-Gel Sci. Technol.*, 1999, **15**, 251–262.
- 25 J. Reszczyńska, T. Grzyb, Z. Wei, M. Klein, E. Kowalska, B. Ohtani and A. Zaleska-Medynska, *Appl. Catal. B Environ.*, 2016, **181**, 825–837.
- 26 H. G. Yang, G. Liu, S. Z. Qiao, C. H. Sun, Y. G. Jin, S. C. Smith, J. Zou, H. M. Cheng and G. Q. (Max) Lu, *J. Am. Chem. Soc.*, 2009, **131**, 4078–4083.
- 27 H. Yoshitake, T. Sugihara and T. Tatsumi, *Chem. Mater.*, 2002, **14**, 1023–1029.
- 28 D. Byun, Y. Jin, B. Kim, J. Kee Lee and D. Park, *J. Hazard. Mater.*, 2000, **73**, 199–206.
- 29 Y. Wang, X. Tang, L. Yin, W. Huang, Y. Rosenfeld Hacohen and A. Gedanken, *Adv. Mater.*, 2000, **12**, 1183–1186.
- 30 J. C. Yu, L. Zhang and J. Yu, *Chem. Mater.*, 2002, **14**, 4647–4653.
- 31 Q. Xiang, J. Yu, B. Cheng and H. C. Ong, *Chem. – Asian J.*, 2010, **5**, 1466–1474.
- 32 K. Ding, Z. Miao, Z. Liu, Z. Zhang, B. Han, G. An, S. Miao and Y. Xie, *J. Am. Chem. Soc.*, 2007, **129**, 6362–6363.
- 33 H.-W. Wang, C.-H. Kuo, H.-C. Lin, I.-T. Kuo and C.-F. Cheng, *J. Am. Ceram. Soc.*, 2006, **89**, 3388–3392.
- 34 C.-C. Wang and J. Y. Ying, *Chem. Mater.*, 1999, **11**, 3113–3120.
- 35 J. Zhu, F. Chen, J. Zhang, H. Chen and M. Anpo, *J. Photochem. Photobiol. Chem.*, 2006, **180**, 196–204.
- 36 S. Ito, S. Yoshida and T. Watanabe, *Chem. Lett.*, 2000, **29**, 70–71.

- 37 S. Valencia, J. M. Marín and G. Restrepo, *Open Mater. Sci. J.*, 2010, **4**, 9–14.
- 38 G. Oskam, A. Nellore, R. L. Penn and P. C. Searson, *J. Phys. Chem. B*, 2003, **107**, 1734–1738.
- 39 J. Livage, M. Henry and C. Sanchez, *Prog. Solid State Chem.*, 1988, **18**, 259–341.
- 40 D. Biskupski, B. Herbig, G. Schottner and R. Moos, *Sens. Actuators B Chem.*, 2011, **153**, 329–334.
- 41 U. Schubert, *J. Mater. Chem.*, 2005, **15**, 3701.
- 42 L. G. Hubert-Pfalzgraf, *Inorg. Chem. Commun.*, 2003, **6**, 102–120.
- 43 J. Livage, *Bull. Mater. Sci.*, 1999, **22**, 201–205.
- 44 J. Jitputti, S. Pavasupree, Y. Suzuki and S. Yoshikawa, *J. Solid State Chem.*, 2007, **180**, 1743–1749.
- 45 A. Leautic, F. Babonneau and J. Livage, *Chem. Mater.*, 1989, **1**, 248–252.
- 46 M. W. Jung, H. J. Oh, J. C. Yang and Y. G. Shul, *Bull. Korean Chem. Soc.*, 1999, **20**, 1394–1398.
- 47 D. Amans, C. Malaterre, M. Diouf, C. Mancini, F. Chaput, G. Ledoux, G. Breton, Y. Guillin, C. Dujardin, K. Masenelli-Varlot and P. Perriat, *J. Phys. Chem. C*, 2011, **115**, 5131–5139.
- 48 J.-P. Jolivet, *Metal Oxide Chemistry and Synthesis: From Solution to Solid State*, John Wiley & Sons, Inc., Chichester, 2000.
- 49 M. Henry, J. P. Jolivet and J. Livage, in *Chemistry, Spectroscopy and Applications of Sol-Gel Glasses*, Springer, 1992, pp. 153–206.
- 50 P. D. Cozzoli, A. Kornowski and H. Weller, *J. Am. Chem. Soc.*, 2003, **125**, 14539–14548.
- 51 A. Rabenau, *Angew. Chem. Int. Ed. Engl.*, 1985, **24**, 1026–1040.
- 52 J. Lin, Y. Lin, P. Liu, M. J. Meziani, L. F. Allard and Y.-P. Sun, *J. Am. Chem. Soc.*, 2002, **124**, 11514–11518.
- 53 D. Beydoun, R. Amal, G. Low and S. McEvoy, *J. Nanoparticle Res.*, 1999, **1**, 439–458.
- 54 E. Stathatos, D. Tsiourvas and P. Lianos, *Colloids Surf. Physicochem. Eng. Asp.*, 1999, **149**, 49–56.
- 55 D. I. Enache, J. K. Edwards, P. Landon, B. Solsona-Espriu, A. F. Carley, A. A. Herzing, M. Watanabe, C. J. Kiely, D. W. Knight and G. J. Hutchings, *Science*, 2006, **311**, 362–365.
- 56 D. M. Blake, P.-C. Maness, Z. Huang, E. J. Wolfrum, J. Huang and W. A. Jacoby, *Sep. Purif. Rev.*, 1999, **28**, 1–50.
- 57 A. L. Linsebigler, G. Lu and J. T. Yates Jr, *Chem. Rev.*, 1995, **95**, 735–758.
- 58 M. Pelaez, N. T. Nolan, S. C. Pillai, M. K. Seery, P. Falaras, A. G. Kontos, P. S. M. Dunlop, J. W. J. Hamilton, J. A. Byrne, K. O'Shea, M. H. Entezari and D. D. Dionysiou, *Appl. Catal. B Environ.*, 2012, **125**, 331–349.
- 59 V. Etacheri, C. Di Valentin, J. Schneider, D. Bahnemann and S. C. Pillai, *J. Photochem. Photobiol. C Photochem. Rev.*, 2015, **25**, 1–29.
- 60 J. Yan, G. Wu, N. Guan, L. Li, Z. Li and X. Cao, *Phys. Chem. Chem. Phys.*, 2013, **15**, 10978.
- 61 Z. Zhao, X. Zhang, G. Zhang, Z. Liu, D. Qu, X. Miao, P. Feng and Z. Sun, *Nano Res.*, 2015, **8**, 4061–4071.
- 62 X. Jiang, Y. Zhang, J. Jiang, Y. Rong, Y. Wang, Y. Wu and C. Pan, *J. Phys. Chem. C*, 2012, **116**, 22619–22624.
- 63 J. Zhu, S. Wang, Z. Bian, S. Xie, C. Cai, J. Wang, H. Yang and H. Li, *CrystEngComm*, 2010, **12**, 2219.
- 64 J. Yu, J. Low, W. Xiao, P. Zhou and M. Jaroniec, *J. Am. Chem. Soc.*, 2014, **136**, 8839–8842.
- 65 H. G. Yang, C. H. Sun, S. Z. Qiao, J. Zou, G. Liu, S. C. Smith, H. M. Cheng and G. Q. Lu, *Nature*, 2008, **453**, 638–641.
- 66 B. Wu, C. Guo, N. Zheng, Z. Xie and G. D. Stucky, *J. Am. Chem. Soc.*, 2008, **130**, 17563–17567.
- 67 F. Tian, Y. Zhang, J. Zhang and C. Pan, *J. Phys. Chem. C*, 2012, **116**, 7515–7519.
- 68 N. Roy, Y. Sohn and D. Pradhan, *ACS Nano*, 2013, **7**, 2532–2540.
- 69 J. Pan, G. Liu, G. Q. M. Lu and H.-M. Cheng, *Angew. Chem. Int. Ed.*, 2011, **50**, 2133–2137.
- 70 J. Pan, X. Wu, L. Wang, G. Liu, G. Q. (Max) Lu and H.-M. Cheng, *Chem. Commun.*, 2011, **47**, 8361–8363.
- 71 X. Y. Ma, Z. G. Chen, S. B. Hartono, H. B. Jiang, J. Zou, S. Z. Qiao and H. G. Yang, *Chem. Commun.*, 2010, **46**, 6608.

- 72 X. Han, Q. Kuang, M. Jin, Z. Xie and L. Zheng, *J. Am. Chem. Soc.*, 2009, **131**, 3152–3153.
- 73 G. Liu, J. C. Yu, G. Q. (Max) Lu and H.-M. Cheng, *Chem. Commun.*, 2011, **47**, 6763.
- 74 C. Chen, G. A. Sewvandi, T. Kusunose, Y. Tanaka, S. Nakanishi and Q. Feng, *CrystEngComm*, 2014, **16**, 8885–8895.
- 75 A. S. Barnard, P. Zapol and L. A. Curtiss, *Surf. Sci.*, 2005, **582**, 173–188.
- 76 A. S. Barnard and L. A. Curtiss, *Nano Lett.*, 2005, **5**, 1261–1266.
- 77 A. Vittadini, A. Selloni, F. P. Rotzinger and M. Grätzel, *Phys. Rev. Lett.*, 1998, **81**, 2954–2957.
- 78 A. Selloni, *Nat. Mater.*, 2008, **7**, 613–615.
- 79 W. Q. Fang, X.-Q. Gong and H. G. Yang, *J. Phys. Chem. Lett.*, 2011, **2**, 725–734.
- 80 J. Li and D. Xu, *Chem. Commun.*, 2010, **46**, 2301–2303.
- 81 G. Liu, C. Sun, H. G. Yang, S. C. Smith, L. Wang, G. Q. (Max) Lu and H.-M. Cheng, *Chem Commun*, 2010, **46**, 755–757.
- 82 S. Liu, J. Yu and M. Jaroniec, *Chem. Mater.*, 2011, **23**, 4085–4093.
- 83 M. M. Maitani, K. Tanaka, D. Mochizuki and Y. Wada, *J. Phys. Chem. Lett.*, 2011, **2**, 2655–2659.
- 84 J.-W. Shiu, C.-M. Lan, Y.-C. Chang, H.-P. Wu, W.-K. Huang and E. W.-G. Diau, *ACS Nano*, 2012, 121106142518005.
- 85 C. Z. Wen, H. B. Jiang, S. Z. Qiao, H. G. Yang and G. Q. (Max) Lu, *J. Mater. Chem.*, 2011, **21**, 7052.
- 86 N. Wu, J. Wang, D. N. Tafen, H. Wang, J.-G. Zheng, J. P. Lewis, X. Liu, S. S. Leonard and A. Manivannan, *J. Am. Chem. Soc.*, 2010, **132**, 6679–6685.
- 87 X. Zhao, W. Jin, J. Cai, J. Ye, Z. Li, Y. Ma, J. Xie and L. Qi, *Adv. Funct. Mater.*, 2011, **21**, 3554–3563.
- 88 Y. Li, W. Xie, X. Hu, G. Shen, X. Zhou, Y. Xiang, X. Zhao and P. Fang, *Langmuir*, 2010, **26**, 591–597.
- 89 C. M. Teh and A. R. Mohamed, *J. Alloys Compd.*, 2011, **509**, 1648–1660.
- 90 A. Mills, C. Hill and P. K. J. Robertson, *J. Photochem. Photobiol. Chem.*, 2012, **237**, 7–23.
- 91 S. Sakthivel, M. C. Hidalgo, D. W. Bahnemann, S.-U. Geissen, V. Murugesan and A. Vogelpohl, *Appl. Catal. B Environ.*, 2006, **63**, 31–40.
- 92 M. Lindner, *Univ. Hann.*, 1997.
- 93 D. W. Bahnemann, S. N. Kholuiskaya, R. Dillert, A. I. Kulak and A. I. Kokorin, *Appl. Catal. B Environ.*, 2002, **36**, 161–169.
- 94 Y. Mao, C. Schoeneich and K. D. Asmus, *J. Phys. Chem.*, 1991, **95**, 10080–10089.
- 95 B. Kraeutler and A. J. Bard, *J. Am. Chem. Soc.*, 1977, **99**, 7729–7731.
- 96 Y. Nosaka, K. Koenuma, K. Ushida and A. Kira, *Langmuir*, 1996, **12**, 736–738.
- 97 A. Chemseddine and H. P. Boehm, *J. Mol. Catal.*, 1990, **60**, 295–311.
- 98 C. von Sonntag and H.-P. Schuchmann, *Angew. Chem. Int. Ed. Engl.*, 1991, **30**, 1229–1253.
- 99 W. F. Chan and R. A. Larson, *Water Res.*, 1991, **25**, 1539–1544.
- 100 W. F. Chan and R. A. Larson, *Water Res.*, 1991, **25**, 1529–1538.
- 101 G. Chen, I. Roy, C. Yang and P. N. Prasad, *Chem. Rev.*, 2016, **116**, 2826–2885.
- 102 Z. Fei Yin, L. Wu, H. Gui Yang and Y. Hua Su, *Phys. Chem. Chem. Phys.*, 2013, **15**, 4844.
- 103 P. Agostinis, K. Berg, K. A. Cengel, T. H. Foster, A. W. Girotti, S. O. Gollnick, S. M. Hahn, M. R. Hamblin, A. Juzeniene, D. Kessel, M. Korbelik, J. Moan, P. Mroz, D. Nowis, J. Piette, B. C. Wilson and J. Golab, *CA. Cancer J. Clin.*, 2011, **61**, 250–281.
- 104 Z. Lu, X. Zhang, Y. Zhao, Y. Xue, T. Zhai, Z. Wu and C. Li, *Polym Chem*, 2015, **6**, 302–310.
- 105 C. S. Shemesh, C. W. Hardy, D. S. Yu, B. Fernandez and H. Zhang, *Photodiagnosis Photodyn. Ther.*, 2014, **11**, 193–203.
- 106 S. Hackenberg, A. Scherzed, W. Harnisch, K. Froelich, C. Ginzkey, C. Koehler, R. Hagen and N. Kleinsasser, *J. Photochem. Photobiol. B*, 2012, **114**, 87–93.

- 107 H. S. Qian, H. C. Guo, P. C.-L. Ho, R. Mahendran and Y. Zhang, *Small*, 2009, **5**, 2285–2290.
- 108 R. R. Anderson and J. A. Parrish, *J. Invest. Dermatol.*, 1981, **77**, 13–19.
- 109 F. Scholkmann, S. Kleiser, A. J. Metz, R. Zimmermann, J. Mata Pavia, U. Wolf and M. Wolf, *NeuroImage*, 2014, **85, Part 1**, 6–27.
- 110 I. Řehoř, V. Vilímová, P. Jendelová, V. Kubiček, D. Jiráček, V. Herynek, M. Kapcalová, J. Kotek, J. Černý, P. Hermann and I. Lukeš, *J. Med. Chem.*, 2011, **54**, 5185–5194.
- 111 K. T. Thurn, E. M. B. Brown, A. Wu, S. Vogt, B. Lai, J. Maser, T. Paunesku and G. E. Woloschak, *Nanoscale Res. Lett.*, 2007, **2**, 430–441.
- 112 J. Seo, H. Chung, M. Kim, J. Lee, I. Choi and J. Cheon, *Small*, 2007, **3**, 850–853.
- 113 S. Yamaguchi, H. Kobayashi, T. Narita, K. Kanehira, S. Sonezaki and Y. Kubota, *Photochem. Photobiol.*, 2010, **86**, 964–971.
- 114 X. Feng, S. Zhang and X. Lou, *Colloids Surf. B Biointerfaces*, 2013, **107**, 220–226.
- 115 J. Xu, Y. Sun, J. Huang, C. Chen, G. Liu, Y. Jiang, Y. Zhao and Z. Jiang, *Bioelectrochemistry*, 2007, **71**, 217–222.
- 116 R. Cai, Y. Kubota, T. Shuin, H. Sakai, K. Hashimoto and A. Fujishima, *Cancer Res.*, 1992, **52**, 2346–2348.
- 117 B. Jovanović, *Integr. Environ. Assess. Manag.*, 2015, **11**, 10–20.
- 118 I. Iavicoli, V. Leso and A. Bergamaschi, *J. Nanomater.*, 2012, **2012**, 1–36.
- 119 G. E. Schaumann, A. Philippe, M. Bundschuh, G. Metreveli, S. Klitzke, D. Rakcheev, A. Grün, S. K. Kumahor, M. Kühn, T. Baumann, F. Lang, W. Manz, R. Schulz and H.-J. Vogel, *Sci. Total Environ.*, 2015, **535**, 3–19.
- 120 K. Schilling, B. Bradford, D. Castelli, E. Dufour, J. F. Nash, W. Pape, S. Schulte, I. Tooley, J. van den Bosch and F. Schellauf, *Photochem. Photobiol. Sci.*, 2010, **9**, 495.
- 121 B. Sha, W. Gao, X. Cui, L. Wang and F. Xu, *J. Appl. Toxicol.*, 2015, **35**, 1086–1101.
- 122 H. Shi, R. Magaye, V. Castranova and J. Zhao, *Part Fibre Toxicol.*, 2013, **10**, 15.
- 123 X. Zhang, W. Li and Z. Yang, *Arch. Toxicol.*, 2015, **89**, 2207–2217.
- 124 A. Chompoosor, K. Saha, P. S. Ghosh, D. J. Macarthy, O. R. Miranda, Z.-J. Zhu, K. F. Arcaro and V. M. Rotello, *Small*, 2010, **6**, 2246–2249.
- 125 E. Fröhlich, B. J. Teubl and E. Roblegg, *BioNanoMaterials*, 2013, **14**, 25–35.
- 126 J. R. McCarthy, *Nanomed.*, 2009, **4**, 693–695.
- 127 A. Fernandez-Fernandez, R. Manchanda and A. J. McGoron, *Appl. Biochem. Biotechnol.*, 2011, **165**, 1628–1651.
- 128 K. Young Choi, G. Liu, S. Lee and X. Chen, *Nanoscale*, 2012, **4**, 330–342.
- 129 S. M. Janib, A. S. Moses and J. A. MacKay, *Adv. Drug Deliv. Rev.*, 2010, **62**, 1052–1063.
- 130 Z. Zhang, L. Wang, J. Wang, X. Jiang, X. Li, Z. Hu, Y. Ji, X. Wu and C. Chen, *Adv. Mater.*, 2012, **24**, 1418–1423.
- 131 Y. Xia, W. Li, C. M. Cobley, J. Chen, X. Xia, Q. Zhang, M. Yang, E. C. Cho and P. K. Brown, *Acc. Chem. Res.*, 2011, **44**, 914–924.
- 132 D. Yoo, J.-H. Lee, T.-H. Shin and J. Cheon, *Acc. Chem. Res.*, 2011, **44**, 863–874.
- 133 T. Krasia-Christoforou and T. K. Georgiou, *J. Mater. Chem. B*, 2013, **1**, 3002–3025.
- 134 S.-M. Lee, Y. Song, B. J. Hong, K. W. MacRenaris, D. J. Mastarone, T. V. O'Halloran, T. J. Meade and S. T. Nguyen, *Angew. Chem. Int. Ed.*, 2010, **49**, 9960–9964.
- 135 Y. Zhu, C. Ding, G. Ma and Z. Du, *J. Solid State Chem.*, 1998, **139**, 124–127.
- 136 Y. C. Zhu and C. X. Ding, *J. Solid State Chem.*, 1999, **145**, 711–715.
- 137 M. Niederberger, M. H. Bartl and G. D. Stucky, *Chem. Mater.*, 2002, **14**, 4364–4370.
- 138 D. Pan, N. Zhao, Q. Wang, S. Jiang, X. Ji and L. An, *Adv. Mater.*, 2005, **17**, 1991–1995.
- 139 S. Biswas, V. Sundstrom and S. De, *Mater. Chem. Phys.*, 2014, **147**, 761–771.

- 140 J. Liqiang, Q. Yichun, W. Baiqi, L. Shudan, J. Baojiang, Y. Libin, F. Wei, F. Honggang and S. Jiazhong, *Sol. Energy Mater. Sol. Cells*, 2006, **90**, 1773–1787.
- 141 Z. Zhao and Q. Liu, *J. Phys. Appl. Phys.*, 2008, **41**, 085417.
- 142 S. Bingham and W. A. Daoud, *J Mater Chem*, 2011, **21**, 2041–2050.
- 143 U. G. Akpan and B. H. Hameed, *Appl. Catal. Gen.*, 2010, **375**, 1–11.
- 144 M. K. Nowotny, L. R. Sheppard, T. Bak and J. Nowotny, *J. Phys. Chem. C*, 2008, **112**, 5275–5300.
- 145 W. Zhou, Y. Zhou and S. Tang, *Mater. Lett.*, 2005, **59**, 3115–3118.
- 146 L. Xing, J. Jia, Y. Wang and S. Dong, *Environ. Prog. Sustain. Energy*, 2013, **32**, 302–306.
- 147 N. V. Gaponenko, I. S. Molchan, G. E. Thompson, P. Skeldon, A. Pakes, R. Kudrawiec, L. Bryja and J. Misiewicz, *Sens. Actuators Phys.*, 2002, **99**, 71–73.
- 148 H. R. Kim, T. G. Lee and Y.-G. Shul, *J. Photochem. Photobiol. Chem.*, 2007, **185**, 156–160.
- 149 A. J. Kenyon, *Prog. Quantum Electron.*, 2002, **26**, 225–284.
- 150 H. Liu, L. Yu, W. Chen and Y. Li, *J. Nanomater.*, 2012, **2012**, 1–9.
- 151 Y. Wang, H. Cheng, L. Zhang, Y. Hao, J. Ma, B. Xu and W. Li, *J. Mol. Catal. Chem.*, 2000, **151**, 205–216.
- 152 W. Zhou, Y. Zheng and G. Wu, *Appl. Surf. Sci.*, 2006, **253**, 1387–1392.
- 153 Q. G. Zeng, Z. M. Zhang, Z. J. Ding, Y. Wang and Y. Q. Sheng, *Scr. Mater.*, 2007, **57**, 897–900.
- 154 J. Zhang, X. Wang, W.-T. Zheng, X.-G. Kong, Y.-J. Sun and X. Wang, *Mater. Lett.*, 2007, **61**, 1658–1661.
- 155 A. Patra, C. S. Friend, R. Kapoor and P. N. Prasad, *Chem. Mater.*, 2003, **15**, 3650–3655.
- 156 J. Liqiang, S. Xiaojun, X. Baifu, W. Baiqi, C. Weimin and F. Honggang, *J. Solid State Chem.*, 2004, **177**, 3375–3382.
- 157 H. Wang, Y. Wang, Y. Yang, X. Li and C. Wang, *Mater. Res. Bull.*, 2009, **44**, 408–414.
- 158 L. Li, C.-K. Tsung, Z. Yang, G. D. Stucky, L. D. Sun, J. F. Wang and C. H. Yan, *Adv. Mater.*, 2008, **20**, 903–908.
- 159 D. Kaczmarek, J. Domaradzki, A. Borkowska, A. Podhorodecki, J. Misiewicz and K. Sieradzka, *Opt. Appl.*
- 160 C.-C. Ting, S.-Y. Chen, W.-F. Hsieh and H.-Y. Lee, *J. Appl. Phys.*, 2001, **90**, 5564–5569.
- 161 C. W. Jia, E. Q. Xie, J. G. Zhao, Z. W. Sun and A. H. Peng, *J. Appl. Phys.*, 2006, **100**, 023529.
- 162 E. Galoppini, *Coord. Chem. Rev.*, 2004, **248**, 1283–1297.
- 163 N. J. Cherepy, G. P. Smestad, M. Grätzel and J. Z. Zhang, *J. Phys. Chem. B*, 1997, **101**, 9342–9351.
- 164 I. Martini, J. H. Hodak and G. V. Hartland, *J. Phys. Chem. B*, 1998, **102**, 9508–9517.
- 165 M. N. Tahir, M. Eberhardt, P. Theato, S. Faiß, A. Janshoff, T. Gorelik, U. Kolb and W. Tremel, *Angew. Chem. Int. Ed.*, 2006, **45**, 908–912.
- 166 K. T. Thurn, T. Paunesku, A. Wu, E. M. B. Brown, B. Lai, S. Vogt, J. Maser, M. Aslam, V. Dravid, R. Bergan and G. E. Woloschak, *Small*, 2009, **5**, 1318–1325.
- 167 J. Lin, J. A. Siddiqui and R. M. Ottenbrite, *Polym. Adv. Technol.*, 2001, **12**, 285–292.
- 168 M. J. Choi, T. Smoother, A. A. Martin, A. M. McDonagh, P. J. Maynard, C. Lennard and C. Roux, *Forensic Sci. Int.*, 2007, **173**, 154–160.
- 169 N. Mandzy, E. Grulke and T. Druffel, *Powder Technol.*, 2005, **160**, 121–126.
- 170 J. L. Deiss, P. Anizan, S. El Hadigui and C. Wecker, *Colloids Surf. Physicochem. Eng. Asp.*, 1996, **106**, 59–62.
- 171 A.-H. Lu, E. L. Salabas and F. Schüth, *Angew. Chem. Int. Ed.*, 2007, **46**, 1222–1244.
- 172 W. B. Russel, D. A. Saville and W. R. Schowalter, *Colloidal Dispersions*, Cambridge University Press, 1989.
- 173 G. Fritz, V. Schädler, N. Willenbacher and N. J. Wagner, *Langmuir*, 2002, **18**, 6381–6390.
- 174 D. H. Napper and A. Netschey, *J. Colloid Interface Sci.*, 1971, **37**, 528–535.
- 175 Z. E. Allouni, M. R. Cimpan, P. J. Høl, T. Skodvin and N. R. Gjerdet, *Colloids Surf. B Biointerfaces*, 2009, **68**, 83–87.

- 176 Z. Ji, X. Jin, S. George, T. Xia, H. Meng, X. Wang, E. Suarez, H. Zhang, E. M. V. Hoek, H. Godwin, A. E. Nel and J. I. Zink, *Environ. Sci. Technol.*, 2010, **44**, 7309–7314.
- 177 P. Bihari, M. Vippola, S. Schultes, M. Praetner, A. G. Khandoga, C. A. Reichel, C. Coester, T. Tuomi, M. Rehberg and F. Krombach, *Part. Fibre Toxicol.*, 2008, **5**, 14.
- 178 E. C. Cho, Q. Zhang and Y. Xia, *Nat. Nanotechnol.*, 2011, **6**, 385–391.
- 179 C. Guiot and O. Spalla, *Environ. Sci. Technol.*, 2013, **47**, 1057–1064.
- 180 N. Lakshminarasimhan, W. Kim and W. Choi, *J. Phys. Chem. C*, 2008, **112**, 20451–20457.
- 181 C. He, Y. Hu, L. Yin, C. Tang and C. Yin, *Biomaterials*, 2010, **31**, 3657–3666.
- 182 T. S. Hauck, A. A. Ghazani and W. C. W. Chan, *Small*, 2008, **4**, 153–159.
- 183 M. L. Amin, J. Y. Joo, D. K. Yi and S. S. A. An, *J. Controlled Release*, 2015, **207**, 131–142.
- 184 L. Hu, Z. Mao and C. Gao, *J. Mater. Chem.*, 2009, **19**, 3108.
- 185 A. Verma and F. Stellacci, *Small*, 2010, **6**, 12–21.
- 186 K. Yin Win and S.-S. Feng, *Biomaterials*, 2005, **26**, 2713–2722.
- 187 L. Chen, J. M. Mccrate, J. C.-M. Lee and H. Li, *Nanotechnology*, 2011, **22**, 105708.
- 188 M. J. D. Clift, B. Rothen-Rutishauser, D. M. Brown, R. Duffin, K. Donaldson, L. Proudfoot, K. Guy and V. Stone, *Toxicol. Appl. Pharmacol.*, 2008, **232**, 418–427.
- 189 S. Patil, A. Sandberg, E. Heckert, W. Self and S. Seal, *Biomaterials*, 2007, **28**, 4600–4607.
- 190 R. Kumar, I. Roy, T. Y. Ohulchanskyy, L. N. Goswami, A. C. Bonoiu, E. J. Bergey, K. M. Trampusch, A. Maitra and P. N. Prasad, *ACS Nano*, 2008, **2**, 449–456.
- 191 T.-H. Chung, S.-H. Wu, M. Yao, C.-W. Lu, Y.-S. Lin, Y. Hung, C.-Y. Mou, Y.-C. Chen and D.-M. Huang, *Biomaterials*, 2007, **28**, 2959–2966.
- 192 W.-K. Oh, S. Kim, M. Choi, C. Kim, Y. S. Jeong, B.-R. Cho, J.-S. Hahn and J. Jang, *ACS Nano*, 2010, **4**, 5301–5313.
- 193 B. J. Teubl, C. Schimpel, G. Leitinger, B. Bauer, E. Fröhlich, A. Zimmer and E. Roblegg, *J. Hazard. Mater.*, 2015, **286**, 298–305.
- 194 A. Villanueva, M. Cañete, A. G. Roca, M. Calero, S. Veintemillas-Verdaguer, C. J. Serna, M. del Puerto Morales and R. Miranda, *Nanotechnology*, 2009, **20**, 115103.
- 195 Y. Zhang, N. Kohler and M. Zhang, *Biomaterials*, 2002, **23**, 1553–1561.
- 196 C. Wilhelm, C. Billotey, J. Roger, J. N. Pons, J.-C. Bacri and F. Gazeau, *Biomaterials*, 2003, **24**, 1001–1011.
- 197 D. L. J. Thorek and A. Tsourkas, *Biomaterials*, 2008, **29**, 3583–3590.
- 198 A. Petri-Fink and H. Hofmann, *IEEE Trans. NanoBioscience*, 2007, **6**, 289–297.
- 199 K. Cho, X. Wang, S. Nie, Z. Chen and D. M. Shin, *Clin. Cancer Res.*, 2008, **14**, 1310–1316.
- 200 C. Leamon, *Adv. Drug Deliv. Rev.*, 2004, **56**, 1127–1141.
- 201 C. P. Leamon and P. S. Low, *Drug Discov. Today*, 2001, **6**, 44–51.
- 202 Y. Lu and P. S. Low, *Adv. Drug Deliv. Rev.*, 2012, **64**, 342–352.
- 203 A. Quintana, E. Raczka, L. Piehler, I. Lee, A. Myc, I. Majoros, A. K. Patri, T. Thomas, J. Mulé and J. R. Baker Jr, *Pharm. Res.*, 2002, **19**, 1310–1316.
- 204 N. F. Saba, X. Wang, S. Müller, M. Tighiouart, K. Cho, S. Nie, Z. (Georgia) Chen and D. M. Shin, *Head Neck*, 2009, **31**, 475–481.
- 205 J. Sudimack and R. J. Lee, *Adv. Drug Deliv. Rev.*, 2000, **41**, 147–162.
- 206 X. Zhao, H. Li and R. J. Lee, *Expert Opin. Drug Deliv.*, 2008, **5**, 309–319.
- 207 Z. M. Qian, H. Li, H. Sun and K. Ho, *Pharmacol. Rev.*, 2002, **54**, 561–587.
- 208 J. J. Huang, Y. B. Ye, Z. Q. Lei, X. J. Ye, M. Z. Rong and M. Q. Zhang, *Phys. Chem. Chem. Phys.*, 2014, **16**, 5480.
- 209 C. Bies, C.-M. Lehr and J. F. Woodley, *Adv. Drug Deliv. Rev.*, 2004, **56**, 425–435.

- 210 V. Bagalkot, L. Zhang, E. Levy-Nissenbaum, S. Jon, P. W. Kantoff, R. Langer and O. C. Farokhzad, *Nano Lett.*, 2007, **7**, 3065–3070.
- 211 O. C. Farokhzad, S. Jon, A. Khademhosseini, T.-N. T. Tran, D. A. LaVan and R. Langer, *Cancer Res.*, 2004, **64**, 7668–7672.
- 212 O. C. Farokhzad, J. Cheng, B. A. Teply, I. Sherifi, S. Jon, P. W. Kantoff, J. P. Richie and R. Langer, *Proc. Natl. Acad. Sci.*, 2006, **103**, 6315–6320.
- 213 L. Zhang, A. F. Radovic-Moreno, F. Alexis, F. X. Gu, P. A. Basto, V. Bagalkot, S. Jon, R. S. Langer and O. C. Farokhzad, *ChemMedChem*, 2007, **2**, 1268–1271.
- 214 B. J. Hicke, A. W. Stephens, T. Gould, Y.-F. Chang, C. K. Lynott, J. Heil, S. Borkowski, C.-S. Hilger, G. Cook, S. Warren and others, *J. Nucl. Med.*, 2006, **47**, 668–678.
- 215 K. Kalyanasundaram and M. Grätzel, *Coord. Chem. Rev.*, 1998, **177**, 347–414.
- 216 T. Paunesku, T. Rajh, G. Wiederrecht, J. Maser, S. Vogt, N. Stojićević, M. Protić, B. Lai, J. Oryhon, M. Thurnauer and G. Woloschak, *Nat. Mater.*, 2003, **2**, 343–346.
- 217 R. W. Cheyne, T. A. Smith, L. Trembleau and A. C. McLaughlin, *Nanoscale Res. Lett.*, 2011, **6**, 1–6.
- 218 M. Niederberger, G. Garnweitner, F. Krumeich, R. Nesper, H. Cölfen and M. Antonietti, *Chem. Mater.*, 2004, **16**, 1202–1208.
- 219 H. Kamiya and M. Iijima, *Sci. Technol. Adv. Mater.*, 2010, **11**, 044304.
- 220 L. de la Garza, Z. V. Saponjic, N. M. Dimitrijevic, M. C. Thurnauer and T. Rajh, *J. Phys. Chem. B*, 2006, **110**, 680–686.
- 221 I. A. Janković, Z. V. Šaponjić, E. S. Džunuzović and J. M. Nedeljković, *Nanoscale Res. Lett.*, 2010, **5**, 81–88.
- 222 I. A. Janković, Z. V. Šaponjić, M. I. Čomor and J. M. Nedeljković, *J. Phys. Chem. C*, 2009, **113**, 12645–12652.
- 223 M. C. Thurnauer, T. Rajh and D. M. Tiede, *Acta Chim. Scandinavica*, 1997, **51**, 610–618.
- 224 M. N. Tahir, P. Theato, P. Oberle, G. Melnyk, S. Faiss, U. Kolb, A. Janshoff, M. Stepputat and W. Tremel, *Langmuir*, 2006, **22**, 5209–5212.
- 225 R. Comparelli, E. Fanizza, M. Curri, P. Cozzoli, G. Mascolo, R. Passino and A. Agostiano, *Appl. Catal. B Environ.*, 2005, **55**, 81–91.
- 226 P. H. Mutin, G. Guerrero and A. Vioux, *J. Mater. Chem.*, 2005, **15**, 3761.
- 227 T. Rajh, J. M. Nedeljkovic, L. X. Chen, O. Poluektov and M. C. Thurnauer, *J. Phys. Chem. B*, 1999, **103**, 3515–3519.
- 228 K. E. Sapsford, W. R. Algar, L. Berti, K. B. Gemmill, B. J. Casey, E. Oh, M. H. Stewart and I. L. Medintz, *Chem. Rev.*, 2013, **113**, 1904–2074.
- 229 Y. Qin, L. Sun, X. Li, Q. Cao, H. Wang, X. Tang and L. Ye, *J. Mater. Chem.*, 2011, **21**, 18003.
- 230 A. M. El-Toni, S. Yin and T. Sato, *J. Colloid Interface Sci.*, 2006, **300**, 123–130.
- 231 A. Jaroenworarluck, W. Sunsaneeyametha, N. Kosachan and R. Stevens, *Surf. Interface Anal.*, 2006, **38**, 473–477.
- 232 E. Jimenez-Villar, V. Mestre, P. C. de Oliveira and G. F. de Sá, *Nanoscale*, 2013, **5**, 12512.
- 233 O. K. Park and Y. S. Kang, *Colloids Surf. Physicochem. Eng. Asp.*, 2005, **257–258**, 261–265.
- 234 S. M. Grayson and J. M. J. Fréchet, *Chem. Rev.*, 2001, **101**, 3819–3868.
- 235 D. A. Tomalia, *New J. Chem.*, 2012, **36**, 264–281.
- 236 L. M. Bronstein and Z. B. Shifrina, *Chem. Rev.*, 2011, **111**, 5301–5344.
- 237 R.-O. Moussodia, L. Balan, C. Merlin, C. Mustin and R. Schneider, *J Mater Chem*, 2010, **20**, 1147–1155.
- 238 M. Li, L. Qun Xu, L. Wang, Y. P. Wu, J. Li, K.-G. Neoh and E.-T. Kang, *Polym. Chem.*, 2011, **2**, 1312–1321.
- 239 R. Abu-Reziq, H. Alper, D. Wang and M. L. Post, *J. Am. Chem. Soc.*, 2006, **128**, 5279–5282.
- 240 Y. Nakanishi and T. Imae, *J. Colloid Interface Sci.*, 2006, **297**, 122–129.
- 241 C.-C. Chu, N. Ueno and T. Imae, *Chem. Mater.*, 2008, **20**, 2669–2676.

- 242 Y. Komine, I. Ueda, T. Goto and H. Fujihara, *Chem. Commun.*, 2006, **0**, 302–304.
- 243 C. S. Love, V. Chechik, D. K. Smith and C. Brennan, *J. Mater. Chem.*, 2004, **14**, 919–923.
- 244 K. Satoh, T. Yoshimura and K. Esumi, *J. Colloid Interface Sci.*, 2002, **255**, 312–322.
- 245 C. Danda, R. Ponnappati, P. Dutta, P. Taranekar, G. Patterson and R. C. Advincula, *Macromol. Chem. Phys.*, 2011, **212**, 1600–1615.
- 246 M.-C. Daniel, J. Ruiz, S. Nlate, J. Palumbo, J.-C. Blais and D. Astruc, *Chem. Commun.*, 2001, **0**, 2000–2001.
- 247 W. Guo, J. J. Li, Y. A. Wang and X. Peng, *J. Am. Chem. Soc.*, 2003, **125**, 3901–3909.
- 248 T. J. Cho, R. A. Zangmeister, R. I. MacCusprie, A. K. Patri and V. A. Hackley, *Chem. Mater.*, 2011, **23**, 2665–2676.
- 249 D.-H. Tsai, T. Joon Cho, S. R. Elzey, J. C. Gigault and V. A. Hackley, *Nanoscale*, 2013, **5**, 5390–5395.
- 250 S. Nakao, K. Torigoe, K. Kon-No and T. Yonezawa, *J. Phys. Chem. B*, 2002, **106**, 12097–12100.
- 251 S. Deol, N. Weerasuriya and Y.-S. Shon, *J. Mater. Chem. B*, 2015, **3**, 6071–6080.
- 252 Y. A. Wang, J. J. Li, H. Chen and X. Peng, *J. Am. Chem. Soc.*, 2002, **124**, 2293–2298.
- 253 D. Rosario-Amorin, X. Wang, M. Gaboyard, R. Clérac, S. Nlate and K. Heuzé, *Chem. – Eur. J.*, 2009, **15**, 12636–12643.
- 254 Y. Liu, R. Brandon, M. Cate, X. Peng, R. Stony and M. Johnson, *Anal. Chem.*, 2007, **79**, 8796–8802.
- 255 C. Duanmu, I. Saha, Y. Zheng, B. M. Goodson and Y. Gao, *Chem. Mater.*, 2006, **18**, 5973–5981.
- 256 T. Gillich, C. Acikgöz, L. Isa, A. D. Schlüter, N. D. Spencer and M. Textor, *ACS Nano*, 2013, **7**, 316–329.
- 257 B. Basly, D. Felder-Flesch, P. Perriat, C. Billotey, J. Taleb, G. Pourroy and S. Begin-Colin, *Chem. Commun.*, 2010, **46**, 985–987.
- 258 J. Young Park, Y. Park and R. C. Advincula, *Soft Matter*, 2011, **7**, 5124–5127.
- 259 A. Walter, A. Garofalo, A. Parat, J. Jouhannaud, G. Pourroy, E. Voirin, S. Laurent, P. Bonazza, J. Taleb, C. Billotey, L. V. Elst, R. N. Muller, S. Begin-Colin and D. Felder-Flesch, *J. Mater. Chem. B*, 2015, **3**, 1484–1494.
- 260 X. He, X. Wu, X. Cai, S. Lin, M. Xie, X. Zhu and D. Yan, *Langmuir*, 2012, **28**, 11929–11938.
- 261 Y. Liu, M. Kim, Y. Wang, Y. A. Wang and X. Peng, *Langmuir*, 2006, **22**, 6341–6345.
- 262 T. Tanaka, K. Shibata, M. Hosokawa, K. Hatakeyama, A. Arakaki, H. Gomyo, T. Mogi, T. Taguchi, H. Wake, T. Tanaami and T. Matsunaga, *J. Colloid Interface Sci.*, 2012, **377**, 469–475.
- 263 M. Kim, Y. Chen, Y. Liu and X. Peng, *Adv. Mater.*, 2005, **17**, 1429–1432.
- 264 S. M. George, I.-S. Hong and J.-K. Kim, *Bull. Korean Chem. Soc.*, 2008, **29**, 1545–1553.
- 265 T. Mizugaki, M. Murata, S. Fukubayashi, T. Mitsudome, K. Jitsukawa and K. Kaneda, *Chem. Commun.*, 2008, **0**, 241–243.
- 266 K. Torigoe, Y. Watanabe, T. Endo, K. Sakai, H. Sakai and M. Abe, *J. Nanoparticle Res.*, 2010, **12**, 951–960.
- 267 S. Svenson, *Eur. J. Pharm. Biopharm.*, 2009, **71**, 445–462.
- 268 X. Hu, L. Zhou and C. Gao, *Colloid Polym. Sci.*, 2011, **289**, 1299–1320.
- 269 B. Singh, N. Hussain, T. Sakthivel and A. T. Florence, *J. Pharm. Pharmacol.*, 2003, **55**, 1635–1640.
- 270 N. Tsubokawa, H. Ichioka, T. Satoh, S. Hayashi and K. Fujiki, *React. Funct. Polym.*, 1998, **37**, 75–82.
- 271 Y. Maeda, T. Toyoda, M. Tanaka, T. Mogi, T. Taguchi, T. Tanaami, T. Matsunaga and T. Tanaka, *Electrochimica Acta*, 2015, **168**, 308–312.
- 272 C.-H. Lai, T.-C. Chang, Y.-J. Chuang, D.-L. Tzou and C.-C. Lin, *Bioconjug. Chem.*, 2013, **24**, 1698–1709.
- 273 V. Balzani, P. Ceroni, M. Maestri, C. Saudan and V. Vicinelli, in *Dendrimers V*, eds. C. A. Schalley and F. Vögtle, Springer Berlin Heidelberg, Berlin, Heidelberg, 2003, vol. 228, pp. 159–191.
- 274 M. Kawa, in *Dendrimers V*, eds. C. A. Schalley and F. Vögtle, Springer Berlin Heidelberg, Berlin, Heidelberg, 2003, vol. 228, pp. 193–204.
- 275 S. Buathong, D. Ung, T. J. Daou, C. Ulhaq-Bouillet, G. Pourroy, D. Guillon, L. Ivanova, I. Bernhardt, S. Bégin-Colin and B. Donnio, *J. Phys. Chem. C*, 2009, **113**, 12201–12212.

- 276 K. Heuzé, D. Rosario-Amorin, S. Nlate, M. Gaboyard, A. Bouter and R. Clérac, *New J. Chem.*, 2008, **32**, 383–387.
- 277 G. M. Stewart and M. A. Fox, *J. Am. Chem. Soc.*, 1996, **118**, 4354–4360.
- 278 M. Alexander Bissett, I. Köper, J. Scott Quinton and J. George Shapter, *J. Mater. Chem.*, 2011, **21**, 18597–18604.
- 279 C. Hirano, T. Imae, M. Tamura and Y. Takaguchi, *Chem. Lett.*, 2005, **34**, 862–863.
- 280 N. Seob Baek, J.-H. Yum, X. Zhang, H. Kyu Kim, M. K. Nazeeruddin and M. Grätzel, *Energy Environ. Sci.*, 2009, **2**, 1082–1087.
- 281 C. M. Cardona, J. Alvarez, A. E. Kaifer, T. D. McCarley, S. Pandey, G. A. Baker, N. J. Bonzagni and F. V. Bright, *J. Am. Chem. Soc.*, 2000, **122**, 6139–6144.
- 282 C. M. Cardona, T. Wilkes, W. Ong, A. E. Kaifer, T. D. McCarley, S. Pandey, G. A. Baker, M. N. Kane, S. N. Baker and F. V. Bright, *J. Phys. Chem. B*, 2002, **106**, 8649–8656.
- 283 H. Liu, J. Guo, L. Jin, W. Yang and C. Wang, *J. Phys. Chem. B*, 2008, **112**, 3315–3321.
- 284 P. Du, W.-H. Zhu, Y.-Q. Xie, F. Zhao, C.-F. Ku, Y. Cao, C.-P. Chang and H. Tian, *Macromolecules*, 2004, **37**, 4387–4398.

II. Inorganic syntheses: Titanium dioxide nanoparticles

Contents

II. Inorganic syntheses: Titanium dioxide nanoparticles.....	- 45 -
II.1. Influence of the coordinating agent on TiO ₂ nanoparticles	- 45 -
II.1.1. Size and morphology.....	- 45 -
II.1.2. Surface moieties	- 48 -
II.1.3. Photocatalytic activity	- 53 -
II.2. Influence of hydrothermal processing parameters on MEEAA-TiO ₂ particles.....	- 56 -
II.2.1. Size and morphology.....	- 56 -
II.2.2. Surface moieties	- 62 -
II.2.3. Photocatalytic activity	- 65 -
II.3. Luminescent TiO ₂ based core/shell structured nanoparticles.....	- 71 -
II.3.1. Luminescent TiO ₂ /SiO ₂ core/shell nanoparticles.....	- 71 -
II.3.2. ZnO/TiO ₂ core/shell nanoparticles.....	- 76 -
II.4. Conclusion	- 83 -

II. Inorganic syntheses: Titanium dioxide nanoparticles

Various photocatalytically active nanomaterials have already been studied in the last decades, including CdS, SnO₂, ZnO, Nb₂O₃ or ZrO₂. Nevertheless, nano-TiO₂ remains one of the most well-known and widely-used photocatalysts due to its high efficiency, low cost, physical and chemical stability, widespread availability, and noncorrosive properties.¹ Due to these properties combined with their non-toxicity, TiO₂ nanoparticle (NP) systems are very promising candidates for medical applications such as photodynamic therapy for cancer, cell imaging, biological analysis, genetic engineering or drug delivery.² To synthesize them, hydrothermal sol-gel synthesis is the preferred method due to its excellent reproducibility, high particle density and crystallinity, as well as a controlled morphology and narrow size distribution of the obtained NPs. Additionally, depending on the chosen reactants the obtained NPs carry characteristic organic surface moieties which for example ensure a perfect particle dispersibility.³⁻⁶

II.1. Influence of the coordinating agent on TiO₂ nanoparticles

Two synthesis approaches characterized by different coordinating agents have been selected. The first TiO₂ NPs were synthesized in the presence of acetyl acetone (AA) and para-toluene sulfonic acid (PTSA). This system has already been intensively studied for the use of photocatalytic (PC) coating materials in terms of their organic surface properties with TGA, crystal structure with x-ray diffraction (XRD) and PC activity mainly after coating onto surfaces and annealing.⁷⁻¹⁰ Therefore, in this particle case its suitability as a PC material has already been proven and the objective was mainly to determine its properties as a colloid. The second TiO₂ NP system was chelated by 2-[2-(2-methoxyethoxy)ethoxy]acetic acid (MEEAA). It has been chosen as this acid has a polyethylene glycol like structure which may be favourable for cellular uptake and may only show a low cytotoxicity. This particle system has not yet been studied in detail.

For studying the differences of these two particle types, here named AA-TiO₂ and MEEAA-TiO₂, samples with a hydrothermal treatment time of 4 h at 160 °C were selected. First their sizes and morphologies, then their surface moieties and PC activities are discussed in the following.

II.1.1. Size and morphology

To determine differences in their size and morphology due to the chelating ligands of the synthesis, XRD, TEM, N₂ sorption and DLS measurements were conducted. The XRD patterns

for both particles types are shown in Figure II - 1. They are typical for NPs as their signals are very broad in contrast to well-defined sharp signals caused by bulk materials.¹¹

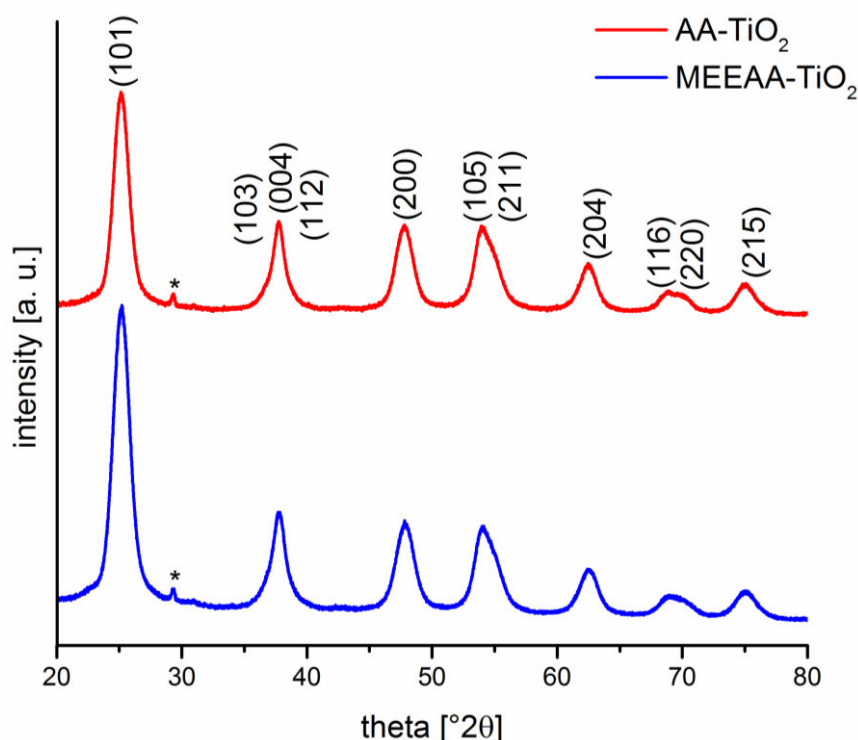


Figure II - 1. Powder X-ray diffraction (XRD) patterns of AA-TiO₂ and MEEAA-TiO₂ assigned to anatase crystal phase. (*background signal due to measurement set-up).

Their patterns were both assigned to the anatase phase; all signals were attributed to hkl indices of this crystal phase. It had already been expected to obtain the anatase phase as in general it can be easily formed at low temperatures as used in these syntheses, while the rutile phase is usually obtained at elevated temperatures of 400 – 1200 °C.^{10,12} Furthermore, the formation of the anatase phase in the case of AA-TiO₂ has already been reported.^{8,10} The XRD patterns of both TiO₂ NP types do not show any differences and even their crystallite sizes determined using the Scherrer equation (using the diffraction peak from the anatase (101) plane) were in both cases between 5 nm and 6 nm (5.5 nm for MEEAA-TiO₂ and 5.6 nm for AA-TiO₂ respectively). TEM images of both particles samples (Figure II - 2) also showed average particle sizes around 5 to 6 nm with slight variances (5.7 ± 1.0 nm for MEEAA-TiO₂ and 6.3 ± 1.5 nm for AA-TiO₂ respectively). This indicates that the obtained NPs are monocrystals. Furthermore, the particles exhibit a prolate spheroidic morphology. Like the XRD spectra, the TEM images do not reveal significant differences between both particle types. Nevertheless, the size of the NPs of the AA-TiO₂ sample seems to vary slightly more as larger particles (e.g. 10 nm) were also found on occasion.

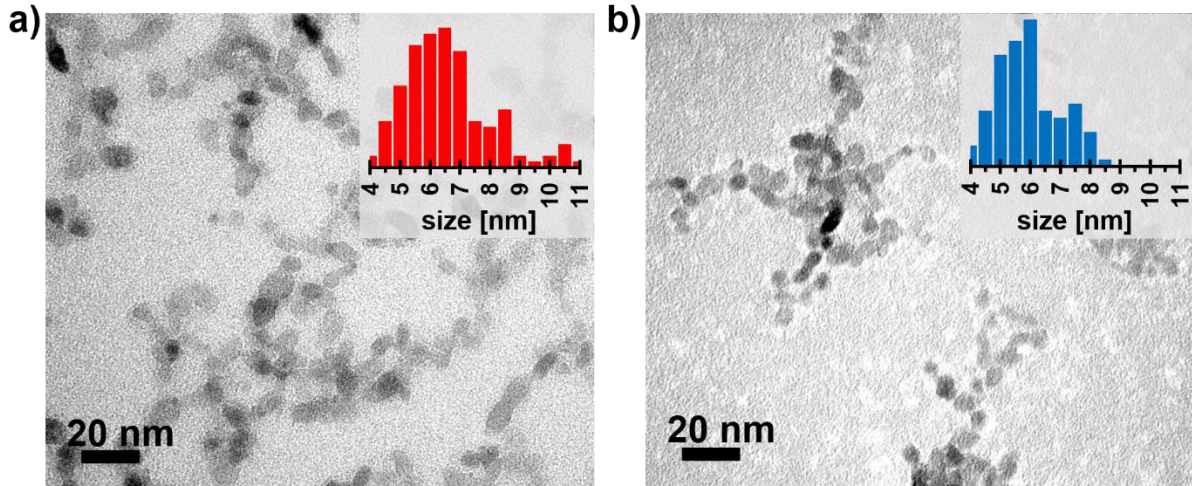


Figure II - 2. Transmission electron microscopy (TEM) of AA-TiO₂ a) and MEEAA-TiO₂ b) and their size distribution, obtained from counting at least 100 particles per sample.

To further examine the particle properties the specific surface area (according to Brunauer Emmet Teller (BET)¹³) was determined by N₂ sorption measurements. The AA-TiO₂ shows a specific surface area of 207.5 m²/g while the surface area of MEEAA-TiO₂ is slightly higher with 231.2 m²/g. This difference may be due to the marginally smaller crystallite size. The obtained experimental surface areas can be compared to the theoretic specific surface area $S_{calc} = \frac{s}{m}$ of a TiO₂ sample. For the calculation one expects $\rho = 3.9 \text{ g/cm}^3$ as the density of anatase¹⁴ and the particle shape is simplified to a perfect sphere with the volume $v = \frac{3}{4} \pi r^3$, surface $s = 4 r^2 \pi$ (r = radius) and the mass $m = \rho * v$. From this, the obtained theoretic surface area $S_{calc} = \frac{s}{m} = \frac{4 r^2 \pi}{\rho * v} = \frac{4 r^2 \pi}{\rho * \frac{3}{4} r^3 \pi} = \frac{3}{\rho * r}$ is 275 m²/g for MEEAA-TiO₂ and 280 m²/g for MEEAA-TiO₂ if the crystallite sizes obtained from the XRD measurements are utilized for the calculation. These values are higher than the experimentally determined specific surface areas. The discrepancies between measured and calculated values are not surprising, if taken into consideration that the specific surface area (determined via BET) and the theoretic calculation can differ up to $\pm 20 \%$ due to errors such as a wide particle size distribution or particle morphology.¹⁵ Therefore, this measurement confirms the measured particle sizes by XRD and TEM.

While the last 3 methods only analysed the particles as dried powder, dynamic light scattering (DLS) measurements allowed the examination of particle behaviour in dispersions. For this, the hydrodynamic diameter was determined using the so-called Z-Average size which is the primary and therefore most stable parameter produced by this technique. The hydrodynamic diameter displays the diameter of a hypothetical hard sphere showing the same translational diffusion coefficient as the examined particle with an assumed hydration layer.¹⁶ Depending on the agglomeration state of the sample, this value shows the size of an agglomerated group

of particles plus hydration layer instead of the size of a single particle. Therefore, this method indicates the dispersion state of the sample or the agglomerate size of the particles, rather than the real particle size. The following Table II - 1 represents the hydrodynamic diameters after synthesis and after an ultrasonic (US) treatment to optimize their dispersion. After synthesis, both particle systems were dispersed in water at pH 2 to 3. This pH is caused by remaining unbound organic acids from the synthesis (i.e. MEEAA or acetic acid which is discussed in detail in II.1.2). Right after synthesis, the hydrodynamic diameter is around 80 nm for both samples. This value can be significantly decreased by dispersion of the particles with US treatment (Branson Sonifier 450, 4 min, duty cycle 30%, strength 7). Therefore, one can assume that after synthesis, the sample is already well dispersed, but small agglomerates can be measured. After US treatment the agglomerates are separated and the particles may even be dispersed as single particles with a hydration layer as the hydrodynamic diameters are only about four times larger than the determined crystallite size of the particles. The polydispersity index (PDI) given shows the width of the measured particle size distribution. The scale ranges from 0 (monodisperse sample) to 1 (polydisperse sample).¹⁷ If the measured PDI is smaller than 0.15 (0.3), the sample is considered to be monodisperse (relatively monodisperse).¹⁸ Thus, the measurement confirms the small particle size distribution of the samples that had already been observed via TEM studies. The (indeed very small) differences in agglomerate sizes between AA-TiO₂ and MEEAA-TiO₂ may be due to the diverse character of the surface ligands.

Table II - 1. Agglomerate sizes of AA-TiO₂ and MEEAA-TiO₂ dispersions at pH = 2 – 3; determined via dynamic light scattering measurements directly after synthesis and after ultrasonic treatment.

	after synthesis		after US treatment	
	hydrodynamic diameter [nm]	PDI [-]	hydrodynamic diameter [nm]	PDI [-]
AA-TiO₂	79.4 ± 1.5	0.2	22.5 ± 0.8	0.2
MEEAA-TiO₂	84.1 ± 1.2	0.2	25.5 ± 0.9	0.2

II.1.2. Surface moieties

While no significant differences in size and morphology were detected for AA-TiO₂ and MEEAA-TiO₂, IR studies revealed discrepancies in their surface functionalities due to the educts utilized for their synthesis. All potential organic surface moieties of both systems are shown in Figure II - 3. Beside hydroxyl groups which are typical for TiO₂ NPs, AA-TiO₂ is coordinated by sulfonate and acetyl acetate groups which decompose into acetates due to heat treatment during their synthesis (Figure II - 3 a). MEEAA-TiO₂ bears MEEAA derivatives on its surface (Figure II - 3 b).



Figure 1 consists of two parts. Part (a) is an FTIR spectrum plot showing transmission [%] on the y-axis and wavenumber [cm^{-1}] on the x-axis, ranging from 3500 to 500. Two curves are shown: a red curve for AA- TiO_2 and a blue curve for MEEAA- TiO_2 . The red curve has peaks labeled: ν OH (around 3400 cm^{-1}), ν CH_2 , CH_3 (around 2900 cm^{-1}), ν_{as} carboxylate (around 1700 cm^{-1}), ν_{s} carboxylate bridging coordination (around 1550 cm^{-1}), ν_{s} carboxylate unidentate + bidentate coordination (around 1400 cm^{-1}), OH bending (around 1350 cm^{-1}), ν C- CH_3 (around 1250 cm^{-1}), ν C-O-C (around 1100 cm^{-1}), ν Ti-O-Ti (around 1000 cm^{-1}), and ν_{as} SO_2 (around 1150 cm^{-1}). The blue curve has peaks labeled: ν OH (around 3400 cm^{-1}), ν_{as} carboxylate, OH bending (around 1700 cm^{-1}), ν_{s} carboxylate bridging coordination (around 1550 cm^{-1}), ν_{s} carboxylate unidentate + bidentate coordination (around 1400 cm^{-1}), ν C-O-C (around 1100 cm^{-1}), and ν Ti-O-Ti (around 1000 cm^{-1}). Part (b) is a schematic diagram of the chemical structure showing the coordination of carboxylate groups on the TiO_2 surface. It illustrates three types of coordination: bidentate (two oxygen atoms of a carboxylate group coordinated to a single Ti atom), unidentate (one oxygen atom of a carboxylate group coordinated to a single Ti atom), and bridging (one oxygen atom of a carboxylate group coordinated to two Ti atoms).

The carboxylate groups can be bound onto the particle surface via three different coordination types (Figure II - 4b): bridging, unidentate and bidentate coordination. While in the asymmetric stretching vibration the coordination modes cannot be distinguished, the symmetric vibrations show bands at different wavenumbers: The symmetric stretching of their bridging coordination can be found at 1442 cm^{-1} (AA-TiO₂) and $1456\text{ -}1423\text{ cm}^{-1}$ (MEEAA-TiO₂).¹⁹ Unidentate and

bidentate coordinations cause signals at 1348 cm^{-1} (AA-TiO₂, only weak) and 1327 cm^{-1} (MEEAA-TiO₂) due to symmetric stretching vibrations.¹⁹ MEEAA-TiO₂ additionally shows the symmetric C-O-C vibration at 1126 cm^{-1} ²⁰, while for AA-TiO₂ the stretching vibration of C-CH₃ (1236 cm^{-1})²¹ is seen as a signal. The spectrum of AA-TiO₂ also proved the presence of sulfonates due to vibration bands at 1159 cm^{-1} and 1124 cm^{-1} (symmetric stretching of SO₂).²⁰ The signals at 1045 cm^{-1} and 1012 cm^{-1} may also be caused by sulfonate groups (asymmetric stretching vibrations).²⁰ The stretching vibration of the Ti-O-Ti bond ($400 - 900\text{ cm}^{-1}$)²² can be detected for both NP systems as expected. Furthermore, the stretching and bending vibrations of the hydroxyl groups of the particles produce signals at about 3200 cm^{-1} and 1620 cm^{-1} , respectively.²³ Those might cover eventual signals caused by other organic groups such as CH₂ and CH₃ (2900 cm^{-1})²⁰ vibrations.

The isoelectric points (IEPs) of AA-TiO₂ and MEEAA-TiO₂ in dispersion (as synthesized) were determined by zeta potential measurements as a function of pH. Figure II - 5 shows both determined curves which exhibit typical zeta potential progressions for TiO₂ NPs. Their IEPs were found at a pH of around 6.3 (AA-TiO₂) and 6.7 (MEEAA-TiO₂), respectively. These values coincide with the general literature values for titanium dioxide NPs ($\text{pH}(\text{IEP}) = 3-7$).²⁴ Furthermore, the isoelectric point also explains the fact that the NP dispersions after synthesis are very stable and mainly without agglomerates as at pH 2 to 3 the particles are highly electrostatically stabilised due to highly positive zeta potentials. It is generally accepted that zeta potentials over $\pm 30\text{ mV}$ indicate a stable particle dispersion.²⁵⁻²⁷

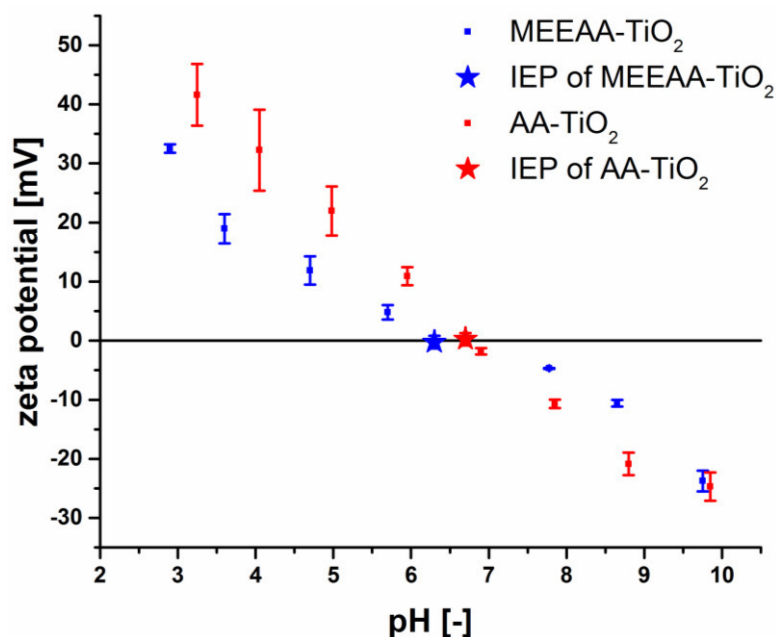


Figure II - 5. Zeta potential titrations of AA-TiO₂ and MEEAA-TiO₂ water dispersions as a function of pH.

To complete the analysis of the surface groups of both particle systems, thermogravimetric (TGA) and differential thermal analyses (DTA) of the (first washed and then dried) particle samples were carried out. The results are shown in Figure II - 6. AA-TiO₂ shows a mass loss of 13 % and MEEAA-TiO₂ of 9 % when heated up to 800 °C (Figure II - 6 a). As at this temperature all organic material is supposed to be eliminated while TiO₂ remains, one can conclude that an AA-TiO₂ particle bears 13 mass-% of organic groups while a MEEAA-TiO₂ particle only 9 mass-%. DTA reveals a broad exothermic signal over the entire measured temperature range for both sample (Figure II - 6 b). MEEAA-TiO₂ shows a maximum between 300 and 400 °C, compared to between 400 and 500 °C for AA-TiO₂.

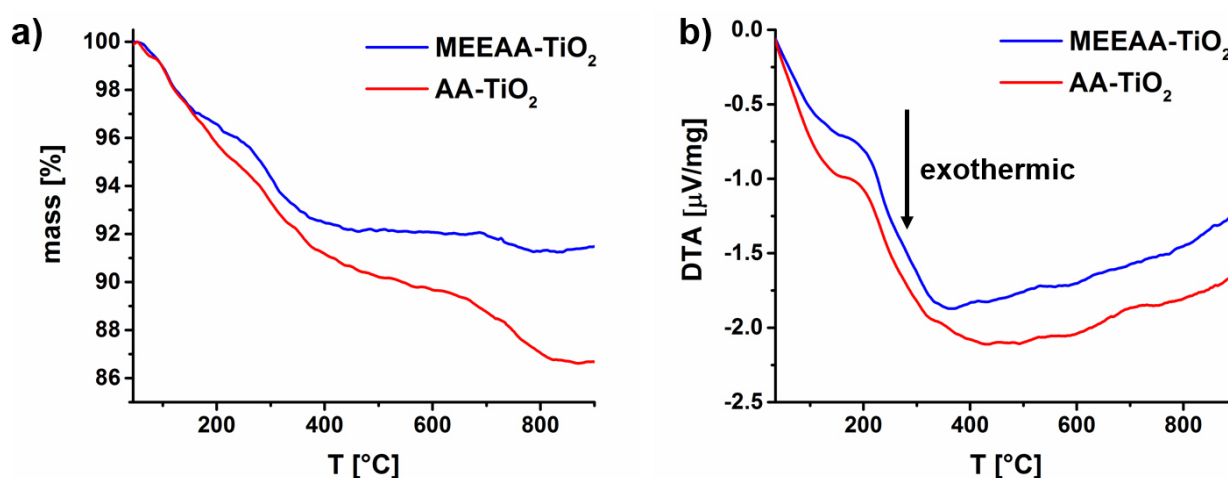


Figure II - 6. Simultaneous thermogravimetric (TGA, a) and differential thermal analysis (DTA, b) performed on dried AA-TiO₂ and MEEAA-TiO₂ particle samples.

The TGA curve of AA-TiO₂ can be divided into 3 sections: under 500 °C there is a fast and almost continuous mass loss, from 500 to 700 °C only a slight mass loss and over 700 °C a second phase of strong mass loss. Comparing these observations to the evolved gas analysis via mass spectroscopy (MS) during the experiment (Figure II - 7), it can be seen that in the first section mainly adsorbed water or hydroxyl groups on the particle surface (because of ionic mass fragments: OH⁺, OH₂⁺) and only small amounts of organics (C₃H₅⁺, CO₂/C₂H₄O⁺) are released around 100 °C. This is followed by a degradation of PTSA (SO₂⁺, SO⁺, CH₃, C₂H₆⁺) and acetate as well as acetylacetonate groups (C₂H₅O⁺, C₂H₅OH⁺, C₂H₄O₂⁺, CO₂/C₂H₄O⁺) around 200 °C. Finally there is only a release of CO₂/C₂H₄O⁺ probably due to further degradation of acetate and acetylacetonate around 300 to 400 °C. The low degradation in the second part is confirmed by the MS data as from 500 to 700 °C, there is only a minimal amount of CO₂/C₂H₄O⁺ detected which indicates that all organic components of the surface groups are eliminated. The mass loss in the last section is due to a further decomposition of the inorganic parts of PTSA (SO₂⁺, SO⁺) over 700 °C.

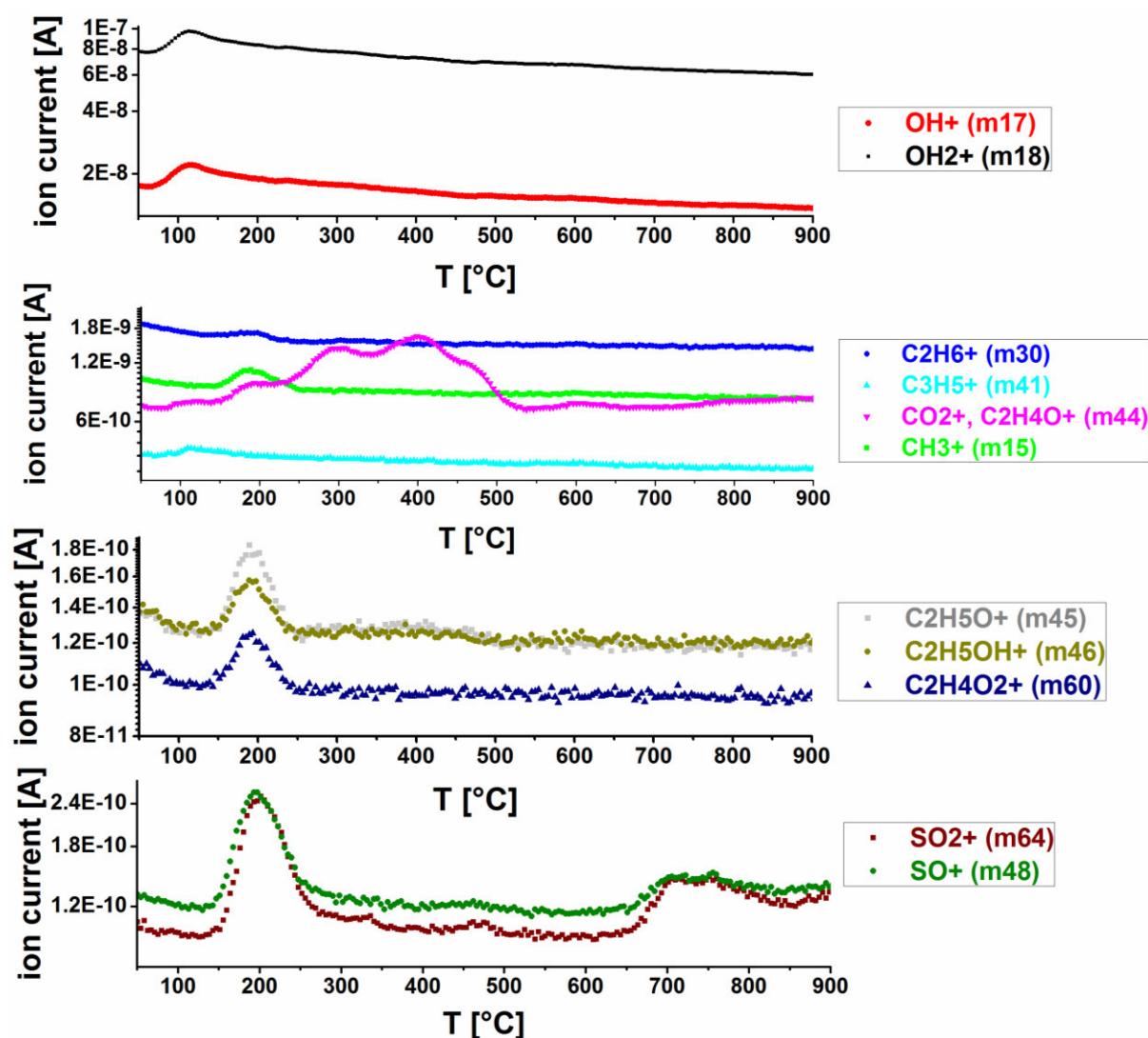


Figure II - 7. Evolved gas analysis by mass spectrometry during TGA/DTA experiments on dried AA-TiO₂ particle sample.

In the case of MEEAA-TiO₂ the TGA curve (Figure II - 6) can also be divided into characteristic decomposition zones and compared to the evolved gas analysis (Figure II - 8). Under 250 °C a first continuous mass loss can be observed, which slows down nearing temperatures close to 250 °C. During this phase, mainly liberated water or hydroxyl groups on the particle surface and only small amount of organics (C₃H₅⁺, CO₂/C₂H₄O⁺) can be detected around 100 °C, followed by the main decomposition of the MEEAA (C₂H₅O⁺, C₂H₅OH⁺, C₂H₄O₂⁺, CH₃, some CO₂/C₂H₄O⁺, and small amounts of C⁺). Between 250 and 450 °C, the mass loss increases again, while only small organic fragments are evolved (CO₂/C₂H₄O⁺ and C⁺). Above 450 °C, there is almost no mass loss indicating that all organic components are already eliminated (only small amounts of evolved CO₂/C₂H₄O⁺ can be still detected).

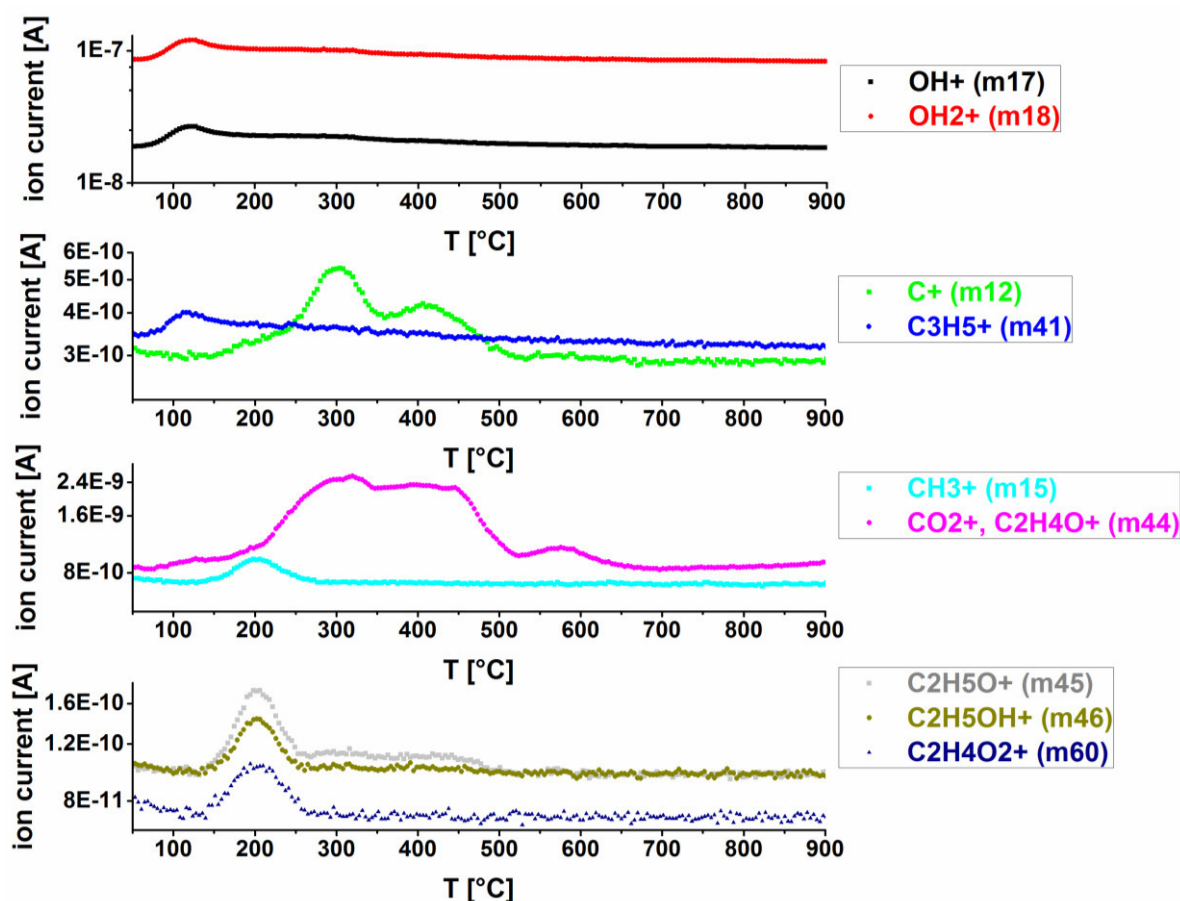


Figure II - 8. Evolved gas analysis by mass spectrometry during TGA/DTA experiments on dried MEEAA-TiO₂ particle sample.

II.1.3. Photocatalytic activity

After having analysed the size, morphology, dispersion state, surface properties and organic surface groups of both particle systems, their PC activity was examined due to its importance for later applications. For the photocatalysis test, dichloroacetic acid (DCA, 1 g/l) was added into the NP (100 mg/l) water dispersion and compressed air was bubbled into the experimental set-up. When UV light was applied, DCA was photocatalytically degraded into CO₂ and Cl⁻ (HCl) as already discussed in Chapter I.1.2. and the produced chloride ions were measured in-situ. The in-situ measurement was chosen as other degradation tests require the removal of the NPs. This would especially be challenging for the particles examined here as they are very small and in a very good dispersion state, making removal by centrifugation difficult and time consuming. The results of the PC degradation tests with AA-TiO₂ and MEEAA-TiO₂ compared to commercial P25 TiO₂ NPs (from Degussa/Evonik) are shown in Figure II - 9. P25 particles were chosen as reference samples as these particles are the best analysed commercial TiO₂ particles, showing an superior PC activity and have therefore often been used as the benchmark system.^{28–31} These particles consist of 80 to 90 % anatase and 10 to 20 %

rutile and possess a primary particle size of 20 to 30 nm.^{29,32} They do not bear organic surface groups and are obtained as powder, which is in general not perfectly dispersible, showing aggregates around 100 nm and agglomerates in solution.^{31,32}

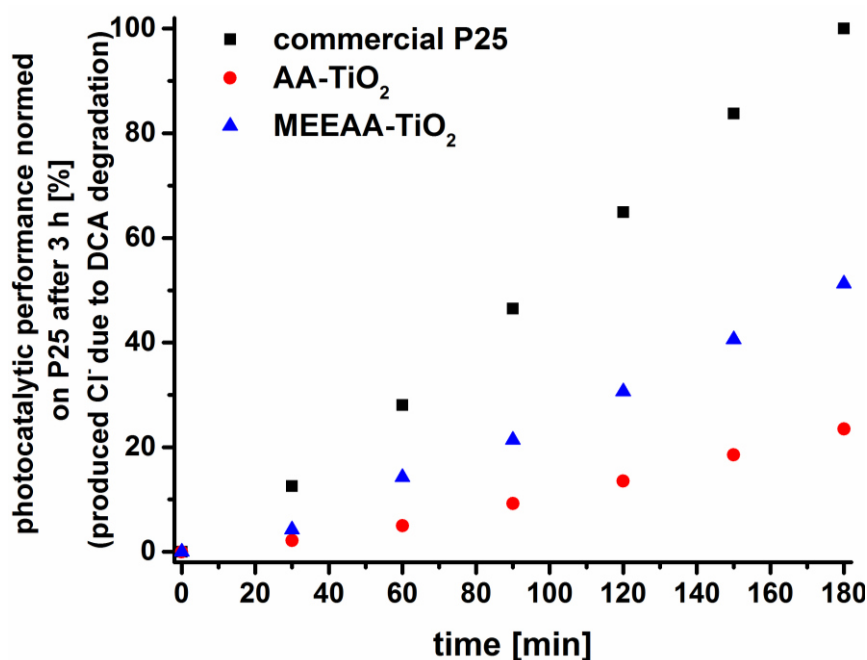


Figure II - 9. Photocatalytic activity of AA-TiO₂ and MEEAA-TiO₂ in comparison to a commercial standard TiO₂ NP (P25); determined by measurement of produced Cl⁻ during the degradation of dichloroacetic acid (DCA). The values are normed on the amount of degraded DCA (produced Cl⁻) by P25 after 3 h photocatalysis test (= 100 %).

If P25 is compared to the synthesized particle samples, its superior PC activity becomes evident. Nevertheless, this is not very significant as the synthesized samples are only obtained in the pure anatase phase and bear organic surface groups, which may both be factors for a decrease in PC activity. Comparing both synthesized particle systems, MEEAA-TiO₂ seems to be twice as active as AA-TiO₂. This can be deduced from the higher amount of organic groups that was found during TGA measurements (II.1.2) on the AA-TiO₂ particle surface. These prevent the possible absorption of DCA or water onto the particle surface as well as decreasing the amount of possible hydroxyl groups bound on the surface, which are crucial for the PC degradation reactions.²⁸ Taking into consideration the later biological or medical applications of the particles, these results may not be representative as the DCA degradation took place under strongly acidic conditions (due to the acidity of this organic compound). In contrast to that, all biological tests have to be carried out at physiological pH (~7.4) and it has already been indicated that the PC activity of a sample can also be influenced by the pH.^{31,33–36} This can be explained by the change of the surface charge on the particle if the pH is varied. It leads first to a different adsorption behaviour of the organic molecule onto the particle surface and second, to a completely changed dispersion state of the sample.³¹ If there are more

agglomerates in the dispersion, less free surface area is offered for photocatalysis resulting in a decreased activity. Furthermore, the PC efficiency of a material can also depend on the nature of the degradable compound which means that the success of the degradation of biological cell components can be significantly different from what was measured for DCA.^{31,36–38} This is first due to the absorption properties of the compound onto the particle surface and second, due to functional groups of the molecule that facilitate OH radical attacks.³¹ Still, this PC activity test is a promising, first indicator for the efficiency of the synthesized particle samples.

II.2. Influence of hydrothermal processing parameters on MEEAA-TiO₂ particles

For the examination of the hydrothermal processing parameters on the properties of the synthesized TiO₂ particles, only MEEAA-TiO₂ samples are discussed in this chapter as this system seemed to be the more promising one concerning its PC activity. Additionally, AA-TiO₂ samples showed the same trends (Appendix I) as MEEAA-TiO₂ in the changes of its size, surface groups and PC activity manipulated by the hydrothermal processing parameters. As well as the standard sample MEEAA-TiO₂ which was treated in the autoclave at 160 °C for 4 h, it was decided to examine four additional samples: 2 treated with other temperatures (180 and 200 °C) for 4 h and two treated with varied durations (1 and 16 h) at 160 °C. First the sizes and morphologies, then the surface moieties and PC activities are discussed in the following analysis (similar to II.1).

II.2.1. Size and morphology*

To determine differences in the size and morphology of MEEAA-TiO₂ treated with different autoclaving parameters, XRD, TEM, N₂ sorption and DLS measurements were conducted. The results of all analyses are summarized in Table II - 2 and will be discussed in detail in the following.

Table II - 2. Particle (XRD, TEM) and agglomerate sizes (DLS) as well as experimental (BET) compared to theoretic specific surface area of MEEAA-TiO₂ samples treated with varied autoclaving parameters.

sample: treatment time / temperature	crystallite size [nm] (XRD)	NP size [nm] (TEM)	hydrodynamic diameter [nm] / PDI [-] pH 2-3, US-treated (DLS)	specific surface area [m²/g] (BET, N₂ sorption)	theoretic specific surface area [m²/g]
1 h / 160 °C	4.8	5.5 ± 1.2	17.8 ± 0.2 / 0.2	253.1	320.5
4 h / 160 °C (standard sample)	5.5	5.7 ± 1.0	23.8 ± 0.3 / 0.2	231.2	279.7
16 h / 160 °C	6.9	6.5 ± 1.0	28.8 ± 0.6 / 0.1	200.8	223.0
4 h / 180 °C	6.5	7.1 ± 1.1	29.0 ± 0.6 / 0.1	214.2	236.7
4 h / 200 °C	7.7	8.1 ± 1.3	32.8 ± 0.8 / 0.1	185.2	199.8

* Parts of this chapter have been submitted to Nanoscale for publication. The submitted title is "Discovering the determining parameters for the photocatalytic activity of TiO₂ colloids based on an anomalous dependence on the specific surface area".

XRD measurements (Figure II - 10) confirmed for all samples a pure anatase crystal phase without any detectable amorphous TiO_2 .

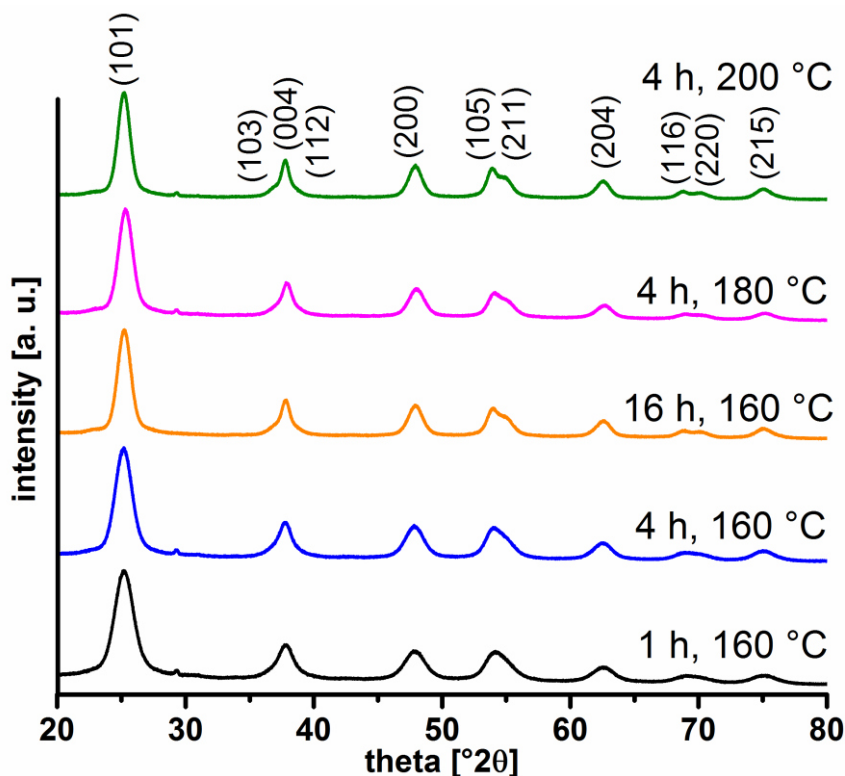


Figure II - 10. Powder X-ray diffraction (XRD) patterns of MEEAA- TiO_2 samples treated with varied autoclaving parameters.

In Table II - 2, the crystallite sizes calculated from XRD, using the Scherrer equation, are compared to the particle sizes determined on TEM images (Figure II - 11). The TEM micrographs show the same size range for the NPs as obtained from XRD, while their average size is slightly larger. This is not significant, however, as the size determination of particles on TEM images yields a large standard deviation due to difficulties to measure the diameter of slightly oval shaped particles uniformly and correctly. Both methods indicate the expected^{39,40} particle growth with increasing treatment time or temperature. The measured specific surface area of the samples S_{exp} , done via gas sorption, confirms the increase in size by declining surface area. It can be compared to the theoretic, calculated specific surface area S_{calc} of a TiO_2 sample. S_{calc} for each sample is listed as well in Table II - 2. These values are close to the experimental ones, confirming the reliability and quality of all experimental measurements. The slight discrepancy between measured and calculated values is not surprising, keeping in mind the unavoidable errors such as a wider particle size distribution and the particle morphology deviation, which are made upon the simplification of assuming a perfect sphere to represent the NPs. To complete the analysis of the influence of processing parameters on the particle size and morphology, dynamic light scattering measurements were carried out (Table

II - 2). The measurements confirm in all cases monodisperse or almost monodisperse samples with probably no agglomerates as already stated for the standard sample in II.1.1.

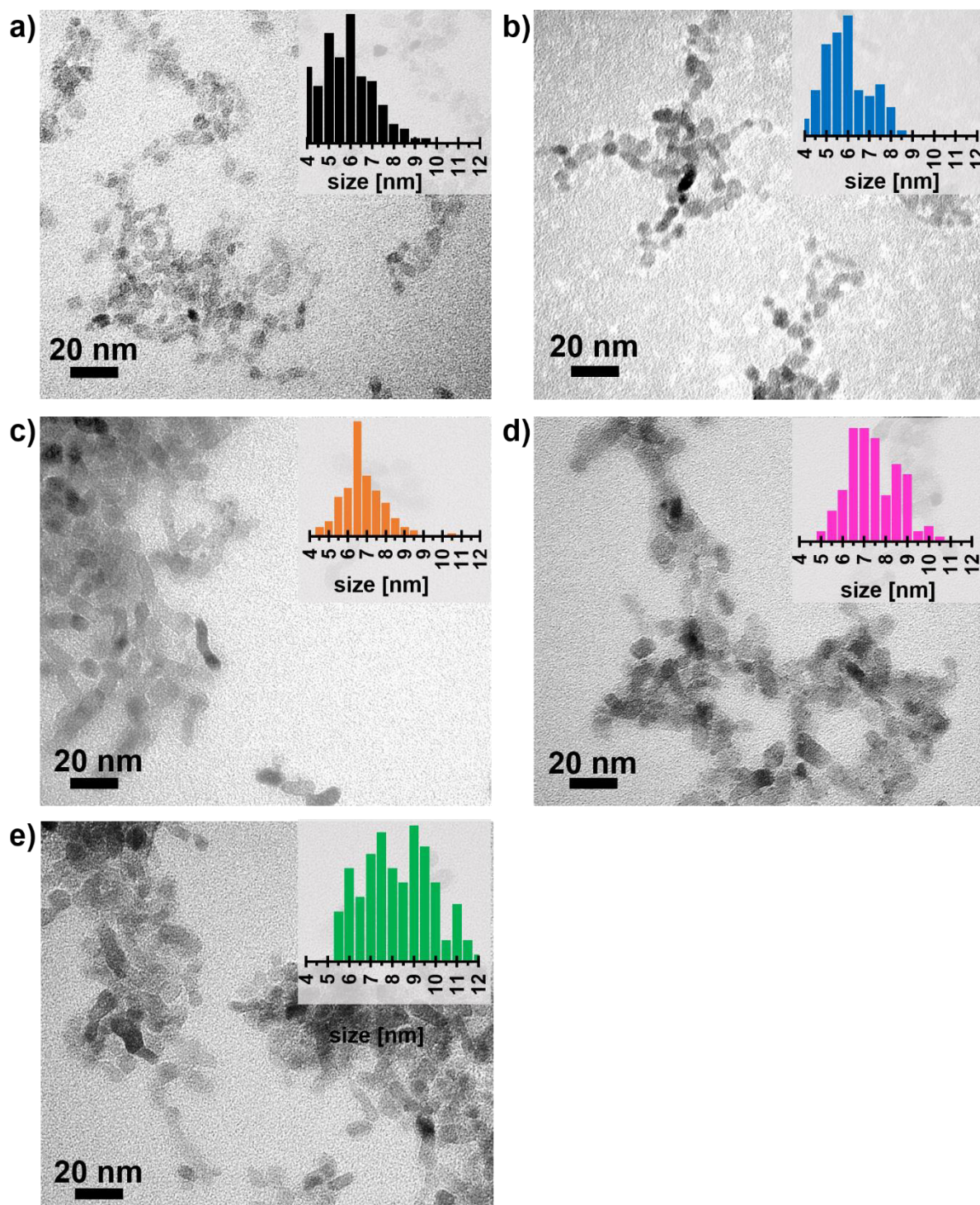


Figure II - 11. Transmission electron microscopy (TEM) of MEEAA-TiO₂ samples treated with varied hydrothermal processing parameters and their particle size distributions, obtained from counting at least 100 particles per sample: a) 1 h, 160 °C; b) 4 h, 160 °C; c) 16 h, 160 °C; d) 4 h, 180 °C; e) 4 h, 200 °C.

To study eventual changes in the particle morphology or in the exposed facets. TEM micrographs and XRD diffractions were studied more intensely. Low magnification TEM does not indicate major difference in morphology between the 5 particle samples. Nevertheless, with increasing treatment temperatures the particles appear to be slightly oval. This visual tendency can also be confirmed by the size evaluations as the measured sizes for the samples with higher processing temperatures (Figure II - 11 d) and e) are statistically scattered over a wider size range. As shown in literature, the morphology of anatase crystals also influences the appearance of their XRD diffraction patterns i.e. the relative intensities of certain diffraction signals.^{41–45} If one takes a closer look on the acquired XRD diffractions, it becomes evident that the relative intensities especially around $38^\circ 2\theta$ and 54 to $55^\circ 2\theta$ change depending on the autoclaving parameters. In Figure II - 12 a) and b), two enlarged studies of the reflex patterns are shown in which the relative signal intensities change with increasing autoclaving time or temperature of the samples.

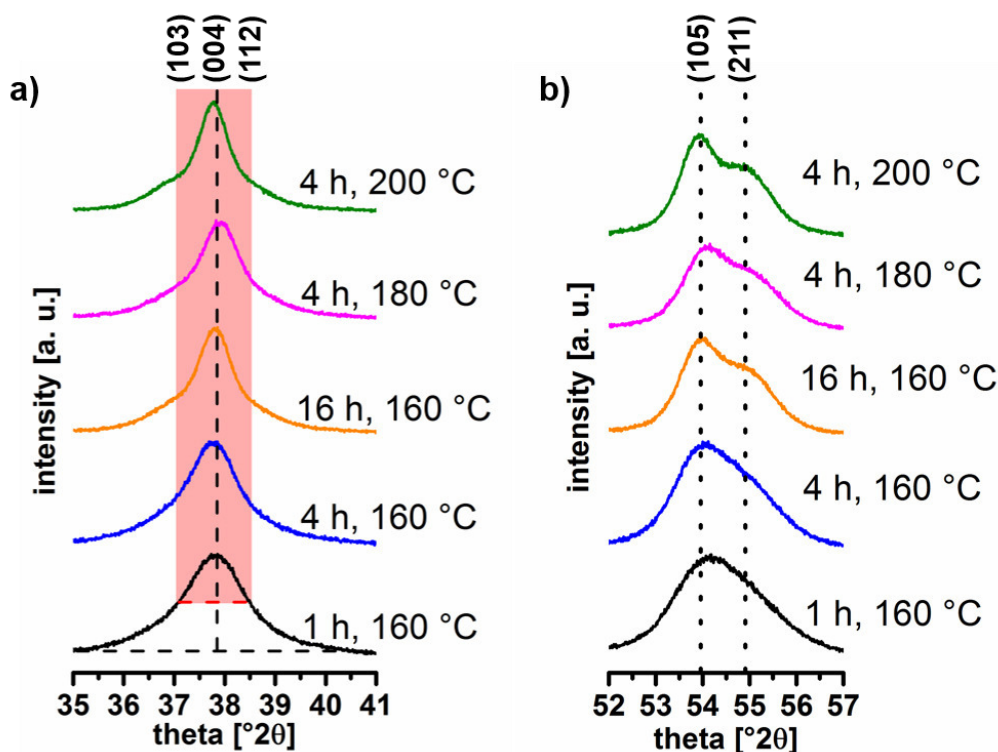


Figure II - 12. Powder X-ray diffraction (XRD) patterns of MEEAA-TiO₂ samples treated with varied autoclaving parameters – enlarged studies of the signals of a) the reflexes 103, 004 and 112 and of b) the reflexes 105 and 211.

The relative intensity of (004) increases compared to (103) and (112) and the relative intensity of (211) decreases compared to (105). If these tendencies are compared to literature, it becomes evident, that the equilibrium shape of anatase with eight {011} facets and two {001} facets shows a pattern similar to the sample 1 h, 160 °C. The intensity increase of (004) diffraction peak and therefore the narrowing of its full width at half-maximum has been

observed for the crystal growth along $[001]$ direction.^{41,44,46} This sharpening of the signal at $37.9^\circ 2\theta$ was both shown for crystals exposing 4 additional facets, namely $\{010\}$,^{42,47–49} and for rod-like morphologies without this type of facets.⁵⁰ A higher intensity of (105) compared to (211) is obtained for rod-like crystals while disc-like morphologies with a high percentage of $\{001\}$ facets would lead to a lower intensity of (105) .^{44,50} Therefore, the XRD analysis suggests an elongation of the crystals with increasing hydrothermal treatment time or temperature i.e. with decreasing specific surface area.

In order to gain further insights, high resolution TEM studies were carried out on the two samples 1 h, 160°C and 4 h, 200°C showing the largest differences in their specific surface area. All below discussed images are shown along $[100]$ zone-axis as determined from FFT (see Figure II - 13).

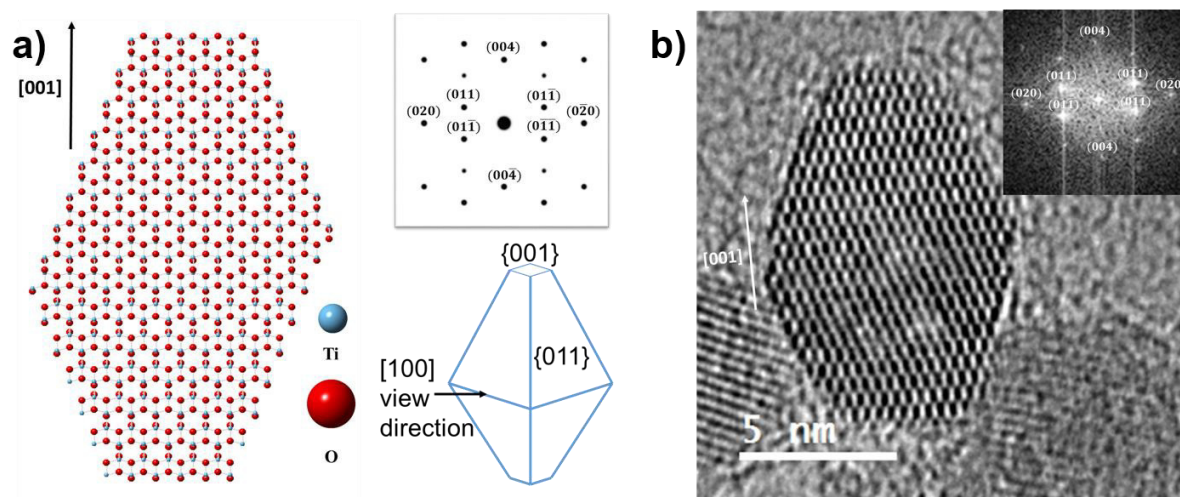


Figure II - 13. Equilibrium shape anatase nanocrystal; a) Structural and corresponding FFT model along $[100]$ view direction as well as 3D sketch with named exposed facets. b) High resolution TEM image and corresponding FFT along $[100]$ view direction.

In the sample 1 h, 160°C only truncated bipyramidal crystals with $\{011\}$ and $\{001\}$ facets were identified (Figure II - 14 a1, a2) which confirm the findings of XRD analysis. In addition, several unexpected crystal morphologies were found, formed by the attachment of at least two primary crystals at the $\{011\}$ facets (Figure II - 14 a3). This phenomenon has already been reported for hydrothermally coarsened anatase particles in acidic water.⁵¹ Nevertheless, these morphologies are not considered to have a high impact on the properties of the examined sample due to their rare appearance. The sample 4 h, 200°C contains, in addition to truncated bipyramidal crystals (Figure II - 13), several other morphologies (Figure II - 14 b). The nanoparticle in Figure II - 14 b1 shows the standard set of $\{011\}$ and $\{001\}$ facets, however, elongation is along $[011]$ direction. The crystal in Figure II - 14 b2 shows a similar rod-like morphology, however, this time it is joined with another nanocrystal near the end of $\{011\}$ facet.

Finally, Figure II - 14 b3 shows a nanoparticle where the surface has a curvature rather than facets.

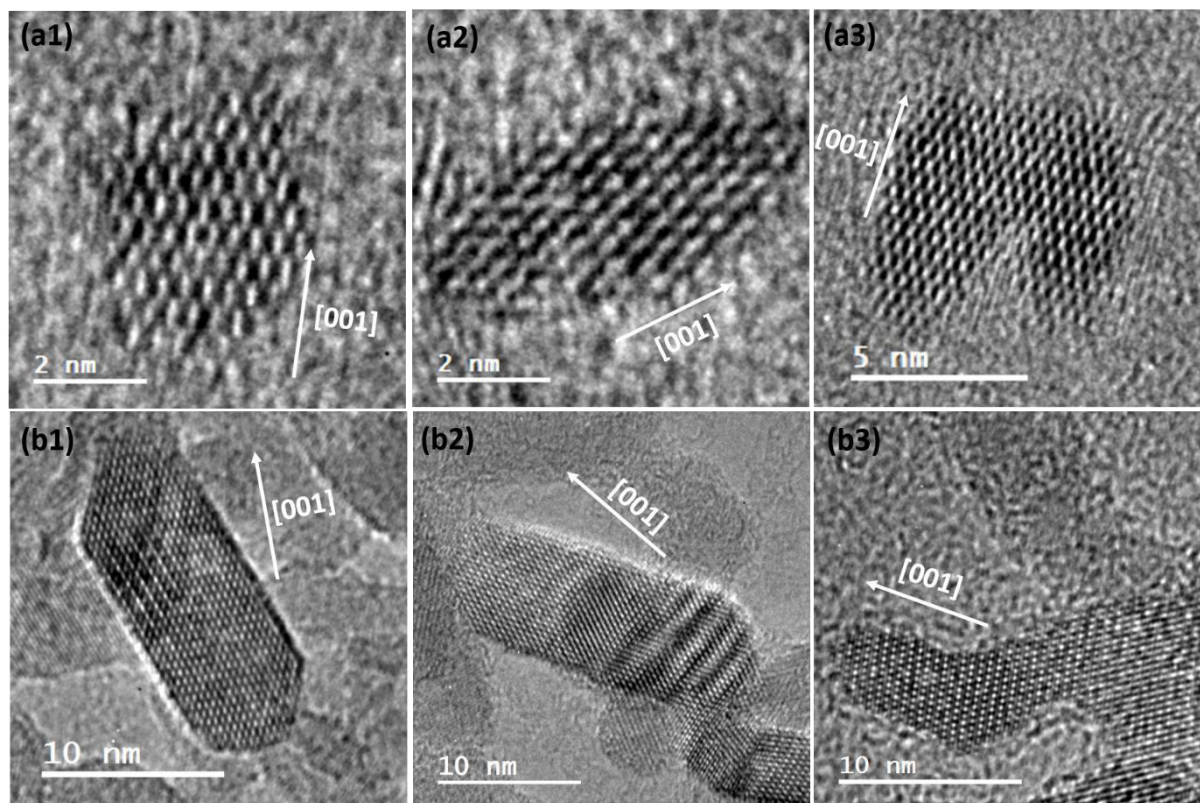


Figure II - 14. High resolution transmission electron microscopy images of TiO_2 nanoparticle samples synthesized at a) 1 h, 160 °C and b) 4 h, 200 °C.

In order to discuss the formation of rod-like particles during increased hydrothermal treatment times and/or temperatures, one has to consider that the formation of nanocrystals from solution consists of nucleation and subsequent crystal growth. Crystal growth in solution (driven by the reduction of surface energy) can either proceed via the growth of a large particle at the expense of smaller ones by addition of single Ti ions (Ostwald ripening) or by oriented attachment of 2 or more nanocrystals. This involves the spontaneous self-organization of neighboring particles in order to share a common crystallographic orientation and subsequent attachment of the particles at their planar interface leading to the development of single homogeneous crystals.^{51,52} The presence of additives can for example impede one of these mechanisms (most commonly the oriented attachment) or guide the growth along a certain crystal plane.^{51–53} The solvent-solute interactions along different orientations of a crystal vary significantly because of the surface atomic arrangements. This results in different surface affinities of the additive towards each facet and in the stabilisation of a specific crystal surface plane as it e. g. lowers the surface energy or changes the surface tension of the bound plane.^{54–56} Some experimental procedures have already reported that carboxylic acids as additives lead to elongated or rod-like crystals.^{50,57,58} However, in contrast to the obtained

nanorods elongated along [011] direction, the crystals were shown to grow preferentially along [001]. Nanorods grown along [001] direction are most probably formed due to either the preferential stabilisation of {010} facets by an additive or the oriented attachment of {001} facets of several single crystals.^{46,51,59} Deduced from these findings, the obtained nanorods grown along [011] direction could be formed due to absorption of MEEAA onto {001} facets leading to a commonly not favored⁵¹ attachment of {011} facets (Figure II - 14 a3, b2). Also the acidic pH and the presences of an excess of water is said to favor the crystal growth via oriented attachment compared to Oswald ripening (even though the cause has not been clarified yet).⁵¹

II.2.2. Surface moieties[†]

To continue the study of the influence of the processing parameters on the NP properties, the following section deals with the behaviour of the surface moieties of the MEEAA-TiO₂ NP systems. For this, zeta potential titrations, TGA studies and IR measurements have been carried out. The IEPs obtained by zeta potential titrations are shown in Table II - 3. All IEP values are between pH 6.4 and 6.7. It is expected that the measuring error for the determination of the IEP is around ± 0.2 and therefore it can be stated that all samples provide the same surface potential. This could be a first indicator that the amount of organic MEEAA groups on the particle surface do not change when the autoclaving parameters are varied. In order to examine this assumption more closely, IR measurements were carried out.

Table II - 3. pHs at IEP of MEEAA-TiO₂ samples with varied processing parameters determined by zeta potential titrations.

treatment time / temperature	1 h / 160 °C	4 h / 160 °C (standard sample)	1 h / 160 °C	4 h / 180 °C	4 h / 200 °C
pH at IEP [-]	6.5	6.7	6.6	6.4	6.6

In Figure II - 15, the obtained DRIFT transmission spectra are shown. It is evident, that the structure or composition of the surface groups is not influenced by the autoclaving parameters. All spectra show the IR bands typical for this NP type which has been discussed in II.1.2. If there is a small change in the amount of organic surface groups on the particle, it cannot be determined by this method. To determine the amount of organic surface groups in the different samples, TGA and DTA measurements were carried out.

[†] Parts of this chapter have been submitted to Nanoscale for publication. The submitted title is "Discovering the determining parameters for the photocatalytic activity of TiO₂ colloids based on an anomalous dependence on the specific surface area".

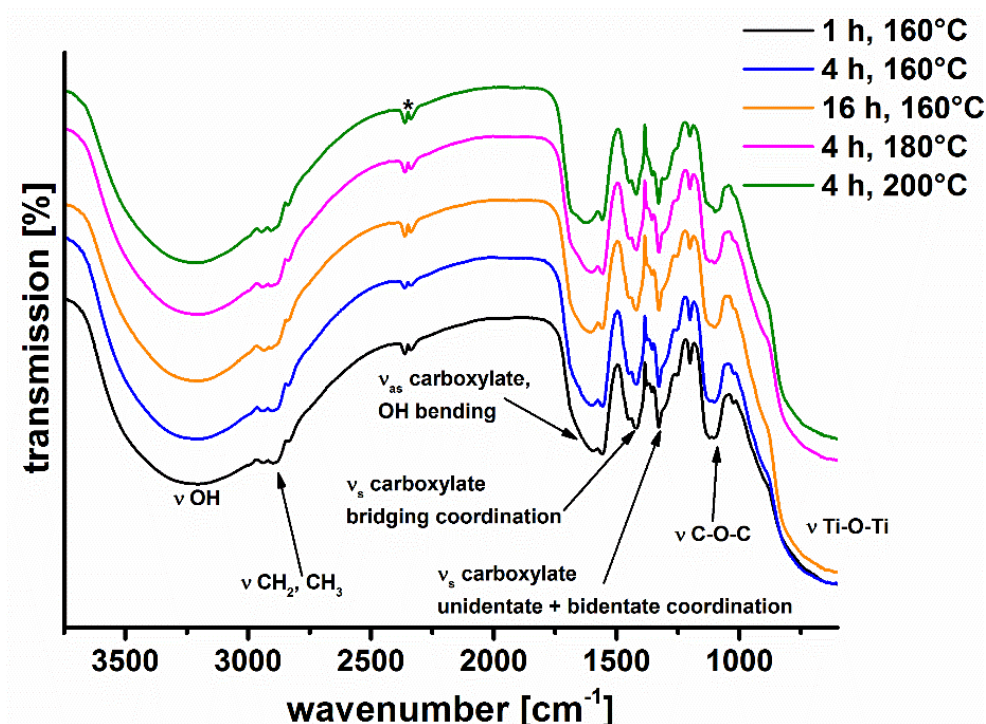


Figure II - 15. IR (DRIFT) spectra of MEEAA- TiO_2 samples synthesized with varied hydrothermal treatment parameters. (* marks a background signal).

In Figure II - 16, both diagrams are displayed. The mass loss takes for all of the samples a similar course due to a characteristic decomposition process of the MEEAA- TiO_2 samples which has been described in II.1.2.

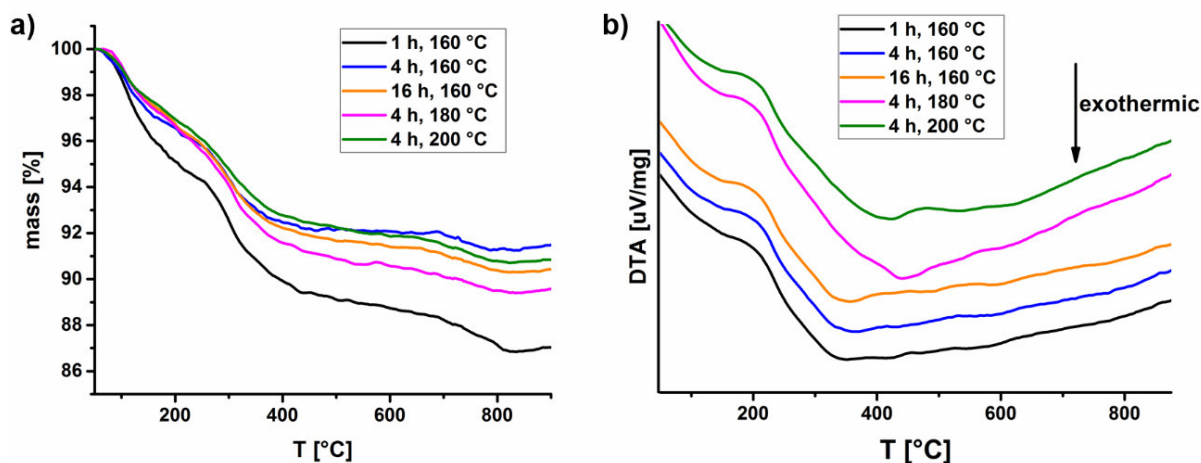


Figure II - 16. a) Simultaneous thermogravimetric (TGA) and b) differential thermal analysis (DTA) performed on dried MEEAA- TiO_2 particle samples synthesized with varied hydrothermal processing parameters.

The amount of organic groups that is removed when heating up to 900 °C, was determined to be between 9 % and 13 %. To examine the amount of surface groups on the particles, the obtained mass of total evolved organic moieties was divided by the experimentally determined specific surface area of each sample (Figure II - 17). The thereby obtained mass of organics,

which can be related to surface groups per square meter, is plotted in dependence of the specific surface area. The results indicate that the amount of organic surface moieties per square meter is the same for all samples. A slight variance such as for sample 4 h, 160 °C may be caused by experimental errors in mass or temperature determination or small sample heterogeneities.^{60,61}

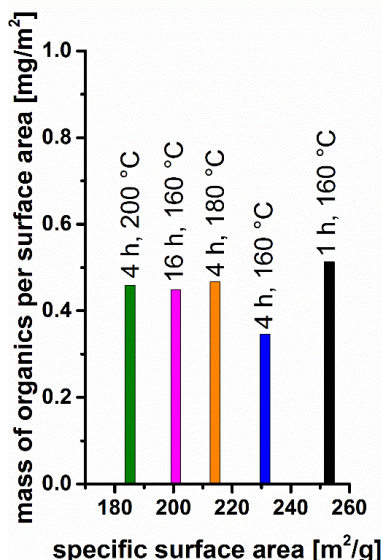


Figure II - 17. Mass of organic surface groups per square meter calculated based on TG analysis and plotted versus the specific surface area of the samples.

The exothermic DTA curve does not show any differences for the MEEAA-TiO₂ samples treated for different time spans; the signal maximum can always be found around 350 °C. In contrast, if the autoclaving temperature is increased, the signal maximum shifts slightly to higher temperatures from ~ 350 °C to ~ 400 °C for an autoclaving temperature of 180 °C and ~ 450 °C for an autoclaving temperature of 200 °C. This may indicate that because of the higher autoclave treatment the organic acid (which is complexed onto the particles) is slightly more heat resistant. This impression can be confirmed by the evolved gas analysis using mass spectrometry during TGA and DTA experiments (Figure II - 18). While most of the evolved mass curves do not show any changes for all samples, in the case of CO₂⁺/C₂H₄O⁺, C₂H₅O⁺ and C⁺ the ion current stays higher up to a temperature of around 750 °C for the samples treated with a higher autoclaving temperature.

To conclude, one can state that the MEEAA coordinated onto the particle surfaces is not significantly modified. In the case of zeta potential titrations and IR measurements, no differences between the samples were measured. Only the evolved mass analysis during TGA studies indicated a small change in the properties of the organic surface groups when the hydrothermal treatment temperature is increased.

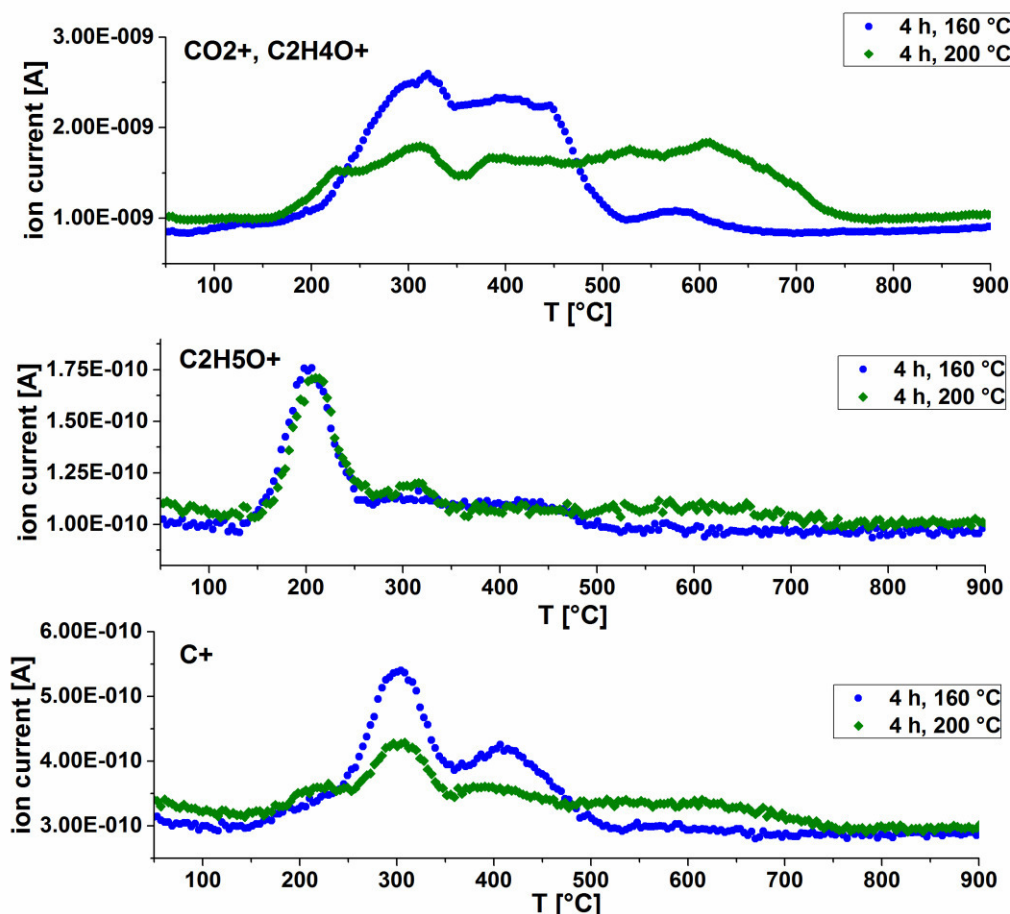


Figure II - 18. Evolved gas analysis by mass spectrometry during TGA/DTA experiments on dried MEEAA-TiO₂ particle samples synthesized with varied hydrothermal processing parameters.

II.2.3. Photocatalytic activity[‡]

To complete the study of MEEAA-TiO₂ samples treated with varying processing parameters, the PC activity of the particles was examined. For this, the PC DCA degradation was carried out for all samples and compared to commercial P25 TiO₂ NPs. The results are shown in Figure II - 19. As one can see in Figure II - 19 a) the same PC activity as of the bench mark material P25 can be achieved or even surpassed by the particle sample treated for 4 h at 200 °C. Furthermore, the photocatalysis curve of P25 is rather linear while of the synthesized particles it seems to be less efficient initially but increases with longer UV-light application time. To explain this, one has to keep in mind that P25 is synthesized via a high temperature pyrogenic process⁶² and therefore does not bear organic surface groups. That is why it decomposes

[‡] Parts of this chapter have been submitted to Nanoscale for publication. The submitted title is "Discovering the determining parameters for the photocatalytic activity of TiO₂ colloids based on an anomalous dependence on the specific surface area". All XAFS measurements, analyses, modelling and discussion were carried out by the researchers of the "Bundesanstalt für Materialprüfung BAM", mainly Wojciech Szczerba. It is used here with Wojciech Szczerba's permission.

directly the test substance DCA right from the beginning. In contrast the MEEAA-TiO₂ particles, are possibly first degrading their own surface groups before starting to decompose the DCA. This explains why at first a smaller amount of generated chloride ions is measured. Moreover, this diagram indicates that the particle samples show in general a higher PC activity with increasing hydrothermal treatment time or temperature. This phenomenon is rather surprising as with increasing treatment temperature or duration, the particles grow resulting in a smaller surface area. According to the literature,^{31,34} the PC activity of NPs decreases with smaller specific surface area as the photocatalysis is a surface-dependent process. In this study the effect is vice versa as displayed in Figure II - 19 b).

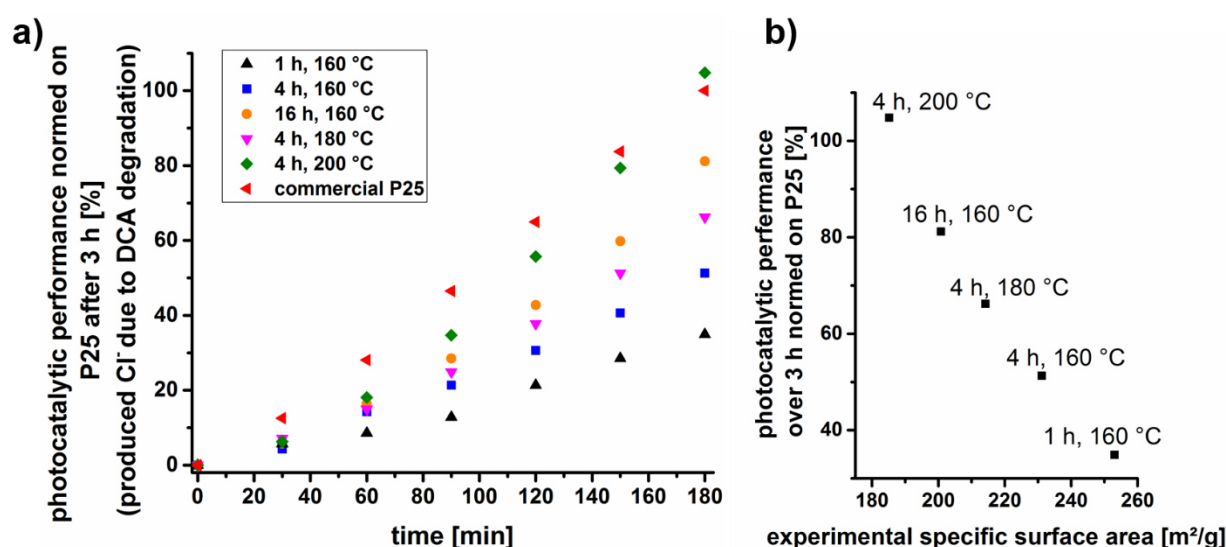


Figure II - 19. Photocatalytic activity of MEEAA-TiO₂ samples synthesized with varied processing parameters in comparison to a commercial standard TiO₂ NP (P25); determined by measurement of produced Cl⁻ during the degradation of dichloroacetic acid (DCA). a) Photocatalytic activity shown over the time of 3 h and b) total photocatalytic performance after 3 h compared to the BET specific surface area determined by N₂ sorption measurements. The values are normed on the amount of degraded DCA (produced Cl⁻) by P25 after 3 h photocatalysis test (= 100 %).

The first guess for a reason explaining this surprising observation could be that the amount of organic groups on the particle surface could have manipulated the PC performance of the samples. As the photocatalysis is a surface process, the coverage by organic molecules decreases the performance. If the smaller particles which are synthesized with lower treatment times and/or temperatures, exhibited significantly more surface moieties than the larger particles, the lower PC activity could be explained. As already shown in II.2.2, the presence of organic surface groups on the anatase particles was confirmed and these may certainly hinder their photocatalysis. However, very important to note is that no significant differences between the samples were found that could explain their anomalous PC performance dependence on the NP size.

Besides organic molecules covering the crystal surface, the presence of oxygen defects in the crystal lattice can influence the PC performance as already mentioned in Chapter I.1.2.^{63–65} To examine the possible presence of oxygen defects, the composition and the valence state of the synthesized samples were investigated by X-ray photoelectron spectroscopy (XPS). The XPS analyses (Figure II - 20 a) reveal that, as expected, Ti, O and C (as well as N from the atmosphere and In from the substrate) were detected within all samples. The Ti $2p_{3/2}$ and Ti $2p_{1/2}$ XPS peaks at 459.5 eV and 465.5 eV (Figure II - 20 b) are characteristic for Ti^{4+} -O bonds in TiO_2 .^{63–66} If a considerable amount of oxygen vacancies was present within the TiO_2 crystal, a peak at the high energy side of the Ti $2p_{3/2}$ XPS peak around 457.0 eV typical for Ti^{3+} species would be expected.^{65,66} This peak was not found in any of the samples indicating the absence of bulk defects (with bulk meaning the particle interior, not surface atoms).⁶³

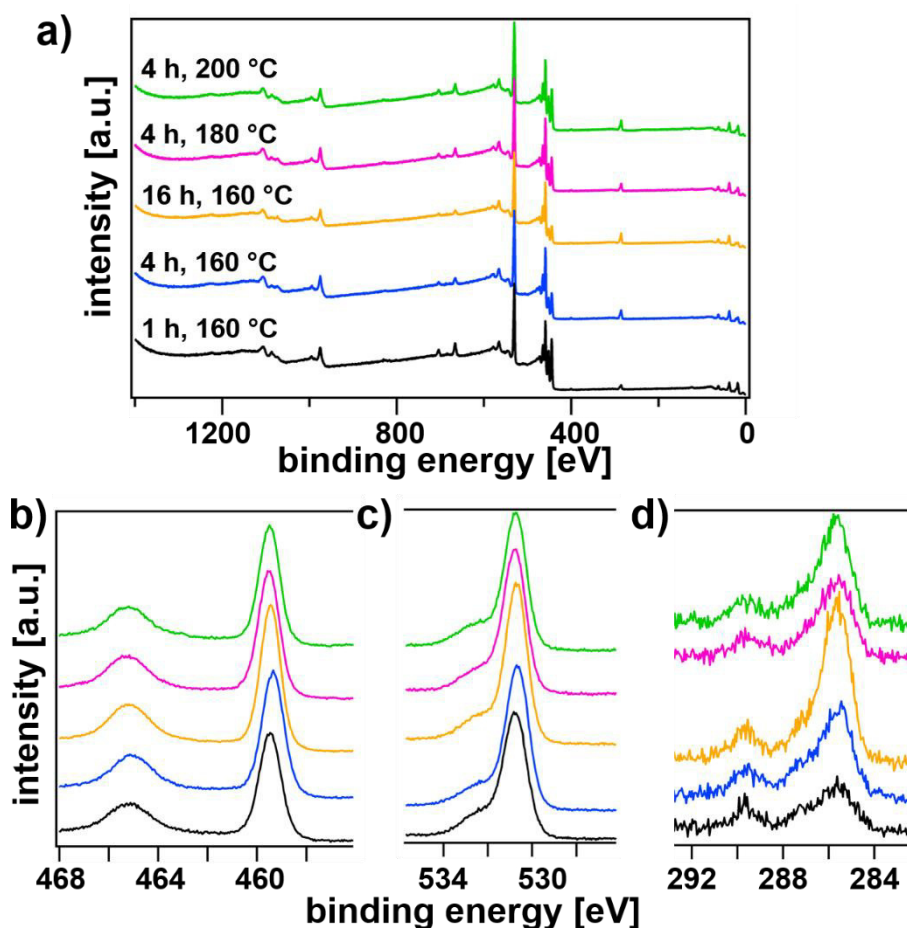


Figure II - 20. a) Spectra obtained by XPS survey of synthesized TiO_2 samples and enlarged studies of the b) Ti $2p$, c) O $1s$ and d) C region.

In the O $1s$ region (Figure II - 20 c), the XPS peak at 530.8 eV is assigned to crystal lattice oxygen ($O-Ti^{4+}$).⁶³ The shoulder around 533 eV is caused by hydroxide species which belong to surface-bound water or MEEAA. In the C region (Figure II - 20 d), the main XPS peak (~286 eV) is caused by contamination from air, while the second peak at the higher binding energy

(~290 eV) may be attributed to carboxyl species from the surface groups of the NPs. To conclude these analyses, the XPS results do not indicate the presence of oxygen defects. However, XPS analysis concerning oxygen vacancies of the investigated anatase powder samples was very difficult as they were synthesized ex-situ and therefore the measurement was negatively influenced by the air contamination and by the In substrate used.

Hence, x-ray absorption fine structure (XAFS) spectroscopy has been carried out as XAFS spectra are very sensitive to differences in the local environment of a given element. The extended x-ray absorption fine structure (EXAFS) featured by oscillations stretching up to 1 keV beyond the absorption edge bear information on the local symmetry of the absorbing element. The Fourier transform delivers a radial distribution function of the surrounding atoms. Such an EXAFS pattern consists usually of a sequence of peaks that are interpreted as coordination shells surrounding the absorber atom. The amplitude of these peaks is proportional to the effective coordination number, which can be affected by the surface-to-volume ratio in the case of nanocrystallites, as well as by the presence of a significant number of vacancies in the given coordination shell. The obtained spectra show, as expected, different peak amplitudes for the different samples, while the peak positions remain the same indicating that the lattice parameters stay unchanged (Figure II - 21).

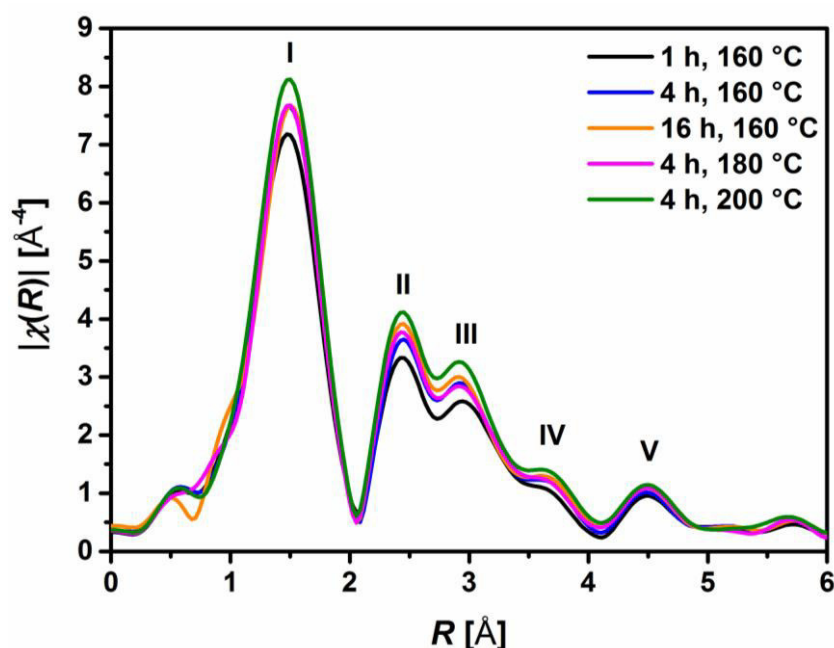


Figure II - 21. The module of the Fourier transformed EXAFS spectra of MEEAA- TiO_2 samples; the differences in the intensities of peak I and II are subject of the analysis.

Peak I is contributed by single scattering events of the nearest six oxygen neighbors. Its amplitude of the coordination shell peak is influenced by present oxygen deficiencies. However, the amplitude of the coordination shell peak might be influenced by the presence of

vacancies as well as by the small sizes of the particles. Unfortunately, the samples have different particle sizes and the intensities of peak I do not show any clear relation neither with respect to the PC activity nor to the crystallite size.

According to the theoretical model calculations peak II is contributed mainly by scattering off the Ti atoms in the second coordination shell. Since the Ti sublattice is assumed not to have a significant number of vacancies the intensity of the second shell peak should be proportional to the crystallite size. Indeed the intensities of peak II exhibit a linear dependence on the crystallite size obtained from XRD (Figure II - 22).

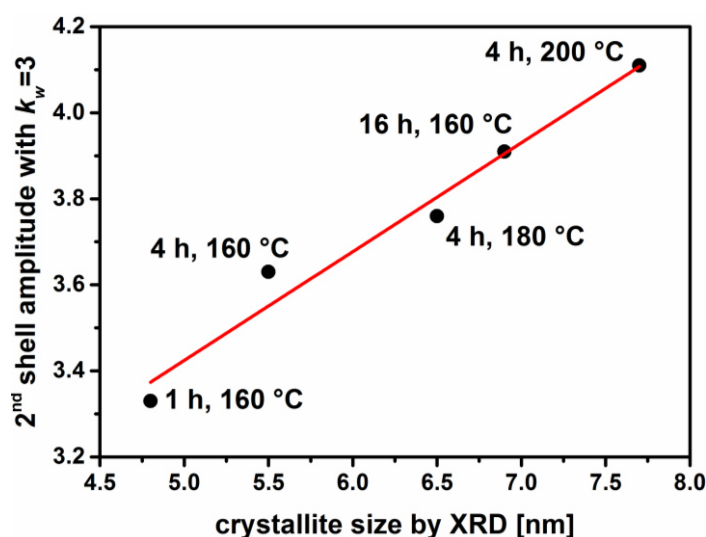


Figure II - 22. The amplitude of the second coordination shell (peak II of the EXAFS pattern) exhibits a linear dependence on the mean crystallite size retrieved from XRD. (The functional relation is $f(x) = 0.25x + 2.15$, $R = 0.985$).

The same proportionality of the EXAFS amplitude intensity to the crystallite size found for peak II should also hold for peak I, if there were no oxygen vacancies. Hence, the peak intensities of the first coordination shell peak can be corrected for the size effect by the relation found from the analysis of Figure II - 22. The directly obtained values of the amplitudes are depicted in Figure II - 23 a) together with the values corrected for the size effect relation. The correction is done in relative terms with respect to the sample with the smallest crystallite size, i.e. 1 h, 160 °C. The difference between the directly measured amplitude values and the corrected ones should be a measure of the surplus of oxygen deficiencies with respect to the sample with the smallest crystallite size. Figure II - 23 b) clearly shows that there is a linear trend in the relation of the amplitude difference and crystallite size. Thus, with increasing hydrothermal treatment time or temperature, the number of oxygen vacancies increases and presumably improves the PC performance: Oxygen deficiencies on the crystal surface can improve the adsorption of O_2 molecules due to interactions with the Ti^{3+} sites (caused by the removal of oxygen atoms).^{63,65} As for PC reactions, the pre-adsorption of molecules on the catalyst surface is a determining step, the enhancement of pre-adsorption of oxygen molecules, results

in a higher PC performance.^{54,68–70} Additionally, Ti^{3+} sites can act as hole scavengers and therefore delay the charge carrier recombination which also improves the PC activity.^{63–65}

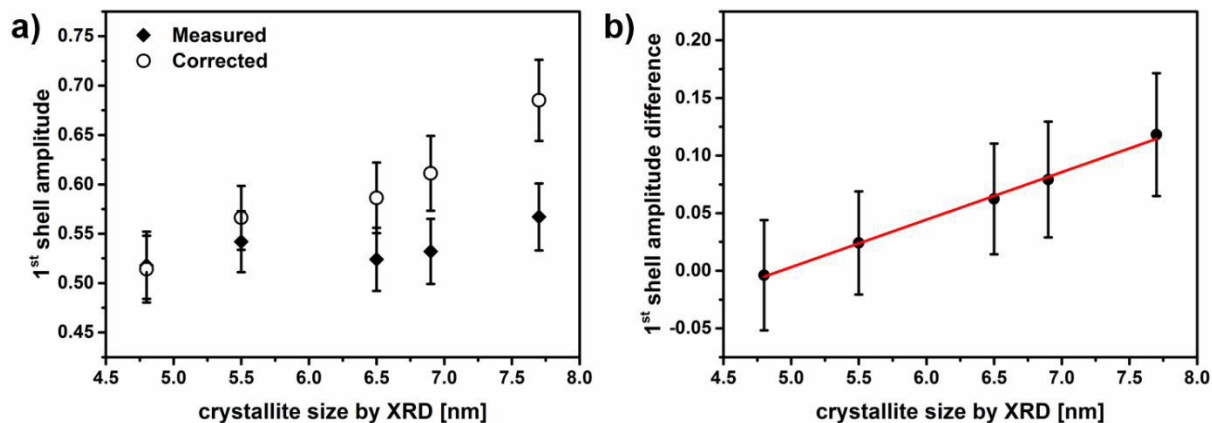


Figure II - 23. a) Amplitudes of the first coordination shell as “measured” (after FEFF9⁶⁷ fit) and corrected for the size effect. b) The difference between the measured EXAFS amplitude of the first coordination shell and the size-effect corrected one is a direct measure of the anion deficiency in the oxygen lattice.

Additionally, high resolution TEM studies and XRD analyses (II.2.1) showed an elongation of the synthesized crystals (along [011] direction) forming rod-like morphologies with increasing autoclaving temperature (or time). Especially in the case of spherical nanocrystals around 10 nm, an increased electron-hole recombination at surface trapping sites is expected which reduces their PC performance.⁵⁰ However, the crystal anisotropy of nanorods is assumed to lead to a lower charge recombination due to the spontaneous charge carrier separation towards the different crystal facets and to an increased delocalization of the carrier as they can freely move throughout the whole crystal lengths.^{49,50,68} This could partly compensate the presence of surface trap states resulting in a higher PC activity of the rod-like crystal samples.

In conclusion, the synergy of both the increase in oxygen deficiencies and the elongation of the nanocrystals must be responsible for a higher PC activity and overrules the expected dependence on the specific surface area.

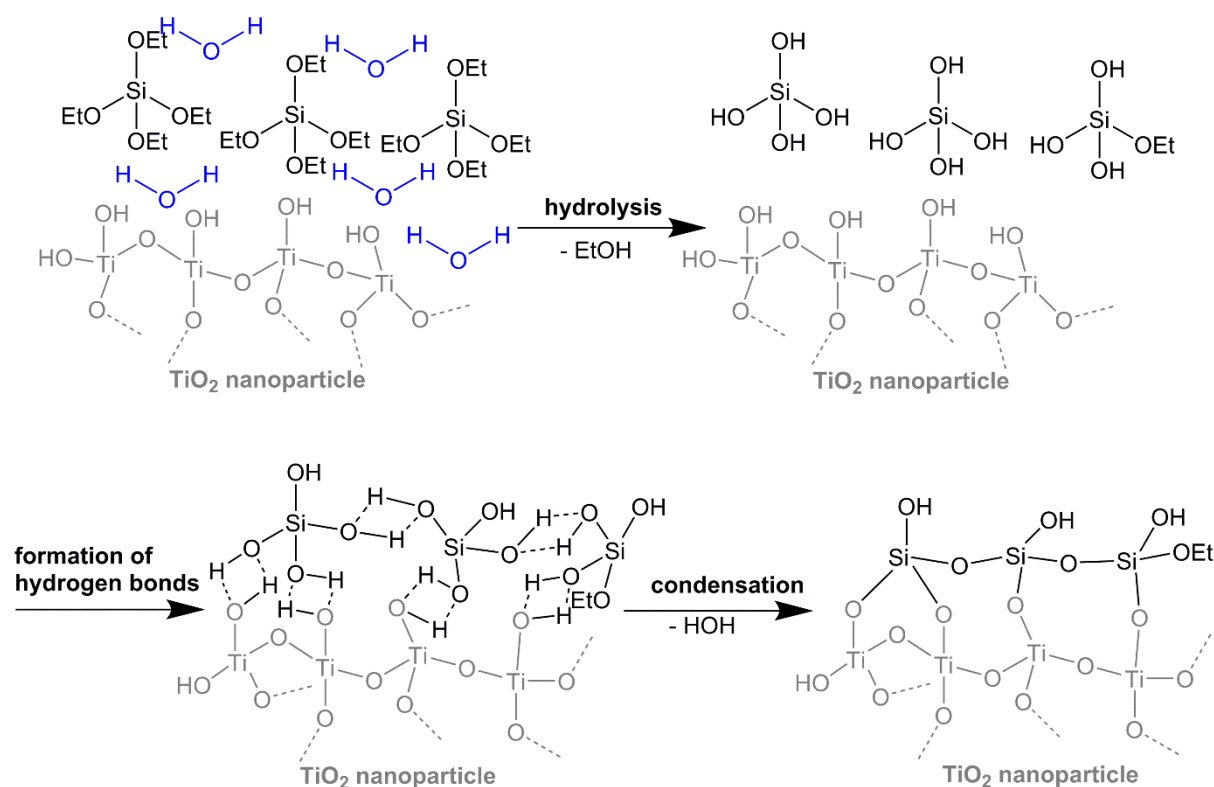
II.3. Luminescent TiO₂ based core/shell structured nanoparticles

After the successful synthesis and characterization of PC anatase NPs, the incorporation of luminescence properties into these systems was a main goal of this work. This is due to the fact that luminescence on the one hand is very helpful to analyse the particle behaviour within cell culture studies: The particle uptake can easily be quantified by luminescence measurements and their position within cells can be detected e. g. via confocal fluorescence microscopy. On the other hand, luminescence enables the use of PC particles not only as therapeutic agents but also possibly as diagnostics: If a targeting surface molecule of the particles specifically binds to tumour cells, these could be visualized due to the luminescence of the particles. This could facilitate the detection of the tumour location and the surgical elimination of tumour tissue. Different strategies to synthesize luminescent TiO₂ based NP systems have been presented in Chapter I.1.4. A common and rather straight forward strategy, is the doping of metal oxide particles with rare earth ions. This usually results in bright luminescence in a colour depending of the nature of the rare earth ion. Nevertheless, this strategy is most often only efficient when the material is heated in the presence of oxygen (calcination).^{71,72} This heat treatment is an eminent disadvantage as it usually leads to aggregation of the particles and disintegration of functional surface groups. Furthermore the doping can also negatively influence the PC activity of the particles as it manipulates the band gap and can therefore enhance recombination of electrons and holes.^{64,73} Another drawback is that first several rare earth ions are classified as carcinogens and second also their supply is limited.^{74–77} Therefore, the current trend is to find substitutes for these elements. Due to these reasons, two different approaches were carried out for the synthesis of luminescent TiO₂ based particle systems avoiding the doping of TiO₂ with rare earth elements.

II.3.1. Luminescent TiO₂/SiO₂ core/shell nanoparticles

The synthesis of luminescent NP systems by doping a silica matrix with organic dyes is well-known and may be transferrable to other NP materials as well.^{78,79} As the TiO₂ NPs were synthesized by heat treatment in an autoclave which would destroy organic dyes, an incorporation of a dye during synthesis was no option. This is why the addition of a silica shell, containing the organic luminescent agent, after the anatase crystal synthesis was chosen as a strategy to obtain a fluorescent particle system. The formation of a well-defined silica shell around TiO₂ NPs has already been carried out various times in literature^{22,23,80–84}, but particles with organic surface groups have not been utilized for this before. This is why the synthesis of a silica shell (without any dye incorporation) was proved first. For this TiO₂ NPs (AA-TiO₂ – 160 °C 4 h which was chosen for the proof of concept in all reactions in this chapter) were coated with a silica shell via a typical *Stoeber* synthesis: tetraorthosilicate was hydrolysed in a

water/ethanol mixture in the presence of ammonium hydroxide as base. The hydrolysed silica precursor condensates onto the present TiO_2 particles, acting as seeds, resulting in Ti-O-Si bonding between the particle surface and TEOS. Scheme II - 1 showing the simplified reactions that take place during the shell formation, can be found below. Further hydrolysis and condensation reactions result in three-dimensional siloxane networks and finally a homogeneous silica shell.^{23,82,83,85} These reactions leading to a particle growth rather occur by addition of monomers to the surface than by aggregation of the small nuclei particles (which would be pure silica particles as side products).⁸⁶ The final particle size and composition can be manipulated by the initial alkoxy silane, water and ammonia concentration.^{86,87} The present base favours condensation over hydrolysis reactions resulting in spherically expanding particles rather than in linear chain structures that could form a gel.⁸⁸



Scheme II - 1. Simplified (and idealized) mechanism of the formation of Si-O-Ti bonds leading to a shell formation around the TiO_2 nanoparticle.

To prove the successful shell formation, the synthesized particle system was analysed via TEM, zeta potential and DLS measurements. Zeta potential measurements showed that the IEP of the coated particle system was at $\text{pH} = 4.6$. If compared to the uncoated TiO_2 with an IEP at the pH of 6.58 and the IEP of pure silica NPs at $\text{pH} = 2.8\text{--}3.5$,^{89,90} the IEP of the measured sample lay in between these materials. This also indicates the successful silica shell formation^{80,81} as the properties of the silica shell superimposes the surface properties of the TiO_2 . Furthermore, the IEP lying in between the characteristic values of the uncoated TiO_2 and

silica NPs, can also indicate an incomplete shell formation or a shell of high porosity which would in both cases be advantageous for the accessibility of the TiO_2 core allowing photocatalytic reactions.⁹¹ TEM images (Figure II - 24) showed that the coated particles were still sphere-like and only slightly larger than the TiO_2 . It is possible to distinguish the silica shell from the titanium dioxide core due to different material densities. According to the TEM images the particle samples seem to be agglomerated which is only due to the preparation method for TEM. DLS measurements on the contrary, show agglomerate sizes of 256.4 ± 5.5 nm with a PDI of 0.27 ± 0.01 for the $\text{TiO}_2/\text{SiO}_2$ system in acidic water which indicates a good dispersion state.

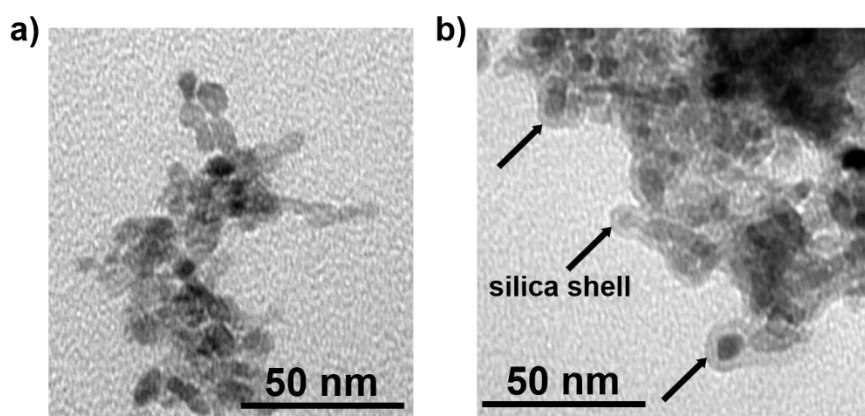
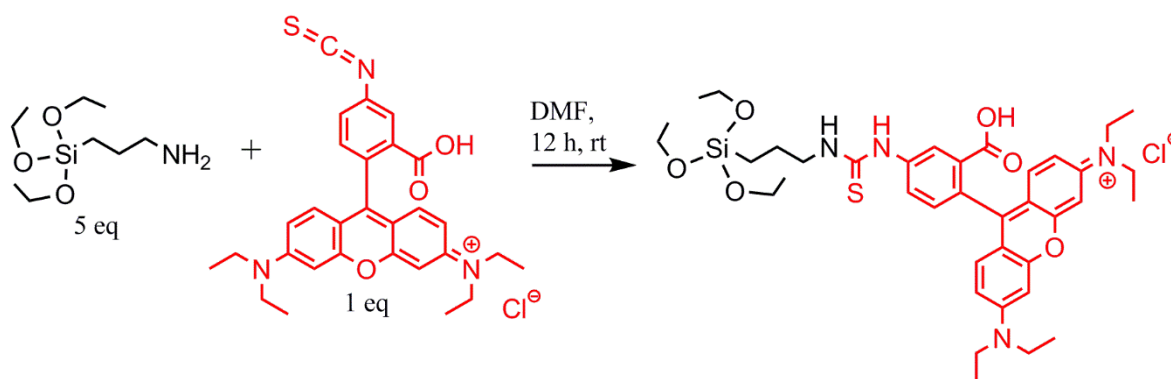


Figure II - 24. TEM images of a) TiO_2 (AA- TiO_2) and b) silica-coated TiO_2 nanoparticles.

After having proved the silica shell formation around the TiO_2 particles, the synthesis of silica shells doped with an organic dye and varying shell thicknesses was carried out. First the commercially available Rhodamine B isothiocyanate (RhBitc) was coupled to aminopropyltriethoxy silane (AMEO) to enable a covalent incorporation of the dye into the silica shell. This was to make sure that the dye cannot leak out of the particle systems after synthesis. The reaction is shown in Scheme II - 2.



Scheme II - 2. Reaction of Rhodamine B isothiocyanate (RhBitc) with aminopropyltriethoxy silane (AMEO).

The silica shell synthesis was carried out as described above but now the silanized dye was mixed with the TEOS before addition. The amount of TEOS was varied (Table II - 4, theoretical molar ratio) to obtain 3 samples ($\text{TiO}_2/\text{SiO}_2_1$ to $\text{TiO}_2/\text{SiO}_2_3$) with different silica shell thicknesses and the amount of dye was always 0.5 weight-% of the added amount of TEOS. This amount of dye was chosen according to literature^{92,93} as the occurrence of self-quenching of the dye with too high concentrations of dye in a silica matrix is a well-known problem. To evaluate the synthesized luminescent particle systems DRIFT, X-ray fluorescence spectroscopy (XRF), zeta potential, photoluminescence (PL) and PC measurements were carried out.

Table II - 4. Theoretical and experimental molar ratios (obtained by XRF) of Ti and Si in $\text{TiO}_2/\text{SiO}_2$ core/shell nanoparticles with increasing shell thicknesses (_1 to _3) doped with Rhodamine dye. Additionally, the reaction yield calculated from the experimental molar ratios is displayed.

sample	Theoretical molar ratio Ti : Si	Experimental molar ratio Ti : Si (XRF)	Yield (%)
$\text{TiO}_2/\text{SiO}_2_1$	1 : 0.07	1 : 0.04	60.0
$\text{TiO}_2/\text{SiO}_2_2$	1 : 0.14	1 : 0.11	76.4
$\text{TiO}_2/\text{SiO}_2_3$	1 : 0.29	1 : 0.19	64.8

The DRIFT spectra of the synthesized particles and the uncoated TiO_2 particle (AA- TiO_2 – DRIFT discussed in II.1.2) as reference are shown in Figure II - 25. They affirmed the formation of a silica shell around the titanium dioxide core: a strong signal at 1066 cm^{-1} and the shoulder at about 1180 cm^{-1} were attributed to asymmetric Si-O-Si bending and stretching vibrations.²³ Vibration of covalent Si-O-Ti bonds between the titanium dioxide core and the silica shell caused a weak signal between 910 cm^{-1} and 960 cm^{-1} .⁸⁵ The weakness of it can be explained by the overlap of the Ti-O-Ti vibration band and the possible existence of only a few Ti-O-Si bonds due to the other organic surface moieties obstructing this binding. Signals at 2927 cm^{-1} , 2856 cm^{-1} and 1400 cm^{-1} corresponded to C-H vibrations of TEOS intermediate reaction products $((\text{OCH}_2\text{CH}_3)_x\text{Si}(\text{OH})_{4-x})$.²³ The band at 1628 cm^{-1} was assigned to O-H bending vibration of Si-O-H groups on the surface of the shell.²³ Depending on the increase of silica shell thickness the IR bands are more pronounced and the organic surface groups of the uncoated particle do almost completely disappear due to their coverage by silica. XRF analysis of the samples showing the experimental molar ratio of Ti to Si, suggested yields of the shell syntheses between 60 % and 76 % (Table II - 4). The IEPs at the pH of 6.3, 5.4 and 4.9 of $\text{TiO}_2/\text{SiO}_2_1$ to $\text{TiO}_2/\text{SiO}_2_3$ were received by zeta potential measurements. With higher silica content and therefore growing shell thickness the pH values shift closer to the IEP of silica

(2.8-3.5). This can be explained by the increasing overlay of the surface potential of TiO_2 by the shell.

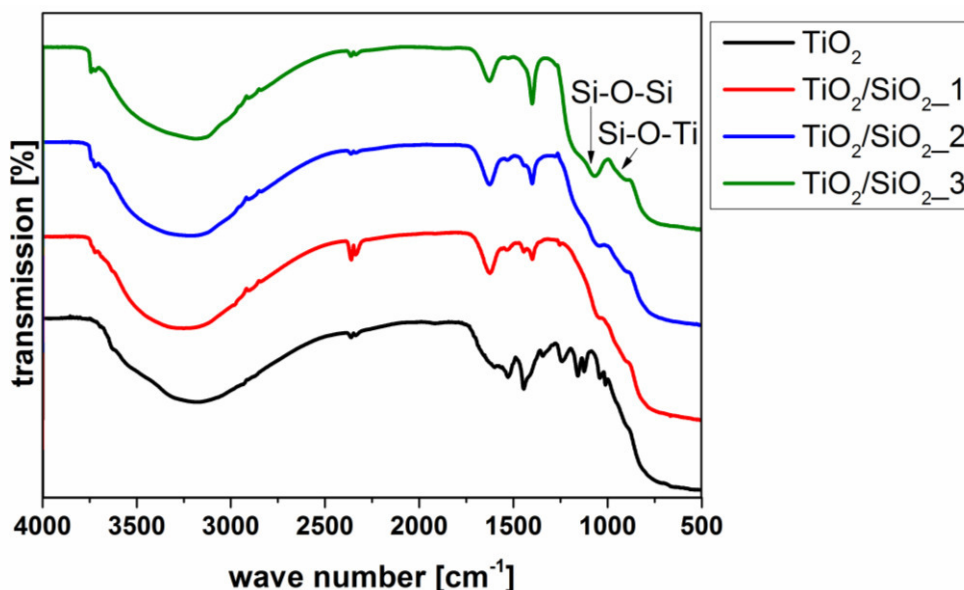


Figure II - 25. IR (DRIFT) spectra of $\text{TiO}_2/\text{SiO}_2$ core/shell particles with increasing shell thicknesses (_1 to _3) compared to the uncoated TiO_2 sample (AA- TiO_2).

The measurements of the fluorescence intensity of $\text{TiO}_2/\text{SiO}_2_{-1}$ to $\text{TiO}_2/\text{SiO}_2_{-3}$ at an excitation wavelength of 555 nm are shown Figure II - 26. As expected the fluorescence intensity rose with increasing shell thickness because the RhBtc content is proportional to the Si content if one assumes a homogeneous placement of RhBtc-AMEO into the shell without preferences.

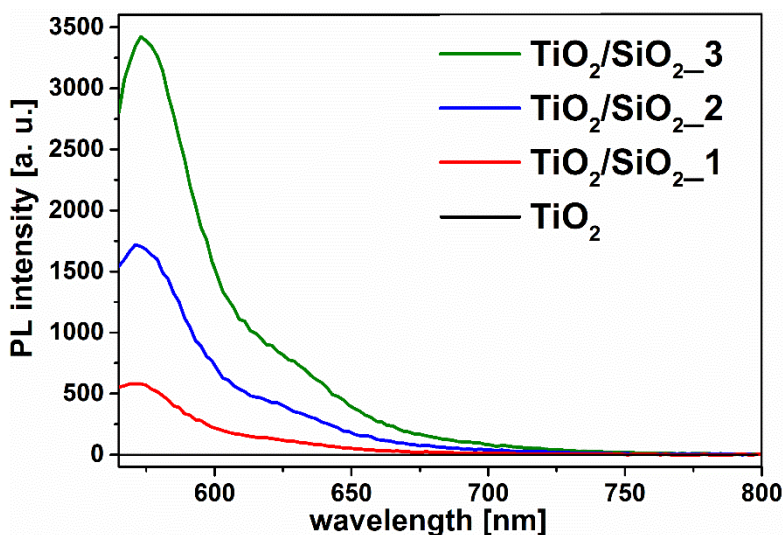


Figure II - 26. Fluorescence spectra of $\text{TiO}_2/\text{SiO}_2$ core/shell particles with increasing shell thicknesses (_1 to _3) compared to the uncoated TiO_2 sample (AA- TiO_2) excited at 555 nm.

For investigating the influence of the silica shell thickness on the PC activity of the TiO_2 core, the decomposition of DCA was utilized (as already described in II.1.3). The PC activity tests (Figure II - 27) reveal that an increasing shell thickness depresses the PC activity.

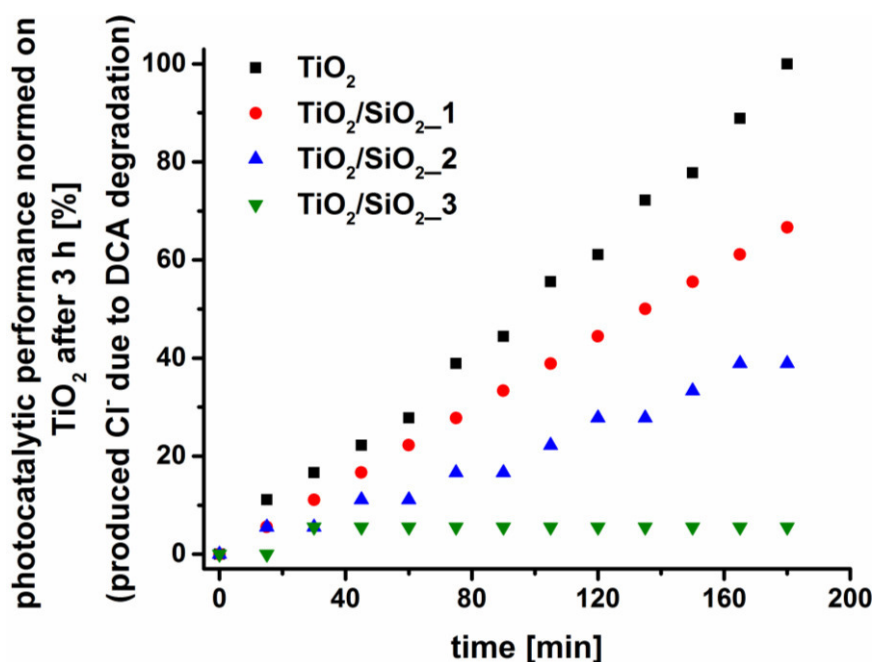


Figure II - 27. Photocatalytic activity of TiO₂/SiO₂ core/shell particles with increasing shell thicknesses (_1 to _3) compared to the uncoated TiO₂ sample (AA-TiO₂); determined by measurement of produced Cl⁻ during the degradation of dichloroacetic acid (DCA). The values are normed on the amount of degraded DCA (produced Cl⁻) by TiO₂ after 3 h photocatalysis test (= 100 %).

This is logically as the shell impedes the interaction of the TiO₂ surface with surrounding water or oxygen. Taking into consideration the PL and PC examinations, it becomes evident that a good PL activity is always on the cost of the PC activity of the NPs. This is due to fact that the amount of dye cannot be increased due to occurring self-quenching and therefore, the higher the wished PC activity, the higher the silica shell has to be and the lower is the PC efficiency. To sum up, this developed particle system can fulfil the requirement of the application as luminescent PC particle system but does not ideally combine both of these properties.

II.3.2. ZnO/TiO₂ core/shell nanoparticles[§]

Another approach to introduce luminescence into a particle system is to synthesize a luminescent core of another appropriate material while the shell still remains to be anatase with the desired properties. In the past, particle setups with a luminescent core were mainly used for quantum dots such as CdS, CdSe and CdTe which are highly luminescent, but most often toxic.^{94,95} This is why they were coated with a silica shell, preventing the toxic substance from leaking and offering a non-toxic surface for functionalization. In our case, it was important to achieve a TiO₂ surface that is highly PC active, while the core provides the PL. As quantum

[§] A part of this chapter has been published and is reused in this work by courtesy of The Royal Society of Chemistry, Original article: S. Koch et al., J. Mater. Chem. C, 2015, 3, 12430-2435.

dots (synthesized in nonpolar organic solvents) are most often not easily transferrable into aqueous solutions and toxic,⁹⁶ in this work the synthesis of ZnO NPs was chosen. These undoped ZnO quantum dots can exhibit PL in the visible wavelength range.^{97–100} The visible emission is supposed to be caused by electron transitions from the conduction band to a deep-level hole defect.^{101,102} These deep-level defects were identified as doubly charged oxygen vacancies originating from the charging of an oxygen vacancy with a photogenerated hole. To ensure the formation of these defects, adsorbed surface groups such as bridging acetates or hydroxyls, scavenging the photoexcited electrons, have to be present.^{100,102} For small particles, due to quantum confinement, the width of the bandgap and therefore also the difference between the conduction band and defect states increases.¹⁰³ Consequently, the emitted (visible) colours that depend on that width are directly related to the NP size.^{101,102} Due to their adjustable colour emission and non-toxicity, these undoped ZnO quantum dots seemed to be good candidates as luminescent cores. For the synthesis the most common sol–gel synthesis^{99,104–108} was chosen using zinc acetate precursors and KOH or LiOH as base in ethanol as solvent. In this study it was possible to determine the accessibility of air during synthesis as yield and synthesis speed driving factor. To visualize this, the particle synthesis was carried out under 3 different conditions: in a closed flask versus an opened flask which allowed air circulation, and a nitrogen flooded flask. Particle growth was only observed in the case of air circulation, which can be seen in Figure II - 28. It shows the PL (Figure II - 28 a) and absorbance (Figure II - 28 b) spectra of the three differently treated samples.

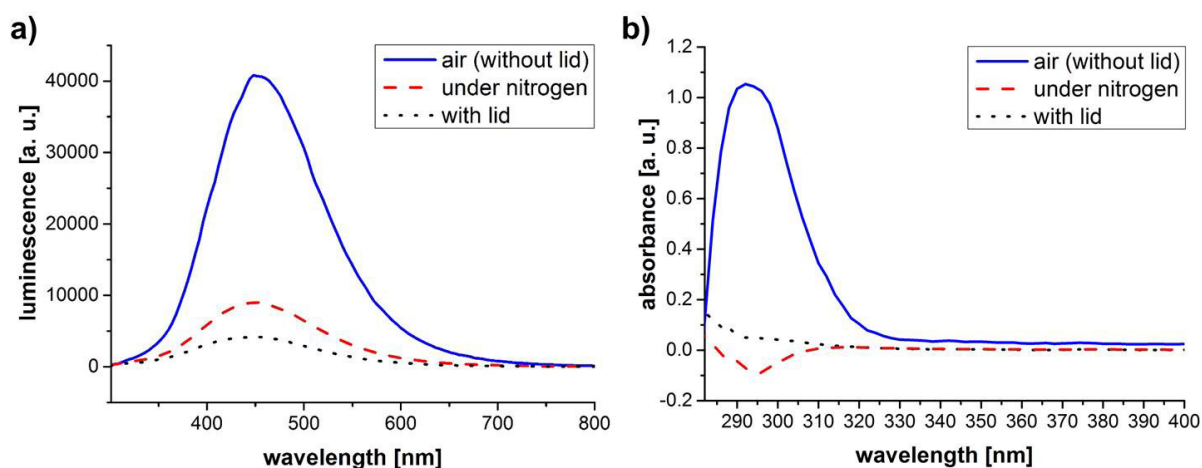


Figure II - 28. a) Luminescence and b) absorbance spectra of ZnO nanoparticles after 4 h of reaction time, synthesized in flasks closed with a lid (dotted line), without a lid allowing air circulation (solid line) or under a nitrogen atmosphere (dashed line). As precursors, low concentrated $\text{Zn}(\text{CH}_3\text{CO}_2)_2$ and LiOH in ethanol were chosen.

Only the sample reacted under air circulation shows a significant PL and absorbance for the wavelength ranges that are expected from what has been described in the literature for ZnO NPs.^{101,104} While a slight PL of the other samples (closed flask, respectively nitrogen flooded)

indicates a minor particle formation. The slightly higher PL intensity of the nitrogen flooded in comparison to the closed reaction batch can be explained by the enhanced formation of oxygen vacancies in a nitrogen atmosphere.⁹⁸ Negative absorbance values in the case of the nitrogen atmosphere are due to the measurement method in well plates. Small variations of the measured sample volumes result in less absorbance and due to the subtraction of ethanol as reference negative values can be obtained. Therefore it can be concluded that accessibility of air is the driving force for an enhanced particle formation. Most possibly the oxygen in the air is the responsible component¹⁰⁹ and enables upscaling due to inlet of air bubbles into the reaction batch.

The successful particle synthesis was not only proved by PL measurements but also via XRD and TEM which is shown in Figure II - 29 (of an upscaled synthesis batch with KOH as base and 100 l/h compressed air inlet).

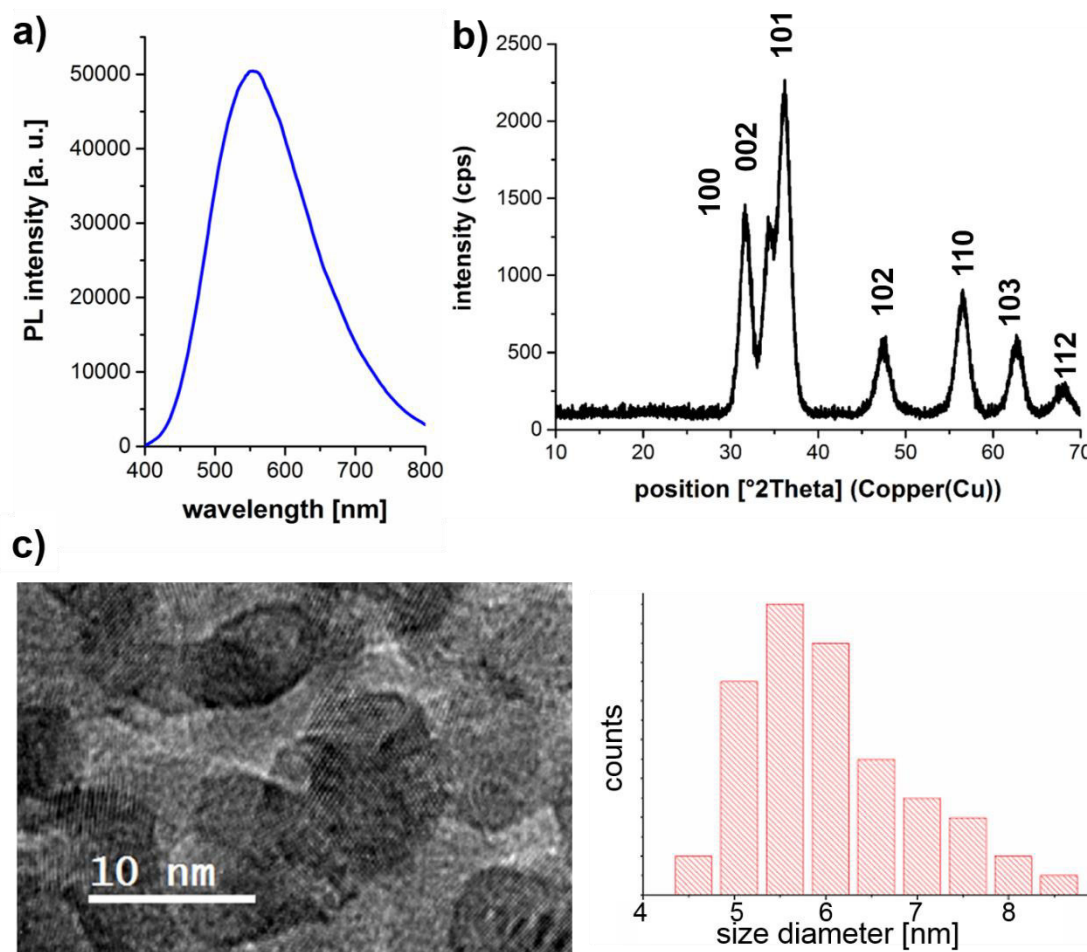


Figure II - 29. a) PL spectra exc. at 350 nm, b) XRD patterns and c) TEM images and the determined particle size distributions of zinc oxide nanoparticles synthesized for 6 h with 100 l/h compressed air flow.

XRD confirms the ZnO crystal structure with a crystallite size of about 6 nm calculated applying Scherrer's formula, which is in agreement with the size determination of the TEM image ($6.0 \text{ nm} \pm 0.9 \text{ nm}$).

In the next step the synthesis of 4 different visible luminescence colours as described in literature^{101,110–112} was also proved (Figure II - 30). Due to variation of the Base LiOH, the particle size and therefore the luminescence wavelength is manipulated resulting in colours from red to green.

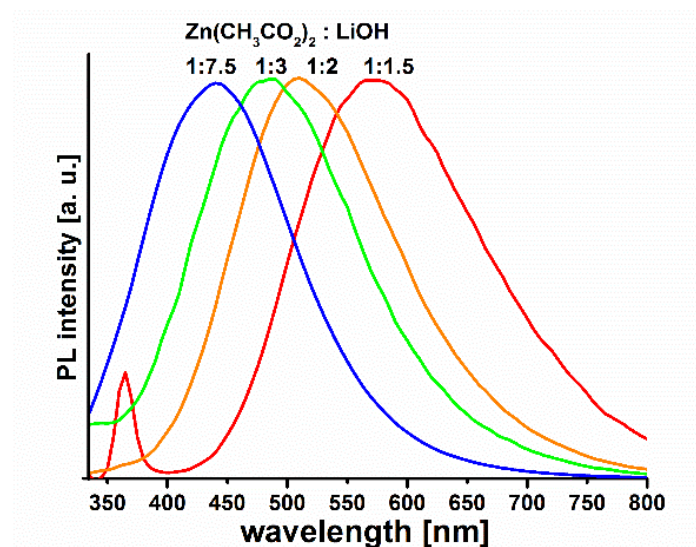
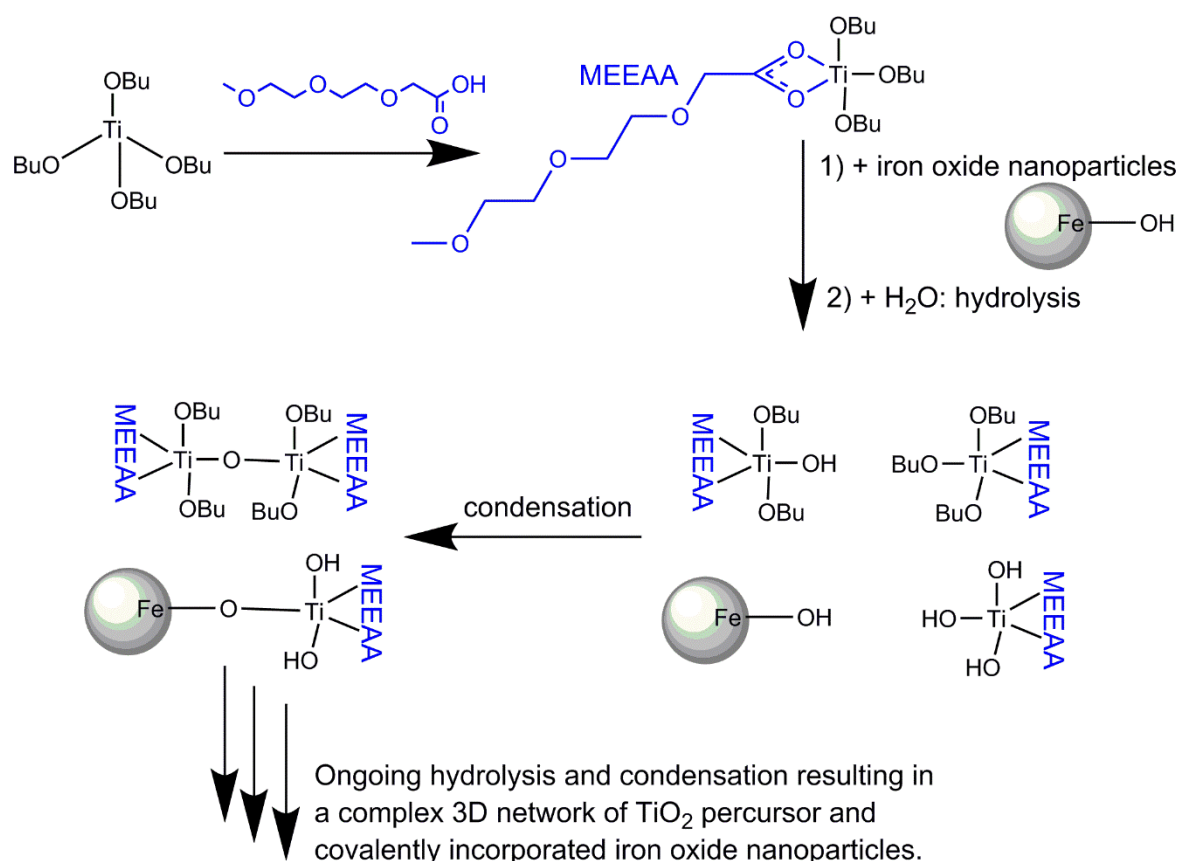


Figure II - 30. PL intensities of ZnO nanoparticles synthesized with $\text{Zn}(\text{CH}_3\text{CO}_2)_2$ and LiOH with the ratios 1:7.5, 1:3, 1:2 and 1:1.5; all spectra are normalized as the NP concentration and therefore the PL intensity of each sample differed due to the ratio of starting materials. (All samples were excited at a wavelength of 290 nm.)

During the synthesis and characterization of all synthesized ZnO NPs, it became evident that these particles easily lose their luminescence behaviour and even dissolve under aqueous acidic conditions. The TiO_2 shell synthesis which is described in the following paragraph, is carried out under these conditions (similar to the synthesis of TiO_2 NPs of II.1 and II.2). Due to this fact, the synthesis of ZnO/ TiO_2 core/shell particles is not possible with the synthesized ZnO NPs and the planned synthesis protocol for TiO_2 cores. Even if most of the literature does not mention the drawback of water sensibility,^{110,112,113} some references tried to improve the water stability of ZnO particles. One possibility is the coating of these particles with polymers made out of triethylene glycol, oleic acid, polyethylene glycol derivatives and/or diethanolamine.^{114–118} These syntheses result in an efficient protection of the ZnO core of acidic water but are not adequate for the coating with TiO_2 as the polymer surfaces are very different from inorganic metal oxide surfaces and therefore a successful TiO_2 condensation onto them it is not guaranteed. Furthermore, one tried to synthesize core/shell particles with silica as shell.^{110–112} While silica would provide similar inorganic metal oxide surface properties for

further reactions, the stability of this system against acids is only slightly enhanced as the shell is too porous to efficiently protect the labile ZnO.¹¹⁹

Simultaneous to the synthesis of a luminescent core, it was examined if the shell formation of TiO₂ around another inorganic metal oxide NP is feasible. For this proof of concept, magnetic iron oxide NPs were chosen as they are easy to synthesize and the washing of these particles is very fast due to their magnetic properties. Additionally, these particles offer hydroxyl groups on their surface which is a condition for coating them with the TiO₂ shell by sol-gel synthesis. For this, magnetic NPs were synthesized via the precipitation method; Fe(II)Cl₂ * 4 H₂O and Fe(III)Cl₃ * 6 H₂O were dissolved in water, then ammonium hydroxide was added resulting in particle precipitation.^{120,121} After washing the particles with water and ethanol, they were added to the TiO₂ precursors (MEEAA and titanium (IV) butoxide). The reaction mixture was then hydrolysed overnight. The most probable reactions during synthesis are shown in Scheme II - 3.



Scheme II - 3. Covalent integration of iron oxide nanoparticles during the preparation of the TiO₂ precursor sol via hydrolysis and condensation reactions (- a simplified reaction mechanism is proposed).

First, the titanium butoxide precursor was partly complexed by the MEEAA under release of butanol. In the scheme only a complex with one acid is shown to avoid any unnecessary oversophistication but it is possible that the titanium ion is in some cases complexed twice^{122,123} by

the acid as almost 2 equivalents of MEEAA were added to the titanium (IV) butoxide. After addition of the core particles, water was added and hydrolysis of residual butoxide groups was initiated. Subsequently, condensation between Ti-OH and Ti-OH or Ti-OBu, but also between Ti-OH and Fe-OH groups, took place forming a complex Ti-O-Ti, Ti-O-Fe and Ti-O-MEEAA network providing an amorphous TiO₂ precursor sol. The covalent integration of the core particles into the titanium dioxide precursor sol was crucial for the later shell formation; if the magnetic particles were added after the hydrolysis and condensation reactions into the already prepared TiO₂ precursor sol, no shell formation occurred. During hydrothermal treatment formed TiO₂ particles did grow beside the magnetic particles and it was possible to eliminate all traces of TiO₂ from the magnetic sample via washing with magnetic separation.

After hydrothermal synthesis, the coated iron oxide NPs were magnetically separated from single TiO₂ NPs that were formed as side products (Figure II - 31 a) and washed several times with slightly basic water. For successful magnetic separation, it was necessary to maintain a slightly basic environment to keep the particles destabilised as due to the heat treatment, the magnetisation of the iron oxide was significantly decreased (Figure II - 31 b). This was already expected as the amount of TiO₂ in the shell were calculated to be 60 weight-% and it is well-known that magnetite and/or maghemite age under heat. For this proof of concept the residual magnetism only had to be strong enough for the washing procedure.

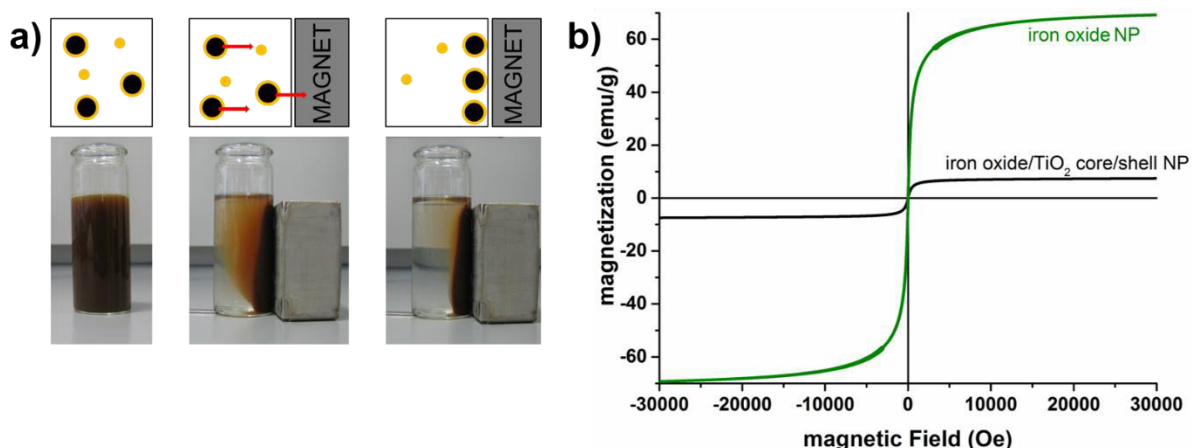


Figure II - 31. a) Schematic presentation (on the top) and photographs (on the bottom) of the magnetic separation of synthesized iron oxide/TiO₂ core/shell particles (depicted with a black core as iron oxide and a yellow shell as TiO₂) from TiO₂ particles (depicted as yellow particles) which were formed as side products. b) Vibrating sample magnetometer measurements (carried out at 293 K) on dried powders of pure iron oxide nanoparticles and the synthesized iron oxide/TiO₂ core/shell particles.

The successful shell formation was proved via zeta potential measurements (Table II - 5); the isoelectric point shifted from 7.3 to approximately 6.2 which is the same isoelectric point exhibited by pure MEEAA-TiO₂ NPs (II.1.2). This indicates the complete formation of a relatively dense TiO₂ shell around the iron oxide as partly covered particles⁹¹ or particles with

porous shells often show their IEP between that of the core and the shell material (II.3.1). In the case of the addition of the core particles after the precursor sol formation, the isoelectric point was still the same as of pure iron oxide particles which indicates (as mentioned before) no successful shell formation.

Table II - 5. The pHs at IEPs of iron oxide, TiO_2 and iron oxide/ TiO_2 NPs determined by zeta potential titrations.

Sample	pH(IEP) [-]
Pure iron oxide NPs	7.3
Iron oxide / TiO_2 NPs (iron oxide added after hydrolysis and condensation of the TiO_2 precursor)	7.1-7.4
Iron oxide / TiO_2 NPs (iron oxide added before hydrolysis and condensation of the TiO_2 precursor)	6.1-6.3
Pure TiO_2 NPs	6.3

Furthermore, XRD measurements confirmed the presence of both anatase and magnetite/maghemite phases (Figure II - 32 a). As one can see on the TEM image (Figure II - 32 b), the sample looks homogenous and the particles are about the same or slightly larger than pure iron oxide particles with a diameter around 10 nm.^{91,120} At acidic pH (1-4), the hydrodynamic diameter of the stably dispersed core/shell samples was around 50 nm (with a PDI of roughly 0.3) while that of iron oxide is in the range of 10–20 nm.¹²¹ A final proof that the formed titanium dioxide is in close surface contact with the core particles, is the complete loss of PC activity of the samples. This phenomenon is due to the heterojunction of both phases, enabling the photogenerated electrons and holes to transfer from TiO_2 to the lower lying conduction band of the iron oxide instead of migrating to the particle surface.^{124–126}

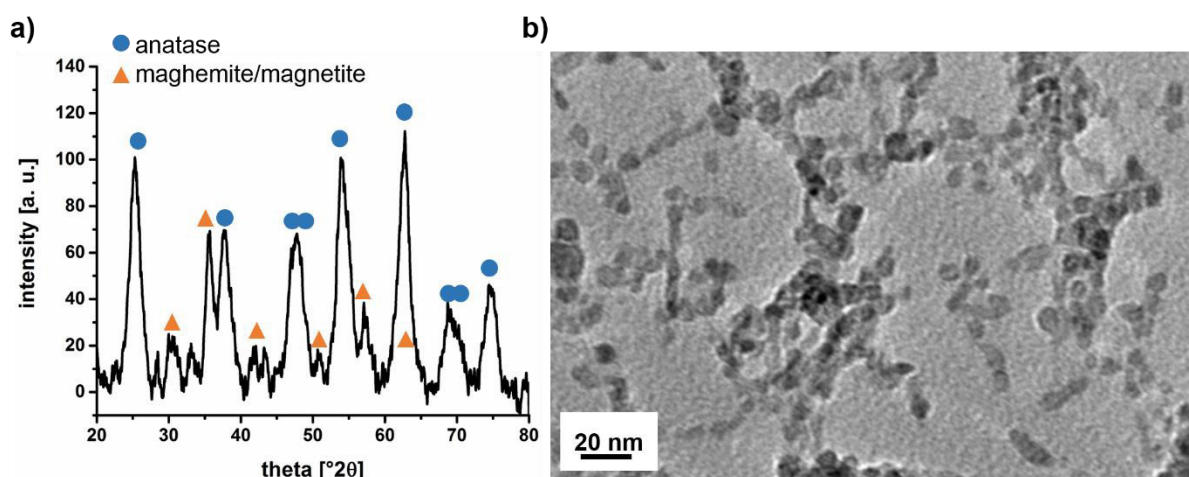


Figure II - 32.a) XRD pattern and b) TEM of synthesized iron oxide/ TiO_2 core/shell nanoparticles.

II.4. Conclusion

Given the results obtained during inorganic syntheses of titanium dioxide NPs and related attempts of core-and-shell particle syntheses to introduce luminescence properties into the systems, one can sum up that two different TiO_2 NPs were successfully synthesized. They were thoroughly analyzed via XRD, TEM, zeta potential measurements, DLS, TGA, nitrogen sorption and DRIFT. While the morphology (oval shape) and size (between 5 nm and 6 nm) of both anatase crystals seem to be very similar, they mainly differ in the surface functions introduced during the synthesis. While the AA- TiO_2 bears acetyl acetate and PTSA groups, the MEEAA- TiO_2 features MEEAA on its surface. The higher PC activity of the MEEAA- TiO_2 compared to the AA- TiO_2 is therefore mainly related to the different surface groups or more precisely the higher amount of functional groups on the AA- TiO_2 . Due to these results, the experiments into the influence of the hydrothermal treatment conditions on the NP properties were conducted with the more promising MEEAA- TiO_2 system. If the autoclaving time or temperature during the synthesis is increased, the crystallite size increases from 4.8 nm to 7.7 nm (1h, 160 °C to 4h, 200 °C). This was verified by XRD, TEM, DLS and nitrogen sorption measurements. While the properties of the surface groups are only marginally influenced by changes in the treatment time and/or duration (as shown via DRIFT, TGA and zeta potential measurements), the PC activity of the sample is significantly improved with increasing particle size. This was in contrast to the initial expectation that PC activity of the samples decreases with increasing size as the specific surface area in the sample is diminished. Their increasing PC performance with decreasing specific surface area were found to be caused by a change in crystal morphology. While small crystallites show the typical equilibrium state truncated tetragonal bipyramidal morphology, crystal growth leads to the formation of rod-like crystals with oxygen vacancies provoked by oriented attachment of single particles (as shown by XAFS, XRD and HR-TEM analyses). Both the more anisotropic crystal shape and the increase in oxygen vacancies improve the photocatalytic activity of the samples - most probably due to a more efficient charge carrier separation. The crystal growth via oriented attachment of {011} facets is presumably caused by the acidic aqueous hydrothermal treatment conditions and the preferential adsorption of the utilized carboxylic acid (MEEAA) onto the high energy {001} facets.

After having successfully synthesized and characterized the stably dispersed, photocatalytically active TiO_2 NPs with sizes smaller than 10 nm, that can even compete with the benchmark material P25, the incorporation of luminescence properties (see below) and the transfer into cell culture applications (Chapter IV) were then investigated. To introduce luminescence properties into the obtained TiO_2 particles, the synthesis of luminescent Rhodamine B doped $\text{TiO}_2/\text{SiO}_2$ core/shell NPs was successfully carried out; the homogeneous

formation of a silica shell around TiO_2 was proved via TEM, DLS and zeta potential measurements. The incorporation of Rhodamine B into the shell was evident due to the luminescence of the final particle system. Unfortunately, the PC activity of the particle system is progressively decreased with increasing silica shell thickness. For the doping of the silica shell with Rhodamine B, the dye concentration is limited due to self-quenching of the dye within the shell. This means, the higher the wished PL, the thicker the silica shell and the lower the PC activity of the $\text{TiO}_2/\text{SiO}_2$ particle system. The synthesis of a ZnO/TiO_2 system still remained challenging; while luminescent ZnO NPs were successfully synthesized, their stability in acidic water was not sufficient for the synthesis of a TiO_2 shell. Nevertheless, it was possible to prove the feasibility of a TiO_2 shell formation around inorganic NPs such as iron oxide NPs. This means, if a sufficiently acid-stable luminescent inorganic particle system is found, the TiO_2 shell formation around it can be realized. For this, it has to be taken into consideration that the excitation of the core material must be above the absorption wavelengths of the TiO_2 shell to ensure the arrival of the excitation wavelength to the core. Additionally, one has to bear in mind that the PC activity of the shell could be negatively influenced by the core. To conclude the attempts of luminescent core/shell particle synthesis, it can be stated that both systems were not deemed sophisticated enough for the use as highly photocatalytically active, luminescent NPs. This is the reason why another way had to be found to integrate the luminescence properties into the NP system. The integration of an organic dye into the coupling agents was identified as most promising pathway (treated in detail in Chapter III). It does not heavily influence the PC activity and the addition is carried out after the particle synthesis which avoids heat treatments of the organic components. Moreover, the excitation and emission wavelengths of the luminescent agent can be selected out of the range of all commercially available dyes and its concentration can most probably be significantly increased compared to a dye doped into a silica shell.

References:

- 1 H. Dong, G. Zeng, L. Tang, C. Fan, C. Zhang, X. He and Y. He, *Water Res.*, 2015, **79**, 128–146.
- 2 Z. Fei Yin, L. Wu, H. Gui Yang and Y. Hua Su, *Phys. Chem. Chem. Phys.*, 2013, **15**, 4844.
- 3 C.-C. Wang and J. Y. Ying, *Chem. Mater.*, 1999, **11**, 3113–3120.
- 4 J. Zhu, F. Chen, J. Zhang, H. Chen and M. Anpo, *J. Photochem. Photobiol. Chem.*, 2006, **180**, 196–204.
- 5 S. Ito, S. Yoshida and T. Watanabe, *Chem. Lett.*, 2000, **29**, 70–71.
- 6 S. Valencia, J. M. Marín and G. Restrepo, *Open Mater. Sci. J.*, 2010, **4**, 9–14.
- 7 M. Bockmeyer, B. Herbig and P. Löbmann, *Thin Solid Films*, 2009, **517**, 1596–1600.
- 8 D. Biskupski, B. Herbig, G. Schottner and R. Moos, *Sens. Actuators B Chem.*, 2011, **153**, 329–334.
- 9 P. Löbmann, *J. Sol-Gel Sci. Technol.*, 2005, **33**, 275–282.
- 10 M. Bockmeyer and P. Löbmann, *J. Sol-Gel Sci. Technol.*, 2008, **45**, 251–259.
- 11 K. Thamaphat, P. Limsuwan and B. Ngotawornchai, *Kasetsart JNat Sci*, 2008, **42**, 357–361.
- 12 C.-C. Wang and J. Y. Ying, *Chem. Mater.*, 1999, **11**, 3113–3120.
- 13 S. Brunauer, P. H. Emmett and E. Teller, *J. Am. Chem. Soc.*, 1938, **60**, 309–319.
- 14 P. S. Awati, S. V. Awate, P. P. Shah and V. Ramaswamy, *Catal. Commun.*, 2003, **4**, 393–400.
- 15 J. Rouquerol, F. Rouquerol, P. Llewellyn, G. Maurin and K. S. W. Sing, *Adsorption by Powders and Porous Solids: Principles, Methodology and Applications*, Academic Press, 2013.
- 16 Malvern Instruments Limited, Dynamic Light Scattering - common terms defined, http://www.biophysics.bioc.cam.ac.uk/wp-content/uploads/2011/02/DLS_Terms_defined_Malvern.pdf, (accessed August 25, 2016).
- 17 R. C. Murdock, L. Braydich-Stolle, A. M. Schrand, J. J. Schlager and S. M. Hussain, *Toxicol. Sci.*, 2008, **101**, 239–253.
- 18 R. Coco, L. Plapied, V. Pourcelle, C. Jérôme, D. J. Brayden, Y.-J. Schneider and V. Préat, *Int. J. Pharm.*, 2013, **440**, 3–12.
- 19 K. Nakamoto, in *Infrared and Raman Spectra of Inorganic and Coordination Compounds*, John Wiley & Sons, Inc., 2008, pp. 333–402.
- 20 D. Lin-Vien, N. B. Colthup, W. G. Fateley and J. G. Grasselli, *The Handbook of Infrared and Raman Characteristic Frequencies of Organic Molecules*, Elsevier, 1991.
- 21 M. Chatry, M. Henry, M. In, C. Sanchez and J. Livage, *J. Sol-Gel Sci. Technol.*, 1994, **1**, 233–240.
- 22 A. M. El-Toni, S. Yin and T. Sato, *J. Colloid Interface Sci.*, 2006, **300**, 123–130.
- 23 X. Feng, S. Zhang and X. Lou, *Colloids Surf. B Biointerfaces*, 2013, **107**, 220–226.
- 24 D. Gummy, C. Morais, P. Bowen, C. Pulgarin, S. Giraldo, R. Hajdu and J. Kiwi, *Appl. Catal. B Environ.*, 2006, **63**, 76–84.
- 25 C. Freitas and R. H. Müller, *Int. J. Pharm.*, 1998, **168**, 221–229.
- 26 D. Li, M. B. Müller, S. Gilje, R. B. Kaner and G. G. Wallace, *Nat. Nanotechnol.*, 2008, **3**, 101–105.
- 27 N. Mandzy, E. Grulke and T. Druffel, *Powder Technol.*, 2005, **160**, 121–126.
- 28 M. Lindner, University Hannover, 1997.
- 29 Y. Li, W. Xie, X. Hu, G. Shen, X. Zhou, Y. Xiang, X. Zhao and P. Fang, *Langmuir*, 2010, **26**, 591–597.
- 30 C. M. Teh and A. R. Mohamed, *J. Alloys Compd.*, 2011, **509**, 1648–1660.
- 31 D. S. Bhatkhande, V. G. Pangarkar and A. A. C. M. Beenackers, *J. Chem. Technol. Biotechnol.*, 2002, **77**, 102–116.
- 32 S. Ottofuelling, F. Von Der Kammer and T. Hofmann, *Environ. Sci. Technol.*, 2011, **45**, 10045–10052.
- 33 S. Sakthivel, B. Neppolian, M. V. Shankar, B. Arabindoo, M. Palanichamy and V. Murugesan, *Sol. Energy Mater. Sol. Cells*, 2003, **77**, 65–82.

- 34 D. W. Bahnemann, S. N. Kholuiskaya, R. Dillert, A. I. Kulak and A. I. Kokorin, *Appl. Catal. B Environ.*, 2002, **36**, 161–169.
- 35 M. H. Habibi and H. Vosooghian, *J. Photochem. Photobiol. Chem.*, 2005, **174**, 45–52.
- 36 U. I. Gaya and A. H. Abdullah, *J. Photochem. Photobiol. C Photochem. Rev.*, 2008, **9**, 1–12.
- 37 M. S. Vohra and K. Tanaka, *Water Res.*, 2003, **37**, 3992–3996.
- 38 A. R. Khataee and M. B. Kasiri, *J. Mol. Catal. Chem.*, 2010, **328**, 8–26.
- 39 D. P. Macwan, P. N. Dave and S. Chaturvedi, *J. Mater. Sci.*, 2011, **46**, 3669–3686.
- 40 B. Herbig, Julius-Maximilians University Würzburg, 2007.
- 41 Q. Xiang, J. Yu, W. Wang and M. Jaroniec, *Chem. Commun.*, 2011, **47**, 6906.
- 42 M. D'Arienzo, J. Carbajo, A. Bahamonde, M. Crippa, S. Polizzi, R. Scotti, L. Wahba and F. Morazzoni, *J. Am. Chem. Soc.*, 2011, **133**, 17652–17661.
- 43 X. Y. Ma, Z. G. Chen, S. B. Hartono, H. B. Jiang, J. Zou, S. Z. Qiao and H. G. Yang, *Chem. Commun.*, 2010, **46**, 6608.
- 44 F. Tian, Y. Zhang, J. Zhang and C. Pan, *J. Phys. Chem. C*, 2012, **116**, 7515–7519.
- 45 X. Zhao, W. Jin, J. Cai, J. Ye, Z. Li, Y. Ma, J. Xie and L. Qi, *Adv. Funct. Mater.*, 2011, **21**, 3554–3563.
- 46 C.-T. Dinh, T.-D. Nguyen, F. Kleitz and T.-O. Do, *ACS Nano*, 2009, **3**, 3737–3743.
- 47 J. Pan, University of Queensland, 2014.
- 48 J. Pan, X. Wu, L. Wang, G. Liu, G. Q. (Max) Lu and H.-M. Cheng, *Chem. Commun.*, 2011, **47**, 8361–8363.
- 49 B. Wu, C. Guo, N. Zheng, Z. Xie and G. D. Stucky, *J. Am. Chem. Soc.*, 2008, **130**, 17563–17567.
- 50 P. D. Cozzoli, A. Kornowski and H. Weller, *J. Am. Chem. Soc.*, 2003, **125**, 14539–14548.
- 51 R. L. Penn and J. F. Banfield, *Geochim. Cosmochim. Acta*, 1999, **63**, 1549–1557.
- 52 R. L. Penn and J. F. Banfield, *Science*, 1998, **281**, 969–971.
- 53 H. Zhang, R. L. Penn, R. J. Hamers and J. F. Banfield, *J. Phys. Chem. B*, 1999, **103**, 4656–4662.
- 54 N. Roy, Y. Sohn and D. Pradhan, *ACS Nano*, 2013, **7**, 2532–2540.
- 55 J. Li and D. Xu, *Chem. Commun.*, 2010, **46**, 2301–2303.
- 56 A. S. Barnard and L. A. Curtiss, *Nano Lett.*, 2005, **5**, 1261–1266.
- 57 X.-L. Li, Q. Peng, J.-X. Yi, X. Wang and Y. Li, *Chem. – Eur. J.*, 2006, **12**, 2383–2391.
- 58 J. Joo, S. G. Kwon, T. Yu, M. Cho, J. Lee, J. Yoon and T. Hyeon, *J. Phys. Chem. B*, 2005, **109**, 15297–15302.
- 59 T. Sugimoto, X. Zhou and A. Muramatsu, *J. Colloid Interface Sci.*, 2003, **259**, 53–61.
- 60 J.-L. Dirion, C. Reverte and M. Cabassud, *Chem. Eng. Res. Des.*, 2008, **86**, 618–625.
- 61 A. Tiwari and B. Raj, *Reactions and Mechanisms in Thermal Analysis of Advanced Materials*, John Wiley & Sons, 2015.
- 62 D. Kwon, S. H. Lee, J. Kim and T. H. Yoon, *Toxicol. Environ. Health Sci.*, **2**, 78–85.
- 63 J. Yan, G. Wu, N. Guan, L. Li, Z. Li and X. Cao, *Phys. Chem. Chem. Phys.*, 2013, **15**, 10978.
- 64 Z. Zhao, X. Zhang, G. Zhang, Z. Liu, D. Qu, X. Miao, P. Feng and Z. Sun, *Nano Res.*, 2015, **8**, 4061–4071.
- 65 X. Jiang, Y. Zhang, J. Jiang, Y. Rong, Y. Wang, Y. Wu and C. Pan, *J. Phys. Chem. C*, 2012, **116**, 22619–22624.
- 66 X. Chen, L. Liu, Z. Liu, M. A. Marcus, W.-C. Wang, N. A. Oyler, M. E. Grass, B. Mao, P.-A. Glans, P. Y. Yu, J. Guo and S. S. Mao, *Sci. Rep.*, 2013, **3**, 1510.
- 67 J. J. Rehr, J. J. Kas, F. D. Vila, M. P. Prange and K. Jorissen, *Phys. Chem. Chem. Phys.*, 2010, **12**, 5503–5513.
- 68 G. Liu, J. C. Yu, G. Q. (Max) Lu and H.-M. Cheng, *Chem. Commun.*, 2011, **47**, 6763.
- 69 A. Vittadini, A. Selloni, F. P. Rotzinger and M. Grätzel, *Phys. Rev. Lett.*, 1998, **81**, 2954–2957.
- 70 A. Selloni, *Nat. Mater.*, 2008, **7**, 613–615.
- 71 I. Cacciotti, A. Bianco, G. Pezzotti and G. Gusmano, *Chem. Eng. J.*, 2011, **166**, 751–764.

- 72 X. Chen and W. Luo, *J. Nanosci. Nanotechnol.*, 2010, **10**, 1482–1494.
- 73 J. Liqiang, Q. Yichun, W. Baiqi, L. Shudan, J. Baojiang, Y. Libin, F. Wei, F. Honggang and S. Jiazhong, *Sol. Energy Mater. Sol. Cells*, 2006, **90**, 1773–1787.
- 74 K. T. Rim, K. H. Koo and J. S. Park, *Saf. Health Work*, 2013, **4**, 12–26.
- 75 E. Nakamura and K. Sato, *Nat. Mater.*, 2011, **10**, 158–161.
- 76 E. Alonso, A. M. Sherman, T. J. Wallington, M. P. Everson, F. R. Field, R. Roth and R. E. Kirchain, *Environ. Sci. Technol.*, 2012, **46**, 3406–3414.
- 77 M. A. de Boer and K. Lammertsma, *ChemSusChem*, 2013, **6**, 2045–2055.
- 78 A. Imhof, M. Megens, J. J. Engelberts, D. T. N. de Lang, R. Sprik and W. L. Vos, *J. Phys. Chem. B*, 1999, **103**, 1408–1415.
- 79 R. Kumar, I. Roy, T. Y. Ohulchanskyy, L. N. Goswami, A. C. Bonoio, E. J. Bergey, K. M. Trampusch, A. Maitra and P. N. Prasad, *ACS Nano*, 2008, **2**, 449–456.
- 80 I. A. Siddiquey, T. Furusawa, M. Sato, K. Honda and N. Suzuki, *Dyes Pigments*, 2008, **76**, 754–759.
- 81 Y.-L. Lin, T.-J. Wang and Y. Jin, *Powder Technol.*, 2002, **123**, 194–198.
- 82 O. K. Park and Y. S. Kang, *Colloids Surf. Physicochem. Eng. Asp.*, 2005, **257–258**, 261–265.
- 83 A. Jaroenworuluck, W. Sunsaneeyametha, N. Kosachan and R. Stevens, *Surf. Interface Anal.*, 2006, **38**, 473–477.
- 84 S. Pazokifard, S. M. Mirabedini, M. Esfandeh, M. Mohseni and Z. Ranjbar, *Surf. Interface Anal.*, 2012, **44**, 41–47.
- 85 Z. Li, B. Hou, Y. Xu, D. Wu and Y. Sun, *J. Colloid Interface Sci.*, 2005, **288**, 149–154.
- 86 C. A. P. Leite, E. F. de Souza and F. Galembeck, *J. Braz. Chem. Soc.*, 2001, **12**, 519–525.
- 87 C. A. R. Costa, C. A. P. Leite and F. Galembeck, *J. Phys. Chem. B*, 2003, **107**, 4747–4755.
- 88 H. Ye, X. Zhang, Y. Zhang, L. Ye, B. Xiao, H. Lv and B. Jiang, *Sol. Energy Mater. Sol. Cells*, 2011, **95**, 2347–2351.
- 89 X. Fu and S. Qutubuddin, *Colloids Surf. Physicochem. Eng. Asp.*, 2001, **179**, 65–70.
- 90 X. Fu and S. Qutubuddin, *Colloids Surf. Physicochem. Eng. Asp.*, 2001, **178**, 151–156.
- 91 K. Mandel, M. Straßer, T. Granath, S. Dembski and G. Sextl, *Chem. Commun.*, 2015, **51**, 2863–2866.
- 92 S. Kim, H. E. Pudavar, A. Bonoio and P. N. Prasad, *Adv. Mater.*, 2007, **19**, 3791–3795.
- 93 E.-B. Cho, D. O. Volkov and I. Sokolov, *Adv. Funct. Mater.*, 2011, **21**, 3129–3135.
- 94 Y. Kobayashi, T. Nozawa, T. Nakagawa, K. Gonda, M. Takeda, N. Ohuchi and A. Kasuya, *J. Sol-Gel Sci. Technol.*, 2010, **55**, 79–85.
- 95 D. Gerion, F. Pinaud, S. C. Williams, W. J. Parak, D. Zanchet, S. Weiss and A. P. Alivisatos, *J. Phys. Chem. B*, 2001, **105**, 8861–8871.
- 96 X. Michalet, F. F. Pinaud, L. A. Bentolila, J. M. Tsay, S. Doose, J. J. Li, G. Sundaresan, A. M. Wu, S. S. Gambhir and S. Weiss, *Science*, 2005, **307**, 538–544.
- 97 A. van Dijken, E. A. Meulenkaamp, D. Vanmaekelbergh and A. Meijerink, *J. Lumin.*, 2000, **87–89**, 454–456.
- 98 A. Asok, M. N. Gandhi and A. R. Kulkarni, *Nanoscale*, 2012, **4**, 4943.
- 99 K. Vanheusden, C. H. Seager, W. L. Warren, D. R. Tallant and J. A. Voigt, *Appl. Phys. Lett.*, 1996, **68**, 403–405.
- 100 L. Spanhel, *J. Sol-Gel Sci. Technol.*, 2006, **39**, 7–24.
- 101 Y. Lv, W. Xiao, W. Li, J. Xue and J. Ding, *Nanotechnology*, 2013, **24**, 175702.
- 102 A. van Dijken, E. A. Meulenkaamp, D. Vanmaekelbergh and A. Meijerink, *J. Lumin.*, 2000, **90**, 123–128.
- 103 K.-F. Lin, H.-M. Cheng, H.-C. Hsu, L.-J. Lin and W.-F. Hsieh, *Chem. Phys. Lett.*, 2005, **409**, 208–211.
- 104 X. Tang, E. S. G. Choo, L. Li, J. Ding and J. Xue, *Chem. Mater.*, 2010, **22**, 3383–3388.
- 105 L. Spanhel and M. A. Anderson, *J. Am. Chem. Soc.*, 1991, **113**, 2826–2833.

- 106 E. A. Meulenkamp, *J. Phys. Chem. B*, 1998, **102**, 5566–5572.
- 107 R. D. Yang, S. Tripathy, Y. Li and H.-J. Sue, *Chem. Phys. Lett.*, 2005, **411**, 150–154.
- 108 K. Rekha, M. Nirmala, M. G. Nair and A. Anukaliani, *Phys. B Condens. Matter*, 2010, **405**, 3180–3185.
- 109 S. Koch, S. Späth, A. Shmeliov, V. Nicolosi and K. Mandel, *J Mater Chem C*, 2015, **3**, 12430–12435.
- 110 X. Xu, C. Xu, X. Wang, Y. Lin, J. Dai and J. Hu, *CrystEngComm*, 2013, **15**, 977–981.
- 111 H.-J. Zhang, H.-M. Xiong, Q.-G. Ren, Y.-Y. Xia and J.-L. Kong, *J. Mater. Chem.*, 2012, **22**, 13159.
- 112 H.-Q. Shi, W.-N. Li, L.-W. Sun, Y. Liu, H.-M. Xiao and S.-Y. Fu, *Chem. Commun.*, 2011, **47**, 11921.
- 113 J. Zhang, G. Gao and F. Liu, *J. Appl. Polym. Sci.*, 2013, **128**, 2162–2166.
- 114 L.-H. Zhao and S.-Q. Sun, *CrystEngComm*, 2011, **13**, 1864–1869.
- 115 X. Tang, E. S. G. Choo, L. Li, J. Ding and J. Xue, *Langmuir*, 2009, **25**, 5271–5275.
- 116 Y.-S. Fu, X.-W. Du, S. A. Kulinich, J.-S. Qiu, W.-J. Qin, R. Li, J. Sun and J. Liu, *J. Am. Chem. Soc.*, 2007, **129**, 16029–16033.
- 117 S. Saliba, C. Valverde Serrano, J. Keilitz, M. L. Kahn, C. Mingotaud, R. Haag and J.-D. Marty, *Chem. Mater.*, 2010, **22**, 6301–6309.
- 118 H.-M. Xiong, Y. Xu, Q.-G. Ren and Y.-Y. Xia, *J. Am. Chem. Soc.*, 2008, **130**, 7522–7523.
- 119 B. Rohe, University Duisburg-Essen, 2005.
- 120 K. Mandel, W. Szczerba, A. F. Thünemann, H. Riesemeier, M. Girod and G. Sextl, *J. Nanoparticle Res.*, 2012, **14**, 1066.
- 121 K. Mandel, F. Hutter, C. Gellermann and G. Sextl, *Colloids Surf. Physicochem. Eng. Asp.*, 2011, **390**, 173–178.
- 122 X.-Q. Chen, G.-B. Gu and H.-B. Liu, *Huaxue Xuebao*, 2003, **61**, 1592–1596.
- 123 X.-Q. Chen and W.-H. Shen, *Chem. Eng. Technol.*, 2008, **31**, 1277–1281.
- 124 C. Wang, L. Yin, L. Zhang, L. Kang, X. Wang and R. Gao, *J. Phys. Chem. C*, 2009, **113**, 4008–4011.
- 125 D. Beydoun, R. Amal, G. Low and S. McEvoy, *J. Mol. Catal. Chem.*, 2002, **180**, 193–200.
- 126 D. Beydoun, R. Amal, G. K.-C. Low and S. McEvoy, *J. Phys. Chem. B*, 2000, **104**, 4387–4396.

III. Synthesis of organic coupling agents and their grafting onto TiO_2 nanoparticles

Contents

III.	Synthesis of organic coupling agents and their grafting onto TiO ₂ nanoparticles ...	- 91 -
III.1.	Synthesis of functional coupling agents.....	- 91 -
III.1.1.	Synthesis of linear and dendritic fluorescent coupling agents.....	- 94 -
III.1.1.a.	Coupling agent I (compound 4)	- 94 -
III.1.1.b.	Coupling agent II.....	- 97 -
III.1.1.c.	Coupling agent III (compound 22)	- 103 -
III.1.2.	Synthesis of dendritic non-fluorescent coupling agents	- 111 -
III.1.2.a.	Coupling agent IV (compound 25).....	- 111 -
III.2.	Grafting of functional coupling agents onto particles.....	- 115 -
III.2.1.	Optimization of grafting protocols with commercial silanes	- 116 -
III.2.2.	Grafting of synthesized coupling agents onto MEEAA-TiO ₂ (200 °C, 4 h). -	123 -
III.2.2.a.	Grafting of coupling agent I	- 123 -
III.2.2.b.	Grafting of coupling agent IV	- 127 -
III.3.	Conclusion	- 133 -

III. *Synthesis of organic coupling agents and their grafting onto TiO₂ nanoparticles*

After the successful design of photocatalytic anatase nanocrystals, their surface functionalization was an essential objective to adapt the particle systems to the demands of their later applications in photodynamic cancer therapy. The elaborate design of organic coupling agents allows the fine tuning of molecular properties such as hydrophilicity, charge, geometry, luminescence or functional groups and the transfer of these characteristics to the entire particle system.

III.1. **Synthesis of functional coupling agents**

For the design of coupling agents, it was important to define the requirements they had to fulfil as functional surface groups of the nanoparticles. The first objective was to mediate the cellular uptake of the particles using these functional groups. It is well-known that the surface charge of particles has a great influence on their cellular uptake and that the surface potential can be easily modified by functional surface groups.^{1–14} Wise selection of functional groups can therefore optimize the cellular NP uptake. Furthermore, they can be used for the coupling of biological molecules onto the particle for example for targeted tumour treatment.^{15–19} A second objective was the introduction of luminescence properties into the particle system. This can be achieved by the incorporation of an organic dye into the coupling agent.^{20–24} Luminescence enables the detection of the particle systems in cell culture studies for better analysis and examination of the particle interaction with the cells.²⁵ It also gives the opportunity for their imaging in human tissue when they are for example used as anti-tumour agents. The final task for the coupling agent was to improve or at least not decrease the solubility and dispersibility of the particles in physiological solutions. These objectives have driven the design of fluorescent and non-fluorescent molecules, which are presented in the following in more detail (Figure III - 1; 1st generation dendritic coupling agents as examples).

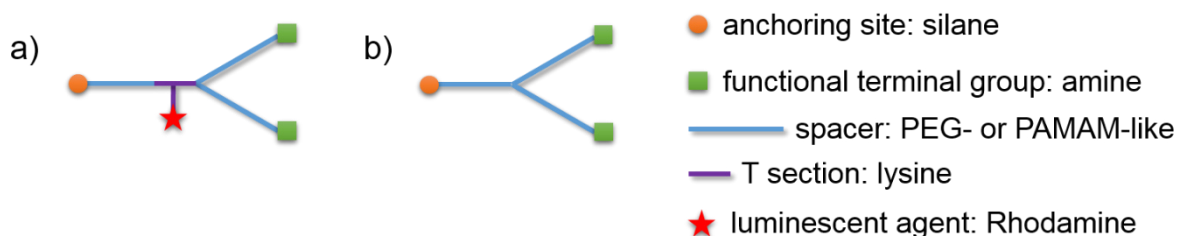


Figure III - 1. Structure of the a) fluorescent and b) non-fluorescent 1st generation dendritic coupling agents.

First, the functional terminal groups of the coupling agents were chosen to be amines as in general positive surface charge at physiological pH leads to a better cellular uptake of the particles.^{3-6,10-12,14} Additionally, by fine tuning of the surface potential it may even be possible to enhance the particle uptake by cancer cells while healthy cells do not show an increased uptake.²⁶ This behaviour is especially preferred for nanoparticles that are used for cancer treatment. To be able to finely tune the positive particle surface potential, we not only relied on linear coupling agents but dendritic structures were also used. By increasing the number of branches and therefore of functional terminal groups of the molecules, the positive charge of the particle surface is step-wise increased while maintaining the number of coupling agents per nanoparticle. This was of the utmost importance for this study as the functionalized TiO₂ nanoparticles were meant to be used as photocatalytic cancer treatment agent. By covering the surface with more coupling agents, the free TiO₂ surface is decreased and as the photocatalysis is a surface process, its efficiency is strongly diminished. By using dendritic structures, one can most probably incline the surface charge while not decreasing the photocatalytic activity. Furthermore, the steric hindrance of dendritic surface agents during grafting is expected to lead to a less dense surface functionalization and therefore “non-passivated” TiO₂ surface is available for catalytic reactions.²⁷ It also has to be mentioned, that amino groups are suitable for couplings with biological molecules that bear succinimidyl esters or carboxylic groups.^{15,17,18} This could enable the coupling of targeting agents like epithelial growth factors receptor antibodies,²⁸ aptamers¹⁹ or folates²⁹ onto the particles for active targeting of cancer cells resulting in a more efficient cancer treatment.

The dendritic structures were chosen to be polyamidoamine (PAMAM) based as these structures are one of the most common structures used in materials science as well as in biotechnology due to their architecture and functionalities.³⁰ These can be easily modified and therefore adapted for various fields of application.³¹⁻³³ PAMAM are said to be in general non-toxic (if low generation dendrons are used) and show a good solubility in physiological solutions due to their hydrophilic properties.^{31,34-36}

Another essential part of the coupling agent was the anchoring site that allows the binding of the organic molecule onto the inorganic particle. For this, silanes like organofunctional ethoxysilanes (RSi(OEt)₃) were the most preferred reagents as silanol groups can covalently bind on titanium surfaces, which exhibit hydroxyl moieties.³⁷⁻³⁹ The subsequent grafting can be carried out under mild conditions e.g. in hydroalcoholic medium by hydrolysis of the ethoxy groups and subsequent condensation with the TiO₂ hydroxyls.^{40,41} The formed Si-O-Ti bond is expected to be stable in water under mild acidic and basic conditions, which is suitable for biomedical applications.

In order to optionally add luminescence properties to the particle system, a dye had to be incorporated into the coupling agent. For this approach, commercial rhodamine derivatives were selected because of their high photostability and quantum yield (especially in aqueous solutions) as well as their good chemical and thermal stability.^{42,43} Furthermore, the luminescence and absorption of the dye had to be over 450 nm as TiO₂ strongly absorbs light up to these wavelengths.^{44,45} This is the case for example for rhodamine B ($\lambda_{\text{abs}} = 554 \text{ nm}$, $\lambda_{\text{pl}} = 576 \text{ nm}$).⁴⁶ The dyes also show a satisfying solubility in water and were proved to be non-toxic, which is both very important for later biomedical applications.^{42,47} Additionally, an efficient coupling of the dye to the rest of the organic coupling agent was of great importance. This is why Rhodamine B isothiocyanate was the first choice as it is an affordable model dye that easily reacts with amines of the coupling agent. For later applications the use of dyes with absorption and luminescence in higher wavelength ranges would be preferred in order to be able to operate within the optical “window” (600-1300 nm)^{48,49} and reach higher light penetration in human tissue. For the incorporation of the luminescent agent into the molecule, a connection is needed between the anchoring site, the luminescent agent and the functional groups (including the dendritic structures). For this the amino acid lysine was chosen as it offers three reactive sites: 2 amino groups and one carboxyl group. The hydrophilic lysine can also improve the solubility of the coupling agent in water. It has the appearance of a T section, which allows a linear connection between the anchoring site and the functional groups (and dendritic structures), while providing a lateral reaction side for the dye.⁵⁰ This was an important requirement as the dye should not be in the periphery of the dendron to not influence the efficiency of the functional terminal groups in their task to modify the surface charge and couple organic molecules. It was also an option to integrate the dye linearly into the molecule between the functional groups and the anchoring site but organic dyes that show two reactive sites in a linear arrangement are commonly not commercially available.

Additionally, we decided to introduce a spacer or linker moiety between the anchoring site and the lysine or in the case of non-fluorescent coupling agents - where no T section is needed - between the anchor and the dendritic structure. This spacer should provide a certain flexibility for a higher grafting efficiency of the coupling agent as it increases the distance between the anchoring site and the large, rather inflexible structures of the dye and the dendritic branches. It should also enhance the colloidal stability of the functionalized particle in water. This is why a polyethylene glycol (PEG)-like spacer has been selected as PEG is nontoxic and provides high colloidal stability of functionalized particles in physiologic media due to its hydrophilic character.⁵¹⁻⁵³

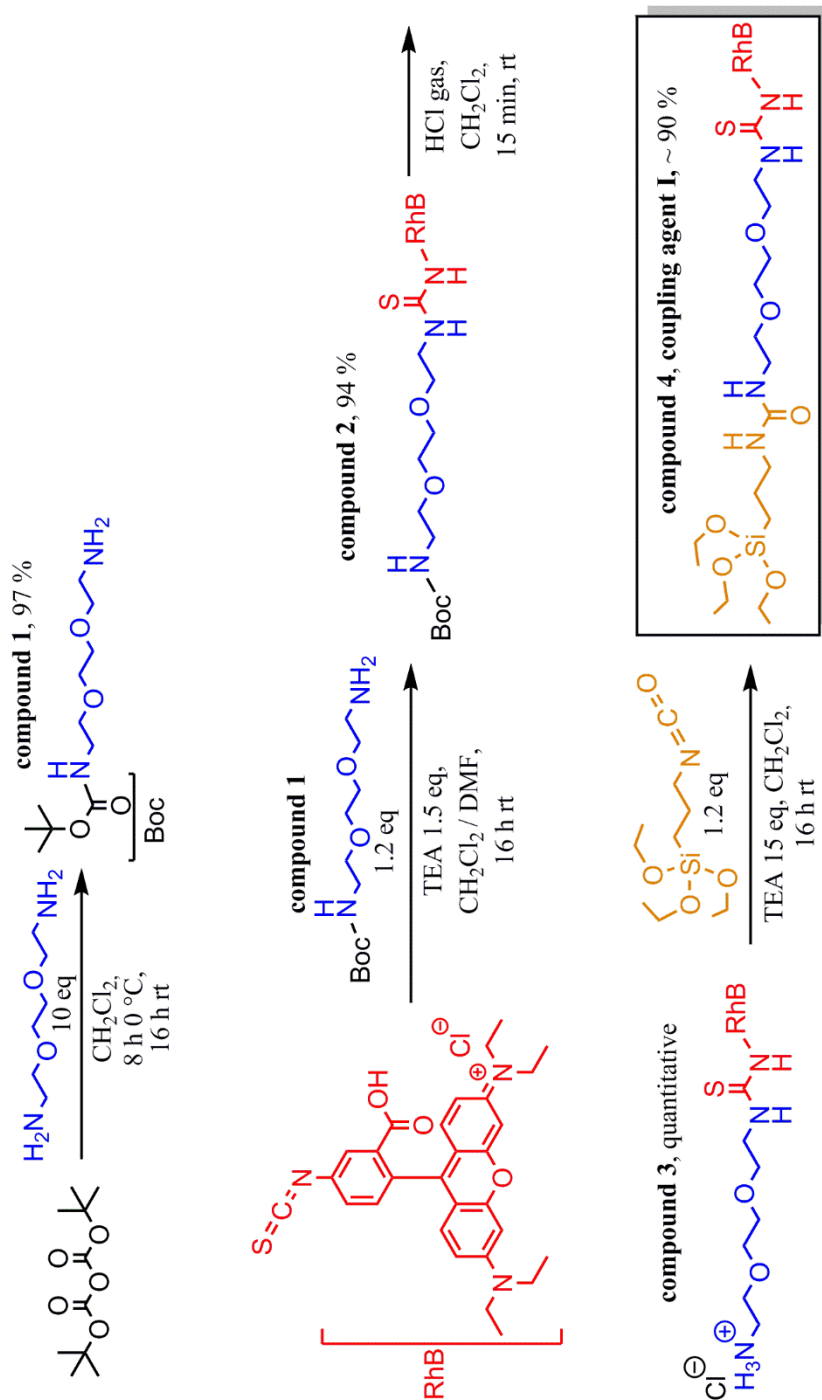
After having defined the targeted structure of the grafting agents, the planned synthesis routes are described in the following sections: First, the synthesis of the linear and dendritic fluorescent coupling agents is discussed (III.1.1) before moving forward to the non-fluorescent grafting agents (III.1.2).

III.1.1. Synthesis of linear and dendritic fluorescent coupling agents

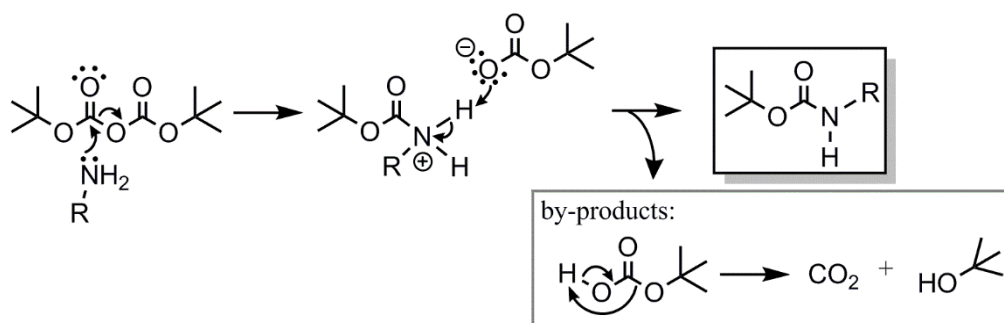
III.1.1.a. Coupling agent I (compound 4)

The first strategy was to synthesize a linear, rather simple molecule that features the same modules as the following more complex fluorescent coupling agents with anchoring site, spacer and dye but was obtained after only 4 reaction steps. It was mainly meant to test the feasibility of the synthesis route, in particular the incorporation of the commercial dye rhodamine B isothiocyanate into the molecule. This coupling agent should help to investigate if the dye survives all reaction conditions for the molecule synthesis and the grafting onto particles (including acidic and basic conditions as well as heat). The synthetic pathway of this so called **compound 4** or **coupling agent I** is described in Scheme III - 1.

The starting material 2,2-(ethylenedioxy)bis(ethylamine) provides on each side a terminal amine. As it was intended to react each side with two different highly reactive molecules, one first had to be protected. Di-tert-butyl dicarbonate (Boc anhydride) was chosen as reagent because its related Boc protection is very resistant against basic conditions, heat (up to 185 °C) and nucleophilic attacks.^{54,55} This was important as the protected starting compound had to survive all following reaction and washing steps with basic treatments. Furthermore, with this protecting group high yields in mono-protected product can be obtained if the molecule that is to be protected is taken in excess and reaction conditions are optimized.^{56,57} During the amine protection carbon dioxide and t-butanol are formed as side products, which is shown in Scheme III - 2. The solvent and the volatile side products were removed under vacuum and the excess 2,2-(ethylenedioxy)bis(ethylamine) was removed by washing the organic phase (CH₂Cl₂) with water. The mono-protected product (**compound 1**) was obtained in 97 % yield containing only traces of di-protected compound not visible in NMR. These traces visualized by thin layer chromatography (TLC) did not take part in the following reaction and were then easily removed by washing.

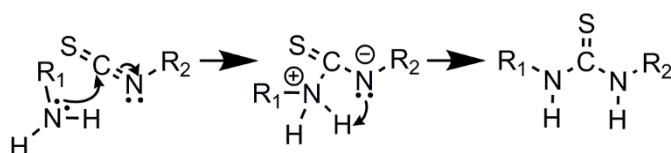


Scheme III - 1. Planned synthesis route of the **coupling agent 1**. The introduced RhB is only shown as 6-RhB while for synthesis a mixture of isomers was used.



Scheme III - 2. Mechanism of the protection of a primary amine with di-tert-butyl dicarbonate.

In the next step, Rhodamine B isothiocyanate (RhBitc) was reacted with the free amine of **compound 1**. The reaction was carried out under basic conditions with the addition of triethylamine (TEA). This ensured that the free amine was not protonated and therefore provided a free electron pair for the nucleophilic attack of the isothiocyanate carbon. The reaction mechanism is shown in Scheme III - 3. As solvents, a mixture of CH₂Cl₂ and dimethylformamide (DMF) was chosen to achieve the solubility of RhBitc salt while minimizing the amount of high boiling point solvent. The reaction was carried out overnight and after evaporation of all volatile components, the crude powder was extensively washed with diethyl ether to remove unreacted **compound 1** (as it had been added in slight excess) as well as traces of di-protected 2,2-(ethylenedioxy)bis(ethylamine) produced during the synthesis of **compound 1**. In order to remove the TEA·HCl salt resulting from the reaction of TEA with the chloride of RhBitc, a wash with basic water was carried out in order to free the TEA. After evaporation of the free TEA, **compound 2** was obtained with a yield of 94 %.

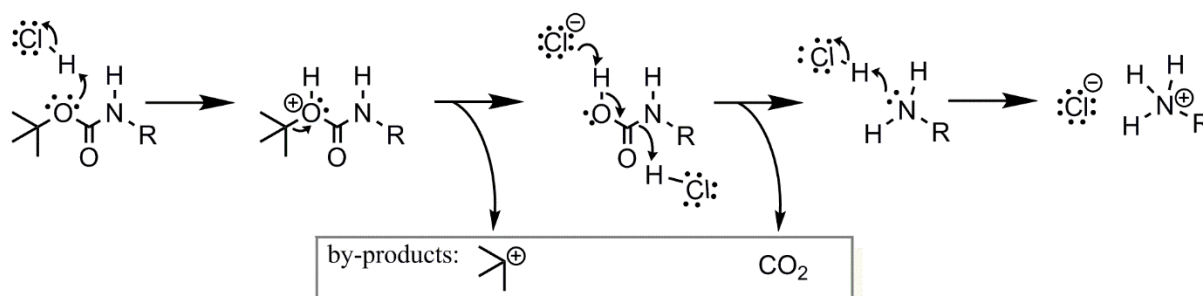


Scheme III - 3. Reaction mechanism of a primary amine with an isothiocyanate.

Now the Boc protecting group of **compound 2** was cleaved by bubbling anhydrous HCl in the CH₂Cl₂ solution. The cleavage takes place through an S_N1 pathway forming the tert-butyl cation. With Cl⁻ as a weak nucleophile, the cation can be slowly converted into tert-butyl chloride or rearranges into isobutene both of which can easily be eliminated out of the reaction batch by evaporation.^{58,59} The reaction mechanism is shown in Scheme III - 4. After evaporation of all volatile components, no further purification was necessary and **compound 3** was obtained as an ammonium salt, in quantitative yield.

For the grafting of the organic molecule, the silane moiety had to be introduced into the **compound 3**. For this the deprotected amine, which was obtained as an ammonium salt was dissolved in CH₂Cl₂ with the help of a large excess of TEA (15 eq - otherwise it was not soluble).

Then it was reacted with a slight excess of triethoxy(3-isocyanatopropyl)silane (1.2 eq). Afterwards, the solvent and excess TEA were evaporated. The residue was thoroughly washed with pentane to remove the unreacted silane.

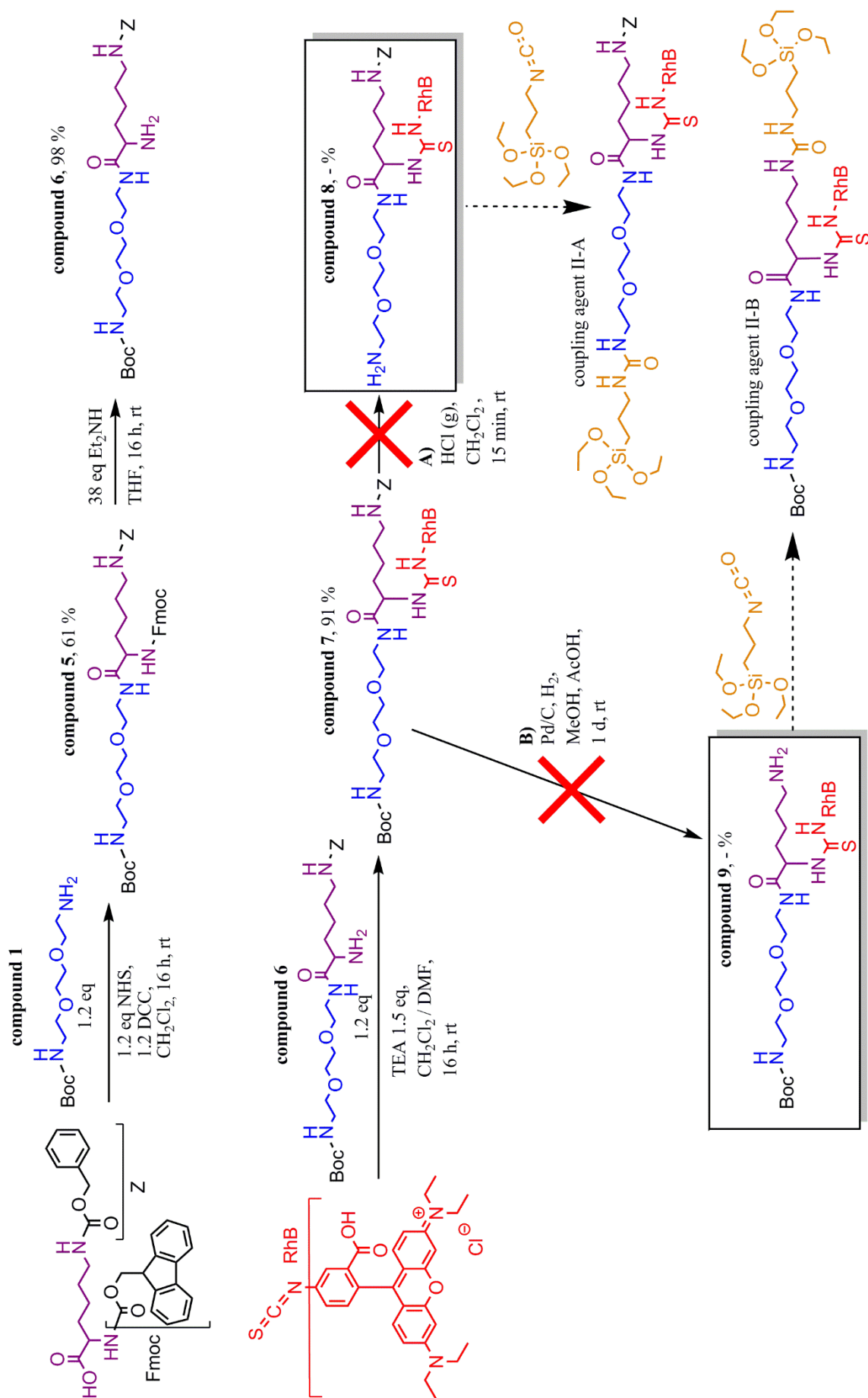


Scheme III - 4. Mechanism of the cleavage of the Boc protecting group from an amine with gaseous HCl.

After evaporation of all traces of pentane, the **compound 4** was obtained in about 90 % yield. It has to be mentioned that traces of TEA•HCl were still present in the compound. Therefore the yield was calculated with the help of the ¹H-NMR integrals. No further purification was needed as the salt was not supposed to interfere with the grafting reactions. **Compound 4**, also called **coupling agent I**, is later on used for the grafting onto TiO₂ nanoparticles. It has to be mentioned that the commercial RhBtc contained impurities, mainly visible in mass spectroscopy (MS). Most of them did not take part into the reactions and were removed during washing procedures. Nevertheless small amounts of rhodamine B amine (identified via MS) were not removed during all reaction steps and therefore reacted with the triethoxy(3-isocyanatopropyl)silane forming a side product to the desired **compound 4**. The amount of this side product is expected to be considerably low as NMR analysis does not show signals that can be assigned to it.

III.1.1.b. Coupling agent II

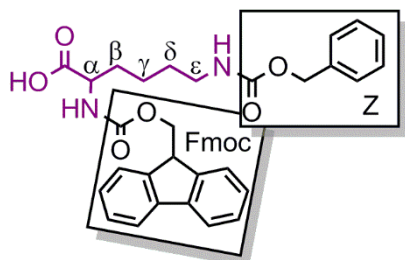
The second linear molecule was synthesized as a reference to the planned dendritic **coupling agent III** (treated later on in this chapter); it has the same basic components but does not contain a dendritic structure. The synthesis procedure of this linear coupling agent, is described in Scheme III - 5. For the design of this molecule, the most crucial point was to use three different protecting groups for amines (contained in the coupling agent) and to place them most ideally to avoid the unwanted deprotection during a reaction or during the cleavage of another protecting group. As a result, benzyloxycarbonyl (Z), tert-butoxycarbonyl (Boc) and 9-Fluorenylmethoxycarbonyl (Fmoc) were chosen as protecting groups. They are shortly introduced now, while more precise descriptions of their coupling and cleavage reactions will be provided later. The Z protecting group is the most popular protecting group in peptide synthesis due to its facile introduction and removal conditions.



Scheme III - 5. Planned synthesis route of the **coupling agent II**. The introduced RhBic is only shown as 6-RhBic while for synthesis a compound mixture of isomers was used.

It can be easily cleaved by catalytic hydrogenation or by acidolysis and is stable to most of the coupling reactions.^{54,55,58} Boc was the first urethane-type protection found that was stable to catalytic hydrogenation (used for Z cleavage) while labile under mild acidic conditions (as already mentioned before).^{54,55,58} The Fmoc group was found to be the perfect completion for Boc and Z as it is completely stable against acids and to a large extent to catalytic hydrogenation while it can be removed with bases such as alkyl amines.^{54,55,58} Comparing the cleavage conditions of all three protecting groups, the Fmoc protecting group was found to be the most labile group as it may be cleaved during prolonged catalytic hydrogenation (used for Z removal).⁵⁸ Additionally, this protecting group could be involuntarily removed during several coupling reactions needed for the synthesis of the coupling agents. For example, the reaction of isocyanates and isothiocyanates with amines had to be carried out under basic conditions and would most probably result in Fmoc cleavage. This is why Fmoc was always cleaved first. One of the two other protecting groups was also planned to be cleaved during the synthesis route, while the last protecting group was meant to be removed after grafting of the final coupling agent onto the nanoparticles.

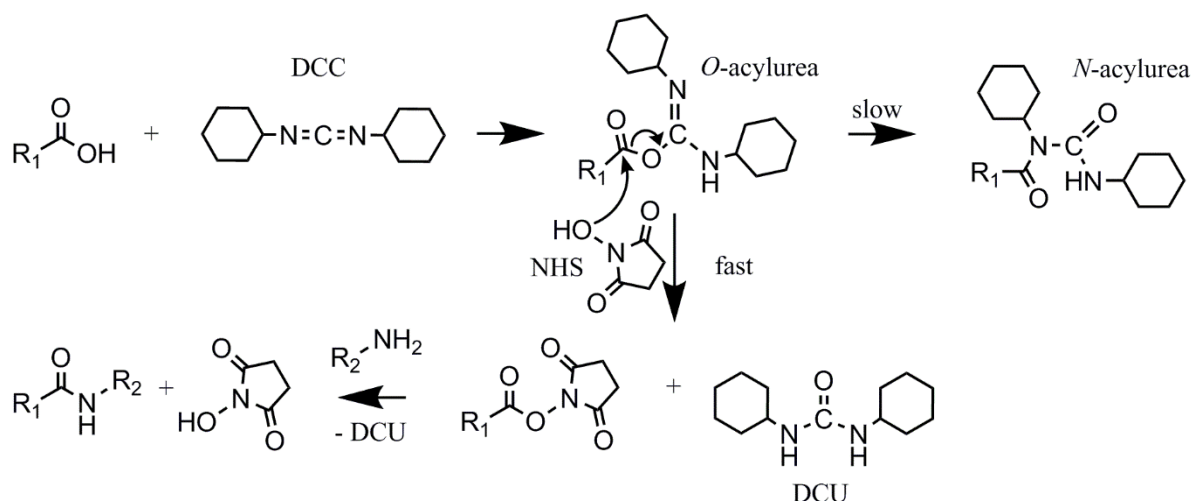
The starting materials for the linear **coupling agent II** were **compound 1** and the commercially available Fmoc-lysine-Z-OH (Scheme III - 6). The amines of this lysine are already Fmoc and Z protected; the *epsilon* amine is Z protected and the *alpha* amine is Fmoc protected.



Scheme III - 6. Fmoc-lysine-Z-OH.

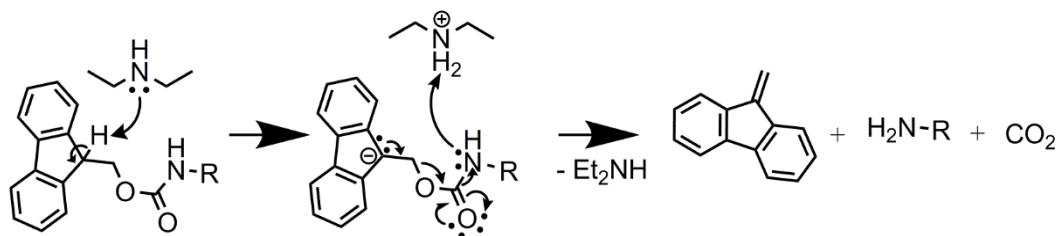
The carboxylic group is the only unprotected reactive group and can form an amide with the unprotected amine of **compound 1**. The coupling between **compound 1** and Fmoc-lysine-Z-OH was carried out by activating the carboxylic acid with *N*-hydroxysuccinimide (NHS) and *N,N'*-dicyclohexylcarbodiimide (DCC). First, the carboxylic acid is added to DCC leading to *O*-acylurea. Then NHS reacts with the *O*-acylurea to form a second, more stable activated ester. This avoids the formation of *N*-acylurea as a side product^{60,61} as NHS reacts with the DCC-activated compound faster than the reaction forming the side product can take place (Scheme III - 7).⁶¹ The activated ester reacts with the amine forming an amide and dicyclohexylurea (DCU).^{60,61} For this reaction Fmoc-lysine-Z-OH was dissolved in CH₂Cl₂ and reacted with DCC and NHS. The formed DCU, which was insoluble in CH₂Cl₂, was filtered off and **compound 1**

was added. The activated carboxyl group reacted with the free amine resulting in an amide bond (releasing the NHS) and the formation of **compound 5**. In order to purify this product, first the organic reaction phase was washed with acidic water to quench unreacted DCC converting it in dicyclourea (which was removed by filtration). Then, washing with basic water removed the main part of NHS and drying and subsequent washing of the powder with diethylether eliminated unreacted starting materials. To withdraw any remaining traces of NHS a silica column was run and pure **compound 5** was obtained with a yield of 61 %.



Scheme III - 7. Amide formation with the help of DCC and NHS.

In order to go on with further reactions, the Fmoc protected amine had to be deprotected under basic conditions.^{58,62,63} For this, a treatment with diethylamine in tetrahydrofuran (THF) was chosen. The cleavage mechanism is shown in Scheme III - 8. In contrast to other nonhydrolytic bases used for the cleavage like piperidine or morpholine, it does not form adducts with the produced dibenzofulvene. This is on one side a risk, as dibenzofulvene can polymerize, forming an insoluble mass or can irreversibly react with the deblocked amine. On the other hand, scavenging this compound by the base is a reversible equilibrium dependent reaction and often incomplete, which results in mixture that is even more difficult to separate.^{58,63}



Scheme III - 8. Mechanism of the Fmoc protecting group cleavage with diethylamine.

The produced CO_2 and the diethylamine were easily removed after the reaction. Nevertheless the obtained side product dibenzofulvene had to be separated from the product by washing. This was achieved by dissolving the crude material in acetonitrile followed by the addition of

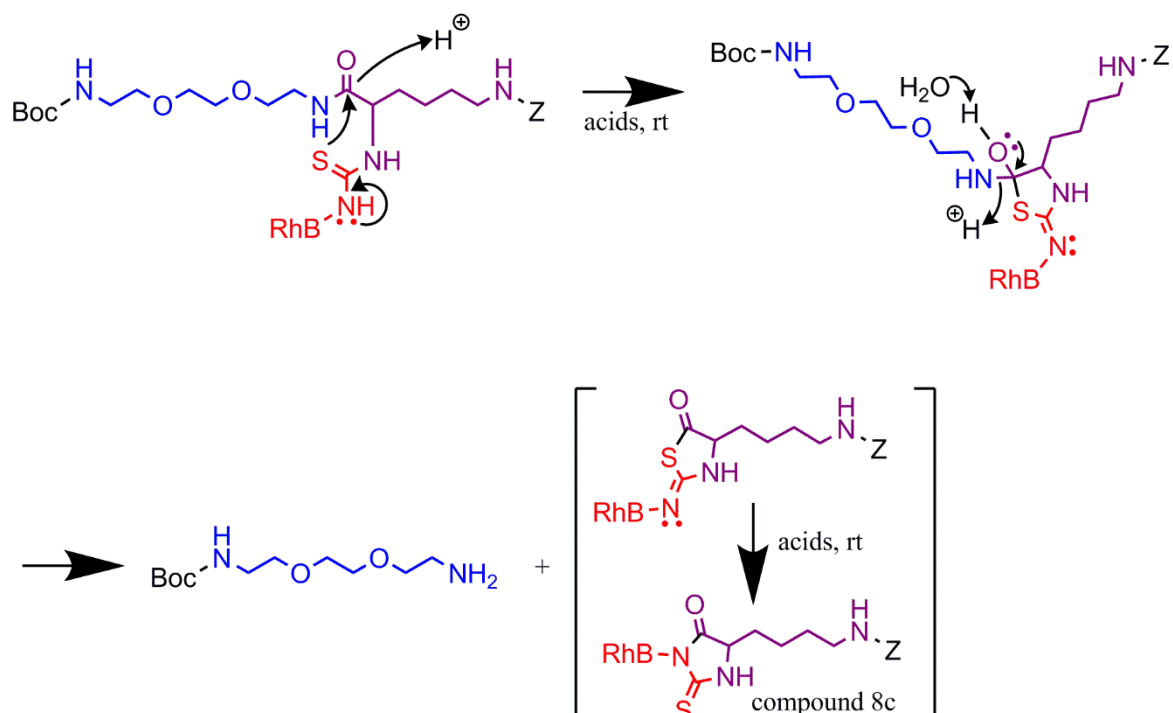
water (with a ratio of 1:9). Now the dibenzofulvene was eliminated from this very polar phase by washing with pentane while the product stayed in the water phase and was then extracted with CH₂Cl₂ after basification of the water phase to yield **compound 6** (98 %). Eventually polymerized dibenzofulvene was not extracted with pentane but also stayed in the water phase as a white mass during extraction of the compound with CH₂Cl₂.

Now, similar to the synthesis of **compound 2** the free amine of **compound 6** was coupled to the luminescent agent (RhBitc) to yield **compound 7** (91 %).

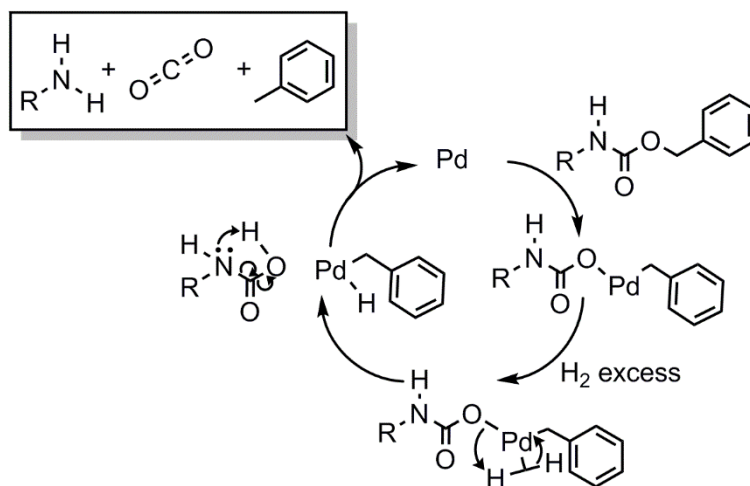
Then two different routes were investigated; either the cleavage of the Boc (Scheme III - 5; route A) or of the Z protecting group (Scheme III - 5; route B). Both reactions were supposed to lead to a free amine that can be reacted with the triethoxy(3-isocyanatopropyl)silane to obtain a final coupling agent, while the remaining protecting group has to be removed after grafting onto the nanoparticles. For the Boc deprotection, a treatment with HCl similar to the one used for **compound 3** was conducted. While the Boc protecting group was entirely removed, **compound 8** was not obtained but fragments of it. If the Boc cleavage was carried out treating **compound 7** with trifluoroacetic acid (TFA, with the same reaction mechanism as the cleavage with HCl), the Boc protecting group was not successfully cleaved and fragments of **compound 7** were obtained. In both cases, MS revealed the amide bond hydrolysis on the *alpha* position of the lysine with the neighbouring thiourea group participation.⁶⁴

The proposed mechanism for this reaction is shown in Scheme III - 9 in the case of weak acids (i.e. without parallel Boc group cleavage). This reaction has only been documented by Lang et al.⁶⁴ who studied the stability of glutamic acid linked to peptides and e. g. a phenyl. The breakage of the amine bond because of the neighbouring thiourea group was observed at pH = 4 in aqueous conditions and at elevated temperatures (80 - 100°C). In the case of **coupling agent II**, no heat was applied but stronger acids (HCl, TFA) were used either under anhydrous (HCl treatment) conditions or in the presence of water traces (TFA treatment).

The same fragmentation of **compound 7** was obtained while carrying out the Z deprotection to obtain **compound 9**. For this deprotection a hydrogenation with the catalyst Pd on carbon was chosen. The proposed mechanism of this reaction is described in Scheme III - 10. It has to be mentioned that while in the case of homogenous catalysis the depicted mechanism seems to be the most probable one, for heterogeneous one (which has been used in this study) it may be different as dissociative adsorption of the reactant onto the Pd particles would be necessary for the catalysis.



Scheme III - 9. Proposed mechanism of amide bond hydrolysis under the participation of the neighboring thiourea group at room temperature and acidic conditions (without additional Boc-cleavage).⁶⁴



Scheme III - 10. Proposed mechanism of the Z protecting group cleavage with the help of catalytic hydrogenation (Pd/C, H₂).

With this treatment the Z protecting group can be cleaved in general while not affecting the Boc protecting group, which is also present in **compound 7**.^{54,55} Following literature, methanol was chosen as the solvent and additionally a small amount of HCl was added to promote the Z group cleavage thanks to protonation of the nitrogen atom.^{65–71} During this deprotection procedure, only the amide bond hydrolysis at the lysine *alpha* position of **compound 7** was achieved while not cleaving the Z protecting group.

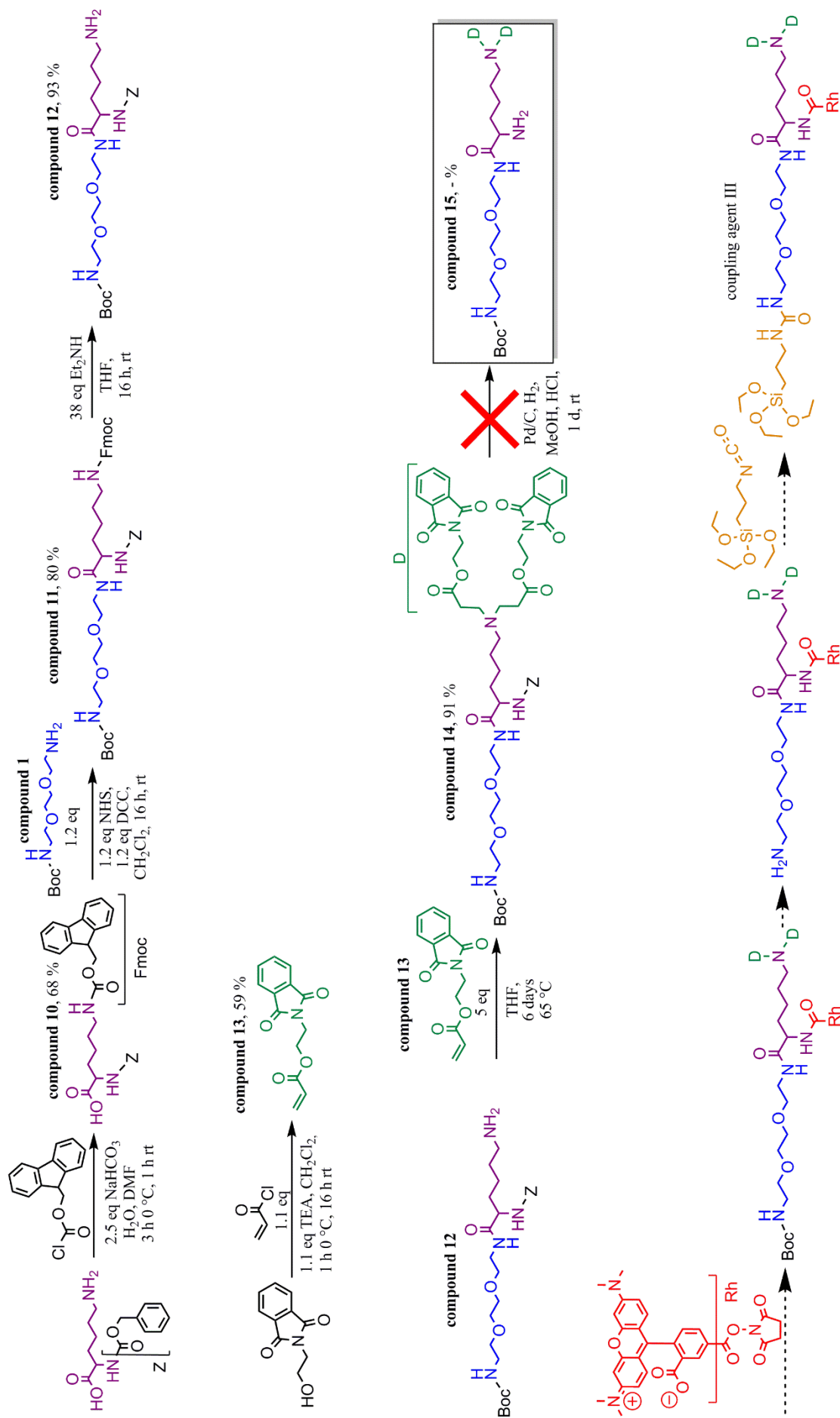
Thus, this specific amide bond is less stable than both carbamates of the Z and Boc protecting groups and it is not possible to complete this synthesis route to obtain **coupling agent II**. It also has to be mentioned that a separation of the dye from the rest of **compound 7** by rupture of the thiourea was detected in MS analysis of the synthesis attempts of **compound 8** and **compound 9**. Nevertheless, this bond breakage is assumed to be caused by the electrospray ionization for MS. In order to avoid the amide bond hydrolysis on the *alpha* position of the lysine with the neighbouring thiourea group participation, the most evident solution was to change the function connecting the dye with the lysine. In the case of an amide bond instead of a thiourea at this position, this reaction was reported not to take place.⁶⁴ This approach was attempted for **coupling agent III** and will be described later on.

III.1.1.c. Coupling agent III (compound 22)

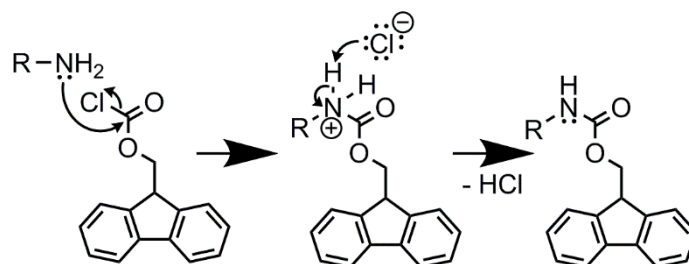
In parallel to the synthesis of **coupling agent II**, the preparation of its dendritic version, named **coupling agent III** was investigated. The first planned synthetic pathway of this 1st generation dendritic coupling agent is described in Scheme III - 11. This molecule contains two dendritic branches with phthalimide-protected amines as end groups. These protecting groups were meant to be cleaved after successful grafting of the coupling agent onto the particles while preventing the reaction of the terminal amines during synthesis.

Due to the design of this molecule the location or cleavage order of the protecting groups had to be slightly changed according to their stability and cleavage mechanisms as mentioned before. As Z-lysine-Fmoc-OH was not commercially affordable, it was first synthesized by the protection of the commercial Z-lysine-OH.

The free epsilon amine was protected by the reaction with 9-Fluorenylmethoxycarbonyl chloride (Fmoc-Cl) as shown in Scheme III - 12. When carrying out Fmoc protection of amino acids, it always has to be considered that di-peptide formation can occur as a side reaction. Especially during protection procedures of the *alpha* amine detectable amounts of dipeptide acids or even tripeptide acids have been reported when chloroformates like Fmoc-Cl were utilized.⁵⁸ The carboxy group of amino acids can be activated by the reaction with a chloroformate forming an anhydride. These intermediates are sufficiently stable in aqueous-organic reaction media to then undergo aminolysis and form a peptide with another amino acid. They are usually difficult to detect and to separate from the product and therefore a major concern for the Fmoc protection of amino acids. These side products were obtained even under Schotten–Baumann conditions (mixture of aqueous and organic solvent and reaction at 0 °C).⁵⁸

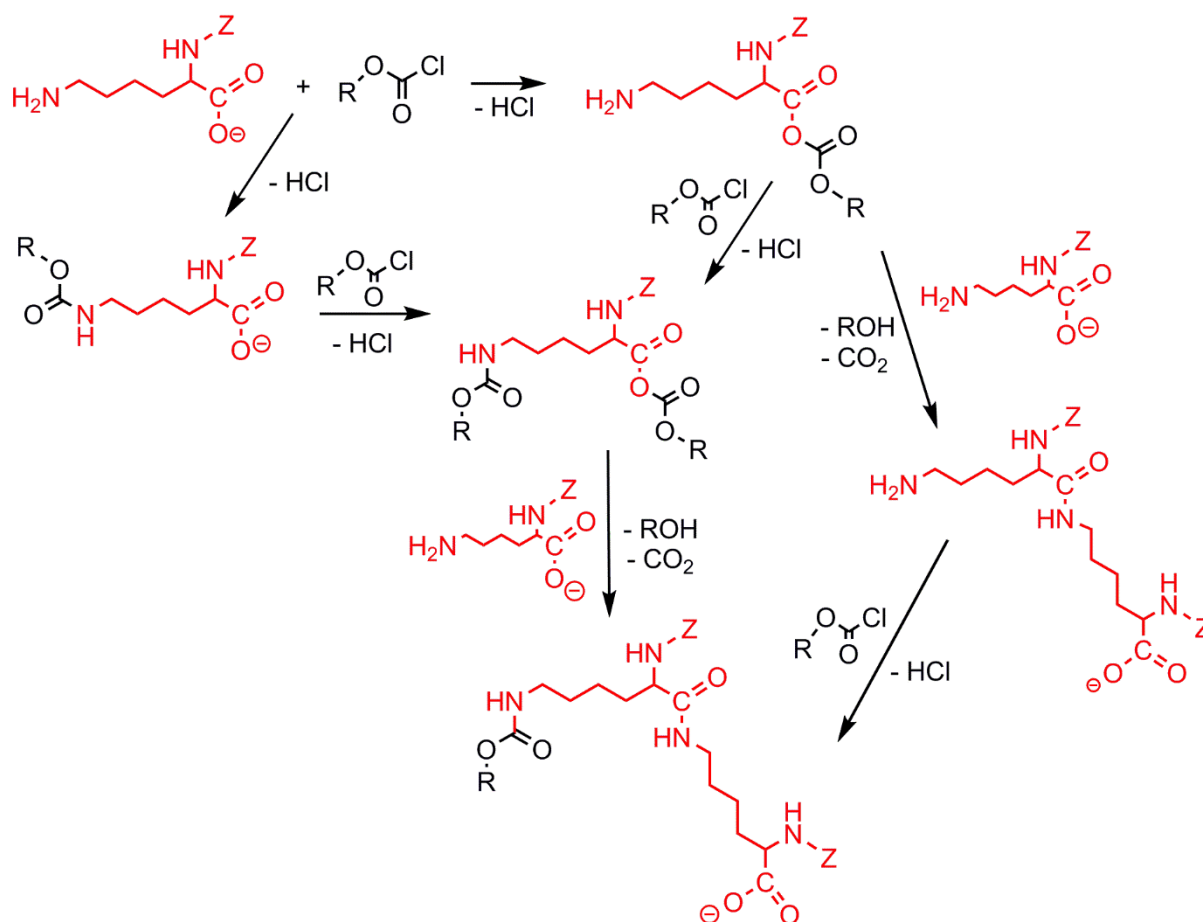


Scheme III - 11. Planned synthesis route of the **coupling agent III**. The introduced NHS-Rhodamine is only shown as 6-carboxytetramethylrhodamine while for the synthesis a compound mixture of 5- and 6-carboxytetramethylrhodamine was used.



Scheme III - 12. Reaction mechanism of Fmoc protection of an amine with FmocCl.

Nevertheless, dipeptide formation during the Fmoc protection of Z-lysine-OH or lysine-Z-OH has in general not been mentioned before.^{67,72,73} Following the reaction protocols from literature,^{67,72,73} Z-lysine-OH was reacted with Fmoc-Cl in a mixture of Na₂CO₃-water solution and an organic solvent. In contrast to former publications, dipeptide formation was detected by TLC and even visible in NMR. The probable reaction mechanism for the formation of dipeptides is shown in Scheme III - 13.



Scheme III - 13. Probable mechanisms of dipeptide formation during Fmoc protection of Z-lysine-OH with FmocCl.

With the help of several washing procedures the Z-lysine-Fmoc-OH was purified; after complete reaction of Fmoc-Cl (controlled by TLC), the crude compound was precipitated by addition of 1 M potassium hydrogensulfate solution. Then the precipitate was washed with

water to remove all salts and with toluene to remove the Fmoc-OH that was generated due to the dipeptide side reaction. Afterwards, the precipitate was washed with diethylether to separate the Z-lysine-Fmoc-OH from the dipeptide. This was possible due to different solubility; the dipeptide was insoluble in this solvent while the product was. Depending on the organic solvent used for synthesis the yield of **compound 10** greatly varied due to the amount of dipeptide that was formed as a side reaction (*Table III - 1*).

*Table III - 1. Obtained yields of **compound 10** depending on the organic solvent used for synthesis.*

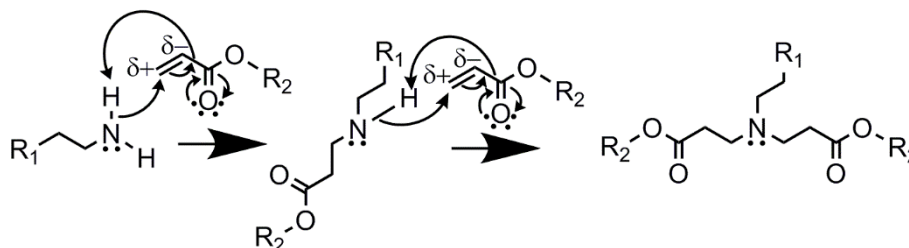
organic solvent	yield
THF	30 %
dioxane	11 %
DMF	68 %

Then **compound 10** was reacted with **compound 1** to obtain **compound 11**. This compound was obtained with a yield of 80 %.

In order to obtain **compound 12** with a yield of 93 %, the Fmoc protecting group was cleaved.

To begin the growth of the dendritic structure, the acrylate (**compound 13**) as reactant had first to be synthesized; *N*-(2-hydroxyethyl)phthalimide was reacted with acryloylchloride in the presence of TEA to scavenge the HCl formed.^{74–78} The reaction mechanism is the same as for the reaction of an amine with an acylchloride, which was explained in Scheme III - 12 for the Fmoc protection of an amine with FmocCl. The product was easily purified as it stayed in the organic phase (CH₂Cl₂) while the unreacted reactants were extracted with water. **Compound 13** was obtained with a yield of 59 %.

Now the creation of the 1st generation dendritic branches was carried out by stirring **compound 13** and **compound 12** in THF for 6 days at 65 °C. During this time the acrylate reacted with the free amine through a double Michael addition as shown in Scheme III - 14.⁷⁹

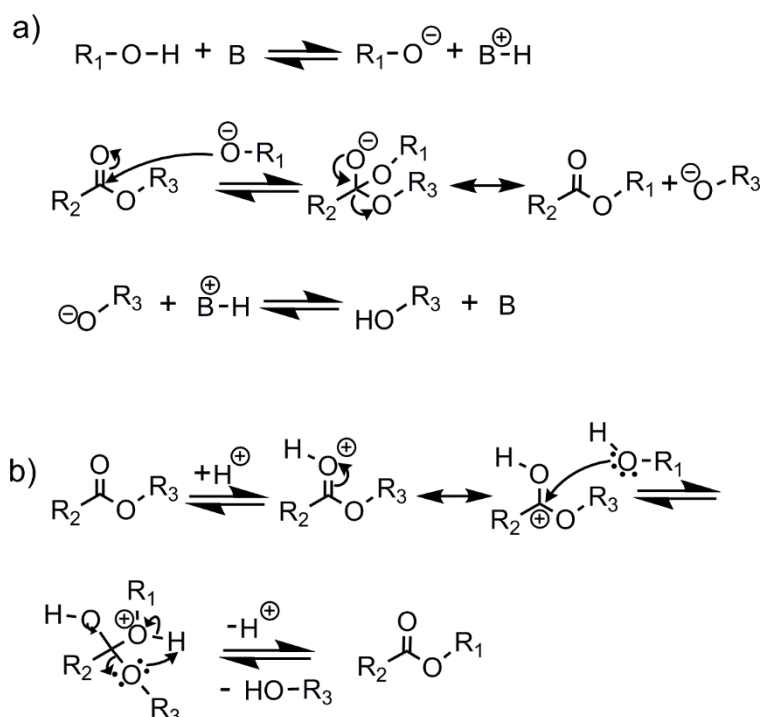


Scheme III - 14. Mechanism of the double Michael addition.

With the help of column chromatography, the excess **compound 13** was separated from the obtained **compound 14** (91 %). As well as THF, dioxane and DMF were tested as possible

reaction solvents that solubilized the reactants sufficiently. Nevertheless, in these solvents only the formation of one branch was achieved.

For the subsequent deprotection of the Z-protected amine of **compound 14** the hydrogenation with Pd on carbon was carried out as described for the attempt to obtain **compound 9**. This treatment does usually not affect the Boc and phthalimide protecting groups present in **compound 14**.^{54,55} During analysis of the expected Z-deprotected **compound 15**, NMR and MS analyses indicated a decomposition of the compound; parts of the dendritic branches were removed by transesterification reactions with the methanol solvent. The base and acid catalysed transesterification mechanism is shown in Scheme III - 15.



Scheme III - 15. The a) base and b) acid catalysed transesterification mechanism with *B* representing a base.⁸⁴

In this specific case *R*₁ would be the methanol solvent, *R*₂ the coupling agent and *R*₃ the benzyl group of Z. How the Pd/H₂ catalyses the transesterification has not been studied in detail yet as acidic or basic catalysis seems to be handier and very few publications can be found that mention such transesterifications using similar catalysts.⁸⁰⁻⁸³

In order to further determine which reaction conditions are leading to a transesterification reaction, several stability tests were carried out on **compound 14**. The results of these examinations are shown in Table III - 2. As this mechanism is an equilibrium driven reaction with an alcohol, it is logical that the presence of methanol or ethanol favoured transesterifications. Additionally, a base or Pd and H₂ had to be present to catalyse this reaction, while acidic conditions did not promote the reaction in this case. If the catalytic

hydrogenation would be carried out in THF no side reactions are supposed to occur and the reaction product would be **compound 15** as expected (given that the Z cleavage is successful).

*Table III - 2. Stability tests with **compound 14** over 24 h (except for the last case: 12 h).*

solvent	catalyst	stability (proved by NMR and/or MS)
methanol	HCl in water	stable
methanol	KOH in water	transesterification
methanol	Pd/C, H ₂	transesterification
THF	Pd/C, H ₂	stable
THF	KOH in water	hydrolysis
ethanol/water	NH ₃ in water	transesterification

Nevertheless, in the following planned reaction steps, washings with basic water were necessary, which also seemed to affect the stability of the compound (like in Table III - 2; THF and KOH) even without the presence of an alcohol. In this case a small percentage of **compound 14** appeared to be hydrolysed under base catalysis resulting in the carboxylic acid and the alcohol. The reaction mechanism of this reaction is similar to Scheme III - 15 a) while R₁ would be a proton. This was the first argument against the use of **compound 14** for the synthesis as a coupling agent but even more crucial was the planned grafting of the final coupling agent onto the particle. This reaction had to be carried out in a hydroalcoholic solvent and in the presence of a base (like in Table III - 2 ethanol/water and NH₃), which both are indispensable for the hydrolysis and condensation reactions of the coupling agent (as discussed in III.2.). Under these conditions, the coupling agent would definitely be destroyed. This is why a modification of the structure of the dendritic branches was necessary; the ester groups were replaced by amide groups, which are more stable and should withstand the subsequent reaction steps.

The alternative synthesis route for the 1st generation dendritic **coupling agent III** is shown in Scheme III - 16. The acrylate was substituted by an acrylamide for the creation of the branches. In order to obtain this reactant, two synthetic steps were required.⁸⁵ First, 2-chloropropylamine hydrochloride was reacted with acryloylchloride in CH₂Cl₂ and in the presence of TEA to scavenge the HCl formed. The reaction mechanism is the same as for the reaction of an amine with an acylchloride, which was explained in Scheme III - 12. The TEA•HCl salt was filtered off and the unreacted reactants were washed away with basic water to obtain pure **compound 16** (88 %).



Scheme III - 16. Planned alternative synthesis route of the **coupling agent III**. The introduced NHS-Rhodamine is only shown as 6-carboxytetramethylrhodamine while for the synthesis a compound mixture of 5- and 6-carboxytetramethylrhodamine was used.

Afterwards, potassium phthalimide was reacted with **compound 16** in DMF (75 °C, 24 h) via Gabriel synthesis to yield **compound 17**, following a S_N2 mechanism. The reaction results in a phthalimide-protected primary amine. The formed KCl as a side product was filtered off and the compound was purified via column chromatography to yield pure **compound 17** (55 %). During this reaction, polymerization of the reactant **compound 16** led to various side products lowering the yield.

In order to obtain **compound 18**, **compound 12** and **compound 17** were reacted in methanol via double Michael addition as described in Scheme III - 14.^{86,87} For this reaction to take place, the reactants had to be heated to 75 °C and stirred for 7 days. In contrast to the acrylate, the acrylamide showed a lower reactivity towards the free amine while easily polymerizing, which led to lower yields of **compound 18** (57 %). The pure desired product was obtained after purification by column chromatography.

Subsequent Z deprotection was carried out via hydrogenation with Pd on carbon as described for the synthesis attempt of **compound 9**. Our findings confirmed other publications that - in the case of lysine - the Z cleavage was only possible with the addition of an acid protonating the heteroatom to facilitate the reaction while strongly acidic conditions led to a parallel Boc deprotection.⁶⁵⁻⁷¹ In the presence of 4 eq acetic acid the Boc protecting group was not affected while an addition of 2 eq HCl already resulted in Boc cleavage. Due to the present acid, **compound 19** was first obtained as a salt and it was possible to extract it with water from the organic phase that contained the unreacted **compound 18**. After basification of the aqueous phase, the pure product as free amine was recovered with dichloromethane (54 % yield).

In order to introduce the dye into the coupling agent, **compound 19** was reacted with 5-/6-carboxytetramethylrhodamine, succinimidyl ester (NHS-Rhodamine) in presence of TEA. DMF was used as solvent to guarantee the solubility of all reactants. After 15 h of reaction, all volatile compounds were removed and the obtained crude product was dissolved in CH₂Cl₂. The desired product was separated from deactivated NHS-Rhodamine (due to hydrolysis), the side product NHS and unreacted **compound 19** by washing with basic and acidic water. This procedure resulted in **compound 20** (85 %).

For Boc protecting group cleavage, similar to the second synthesis attempt of **compound 8**, **compound 20** was dissolved in CH₂Cl₂ and TFA was added to obtain **compound 21** after reaction overnight in quantitative yield. Finally, the silane moiety was added to the **compound 21**. In order to do so, the deprotected amine, which was obtained as an ammonium salt, was dissolved in CH₂Cl₂ with the help of an excess of TEA. Then it was reacted with triethoxy(3-isocyanatopropyl)silane overnight. Afterwards, the solvent and excess TEA were evaporated

to obtain **compound 22**, also called **coupling agent III**, in quantitative yield. It has to be mentioned that the side product TEA•TFA was still present in the compound. This small quantity of salt was not supposed to interfere in subsequent grafting reactions.

The feasibility to introduce rhodamine into the coupling agent via amide bond formation and to finalize the **coupling agent III** has been herein proved. Nevertheless, the commercial NHS-rhodamine was only available in small quantities. Consequently, the **coupling agent III** was obtained in quantities too limited to be used for grafting approaches. In general, the NHS-activated as well as the non-activated 5-/6-carboxytetramethylrhodamine are both commercially not available with a reasonable price and quantity. This is why for future studies, the synthesis of carboxytetramethylrhodamine and its subsequent activation for amide formation would be advisable and has already been proved to be feasible in literature.⁸⁸

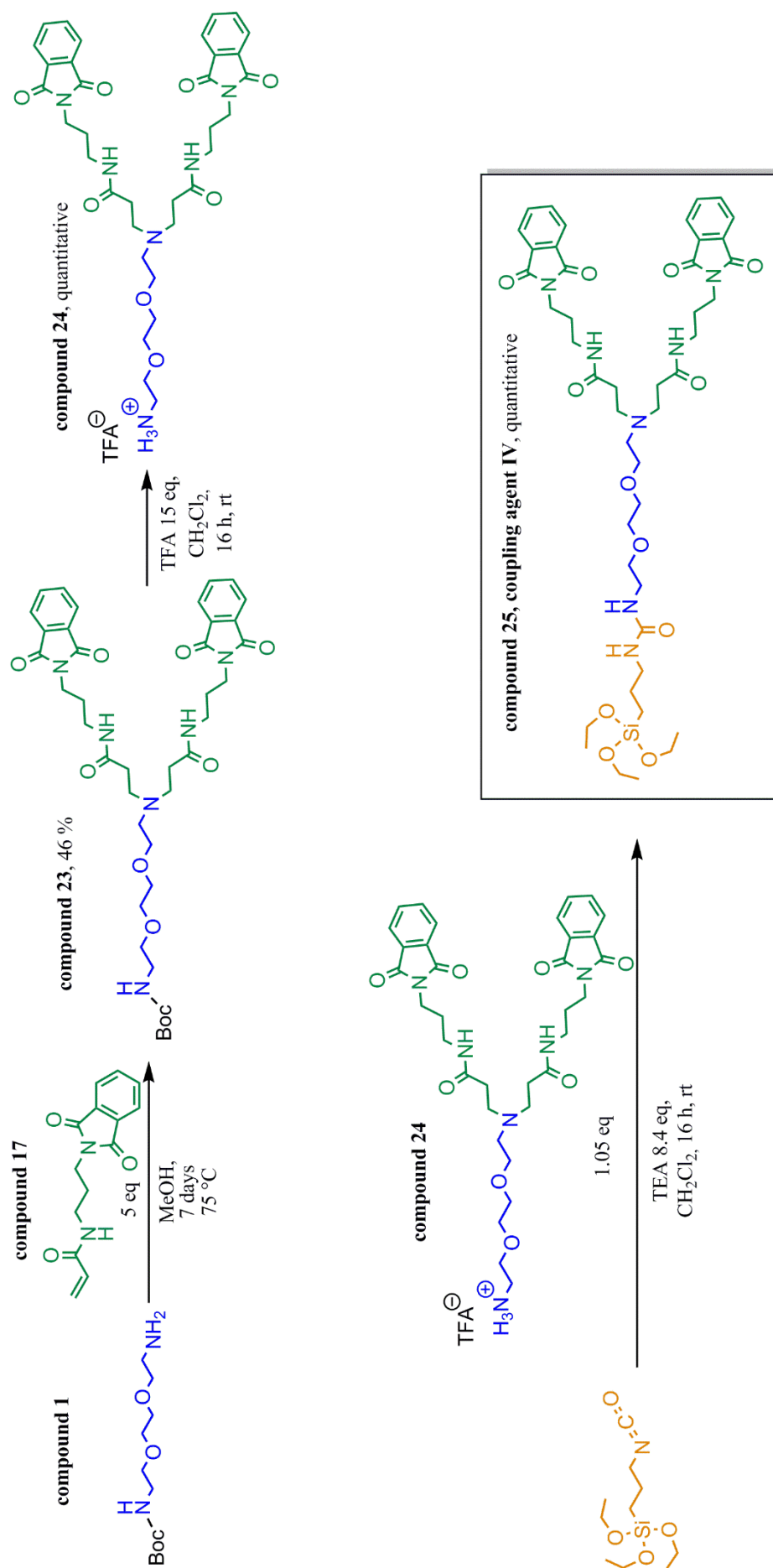
III.1.2. Synthesis of dendritic non-fluorescent coupling agents

The approach to synthesize non-fluorescent coupling agents emerged out of the problems occurring during the synthesis of the **coupling agents II** and **III**. Non-fluorescent dendritic coupling agents are useful to study the charge-dependent cellular uptake as they can finely manipulate the particle surface charge. They will also be a suitable tool to study the dendritic effect of the positively charged terminal groups without having to consider charge effects of an incorporated dye. Analysis techniques that do not rely on fluorescence, can be used to detect the functionalized nanoparticles; for example confocal Raman microscopy. This is why the synthesis of non-fluorescent coupling agents is valuable to gain more insights into the behaviour of functionalized NP systems.

III.1.2.a. Coupling agent IV (compound 25)

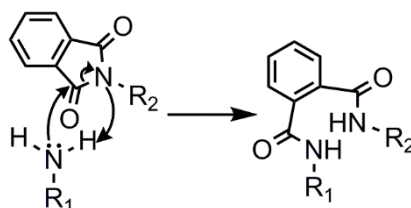
The first non-fluorescent coupling agent is a 1st generation dendron showing a similar structure to **coupling agent III** while not containing the lysine and the rhodamine B components. Its synthesis route is described in Scheme III - 17.

In order to obtain **compound 23**, **compound 1** and **compound 17** were reacted under the same conditions as used for **compound 18**. In the same way, the yield (46 %) of the purified **compound 23** (after column chromatography) was considerably low due to polymerization reactions of the acrylamide. Subsequent Boc deprotection was carried out with the help of a TFA treatment, similar to the second synthesis attempt of **compound 8**. The resulting **compound 24** was obtained as a TFA salt in quantitative yield and not transformed into a salt-



Scheme III - 17. Planned synthesis route of the coupling agent IV.

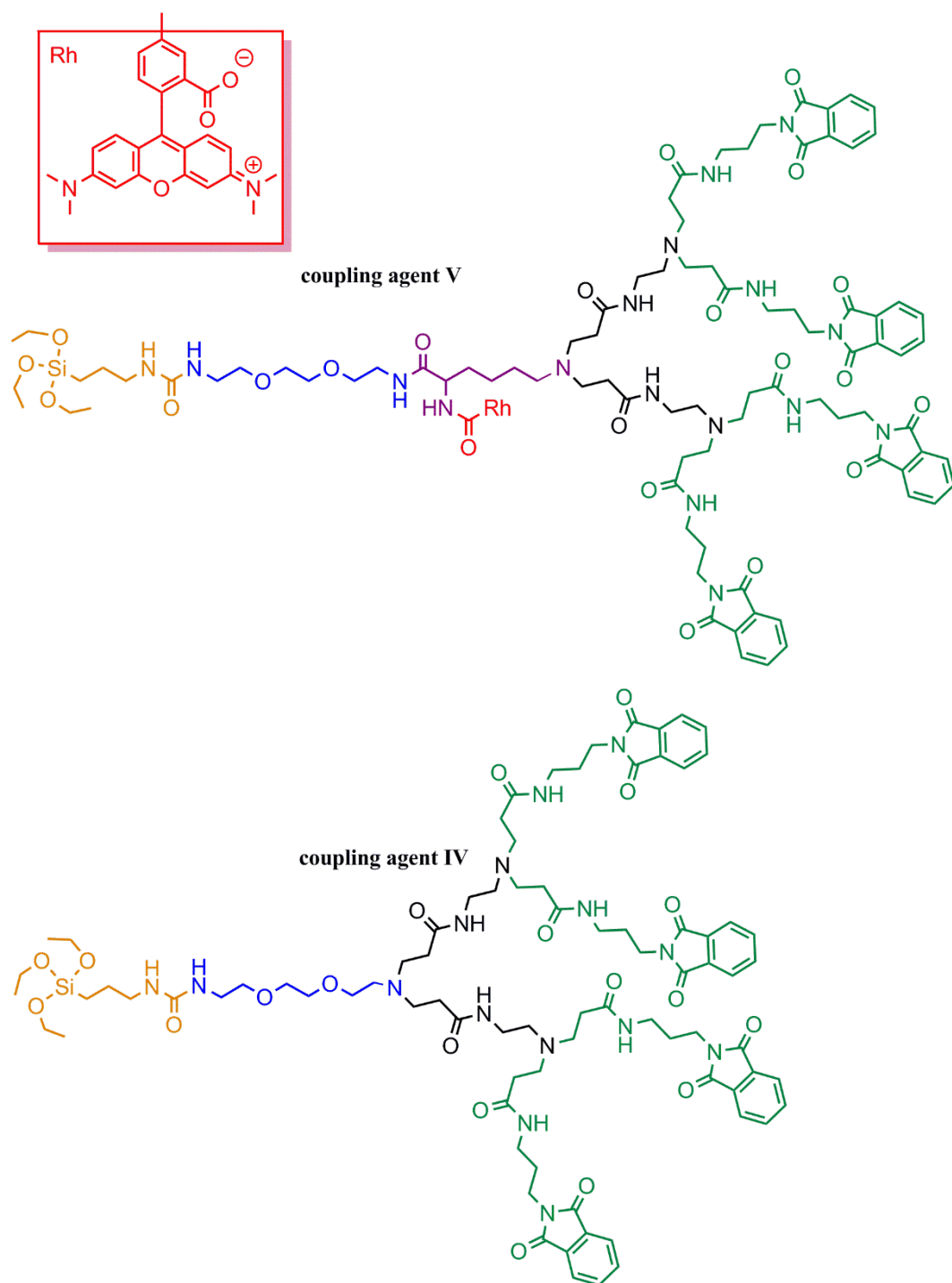
free compound as this free amine acts as a strong base, reacting with the phthalimide protecting group during storage. The proposed mechanism for this reaction is described in Scheme III - 18 and may lead mainly to a cyclisation of the molecule (or to a smaller extent in a polymerization, which was not detectable in MS). The cyclisation of **compound 24** was concluded as MS showed the same mass but NMR indicated the shift of the protons whose environment changed due to the reaction. Additionally, the subsequent urea formation did not take place due to no available primary amine.



Scheme III - 18. Proposed mechanism for the phthalimide ring opening by a primary amine.

For the synthesis of **compound 25**, **compound 24** was reacted with triethoxy(3-isocyanatopropyl)silane in presence of TEA similar to the synthesis of **compound 4**. TEA withdrew the TFA from the primary amine of **compound 24** making it accessible for a reaction with the isocyanate. The isourea formation proceeded faster than the before described reaction of the amine with the phthalimide group resulting in **compound 25** in quantitative yield. This **coupling agent IV**, is later on used for the grafting onto TiO₂ nanoparticles.

The synthesis of 2nd generation dendritic **coupling agent V** and **coupling agent VI** (Scheme III - 19) with a similar structure either to **coupling agent III** or to **coupling agent IV** was started but as the coupling agents were not completed, these synthesis routes are not discussed here. Nevertheless, the synthesis protocols can be found in the experimental part of this manuscript (**compound 26** to **compound 30**).



Scheme III - 19. 2nd generation dendritic coupling agents.

III.2. Grafting of functional coupling agents onto particles

After the synthesis of the organic coupling agents, their grafting onto TiO₂ nanoparticles was carried out. The surface modification of TiO₂ groups was realized via the reaction of the surface hydroxyl groups of the particles with the silanol group of the grafting agents resulting in covalent bonds. As grafting agents, organo-silanes were chosen as their reactive silane groups can typically covalently react onto inorganic substrates (like silica, gold or metal oxides)⁸⁹ while they do not react with organic molecules. The chosen trimethoxy- or triethoxy-organo-silanes were preferred to trichloro-organo-silanes as these are less reactive ($R-Si(OC_2H_5)_3 < R-Si(OCH_3)_3 < R-SiCl_3$) and may lead to a more uniform grafting due to less self-condensation before or during grafting.

As the particles were obtained in aqueous solution during synthesis and mainly showed hydrophilic properties, the grafting conditions had to be in aqueous solutions. Furthermore, the presence of water is favourable for the silanization, since it promotes the hydrolysis of the alkoxy-organo-silanes. Hydrolysis has first to take place before further condensation reactions can proceed - as already shown in Chapter II.3.1. Additionally, the reaction medium was chosen to be hydroalcoholic as hydrophilic and protic solvents usually accelerate the hydrolysis of silanes increasing the reaction kinetics.^{90,91} In the case of silanization, the amount of free hydroxyl groups on a surfaces is often too low to form more than one siloxane group on it, which may be the case for the TiO₂ particles used, bearing additional organic groups on their surface (as discussed in Chapter II.1. and II.2.). This is the reason why cross-linking reactions between the coupling agents also occur leading to a densification of the siloxane layer and thus to an even stronger attachment of the layer around the particle surface.⁹² Nevertheless, the already present organic surface moieties may also impede the cross-linking reactions between the coupling agents.

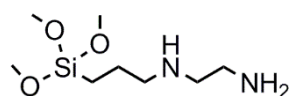
In addition to the silanization, an unwanted polycondensation of the organo-silane can also take place leading to the formation of silane aggregates. If these aggregates condensate onto the particle surfaces the homogeneity of the surface layer can be greatly diminished.⁹³ The preferential reaction of silanes can be mediated by the addition of an acid or a base as catalysts. Acids tend to promote the formation of net like structures (due to slower hydrolysis) while bases promote particle like structures (due to faster hydrolysis).^{94,95} The functionalization of a material works with both catalysts but under acidic conditions oligomerization is more probable.⁹⁶ This is why a base is usually chosen to promote the surface functionalization of nanoparticles. Most often ammonia is used as the base but also other amines with exchangeable protons like ethylamine or diethylamine are an option.^{95,97,98} Even if base catalysed functionalization is preferred, the acidic catalysis approach also had to be taken into

consideration as the synthesized TiO₂ nanoparticles are nicely dispersed only under acidic conditions, which is important for the accessibility of hydroxyl surface groups. The stabilisation of the nanoparticles under basic conditions with the help of an stabilising agent is an option that has been chosen before.^{99–101} However, the stabiliser can also impede the surface accessibility of the particles and the removal of it after grafting cannot be guaranteed. This influences the final surface properties and can have negative effects on the later cell culture application. Due to this, the stabilisation of particles with stabilising agents was not chosen for the graftings carried out in this work.

Furthermore, the reaction of organo-silanes can also be influenced by the experimental parameters like the reaction time, temperature and solvent or water concentration chosen for the surface functionalisation. Raising the temperature for example accelerates the reaction kinetics and therefore decrease the reaction time, which is mainly dependent on the reactivity of the silane and can vary from several minutes to hours.¹⁰² Additionally, the slower the silane addition is, the more efficient the surface coverage.¹⁰³ The concentration of particles in the reaction solution should also be relatively low, to avoid cross-linking between the particles through siloxane bridges.

III.2.1. Optimization of grafting protocols with commercial silanes

Due to the before mentioned factors influencing the successful grafting of organo-silanes onto particle surfaces, the commercial silane [3-(2-aminoethylamino)propyl]trimethoxysilane (Scheme III - 20) was used to first determine an optimized grafting protocol. This molecule was chosen as a model as it also shows hydrophilic properties and an amine end group similar to the synthesized coupling agents (III.1). Grafting conditions¹⁰⁴ such as ethanol to water concentration, were chosen according to the results of the silica shell formation around the synthesized TiO₂ particles as discussed in Chapter II.3.1. In order to determine the most suitable catalyst, graftings were carried out first with the addition of ammonia as a catalyst (improving the functionalization of the particles by the silane). A second reaction protocol included the addition of nitric acid for the silane addition as it provides good particle stability and later ammonia to complete the grafting reaction, in an attempt to combine both advantages of the catalysts.



Scheme III - 20. [3-(2-Aminoethylamino)propyl]trimethoxysilane.

In order to determine the minimum of silane needed for the grafting reactions, the theoretical amount of silanes needed to obtain a monolayer on the particles was calculated. The following assumptions were made: the surface area of the particle samples that is available for grafting is the BET surface area determined by N₂ sorption and the restricting factor for the monolayer density on a surface is the distance between uncoupled hydrolysed silanes.⁸⁹ As the maximal length of a Si-OH...HO-Si sequence is $d = 0.6 \text{ nm}$,⁸⁹ this is the diameter of the assumed covered circular area $A = \left(\frac{d}{2}\right)^2 * \pi$ of a single hydrolysed organo-silane ($N = 1$). The surface coverage c by an organo-silane is therefore:

$$c = \frac{n}{A} = \frac{N}{N_A * A} = \frac{1}{N_A * \left(\left(\frac{d}{2}\right)^2 * \pi\right)} = 5.874 * 10^{-6} \frac{\text{mol}}{\text{m}^2}$$

with N_A as Avogadro's constant ($6.022 * 10^{23} \frac{1}{\text{mol}}$) and the chemical amount $n = \frac{N}{N_A}$. The calculated amount of silane for each of the particle samples utilized for grafting in this chapter are shown in Table III - 3.

Table III - 3. Calculation of the theoretic amount of silane needed depending on the specific surface area of the particle sample.

particle samples	specific surface area S (N ₂ sorption) [m ² /g]	theoretic amount a of required silane per mg particles: $a = c * S$ [μmol/mg]
AA-TiO ₂	207.5	1.22
MEEAA-TiO ₂ (200 °C 4 h)	185.2	1.09

Following this, concentrations from 50 μmol to 0.5 μmol [3-(2-aminoethylamino)propyl]-trimethoxysilane per mg nanoparticle were used. The AA-TiO₂ particles (160 °C, 4 h) were chosen as model particles for both the basic and acidic (to later basic) grafting protocols. After grafting the silane onto them, the samples were characterized via zeta potential, DLS, as well as DRIFT measurements. The results are shown in Table III - 4 (zeta potential and DLS analyses) and in Figure III - 2 (DRIFT). DLS measurements have been carried out in ethanol, to visualize a successful functionalization of the nanoparticles as the non-functionalized particles are not stably dispersed in ethanol resulting in large agglomerate sizes. The organo-silane mediates a stabilisation in ethanol; this means if the agglomerate size is significantly decreased, the functionalization has been successful and the particle surface is sufficiently modified to ensure a tuning of the surface properties of the particles by the organic grafting agent. The results of DLS measurements all indicate a successful functionalization as the agglomerate size of the (former not stably dispersed) particles in ethanol is smaller than 50 nm

after the silane grafting. It appears that the agglomerate size can be decreased with increasing amounts of silanes due to a larger number of functional groups on the particle system that enhance the dispersibility in ethanol. If the amount of grafting agent is increased further, the diameter of the entire particle sample is also increased, which results in slightly larger agglomerate sizes. Nevertheless, the difference in agglomerate sizes should not be considered too important as the small variations in agglomerate size can also be due to varying dispersion efficiency by ultrasonic treatment.

Table III - 4. Analysis (zeta potential and DLS) of AA-TiO₂ functionalized with [3-(2-aminoethylamino)propyl]trimethoxysilane under basic or acidic (to later basic) conditions.

Sample prepared under basic conditions, ratio of silane to NP [μmol/mg]	pH(IEP) determined by zeta potential titration	Agglomerate size [nm] (PDI [-]) in ethanol	Sample prepared first under acid (to later basic) conditions, ratio of silane to NP [μmol/mg]	pH(IEP) determined by zeta potential titration	Agglomerate size [nm] (PDI [-]) in ethanol
50	8.5	42.9 ± 0.4 (0.29 ± 0.01)	50	7.3	34.8 ± 0.3 (0.29 ± 0.03)
10	8.0	36.3 ± 0.1 (0.31 ± 0.01)	10	7.0	32.3 ± 0.2 (0.22 ± 0.01)
5	8.0	37.7 ± 0.2 (0.29 ± 0.01)	5	7.2	22.4 ± 0.1 (0.21 ± 0.01)
1	7.9	42.0 ± 0.4 (0.27 ± 0.01)	1	6.9	24.3 ± 0.2 (0.23 ± 0.01)
0.5	7.8	49.8 ± 0.2 (0.49 ± 0.01)	0.5	6.9	30.8 ± 0.9 (0.28 ± 0.01)
0 (AA-TiO ₂ as reference)	6.9	1325.3 ± 36.5 (0.04 ± 0.03)	0 (AA-TiO ₂ as reference)	6.9	1325.3 ± 36.5 (0.04 ± 0.03)

This is why the determined pHs of the IEPs (Table III - 4) and DRIFT (Figure III - 2) spectra were taken to decide on the most efficient grafting protocol. The IEPs of the samples shift towards more basic pHs with increasing amounts of organosilane added during the grafting. This indicates that the more reactant is present, the more silane is grafted onto the TiO₂ NPs, i.e. the more amines are present on the surface overlaying the original surface potential of the TiO₂ particles. Comparing both grafting protocols, it is evident that the pHs of the IEPs of the samples synthesized with the basic protocol are in all cases more basic than in the case of the

protocol starting under acidic conditions. This indicates a more efficient grafting under basic conditions.

The DRIFT spectra show an increase in the relative intensities of the characteristic absorption bands of the grafted organo-silane. The intensities of the bending vibrations of CH₂ and NH at 1450 cm⁻¹ and 1590 cm⁻¹ incline with higher amounts of added grafting agent for both grafting conditions. This becomes evident if one compares these maxima for example with the local absorption minima close to 1500 cm⁻¹. However, it has to be mentioned that these spectra cannot be quantitatively analysed as firstly the baseline corrections are rather difficult due to the high absorption of TiO₂ (below ~ 1000 cm⁻¹) and secondly no specific vibration band was found without intensity changes for all measured samples. Already with the smallest organo-silane addition, the vibration bands of the organic moieties (acetylacetonate and p-toluene sulfonic acid) resting from TiO₂ synthesis seem to be drastically decreased. This can be explained by the surface sensitivity of DRIFT measurements; the grafted silane present on the surface may overlay the signals of the other present molecules.

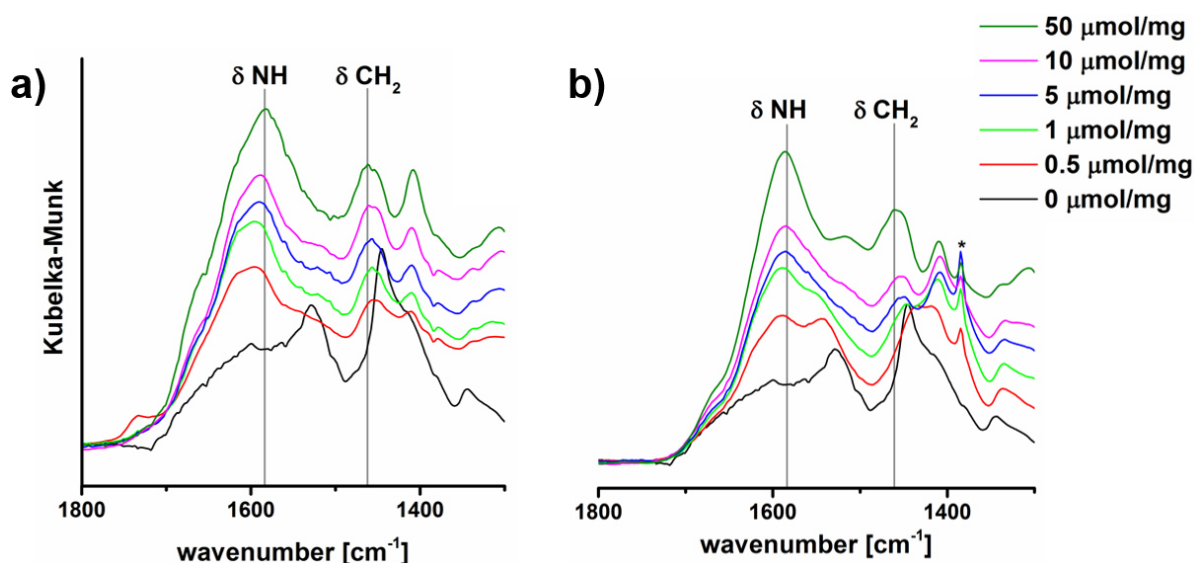
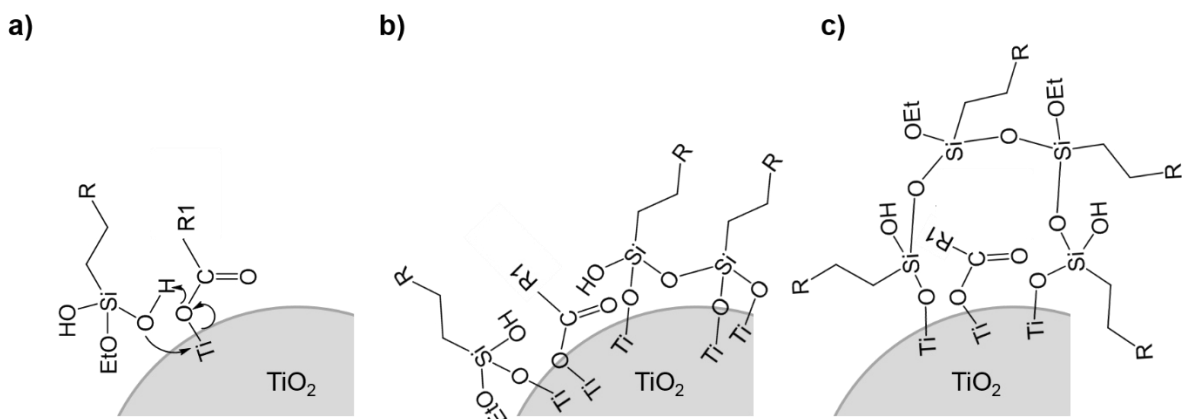


Figure III - 2. IR (DRIFT) spectra of AA-TiO₂ functionalized with [3-(2-aminoethylamino)propyl]trimethoxysilane under a) basic or b) acidic (to later basic) conditions. (*adsorbed HNO₃ of the grafting procedure)

In this context it is also not clear, if the grafted silane layer substitutes the organic surface moieties (Scheme III - 21 a), leaves space for them (Scheme III - 21 b), covers for them (Scheme III - 21 c) or does a combination of all these possibilities. Comparing the samples of both grafting protocols modified with 0.5 or 0 μmol/mg organo-silane, the basic protocol seems to be slightly more efficient as the vibration bands of the organic surface groups from NP synthesis are less intense compared to the vibration bands of the grafted [3-(2-aminoethylamino)propyl]trimethoxysilane, i.e. the CH₂ and NH vibrations.



Scheme III - 21. Possible interactions between the grafted silanes and surface moieties of TiO₂ particles (R, R1 = organic groups): silanes a) substitute the surface group, b) leave space for it or c) enclose it.

Thus, the results obtained by DRIFT measurements seem to confirm the outcomes of zeta potential analyses and the basic protocol is considered to be the more suitable protocol as the grafting of silane onto the particles is more efficient. This is important as it means that less side products caused by oligomerization are formed and the total amount of silane needed for the grafting is lower. As the basic protocol was therefore chosen for future graftings, the photocatalytic activity of the samples (functionalized via the basic protocol) with the smallest amounts of silane (1 and 0.5 $\mu\text{mol}/\text{mg}$), was examined to determine the influences of the surface functionalization on the photocatalytic activity. The results are shown in Figure III - 3. The activity of AA-TiO₂ functionalized with 1 $\mu\text{mol}/\text{mg}$ and 0.5 $\mu\text{mol}/\text{mg}$ [3-(2-aminoethylamino)propyl]trimethoxysilane is reduced to 56 % and 64 % compared to the unmodified particles.

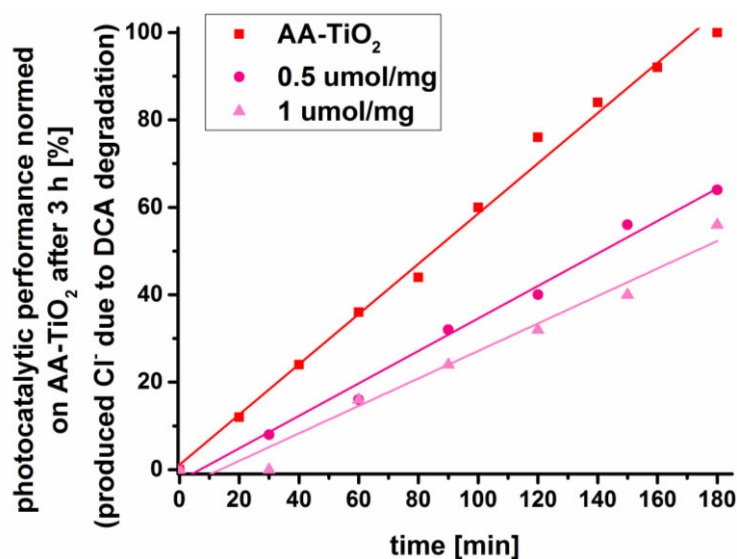
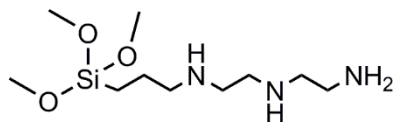


Figure III - 3. Photocatalytic activity of AA-TiO₂ functionalized with 1 $\mu\text{mol}/\text{mg}$ or 0.5 $\mu\text{mol}/\text{mg}$ [3-(2-aminoethylamino)propyl]trimethoxysilane in comparison to the unmodified AA-TiO₂. The values are normed on the amount of degraded dichloroacetic acid (DCA, i.e. produced Cl⁻) by AA-TiO₂ after 3 h photocatalysis test (= 100%).

In order to study if a further decrease in the amount of grafting agent still results in an efficient functionalization but a higher preserved photocatalytic activity, (3-trimethoxysilylpropyl)-diethylenetriamine was utilized as a model organo-silane (Scheme III - 22).



Scheme III - 22. (3-Trimethoxysilylpropyl)-diethylenetriamine.

This molecule bears more CH₂ and NH groups and therefore the shift of the IEPs of the functionalized particles was expected to be more pronounced. Additionally, it has a higher molecular weight, which is more similar to the synthesized organo-silanes and might impede the photocatalytic activity more significantly. The results obtained from grafting AA-TiO₂ with N¹-(3-trimethoxysilylpropyl)diethylenetriamine in concentrations from 1 to 0.05 μmol/mg particle are summarized in Table III - 5.

Table III - 5. Analysis (zeta potential, DLS and photocatalytic efficiency) of AA-TiO₂ functionalized with N¹-(3-trimethoxysilylpropyl)diethylenetriamine under basic conditions.

Sample prepared under basic conditions, ratio of silane to NP [μmol/mg]	pH(IEP) determined by zeta potential titration	Agglomerate size [nm] (PDI [-]) in ethanol	Photocatalytic efficiency compared to the unmodified particle samples after 3 h photocatalysis test
1	8.7	59.0 ± 19.0 (0.48 ± 0.24)	64 %
0.5	8.5	62.1 ± 5.7 (0.64 ± 0.20)	73 %
0.1	7.7	1200 ± 145 (0.38 ± 0.05)	67 %
0.05	7.3	932 ± 178 (0.17 ± 0.05)	82 %
0 (AA-TiO ₂ as reference)	6.9	1325.3 ± 36.5 (0.04 ± 0.03)	100 %

In comparison to the 1 and 0.5 μmol/mg [3-(2-aminoethylamino)propyl]-trimethoxysilane grafted under basic conditions (Table III - 4), the pHs of the IEPs of N¹-(3-trimethoxysilylpropyl)diethylenetriamine are as expected more basic (8.7 and 8.5 compared to 7.9 and 7.8 for 1 and 0.5 μmol/mg, respectively). Additionally, the slightly higher hydrodynamic diameters of the samples (around 60 nm instead of around 45 nm for both 1 and 0.5 μmol/mg) are supposed to be mainly caused by the longer organic chain of the silane. Surprisingly, the larger silane reduces the PC performance slightly less (64 % and 73 % compared to 56 % and 64 % for 1 and 0.5 μmol/mg, respectively). Possible explanations can be a better dispersion state and higher positive surface charge at the acidic pH of the DCA degradation test. This results in more accessible NP surface area and favours molecular adsorption, which is

supposed to lead to a more efficient catalytic degradation of DCA. Concerning the smaller concentration of silane per mg NP (0.1 and 0.05 $\mu\text{mol/mg}$), one can conclude from DLS (large agglomerate sizes) and zeta potential analyses (only small shifts of the pHs of the IEPs) that these quantities are not sufficient to significantly influence the surface properties of the particles. Therefore, these quantities are considered too low to provide an efficient surface functionalization of the NPs.

Due to these results a concentration of 0.5 to 1 μmol silane per mg AA-TiO₂ seems to be optimal to obtain a significant change in the surface properties of the particles. These concentrations are slightly smaller than the calculated one (1.22 $\mu\text{mol/mg}$), which could indicate that the formed silane layer is not completely closed around the NP. This should therefore provide a sufficient surface availability for PC reactions. However, the decrease in the PC activity of 30 to 40 % cannot be avoided if one intends to manipulate the surface properties via functionalization with organo-silanes.

After having proved the feasibility of modifying the AA-TiO₂ nanoparticles with organo-silanes and having determined the most efficient grafting conditions, the photocatalytically most active particle sample MEEAA-TiO₂ synthesized at 200 °C for 4 h was also functionalized with N¹-(3-trimethoxysilylpropyl)diethylenetriamine to determine the most appropriate silane concentration for this system. This system was also chosen to be functionalized later on with the synthesized coupling agents (III.2.2). The obtained results are summarized in Table III - 6.

Table III - 6. Analysis (zeta potential, DLS and photocatalytic efficiency) of MEEAA-TiO₂ functionalized with N¹-(3-trimethoxysilylpropyl)diethylenetriamine under basic conditions. The values obtained during the photocatalysis tests are normed on the amount of degraded DCA (produced Cl⁻) by MEEAA-TiO₂ after 3 h photocatalysis test (= 100%).

ratio of silane to NP [$\mu\text{mol/mg}$]	pH(IEP) determined by zeta potential titration	Agglomerate size [nm] (PDI [-]) in EtOH	Photocatalytic efficiency compared to the unmodified particle samples after 3 h photocatalysis test
4	7.1	41.3 \pm 0.6 (0.23 \pm 0.01)	78 %
2	7.3	41.6 \pm 0.6 (0.24 \pm 0.02)	67 %
1	7.1	36.1 \pm 0.6 (0.23 \pm 0.03)	62 %
0.5	7.3	62.8 \pm 0.5 (0.37 \pm 0.01)	81 %
0 (MEEAA-TiO ₂ as reference)	6.6	1672 \pm 520.4 (0.18 \pm 0.12)	100 %

While the grafting with 0.5 $\mu\text{mol}/\text{mg}$ seems to form a less dense layer, which is expressed by a larger agglomerate size, all other concentrations show no significant differences in agglomerate size or PC activity. It is assumed that with the amount of 1 $\mu\text{mol}/\text{mg}$ a monolayer is formed on the NP surfaces and therefore further condensation onto the surfaces is hindered by the organic chains of the silanes. For increasing the silane layer on the particles, significantly more grafting agent is needed. This assumption is supported by the theoretic calculations, which indicated exactly a concentration of 1 $\mu\text{mol}/\text{mg}$ for a monolayer on the chosen MEEAA-TiO₂ (200 °C 4 h). In comparison to the functionalized AA-TiO₂ the IEP of the MEEAA-TiO₂ samples are slightly less shifted which could indicate either a less efficient grafting or a higher influence of the organic surface groups that are already present on the particle samples after synthesis.

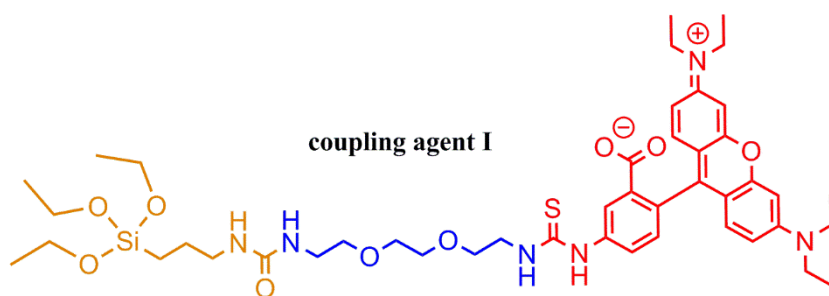
Based on the obtained results, the concentration of 2 $\mu\text{mol}/\text{mg}$ silane per NP was chosen as ideal concentration for the future graftings (of synthesized coupling agents, discussed in III.2.2). This concentration seemed to be a good equilibrium between a sufficient amount of silane to guarantee a successful grafting even with larger, bulkier silanes and the probable waste of excess silane.

III.2.2. Grafting of synthesized coupling agents onto MEEAA-TiO₂ (200 °C, 4 h)

After having optimized the grafting protocol and determined suitable concentrations for the functionalization of the most efficient photocatalytic nanoparticles, namely MEEAA-TiO₂ synthesized at 200 °C for 4 h, the graftings of the synthesized **coupling agents I** and **IV** were carried out with the chosen concentration of 2 μmol silane per mg NP.

III.2.2.a. Grafting of coupling agent I

The successful grafting of **coupling agent I** (Scheme III - 23) onto MEEAA-TiO₂ was examined with the help of zeta potential, DLS, IR and PL measurements.



Scheme III - 23. Coupling agent I.

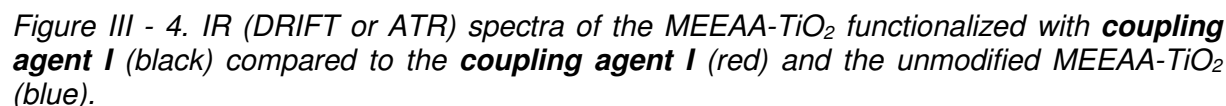
The obtained IEP and the agglomerate size for the functionalized NP system are shown in Table III - 7 and compared to the unmodified system as reference.

*Table III - 7. pH of IEP (zeta potential) and agglomerate size (DLS) of MEEAA-TiO₂ functionalized with **coupling agent I** compared to the unmodified NP system.*

ratio of coupling agent I to MEEAA-TiO ₂ NP [μmol/mg]	pH(IEP) determined by zeta potential titration	Agglomerate size [nm] (PDI [-]) in water pH = 10
2	5.4	461 ± 26 (0.45)
0 (= reference)	6.6	10.000 ± 2.000

The pH of the IEP shifts significantly, indicating a successful surface modification. Keeping in mind the structure of **coupling agent I**, it is evident that the surface potential of the modified particle is mainly dominated by the functional groups of rhodamine B, i.e. the carboxyl and the tertiary amines. As the pK_a value of rhodamine B is reported to be 3.0 to 3.7,^{105,106} it is not surprising that the IEP shifts towards more acidic pH values. According to the measurements, the highest zeta potential of the functionalized sample was reached using basic pHs. This is why the DLS measurements were carried out at the pH of 10 to ensure the best electrostatic stabilisation of the particle dispersion. In contrast to this, the dispersibility of the unmodified TiO₂ NPs was very low at this pH. This is why the modified NPs show significantly smaller agglomerate sizes. Nevertheless, the measured hydrodynamic diameter is still very large compared to well-dispersed particle samples without modification or modified with the commercial amino-silanes. This is most probably caused by the low solubility of rhodamine in water¹⁰⁷ which is not favoring a good dispersion state of the functionalized NPs.

A further confirmation of the successful NP functionalization are the obtained IR spectra (Figure III - 4) of the unmodified particles (exposed to grafting conditions to obtain a reliable reference), the **coupling agent I** before grafting and the particle system functionalized with the **coupling agent I**. Characteristic absorption bands of the **coupling agent I** can also be identified on the functionalized particles (marked in Figure III - 4 with arrows). The absorption bands with wave numbers from 2980 to 2870 cm⁻¹ are caused by asymmetric stretching of CH₃ (2978 cm⁻¹) and CH₂ (2927 cm⁻¹) as well as symmetric stretching of CH₂ (2870 cm⁻¹) of the **coupling agent I**. The signals between 1750 and 1000 cm⁻¹ are dominated by vibrations of the Rhodamine B component which cover signals of the rest of the molecule and were assigned based on literature:^{108–110} The stretching of the xanthene ring (ν CC, ν CO, ν COC) causes signals at 1645 and 1272 cm⁻¹. Bending and stretching vibrations of the aromatic rings (CCH, CC) absorb at 1334 and 1176 cm⁻¹. The vibrations of the carboxyl group cause signals



In order to finalize the examinations of the NP system functionalized **with coupling agent I**, its photocatalytic (PC) activity was assessed and compared to the unmodified NPs reference. The outcomes are shown in Figure III - 6. Based on the results obtained for the particles modified with commercial silanes (III.2.1), it was expected that the PC performance is going to be decreased after the grafting of **coupling agent I**. Nevertheless, the PC activity was significantly increased which is surprising as the grafting of the silane reduced the TiO₂ surface area available for photocatalysis. There are two possible explanations for this behaviour; either the rhodamine acts as photosensitizer or the modified surface charge enhances molecular adsorption.

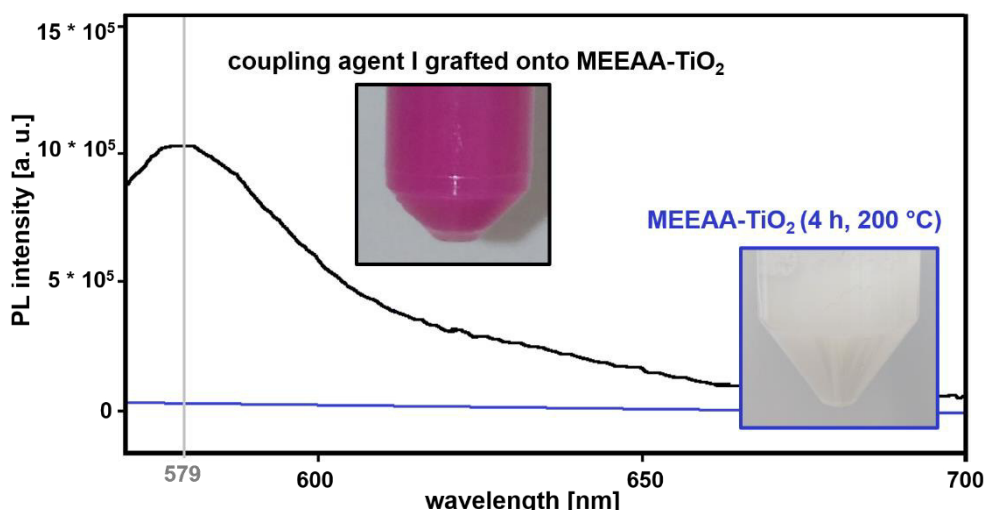


Figure III - 5. PL spectrum of unmodified (blue) and functionalized (black) MEEAA-TiO₂ (with **coupling agent I**); excited at 556 nm (i.e. at the absorption maximum of the functionalized particle system). Additionally, photographs of both particle samples as dispersions in water at pH = 10 are shown.

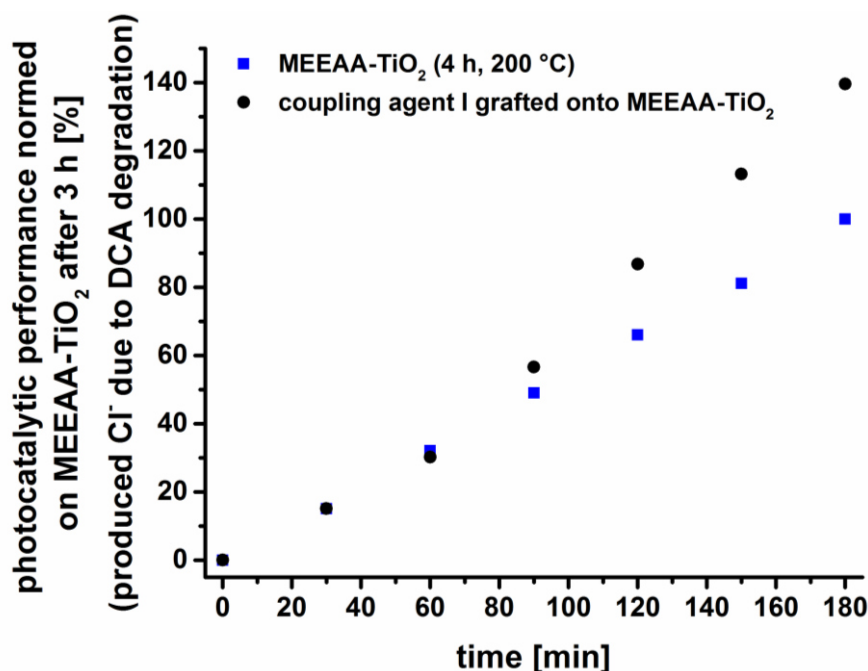


Figure III - 6. PC activity of MEEAA-TiO₂ functionalized with **coupling agent I** (black) compared to the unmodified MEEAA-TiO₂ (blue). The values are normed on the amount of degraded DCA (produced Cl⁻) by MEEAA-TiO₂ (4 h, 200 °C) after 3 h photocatalysis test (= 100 %).

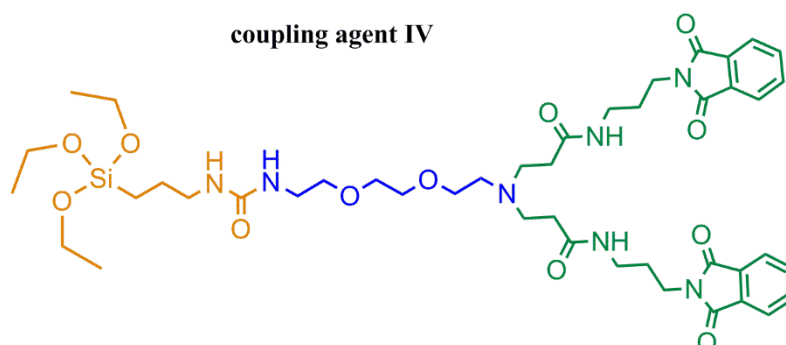
It is well-known, that dyes that are in contact with semiconductor surfaces can transfer absorbed energy.¹¹¹ As rhodamine B absorbs light of a different wavelength range compared to TiO₂, the energy transfer of the dye onto the NP would increase the PC performance as more light is absorbed in total, i.e. more electron-hole pairs are created that can take part in PC reactions. Rhodamine B seems suitable for this approach¹¹² but it is questionable if this is really happening or/and having a significant influence on the PC performance of the sample

as the applied UV-light for the PC test should only lie between 300 and 400 nm and the main absorbance of rhodamine B takes place over 460 nm.¹¹³ It is considered as more probable that the modified surface charge (significant shift of the pH of the IEP) or the properties of the surface moieties may either favour the adsorption of the dichloroacetic acid used as degradable substance or of the water or oxygen molecules. This would also lead to a more efficient photocatalysis as every photocatalytic reaction demands pre-adsorption of the participating molecules.¹¹⁴

To sum up, while a PL nanoparticle system with a good PC activity was successfully obtained, its surface charge and agglomerate size is not adequate for the use as positively charged anti-tumour agent. This is why the introduction of amines as functional terminal groups within the surface agent has to be achieved.

III.2.2.b. Grafting of coupling agent IV

Concerning this matter, the successfully synthesized **coupling agent IV** (Scheme III - 24) was grafted onto MEEAA-TiO₂ (4 h, 200 °C). The obtained modified NP system was again analysed with zeta potential and DLS (Table III - 8).



Scheme III - 24. Coupling agent IV.

Table III - 8. IEP (zeta potential) and agglomerate size (DLS) of MEEAA-TiO₂ functionalized with **coupling agent IV** compared to the unmodified NP system.

ratio of coupling agent IV to MEEAA-TiO ₂ NP [μmol/mg]	pH(IEP) determined by zeta potential titration	Agglomerate size [nm] (PDI [-]) in water pH = 3
2	6.2	658.1 ± 21.2 (0.8)
0 (= reference)	6.6	32.8 ± 0.8 (0.1)

Considering the structure of **coupling agent IV**, the only marginal shift of the IEP of the functionalized NPs in comparison to the NPs before grafting is no surprise as the organic molecule does not bear any ionic groups and should therefore not influence the surface charge of the NPs. This is why the zeta potential measurements are not appropriate to prove the grafting in this particular case. The agglomerate size of the samples was considerably

augmented after the functionalization which may be explained by a less efficient electrostatic stabilisation of the samples due to the uncharged coupling agent. However, it could also point out that the functionalization led to the formation of NP clusters resulting in the aggregation of particles. IR measurements (Figure III - 7) were able to finally prove the grafting of the **coupling agent IV** onto MEEAA-TiO₂.

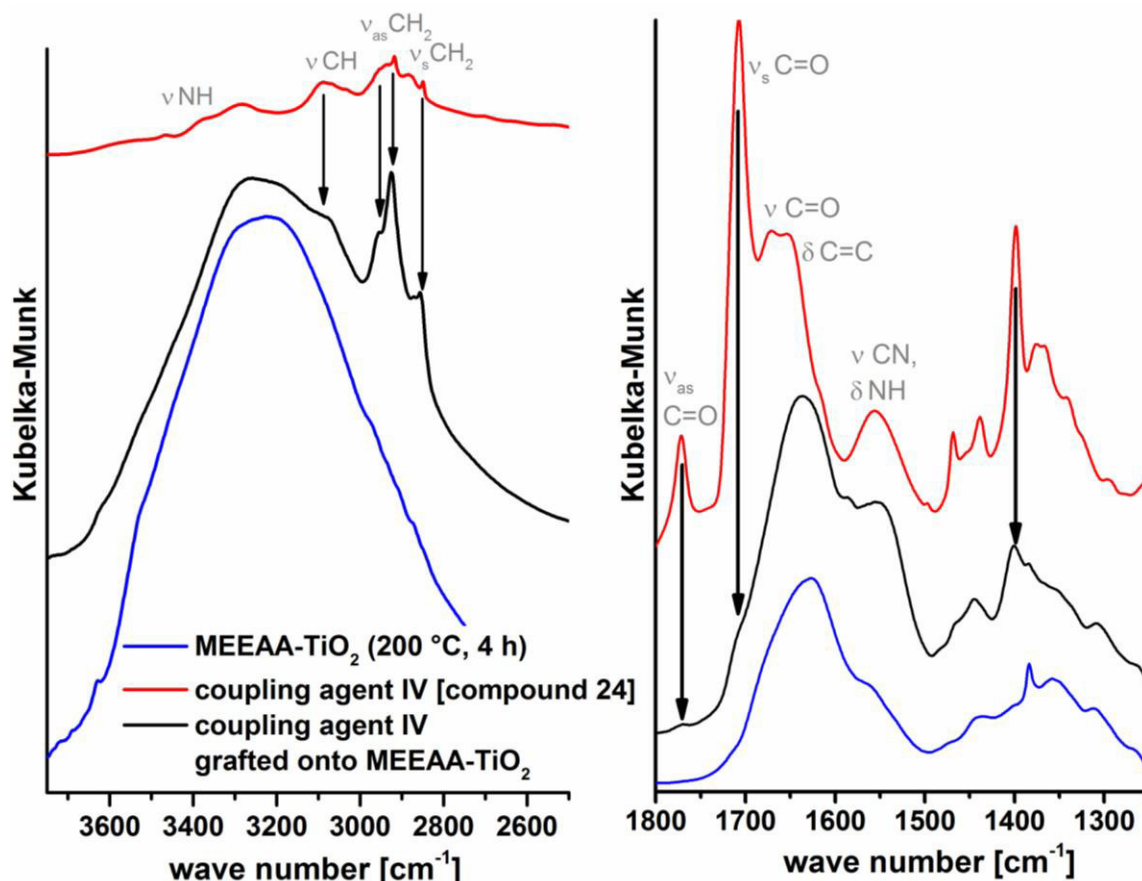
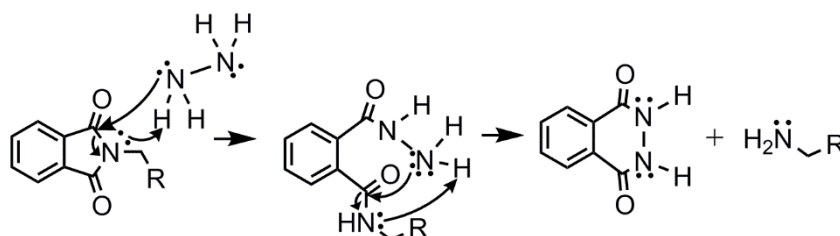


Figure III - 7. IR (DRIFT or ATR) spectra of the MEEAA-TiO₂ functionalized with **coupling agent IV** (black) compared to the **coupling agent IV** (red – compound 24) and the unmodified MEEAA-TiO₂ (blue) in the region a) 3750-2500 cm⁻¹ and b) 1800-1250 cm⁻¹.

For these measurements **compound 24** (Scheme III - 17) instead of **compound 25** (Scheme III - 17) was used as it was more stable and therefore easier to handle during the analysis while already providing the most important molecular functions of the coupling agent. Its IR spectrum is compared to the spectra of the unmodified NPs and of the **coupling agent IV** grafted onto the NPs. Characteristic absorption bands of the **compound 24** can also be identified on the functionalized particles (marked in Figure III - 7 with arrows). Symmetric stretching of NH in amides absorbs at 2285 cm⁻¹ and symmetric stretching of CH in the aromatic rings of the phthalimide at 3085 cm⁻¹. The absorption bands with wave numbers from 2955 to 2850 cm⁻¹ are caused by asymmetric and symmetric stretching of CH₂. The signals at 1770 and 1706 cm⁻¹ are dominated by asymmetric and symmetric stretching vibrations of the

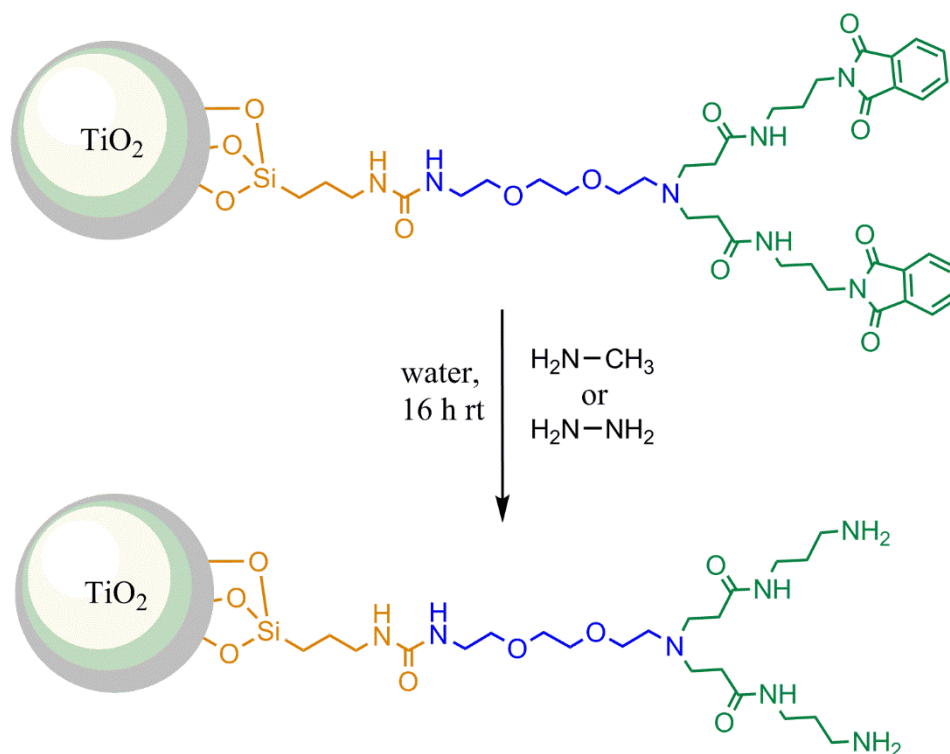
C=O in the imides and the C=C deformation of the aromatic rings cause a band around 1669 cm⁻¹.¹¹⁵ The vibrations of the amide groups (amide I: ν C=O, amide II: ν CN, δ NH) of **coupling agent IV** cause signals at 1669 and 1555 cm⁻¹.¹⁰⁴ It has to be admitted that not all of the characteristic bands can be found on the functionalized NP sample and the ones that can be identified are less intense compared to the samples modified with **coupling agent I**. This could indicate a less efficient grafting in the case of **coupling agent IV**.

In order to further analyse the obtained sample and to evaluate its suitability for future applications as anti-tumour agent, it is of utter importance to remove the phthalimide protecting groups to obtain terminal primary amines and therefore positively charged particle surfaces at physiological pH. The deprotection of phthalimide protected amines is usually carried out with bases containing a primary amine such as methylamine or hydrazine.^{55,116–121} The reaction mechanism for the phthalimide cleavage with hydrazine is shown in Scheme III - 25.



Scheme III - 25. Mechanism of the phthalimide protecting group cleavage with the help of hydrazine.

In this study, 3, 10, 100 or 1000 molar equivalents of amine of the base (either methylamine or hydrazine) per phthalimide group of the **coupling agent IV** and a reaction time of 16 h at room temperature were chosen. Because of the nature of the NP dispersion, water was used as solvent for this reaction. The theoretic amount of **coupling agent IV** per mg NP (which was used for the grafting) was used as basis for these calculations. The concentration rows of the bases were supposed to allow the determination of the most appropriate amount of base, which guarantees an efficient phthalimide cleavage while not destroying the Si-O-Ti bonds via basic hydrolysis. The planned deprotection of the grafted **coupling agent IV** is shown in Scheme III - 26. A successful deprotection should result in the disappearance of the absorption bands in IR of the phthalimide groups (especially the stretching vibrations of C=O in the imide). However, for the sample examined in this study, these changes may be very difficult to detect due to the low intensity of the absorption bands of **coupling agent IV** grafted onto MEEAA-TiO₂. Furthermore, the pHs of the IEPs of the samples should show a significant basic shift and the dispersion state of the NPs was expected to be improved because of better electrostatic stabilisation.



*Scheme III - 26. Phthalimide protecting group cleavage of the grafted **coupling agent IV**.*

All IEPs of the obtained samples lay in the pH range of 5.8 to 6.1 (for more details see Appendix II) which clearly is no significant shift towards basic pH and rather resembles the IEP of the unmodified MEEAA-TiO₂. Also, the hydrodynamic diameters of the samples were not significantly decreased (for more details see Appendix II). While the shift in the pH of the IEP could indicate that the entire coupling agent is removed from the particle surface instead of a phthalimide group cleavage, the DLS measurements do not confirm this assumption as the agglomerate sizes were not decreased (which is expected for a “cleaned” MEEAA-TiO₂ surface). For more insights, DRIFT measurements were conducted. Independent of the type (methylamine or hydrazine) or concentration of base used, there was no difference in the obtained DRIFT spectra between all base-treated samples. This is why the spectrum of the sample (**coupling agent IV**-MEEAA-TiO₂) treated with 10 eq methylamine is shown as representative example in Figure III - 8 and compared to the unmodified MEEAA-TiO₂, the unmodified MEEAA-TiO₂ treated with methylamine and the **coupling agent IV**-MEEAA-TiO₂. Comparing the unmodified MEEAA-TiO₂ to the unmodified MEEAA-TiO₂ treated with methylamine, it is evident that the base treatment does not change the nature of MEEAA surface groups. Small variances in the spectra such as between 1700 and 1600 cm⁻¹ are most probably caused by a varying amount of adsorbed water in the samples. The characteristic absorption bands of **coupling agent IV**-MEEAA-TiO₂ are partly maintained during the base treatment (indicated with arrows in Figure III - 8).

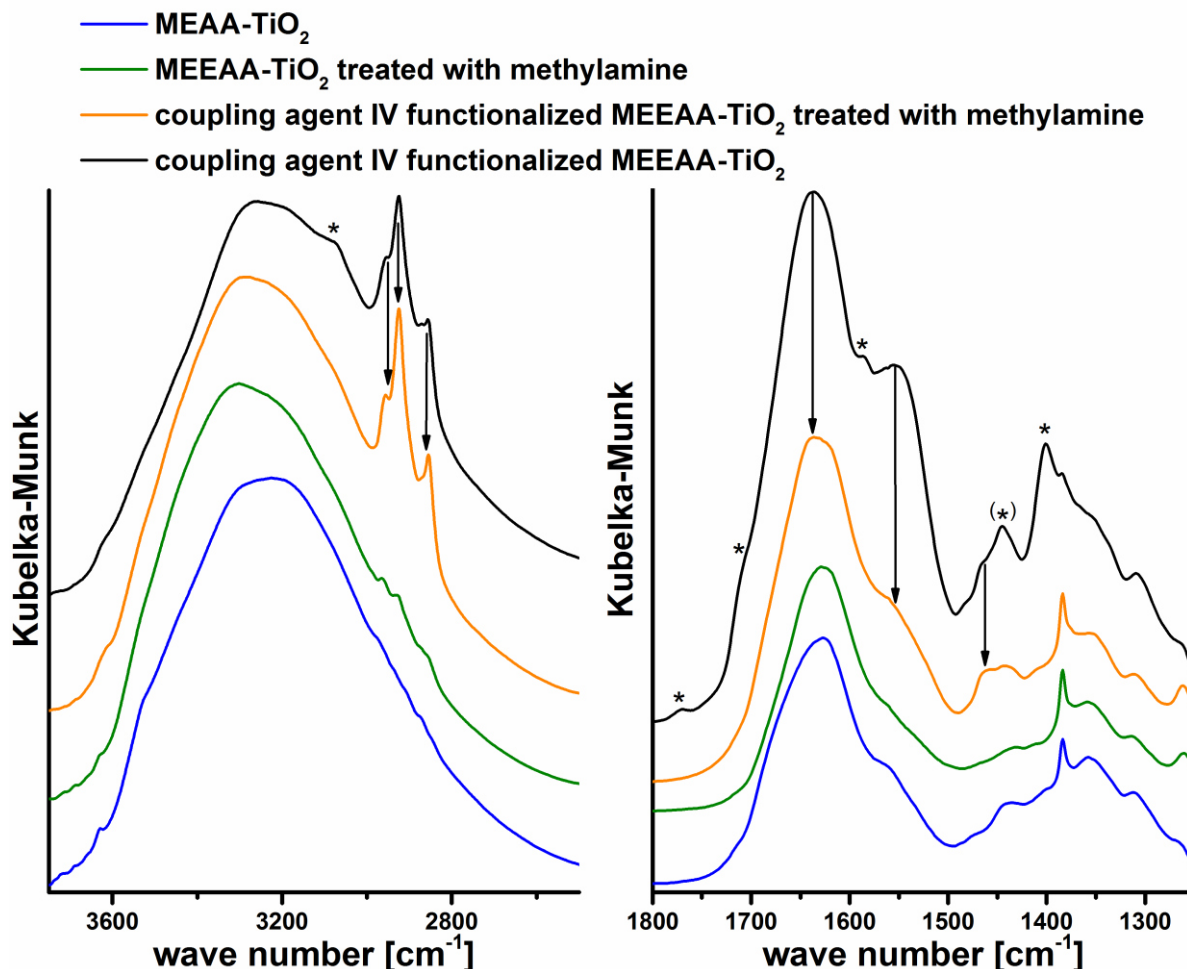


Figure III - 8. IR (DRIFT) spectra of the **coupling agent IV-MEEAA-TiO₂** treated with 10 eq methylamine (orange) compared to the unmodified MEEAA-TiO₂ (blue), the unmodified MEEAA-TiO₂ treated with methylamine (green) and the **coupling agent IV-MEEAA-TiO₂** (black) in the region a) 3800-2500 cm⁻¹ and b) 1800-1250 cm⁻¹.

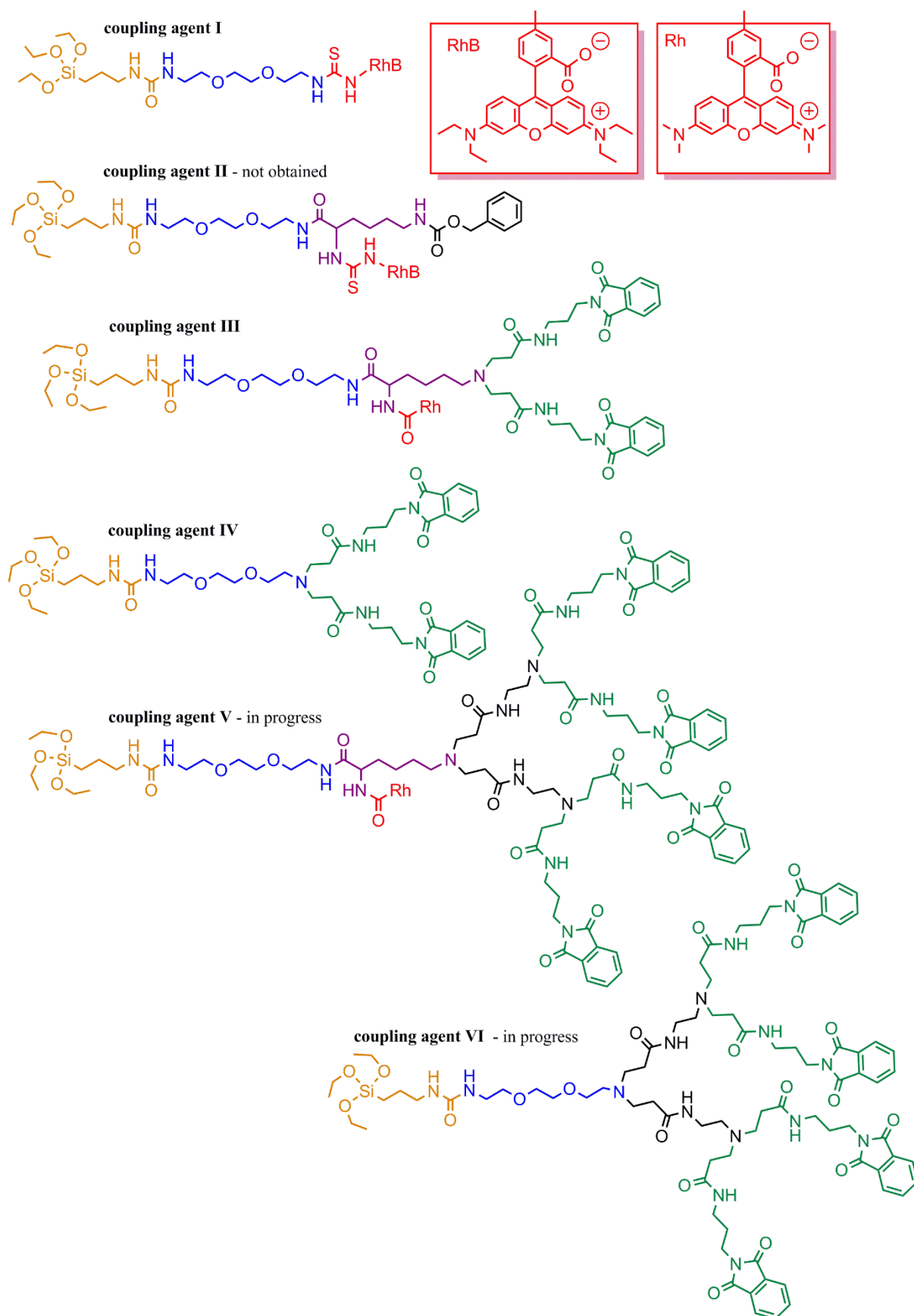
The most evident signals are the asymmetric and symmetric stretching of CH₂ (from 2955 to 2850 cm⁻¹) which prove the presence of organic coupling agent components on the particles. Other signals (marked with * in Figure III - 8) such as the symmetric stretching of CH in the aromatic rings of the phthalimide (3085 cm⁻¹) or asymmetric and symmetric stretching vibrations of the C=O in the imides (1770 and 1706 cm⁻¹) seem to be no longer detectable. Due to the low intensity of the before mentioned absorption bands, it is not clear if they disappeared because of phthalimide cleavage or destruction of parts of the coupling agent or if they are just partly covered for example by vibrations of higher amounts of adsorbed water.

Based on these not very conclusive results, one can deduce that possibly no cleavage of the phthalimide group occurred, while a destruction of parts of the coupling agent or the partial removal of the entire coupling agent by Si-O-Ti cleavage seem to be an option. While there are still a lot of options to improve the deprotection procedure such as the use of temperature or decrease in present water along with the use of other solvents, the evaluation of the

deprotection success will always remain challenging with this functionalized NP sample. One obstacle is the difficulty to first determine the grafting success as the characteristic vibration bands in DRIFT of the grafted **coupling agent IV** are weak and IEP does only shift minimally. This means it is not possible to distinguish between the unsuccessful cleavage with the coupling agent remaining intact and the removal of parts of the coupling agent during the phthalimide cleavage procedure. For more meaningful investigations, the use of other NPs with less absorptive material (such as silica) and no organic groups (such as P25 TiO₂ or silica) would be advisable to obtain more significant changes in the DRIFT spectra. However, this was not the aim of this work and is therefore not treated herein.

III.3. Conclusion

In this chapter the synthesis of organic coupling agents and their subsequent grafting onto the before synthesized TiO₂ NPs was investigated. Concerning the organic syntheses, four either luminescent or non-luminescent dendritic or linear structures were aimed at as shown in Scheme III - 27. The first three coupling agents all contain a rhodamine dye. The **coupling agent I** as linear molecule without terminal amine group was successfully obtained and proved the stability of the luminescence agent during all synthesis and washing steps. The **coupling agent II** was supposed to combine the incorporation of the dye with a terminal functional group. Several synthesis steps were successfully carried out up to the coupling of the non-luminescent components of the coupling agent to the dye by establishing a thiourea linkage. However, this thiourea linkage on the *alpha* position of the lysine was responsible for the rearrangement (cycle formation) of the molecule under acidic conditions. The lability of the amide linkage next to the thiourea has never been reported for lysine under the reaction conditions used (strong acids, room temperature). In this context, the cleavage of both the Boc and Z protection group was not possible and the synthetic pathway was not continued. Nevertheless, the insights gained during the synthesis of **coupling agent II** helped to synthesize **coupling agent III**, a luminescent 1st generation dendritic molecule. This was by far the most complex synthesis route with several obstacles that had to be overcome; for example, the dipeptide formation during Fmoc-protection of Z-lysine was effectively reduced to a minimum by the use of DMF as organic solvent (instead of THF or dioxane). The instability of the ester bond of the first established dendron under hydrogenation due to transesterification reactions (in presence of an alcohol) was rather surprising as well and initiated further examinations of the stability of this bond. It became evident, that these ester bonds will partly be transformed by transesterification reactions due to the basic hydroalcoholic milieu used. Using an amide instead of the ester function, provided a stable molecule up to the final reaction step. Thanks to the experiences made during the synthesis of **coupling agent II**, instead of rhodamine isothiocyanate, the NHS-rhodamine was used. This guaranteed the stability of the compound during the subsequent reaction steps. **Coupling agent III** was therefore successfully obtained. **Coupling agent IV**, a dendritic non-luminescent coupling agent bears the same dendritic branches as **coupling agent III** while not containing the lysine moiety or a dye. This compound was also successfully obtained. The synthesis of 2nd generation dendritic **coupling agent V** and **coupling agent VI** with a similar structure either to **coupling agent III** or to **coupling agent IV** was started but is still in progress. While the quantity of the successfully synthesized **coupling agent III** was too low to proceed with the grafting reaction, both **coupling agent I** and **IV** were available for it.



Scheme III - 27. Organic coupling agents synthesized in this chapter.

For the grafting, first the most adequate grafting procedure was successfully determined with commercial silanes ([3-(2-aminoethylamino)propyl]-trimethoxysilane, *N*'-(3-trimethoxysilylpropyl)diethylenetriamine). Basic hydroalcoholic grafting conditions seemed to be superior to a protocol starting under acidic conditions while both procedures led to a successful particle modification. The surface charge of the particles was effectively manipulated as shown by zeta potential measurements, while the PC activity of the TiO₂ particles was slightly reduced (a reduction of 20 – 40 % was generally determined). In the case of MEEAA-TiO₂ (4 h, 200 °C), an amount of 1 to 4 µmol of added silane per mg NPs resulted in similar results concerning the surface charge and PC activity. This indicates that a monolayer is formed that impedes further condensation of silane molecules because of the steric hindrance of the organic groups of the grafting agent. The amount of 1 µmol/mg as minimal amount of silanes needed to obtain a monolayer on the particles is in good agreement with the calculated amount of 1.09 µmol/mg (for MEEAA-TiO₂). The addition of considerably higher amounts of silane (as tested with AA-TiO₂) presumably leads to the growth of further molecular layers around the NPs.

This is why 2 µmol silane per mg NP was chosen as optimal amount for the grafting of the synthesized **coupling agents I and IV** onto MEEAA-TiO₂ (4 h, 200 °C). The successful grafting of **coupling agent I** was confirmed by all used analysis methods (IR, DLS, zeta potential measurements). The surface potential of the NPs was significantly modified by the functionalisation which led to a considerably negative surface charge at physiological pH. In the context of the planned later applications in cell culture tests, a positive surface charge is desired and therefore, this result stressed the need of basic groups such as primary amines in the coupling agents. Also the dispersion state of the modified particles in water was not satisfying which is not surprising as rhodamine is known to have a low solubility in it. An integration of terminal amine groups into the coupling agent would therefore also certainly improve the dispersibility of the sample. Nevertheless, the obtained modified NPs showed a very high PL and an excellent PC activity even outreaching the results of unmodified samples. This surprising PC performance was supposed to be caused by the significantly changed surface charge which may favour the adsorption of molecules taking part into the photocatalytic reactions. The successful grafting of **coupling agent IV** was confirmed by IR even though the detected characteristic absorption bands were of low intensity. The IEP of the sample was not significantly changed which may be owed to the absence of ionic components in the coupling agent. The attempts which were carried out in order to cleave the phthalimide protection group of the grafted **coupling agents IV**, were not conclusive and have not yet been successful.

Summing up, the feasibility to synthesize luminescent and non-luminescent dendritic coupling agents as well as their grafting onto the before synthesized TiO₂ NPs was successfully shown

(while the complete synthesis of all planned coupling agents is still under progress). The potentials as well as obstacles of the organic synthesis routes and grafting procedures of these coupling agents were clearly shown. For future studies the synthesis of luminescent coupling agents (in particular) should be further investigated and optimized. Also, the phthalimide protecting group cleavage of grafted coupling agents still has to be developed. Additionally, it could be considered to use the phthalimide protected coupling agents as obtained because of the probable anti-tumour activity of phthalimide groups.¹²²

References:

- 1 M. J. D. Clift, B. Rothen-Rutishauser, D. M. Brown, R. Duffin, K. Donaldson, L. Proudfoot, K. Guy and V. Stone, *Toxicol. Appl. Pharmacol.*, 2008, **232**, 418–427.
- 2 S. Patil, A. Sandberg, E. Heckert, W. Self and S. Seal, *Biomaterials*, 2007, **28**, 4600–4607.
- 3 R. Kumar, I. Roy, T. Y. Ohulchanskyy, L. N. Goswami, A. C. Bonoio, E. J. Bergey, K. M. Trampusch, A. Maitra and P. N. Prasad, *ACS Nano*, 2008, **2**, 449–456.
- 4 C. He, Y. Hu, L. Yin, C. Tang and C. Yin, *Biomaterials*, 2010, **31**, 3657–3666.
- 5 W.-K. Oh, S. Kim, M. Choi, C. Kim, Y. S. Jeong, B.-R. Cho, J.-S. Hahn and J. Jang, *ACS Nano*, 2010, **4**, 5301–5313.
- 6 A. Villanueva, M. Cañete, A. G. Roca, M. Calero, S. Veintemillas-Verdaguer, C. J. Serna, M. del Puerto Morales and R. Miranda, *Nanotechnology*, 2009, **20**, 115103.
- 7 B. J. Teubl, C. Schimpel, G. Leitinger, B. Bauer, E. Fröhlich, A. Zimmer and E. Roblegg, *J. Hazard. Mater.*, 2015, **286**, 298–305.
- 8 Y. Zhang, N. Kohler and M. Zhang, *Biomaterials*, 2002, **23**, 1553–1561.
- 9 C. Wilhelm, C. Billotey, J. Roger, J. N. Pons, J.-C. Bacri and F. Gazeau, *Biomaterials*, 2003, **24**, 1001–1011.
- 10 T.-H. Chung, S.-H. Wu, M. Yao, C.-W. Lu, Y.-S. Lin, Y. Hung, C.-Y. Mou, Y.-C. Chen and D.-M. Huang, *Biomaterials*, 2007, **28**, 2959–2966.
- 11 A. Verma and F. Stellacci, *Small*, 2010, **6**, 12–21.
- 12 D. L. J. Thorek and A. Tsourkas, *Biomaterials*, 2008, **29**, 3583–3590.
- 13 T. S. Hauck, A. A. Ghazani and W. C. W. Chan, *Small*, 2008, **4**, 153–159.
- 14 L. Chen, J. M. Mccrate, J. C.-M. Lee and H. Li, *Nanotechnology*, 2011, **22**, 105708.
- 15 S. Setua, D. Menon, A. Asok, S. Nair and M. Koyakutty, *Biomaterials*, 2010, **31**, 714–729.
- 16 A. M. Derfus, W. C. Chan and S. N. Bhatia, *Adv. Mater.*, 2004, **16**, 961–966.
- 17 A. Quintana, E. Raczka, L. Piehler, I. Lee, A. Myc, I. Majoros, A. K. Patri, T. Thomas, J. Mulé and J. R. Baker Jr, *Pharm. Res.*, 2002, **19**, 1310–1316.
- 18 V. Bagalkot, L. Zhang, E. Levy-Nissenbaum, S. Jon, P. W. Kantoff, R. Langer and O. C. Farokhzad, *Nano Lett.*, 2007, **7**, 3065–3070.
- 19 O. C. Farokhzad, S. Jon, A. Khademhosseini, T.-N. T. Tran, D. A. LaVan and R. Langer, *Cancer Res.*, 2004, **64**, 7668–7672.
- 20 T. Palacin, H. L. Khanh, B. Joussetme, P. Jegou, A. Filoramo, C. Ehli, D. M. Guldi and S. Campidelli, *J. Am. Chem. Soc.*, 2009, **131**, 15394–15402.
- 21 M. A. Fox, J. K. Whitesell, D. Magde and L.-Y. Zhu, *Molecules*, 2009, **14**, 3851–3867.
- 22 Y.-C. Chen, T.-Y. Juang, T.-M. Wu, S. A. Dai, W.-J. Kuo, Y.-L. Liu, F. M. C. Chen and R.-J. Jeng, *ACS Appl. Mater. Interfaces*, 2009, **1**, 2371–2381.
- 23 P. G. Hoertz, R. A. Carlisle, G. J. Meyer, D. Wang, P. Piotrowiak and E. Galoppini, *Nano Lett.*, 2003, **3**, 325–330.
- 24 K. G. Thomas and P. V. Kamat, *Acc. Chem. Res.*, 2003, **36**, 888–898.
- 25 K. T. Thurn, T. Paunesku, A. Wu, E. M. B. Brown, B. Lai, S. Vogt, J. Maser, M. Aslam, V. Dravid, R. Bergan and G. E. Woloschak, *Small*, 2009, **5**, 1318–1325.
- 26 T. Osaka, T. Nakanishi, S. Shanmugam, S. Takahama and H. Zhang, *Colloids Surf. B Biointerfaces*, 2009, **71**, 325–330.
- 27 L. M. Bronstein and Z. B. Shifrina, *Chem. Rev.*, 2011, **111**, 5301–5344.
- 28 E. B. Dickerson, E. C. Dreaden, X. Huang, I. H. El-Sayed, H. Chu, S. Pushpanketh, J. F. McDonald and M. A. El-Sayed, *Cancer Lett.*, 2008, **269**, 57–66.

- 29 C. Leamon, *Adv. Drug Deliv. Rev.*, 2004, **56**, 1127–1141.
- 30 R. Esfand and D. A. Tomalia, *Drug Discov. Today*, 2001, **6**, 427–436.
- 31 I. J. Majoros, A. Myc, T. Thomas, C. B. Mehta and J. R. Baker, *Biomacromolecules*, 2006, **7**, 572–579.
- 32 A. R. Menjoge, R. M. Kannan and D. A. Tomalia, *Drug Discov. Today*, 2010, **15**, 171–185.
- 33 A. W. Bosman, H. M. Janssen and E. W. Meijer, *Chem. Rev.*, 1999, **99**, 1665–1688.
- 34 O. M. Milhem, C. Myles, N. B. McKeown, D. Attwood and A. D'Emanuele, *Int. J. Pharm.*, 2000, **197**, 239–241.
- 35 R. Jevprasesphant, J. Penny, R. Jalal, D. Attwood, N. B. McKeown and A. D'Emanuele, *Int. J. Pharm.*, 2003, **252**, 263–266.
- 36 N. Malik, R. Wiwattanapatapee, R. Klopsch, K. Lorenz, H. Frey, J. W. Weener, E. W. Meijer, W. Paulus and R. Duncan, *J. Controlled Release*, 2000, **65**, 133–148.
- 37 Y. Nakanishi and T. Imae, *J. Colloid Interface Sci.*, 2006, **297**, 122–129.
- 38 S. Marcinko and A. Y. Fadeev, *Langmuir*, 2004, **20**, 2270–2273.
- 39 R. Helmy and A. Y. Fadeev, *Langmuir*, 2002, **18**, 8924–8928.
- 40 J. Zhao, M. Milanova, M. M. C. G. Warmoeskerken and V. Dutschk, *Colloids Surf. Physicochem. Eng. Asp.*, 2012, **413**, 273–279.
- 41 M. Iijima, M. Kobayakawa and H. Kamiya, *J. Colloid Interface Sci.*, 2009, **337**, 61–65.
- 42 X.-F. Yang, X.-Q. Guo and Y.-B. Zhao, *Talanta*, 2002, **57**, 883–890.
- 43 T. Fujii, A. Ishii and M. Anpo, *J. Photochem. Photobiol. Chem.*, 1990, **54**, 231–237.
- 44 S. V. Ingale, P. B. Wagh, A. K. Tripathi, R. S. Srivastav, I. K. Singh, R. C. Bindal and S. C. Gupta, *Soft Nanosci. Lett.*, 2012, **02**, 67–70.
- 45 Y. R. Dai and L. F. Yin, *Catal Sci Technol*, 2014, **4**, 456–463.
- 46 A. S. Kristoffersen, S. R. Erga, B. Hamre and Ø. Frette, *J. Fluoresc.*, 2014, **24**, 1015–1024.
- 47 I. Řehoř, V. Vilímová, P. Jendelová, V. Kubiček, D. Jiráček, V. Herynek, M. Kapcalová, J. Kotek, J. Černý, P. Hermann and I. Lukeš, *J. Med. Chem.*, 2011, **54**, 5185–5194.
- 48 R. R. Anderson and J. A. Parrish, *J. Invest. Dermatol.*, 1981, **77**, 13–19.
- 49 F. Scholkmann, S. Kleiser, A. J. Metz, R. Zimmermann, J. Mata Pavia, U. Wolf and M. Wolf, *NeuroImage*, 2014, **85**, Part 1, 6–27.
- 50 C.-H. Lai, T.-C. Chang, Y.-J. Chuang, D.-L. Tzou and C.-C. Lin, *Bioconjug. Chem.*, 2013, **24**, 1698–1709.
- 51 J. Manson, D. Kumar, B. J. Meenan and D. Dixon, *Gold Bull.*, 2011, **44**, 99–105.
- 52 N. Kohler, G. E. Fryxell and M. Zhang, *J. Am. Chem. Soc.*, 2004, **126**, 7206–7211.
- 53 A. C. Balazs, T. Emrick and T. P. Russell, *Science*, 2006, **314**, 1107–1110.
- 54 A. Isidro-Llobet, M. Alvarez and F. Albericio, *Chem. Rev.*, 2009, **109**, 2455–2504.
- 55 Theodora W. Greene and W. Peter G. M., *Protective Groups in Organic Synthesis*, John Wiley & Sons, Inc., New York, 3rd edition., 1999.
- 56 R. N. Zuckermann, E. J. Martin, D. C. Spellmeyer, G. B. Stauber, K. R. Shoemaker, J. M. Kerr, G. M. Figliozzi, D. A. Goff and M. A. Siani, *J. Med. Chem.*, 1994, **37**, 2678–2685.
- 57 D. W. Lee, H. Ha and W. K. Lee, *Synth. Commun.*, 2007, **37**, 737–742.
- 58 A. B. Hughes, Ed., *Amino acids, peptides and proteins in organic chemistry*, Wiley-VCH, Weinheim, 2009.
- 59 I. W. Ashworth, B. G. Cox and B. Meyrick, *J. Org. Chem.*, 2010, **75**, 8117–8125.
- 60 E. Valeur and M. Bradley, *Chem Soc Rev*, 2009, **38**, 606–631.
- 61 C. A. G. N. Montalbetti and V. Falque, *Tetrahedron*, 2005, **61**, 10827–10852.
- 62 G. Fields, in *Peptide Synthesis Protocols*, eds. M. Pennington and B. Dunn, Humana Press, 1995, pp. 17–27.
- 63 S. Höck, R. Marti, R. Riedl and M. Simeunovic, *Chim. Int. J. Chem.*, 2010, **64**, 200–202.
- 64 L. Lang, Y. Ma, D. O. Kiesewetter and X. Chen, *Mol. Pharm.*, 2014, **11**, 3867–3874.
- 65 G.-H. Chen, P. Pan, Y. Chen, X.-B. Meng and Z.-J. Li, *Tetrahedron*, 2009, **65**, 5922–5927.

- 66 P. R. Sultane, T. B. Mete and R. G. Bhat, *Tetrahedron Lett.*, 2015, **56**, 2067–2070.
- 67 M. Rodriguez, M. Amblard, M.-C. Galas, M.-F. Lignon, A. Aumelas and J. Martinez, *Int. J. Pept. Protein Res.*, 1990, **35**, 441–451.
- 68 M. R. Burns, C. L. Carlson, S. M. Vanderwerf, J. R. Ziemer, R. S. Weeks, F. Cai, H. K. Webb and G. F. Graminski, *J. Med. Chem.*, 2001, **44**, 3632–3644.
- 69 R. Srinivas, A. Garu, G. Moku, S. B. Agawane and A. Chaudhuri, *Biomaterials*, 2012, **33**, 6220–6229.
- 70 M. Bergmann and L. Zervas, *Berichte Dtsch. Chem. Ges. B Ser.*, 1932, **65**, 1192–1201.
- 71 J. Montenegro and S. Matile, *Chem. – Asian J.*, 2011, **6**, 681–689.
- 72 C. Marrano, P. de Macédo, P. Gagnon, D. Lapierre, C. Gravel and J. W. Keillor, *Bioorg. Med. Chem.*, 2001, **9**, 3231–3241.
- 73 J. C. Slootweg, J. Kemmink, R. M. J. Liskamp and D. T. S. Rijkers, *Org. Biomol. Chem.*, 2013, **11**, 7486.
- 74 J. De Abajo, E. L. Madruga, J. San Roman, J. G. De La Campa and J. Guzman, *Polymer*, 1992, **33**, 1090–1095.
- 75 D. M. Patel, M. I. Shekh, K. P. Patel and R. M. Patel, *J. Chem. Pharm. Res.*, 2015, **7**, 470–480.
- 76 A. A. Khalil, *J. Appl. Polym. Sci.*, 2006, **99**, 2258–2262.
- 77 T. M. Pyriadi and N. J. Alasli, *J. Polym. Sci. Part Polym. Chem.*, 1989, **27**, 2491–2496.
- 78 T. M. Pyriadi and F. M. Ali Alsalam, *J. Polym. Sci. Part Polym. Chem.*, 1997, **35**, 3125–3130.
- 79 B. D. Mather, K. Viswanathan, K. M. Miller and T. E. Long, *Prog. Polym. Sci.*, 2006, **31**, 487–531.
- 80 M. M. Dell'Anna, V. F. Capodiferro, M. Mali and P. Mastrolilli, *J. Organomet. Chem.*, 2016, **818**, 106–114.
- 81 D. R. Edwards, A. A. Neverov and R. S. Brown, *Inorg. Chem.*, 2011, **50**, 1786–1797.
- 82 T. Iwasaki, Y. Maegawa, Y. Hayashi, T. Ohshima and K. Mashima, *J. Org. Chem.*, 2008, **73**, 5147–5150.
- 83 Y. Maegawa, K. Agura, Y. Hayashi, T. Ohshima and K. Mashima, *Synlett*, 2012, **2012**, 137–141.
- 84 E. F. Aransiola, T. V. Ojumu, O. O. Oyekola, T. F. Madzimbamuto and D. I. O. Ikhu-Omoregbe, *Biomass Bioenergy*, 2014, **61**, 276–297.
- 85 J.-C. Alfred, J. Daunis and R. Jacquier, *Macromol. Chem. Phys.*, 1996, **197**, 389–401.
- 86 A. Akinc, A. Zumbuel, M. Goldberg, E. S. Leshchiner, V. Busini, N. Hossain and S. A. Bacallado, *Nat. Biotechnol.*, 2006, **26**, 561–569.
- 87 K. McAdam, H. Kimpton, C. Vas, D. Rushforth, A. Porter and B. Rodu, *Chem. Cent. J.*, DOI:10.1186/s13065-015-0132-1.
- 88 A. Desvergne, Y. Cheng, S. Grosay-Gaudrel, X. Maréchal, M. Reboud-Ravaux, E. Genin and J. Vidal, *J. Med. Chem.*, 2014, **57**, 9211–9217.
- 89 P. Somasundaran, *Encyclopedia of Surface and Colloid Science*, CRC Press, 2006.
- 90 I. J. Bruce and T. Sen, *Langmuir*, 2005, **21**, 7029–7035.
- 91 M. W. Daniels, J. Sefcik, L. F. Francis and A. V. McCormick, *J. Colloid Interface Sci.*, 1999, **219**, 351–356.
- 92 F. Luderer and U. Walschus, in *Immobilisation of DNA on Chips I*, ed. C. Wittmann, Springer Berlin Heidelberg, 2005, pp. 37–56.
- 93 M. P. J. Peeters, *J. Sol-Gel Sci. Technol.*, 1999, **19**, 131–135.
- 94 C. J. Brinker and G. W. Scherer, *Sol-Gel Science: The Physics and Chemistry of Sol-Gel Processing*, Academic Press, 2013.
- 95 A. M. Buckley and M. Greenblatt, *J. Chem. Educ.*, 1994, **71**, 599.
- 96 C. R. Silva and C. Airoidi, *J. Colloid Interface Sci.*, 1997, **195**, 381–387.
- 97 F. D. Osterholtz and E. R. Pohl, *J. Adhes. Sci. Technol.*, 1992, **6**, 127–149.
- 98 E. J. A. Pope and J. D. Mackenzie, *J. Non-Cryst. Solids*, 1986, **87**, 185–198.
- 99 I. Pastoriza-Santos, J. Pérez-Juste and L. M. Liz-Marzán, *Chem. Mater.*, 2006, **18**, 2465–2467.
- 100 C. Graf, D. L. J. Vossen, A. Imhof and A. van Blaaderen, *Langmuir*, 2003, **19**, 6693–6700.

- 101 S.-Y. Lin, Y.-T. Tsai, C.-C. Chen, C.-M. Lin and C. Chen, *J. Phys. Chem. B*, 2004, **108**, 2134–2139.
- 102 M.-C. Brochier Salon and M. N. Belgacem, *Colloids Surf. Physicochem. Eng. Asp.*, 2010, **366**, 147–154.
- 103 R. Denoyel, J. C. Glez and P. Trens, *Colloids Surf. Physicochem. Eng. Asp.*, 2002, **197**, 213–223.
- 104 L. A. Mitcova, Université de Bordeaux, 2014.
- 105 T. Kasnavia, D. Vu and D. A. Sabatini, *Ground Water*, 1999, **37**, 376–381.
- 106 M. Mohammadi, A. J. Hassani, A. R. Mohamed and G. D. Najafpour, *J. Chem. Eng. Data*, 2010, **55**, 5777–5785.
- 107 H. M. H. Gad and A. A. El-Sayed, *J. Hazard. Mater.*, 2009, **168**, 1070–1081.
- 108 L. Wang, A. Roitberg, C. Meuse and A. K. Gaigalas, *Spectrochim. Acta. A. Mol. Biomol. Spectrosc.*, 2001, **57**, 1781–1791.
- 109 M. Majoube and M. Henry, *Spectrochim. Acta Part Mol. Spectrosc.*, 1991, **47**, 1459–1466.
- 110 N. O. Mchedlov-Petrosyan, L. A. Fedorov, S. A. Sokolovskii, Y. N. Surov and R. S. Maiorga, *Bull. Russ. Acad. Sci. Div. Chem. Sci.*, 1992, **41**, 403–409.
- 111 S. Biswas, V. Sundstrom and S. De, *Mater. Chem. Phys.*, 2014, **147**, 761–771.
- 112 J. Zhao, T. Wu, K. Wu, K. Oikawa, H. Hidaka and N. Serpone, *Environ. Sci. Technol.*, 1998, **32**, 2394–2400.
- 113 P. Bartasun, H. Cieliski, A. Bujacz, A. Wierzbicka-Wo? and J. Kur, *PLoS ONE*, 2013, **8**, e55697.
- 114 R. Comparelli, E. Fanizza, M. Curri, P. Cozzoli, G. Mascolo, R. Passino and A. Agostiano, *Appl. Catal. B Environ.*, 2005, **55**, 81–91.
- 115 A. M. Al-Azzawi and M. S. A. Al-Razzak, *Int J Res Pharm Chem*, 2013, **3**, 682–90.
- 116 O. S. Curley, J. E. McCormick, R. S. McElhinney and T. B. H. McMurry, *Arkivoc*, 2003, **7**, 180–189.
- 117 S. Wolfe and S. K. Hasan, *Can. J. Chem.*, 1970, **48**, 3572–3579.
- 118 M. A. González and D. Pérez-Guaita, *Tetrahedron*, 2012, **68**, 9612–9615.
- 119 S.-H. Chung, T.-J. Lin, Q.-Y. Hu, C.-H. Tsai and P.-S. Pan, *Molecules*, 2013, **18**, 12346–12367.
- 120 M. V. Ramakrishnam Raju, E. Chandra Prakash, H.-C. Chang and H.-C. Lin, *Dyes Pigments*, 2014, **103**, 9–20.
- 121 N. Engelhardt, A. Ernst, A.-L. Kampmann and R. Weberskirch, *Macromol. Chem. Phys.*, 2013, **214**, 2783–2791.
- 122 N. Kasoju, D. K. Bora, R. R. Bhonde and U. Bora, *J. Nanoparticle Res.*, 2010, **12**, 801–810.

IV. Cell culture examinations of synthesized TiO_2 particle systems

Contents

IV.	Cell culture examinations of synthesized TiO ₂ particle systems	- 143 -
IV.1.	Stabilisation of TiO ₂ nanoparticles in cell culture media	- 144 -
IV.2.	Cytotoxicity of TiO ₂ nanoparticles	- 151 -
IV.3.	Tumour treatment effect of MEEAA-TiO ₂ particles	- 154 -
IV.4.	Conclusion.....	- 164 -

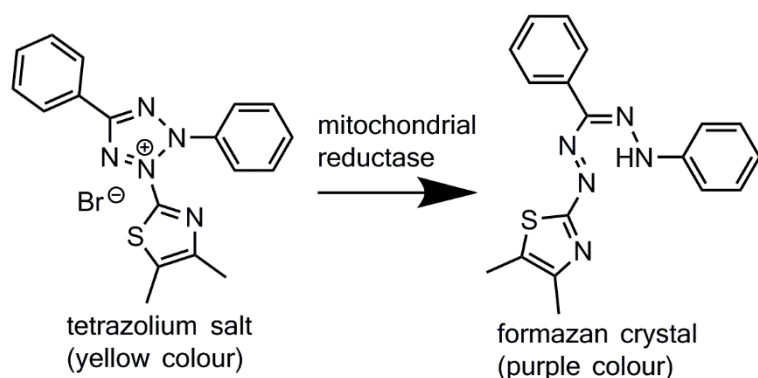
IV. Cell culture examinations of synthesized TiO₂ particle systems

The first step for future applications of TiO₂ nanoparticles in the biomedical field is the examination of their *in vitro* cytotoxicity. A compound is considered to be cytotoxic *in vitro* if it interferes with the cells, which includes cellular attachment, significant morphology alterations, an adverse cell growth rate or cell death.¹ Nevertheless, the most common and reliable method for the evaluation of cytotoxicity is the evaluation of the relative number of dead cells compared to viable cells. The cytotoxicity of the synthesized nanoparticles (NPs) towards malignant and non-malignant cell types has to be examined as this is very important for later applications as tumour treatment agent; the particles should be non-toxic (in their inactivated form) towards all cell types to provide a specific photocatalytic (PC) tumour treatment when ultraviolet (UV) light is applied.

FaDu cells and primary human mesenchymal stem cells have been selected as representative cell systems for all *in vitro* tests in this chapter. FaDu is a well-established cell line of head and neck squamous cell carcinoma (HNSCC). Previously, cancer cell elimination of HNSCC by photoactivated NPs has been described.² In the current investigation, FaDu cells were used for the cytotoxicity tests with respect to possible applications of TiO₂ NPs as a photosensitising agent in experimental cancer therapy in future. Furthermore, human bone marrow-derived mesenchymal stem cells (BMSC) were applied in order to examine toxicity in non-malignant cells. Due to their phenotypic and cellular plasticity, stem cells are considered a promising test system for cytotoxicity evaluations.³ For further cytotoxicity assessments also HLaC78 cells as another tumour cell line and primary human fibroblasts as a non-malignant cell type, which are present in the tissue of interest, were selected.

The duration of NP incubation with the cells before cytotoxicity assessment was chosen to be 24 h as the particle uptake is said to start as early as one hour after NP addition and proceeds at least for 24 hours.⁴ The chosen 3-(4,5-dimethylthiazol-2-yl)-2,5-diphenyl tetrazolium bromide (MTT) assay detects the viability of cells; only viable cells bearing intact mitochondria are able to metabolise the applied yellow tetrazolium MTT salt into a purple formazan crystal (Scheme IV - 1).⁵⁻⁷ This colour change can be easily detected using an automated spectrophotometric microplate reader. It is a well-established method used for various categories of malignant and non-malignant cells and cell lines *in vitro* in immunological investigations, cancer research and material biocompatibility evaluations.^{1,8-10} The advantage of this assay is that it only needs a small amount of cells and is quite sensitive towards cytotoxic events, which allows the miniaturization of the test into 96-well plate formats.^{1,9,11} The assay protocol is considerably simple and rapid, reproducible and economic.^{9,10} As the water-insoluble formazan requires the addition of DMSO, the assay is a lytic end point assay, giving

for example no opportunity for additional spectrophotometric readings.¹ Also the pH dependence of the absorption spectrum of reduced MTT has to be considered for obtaining reliable results.⁷



Scheme IV - 1. Reduction of tetrazolium salt into formazan.¹²

The use of MTT assays to determine the cytotoxicity of particles such as TiO₂ NPs is already well established.⁷ Using this method it has to be kept in mind that the metal ions derived from the particle samples (like Zn²⁺ in the case of ZnO NPs) can inhibit the MTT reduction reaction. Furthermore, NPs can also deplete free MTT by interactions and therefore cause false negative results. Concerning the readout, present NPs can increase the light absorption and therefore also falsify the outcomes.⁷ This is why for every NP sample blind tests with only the NPs and MTT have to be carried out to ensure reliable measurements.

Prior to the toxicity determinations, the particles had to be transferred into cell culture medium (and stabilised). This procedure is discussed in the following chapter (IV.1). Subsequently the cytotoxicity of both stabilised and not-stabilised particles was examined (IV.2). Finally, an observed tumour treatment effect of the examined particle samples is described in IV.3.

IV.1. Stabilisation of TiO₂ nanoparticles in cell culture media*

For the use of nanoparticles in *in vitro* or *in vivo* tests the particles have to be transferred into physiological solutions. Doing this, a problem arises: without appropriate surface modification, NPs tend to agglomerate and sediment in these solutions due to their pH and salt content.^{13–15} This was also the case for the synthesized AA-TiO₂ and MEEAA-TiO₂ standard particles that were used for these examinations. The particles already lost their dispersion state

* Parts of this chapter have been published and are reused in this work by courtesy of Elsevier, original article: S. Koch et al., Colloids Surf., B, 2016, 143, 7–14.

if they were brought to neutral pH, which was necessary for the transfer into cell culture media. Agglomerate sizes of several μm were observed (Figure IV - 1).

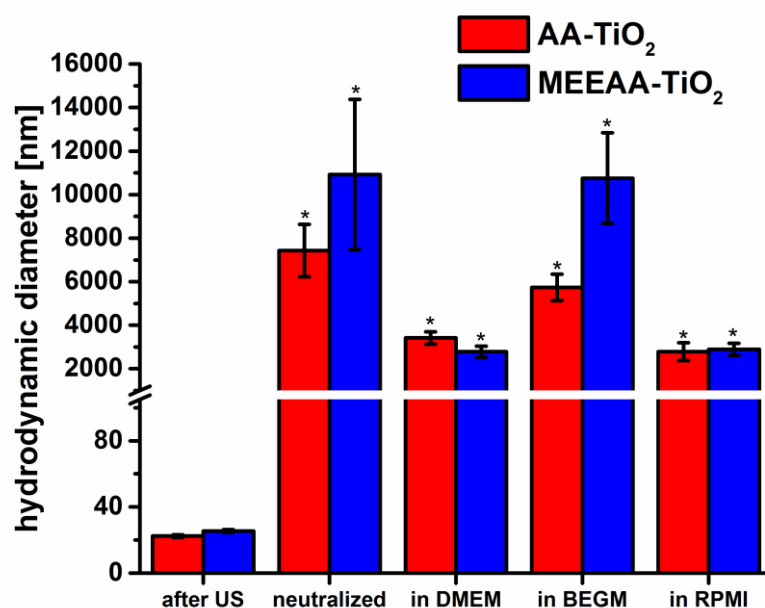


Figure IV - 1. Average hydrodynamic diameter (Z-average) of AA-TiO₂ and MEEAA-TiO₂ after synthesis and ultrasonic treatment (US), after neutralisation and after transfer into DMEM, BEGM or RPMI. *Standard deviations of these values may not be reliable as DLS measurements were impeded by sedimentation of the NPs.

In aqueous solutions the colloids are mainly stabilised by electrostatic repulsion between equally charged particles¹⁶. This electrostatic stabilisation is always limited to a certain pH range as at a particular concentration of OH^- or H_3O^+ , these ions may neutralize the surface charge of the particles up to their isoelectric point resulting in flocculation.^{17,18} In the same way, an increase of ionic strength of the solution, for example due to dissolved salts, results in destabilisation of colloidal dispersions, which is well described by the DLVO (Derjaguin-Landau-Verwey-Overbeek) theory.¹⁹ This is why, after transfer into cell culture media (DMEM, BEGM or RPMI), the agglomerate sizes of the samples had not been significantly reduced and sedimentation of the particles occurred immediately. In order to ensure a consistent assessment of the therapeutic and diagnostic potential of NPs in cell culture experiments or animal testing, this issue needs to be addressed: studies concerning particle concentrations are only reliable when carried out with stable dispersions that guarantee an accurate dosing. The effect of different sized particles on cells can only be studied if the particles do not form large agglomerates.^{13,20,21} In the case of PC NPs, agglomeration also leads to an unwanted reduction of surface area and therefore lower PC efficiency.^{13,22}

Thus, a suitable stabilising agent had to be found to achieve stable, non-agglomerated NP dispersions in cell culture media. In order to do so, several stabilising agent have been

screened: fetal bovine serum (FBS) and bovine serum albumin (BSA) were used as biological stabilising agents since they have been previously applied for this purpose,^{13–15,20} and thus serve as reference systems. BSA can be found abundantly in bovine blood plasma^{14,15,20} and FBS is commonly added as a growth supplement to cell culture media.^{13,14} They both form a protein corona around particles through ionic interactions and therefore act as stabilisers^{23,24} due to mainly electrostatic but also to a certain extent weak steric effects.¹⁴ Furthermore, polycarboxylate ethers (like Melflux®4930 F, Melpers®V4343 and Sika®ViscoCrete®-10110178) as combined ionic and steric surfactants have been chosen as stabilising agent. Their great potential for various NPs in solutions has been demonstrated recently.^{18,25,26} Polycarboxylate ethers have been commonly used in the cement industry as superplasticisers that adsorb onto silicate particles, improving the particle mobility and flow behaviour of cement. The polycarboxylate ether comb-polymers consist of a polycarboxylate backbone and polyethylene oxide side chains bound to the backbone as esters. They adsorb onto the nanoparticle surface via coulombic attractions between the negatively charged backbone and the positively charged particle surface.²⁷ Due to the charge of the backbone and steric effects of the comb-polymer side chains, the particles are electrosterically stabilised.¹⁸ Although this property means they are promising candidates for particle stabilisation in environments with high ionic strength, to the best of our knowledge, these stabilising agents have never been applied in cell culture experiments so far.

The particles were stabilised following the protocol described in literature.^{15,20} The surface-active agents (FBS, BSA, Melflux, Melpers or Sika ViscoCrete) were added to the US treated samples at pH 2–3 where the particles are ideally dispersed, as this ensures that the complete surface of each individual NP is accessible by the stabiliser molecules for adsorption. When the dispersions were then neutralised, the stabilisers prevented particle agglomeration. In order to quantitatively evaluate the stabilisation efficiency, DLS and sedimentation studies were carried out. The agglomerate size of the stabilised particles was only measured immediately after the transfer to cell culture media as the hydrodynamic diameter stayed the same over 24 h, which has been proved by Ji et al.¹⁴ The sedimentation of the stabilised NPs in cell culture media was examined by measuring the absorbance (at 490 nm) of the supernatant (= upper 10 %) of the samples immediately and at 24 h after NP transfer. Due to light scattering by the particles, the absorbance decreased with lower particle concentration in the supernatant when the particles sedimented. The absorbance directly after particle transfer was taken as 100 % stably dispersed particles and the measured reference (medium with stabiliser but without particles) was considered as 0 % stably dispersed particles. Taking these numbers into account the percentage of particles that were still stably dispersed after 24 h was calculated. The results for AA-TiO₂ are shown in Figure IV - 2. The results for MEEAA-TiO₂

can be found in the Appendix III. Slight differences between these results are due to different surface groups and varied surface charges, however, the results are overall very similar.

a) Percentage of NP, still stably dispersed after 24 h

A: 100%	B: >74 %				C: 50-74 %				D: 25-49 %				E: <25 %				
AA-TiO ₂ (0.5 mg/ml)																	
1 mg NP : x mg																	
DMEM				BEGM				RPMI									
1	10	50	100	1	10	50	100	1	10	50	100						
BSA	D	C	A	B	E	E	E	E	E	E	E	E					
FBS	-	C	C	A	-	E	E	E	-	A	A	A					
Melflux	A	E	C	-	A	D	C	-	A	E	C	-					
Melpers	B	A	B	C	-	E	D	A	-	E	C	E					
Sika ViscoCrete	-	C	A	A	-	E	A	A	-	B	A	A					

b) Z-Av d in [nm]

a: <100	b: 101-200				c: 201-300				d: 301-500				e: 501-700				f: > 700			
AA-TiO ₂ (0.5 mg/ml)																				
1 mg NP : x mg																				
DMEM				BEGM				RPMI												
1	10	50	100	1	10	50	100	1	10	50	100									
BSA	e	a	c	d	-	f	f	f	f	d	f	f								
FBS	-	c	b	b	-	f	f	f	-	c	c	b								
Melflux	a	b	d	-	a	b	d	-	a	b	d	-								
Melpers	b	b	c	c	-	f	f	f	-	e	f	f								
Sika ViscoCrete	-	e	b	c	-	f	b	c	-	d	b	c								

Figure IV - 2. AA-TiO₂ (0.5 mg/ml) in different cell culture media (DMEM, BEGM, RPMI) stabilised with 1 mg, 10 mg, 50 mg or 100 mg BSA, FBS, Melflux, Melpers or Sika ViscoCrete per 1 mg NP. a) Percentage of particles still stably dispersed after 24 h with decreasing dispersion stability from A: 100% (dark green) to E: <25 % (dark red). b) Agglomerate size (Z-average) with increasing hydrodynamic diameter from a: <100 nm (dark green) to f: >700 nm (dark red).

The commonly used stabilisers BSA and FBS (in the chosen concentration range) only show stabilising effects in the FBS-containing DMEM (and RPMI). This indicates that for these biological stabilisers a high amount of cell culture supplement, FBS, is additionally needed to build up a larger protein corona that is sufficient to stabilise the particles. BSA does not seem to be an adequate stabilising agent for the examined NPs as BSA only adsorbs at strong negatively charged oxide surfaces^{14,15,28} and the examined particles only exhibit a low negative charge at physiological pH (~7.4). A cell culture medium can be seen as an electrolytic solution with high ionic strength¹⁴ comparable to a 0.12 M NaCl solution.¹³ As the zeta potential of BSA itself decreases in salt solutions²⁹ due to interactions with the salts, the electrostatic stabilisation of particles by BSA is less efficient in cell culture media. In contrast to BSA, FBS stabilises the NPs independent of their surface charge due to a synergistic effect of its components such as globulin, BSA and transferrin.¹⁴ Therefore, it seems to be more suitable as a stabilising agent for the examined only slightly charged TiO₂ NPs. Additionally, several studies have already indicated that even if FBS contains a large amount of BSA, the albumin that is initially adsorbed onto the NP surfaces is usually replaced within several minutes up to a few hours by other less abundant but more specific proteins like apolipoproteins.^{30–32} This may also be an explanation for the higher stabilisation efficiency of FBS compared to BSA. The stabilisation of AA-TiO₂ and MEEAA-TiO₂ by polycarboxylate ethers (Melflux, Melpers and Sika ViscoCrete) seems to be independent of the addition of FBS as a supplement. This may

be due to the mainly steric stabilisation of polycarboxylate ethers (see below) not favouring ionic interactions with FBS.

As suggested by Mandel et al.,¹⁸ polycarboxylate ethers develop hydrogen bridging bonds between their carboxylic groups and the hydroxyl groups on the particle surface, when added at acidic pH to the particle dispersion (Figure IV - 3 a). This means that with this procedure, surfactants are not only weakly adsorbed but to a certain extent sufficiently anchored onto the particles. Thus they chemically functionalize the particles so that they show the surface characteristics of the polymer. Therefore, the measured isoelectric points of the functionalized particles were found at acidic pH values depending on the composition of the polycarboxylate ether (Melflux and Sika-ViscoCrete around pH 2 and Melpers around pH 3; these values are also confirmed in other works).^{18,33} The surfactant sterically stabilises the particles via the bulky polyethylene oxide side chains. With increased pH (>2) the unbound carboxylic acid groups of the polymer backbone start to deprotonate, resulting in an electrostatic stabilisation that adds to the steric stabilisation. At neutral pH, these systems exhibit both the electrostatic and steric repulsion mechanisms, known as electrosteric stabilisation (Figure IV - 3 b). For this reason this class of polycarboxylate ethers are ideally suited for NP stabilisation in cell culture media as the charged groups render the polymers (respective to functionalized particles) dispersible in water. However, even if the electrostatic stabilisation efficiency is very low in cell culture media, due to the prevailing high ionic strength, the steric repulsion keeps the particles separated. In summary, the stabilisation of the particles with polycarboxylate ethers is not influenced by the pH, ionic strength or chemical composition of the media. This has also been shown for other well-anchored polyethylene oxide moieties in literature.³⁴

As a result, the efficiency of polycarboxylate ethers as stabilisers mainly depends on their anchoring strength onto the particles, the particle surface coverage and the polymer composition (e.g. chain lengths). From the experiments shown in Figure IV - 2 it can be concluded that the most efficient stabilising agent is Melflux. It provides a stable dispersion for both particle systems in all media with 1 mg stabiliser per mg nanoparticle. Agglomerate sizes smaller than 100 nm are obtained in all three cell culture media. In comparison to the other polycarboxylate ethers (Sika ViscoCrete with 2000 g/mol side chain and Melpers with 500 g/mol side chain) this polymer has the longest polyethylene side chains (3000 g/mol), providing the best steric stabilisation. Due to its side chain lengths, Sika ViscoCrete is the second best of the tested polycarboxylate ethers.

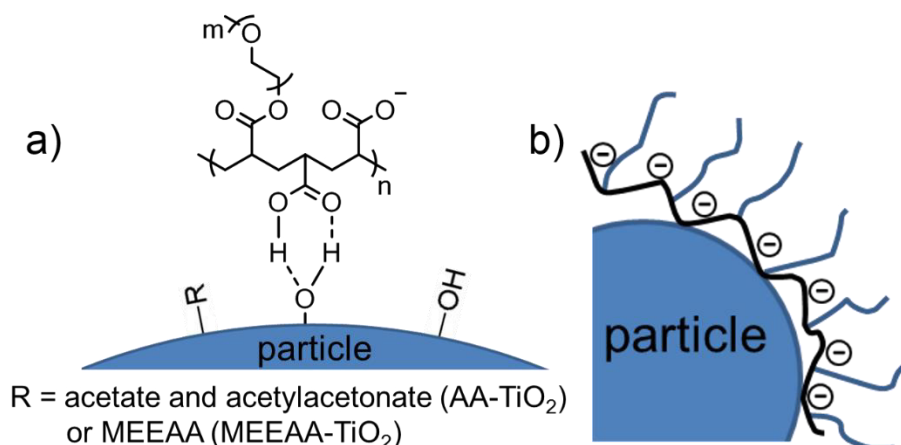


Figure IV - 3. Schemes of particles stabilised with a polycarboxylate ether at physiological pH showing a) the binding of the polymer onto the particle surface and b) one polymer chain adsorbed onto the particle surface, stabilising the particle electrosterically.

For further examinations (in RPMI medium) Melflux, the most efficient stabiliser, and FBS, as a control from the literature, have been selected. The best stabilising agent concentrations were chosen with the help of DLS measurements (Figure IV - 4). The agglomerate sizes of the particles first decreased with increasing stabilising agent concentrations and then finally started to increase again. This can be explained as with a low concentration there are not enough stabiliser molecules to completely cover the surface of every single particle and, due to their partly uncovered surface, particles still form agglomerates. With increasing stabiliser concentration, there are enough surface-active molecules to stabilise smaller agglomerates. When an ideal concentration is reached, each NP is surrounded with a monolayer of stabilising agent; this results in a perfectly stabilised dispersion. With increasing stabiliser concentration, further stabilising agent layers are formed around each particle.¹⁵

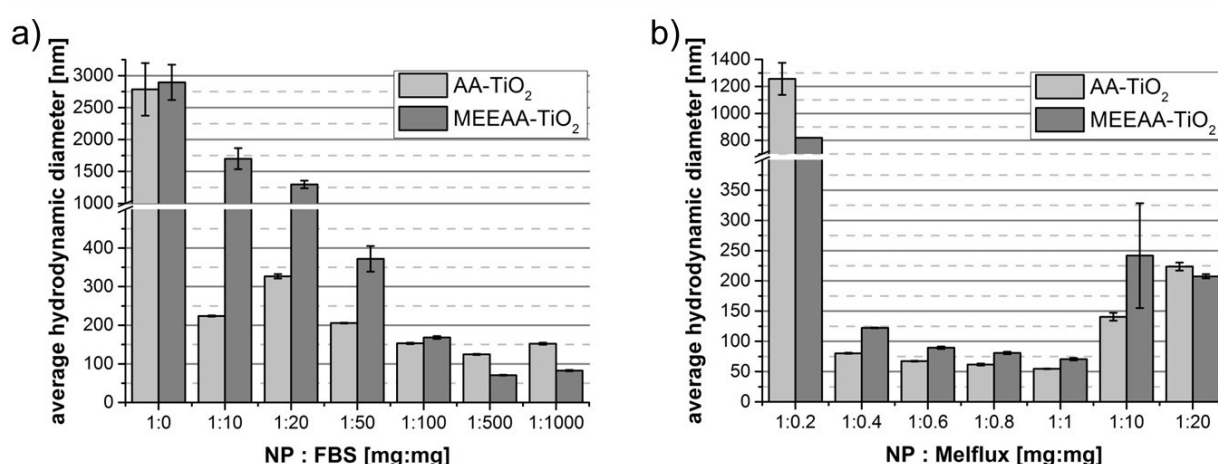


Figure IV - 4. Average hydrodynamic diameter of AA- TiO_2 and MEEAA- TiO_2 (0.5 mg/ml) in RPMI stabilised with a) FBS or b) Melflux.

Due to this and possible bridging effects of the stabiliser between particles, resulting in a connection of particles, the agglomerate size starts to increase again. The smallest stabiliser

concentration required to achieve a stable NP dispersion was 100 mg and 0.4 mg per 1 mg NP for FBS and Melflux, respectively. Both stabilisers prevented the formation of agglomerates larger than 200 nm, which is promising with respect to a facilitated cellular uptake effect.³⁵

The sedimentation study over 24 h confirmed the successful stabilisation of the dispersions with these stabiliser concentrations; Figure IV - 5 shows the absorbance measurements over time a) and photographs b) at 0 h and 24 h after NP transfer into RPMI.

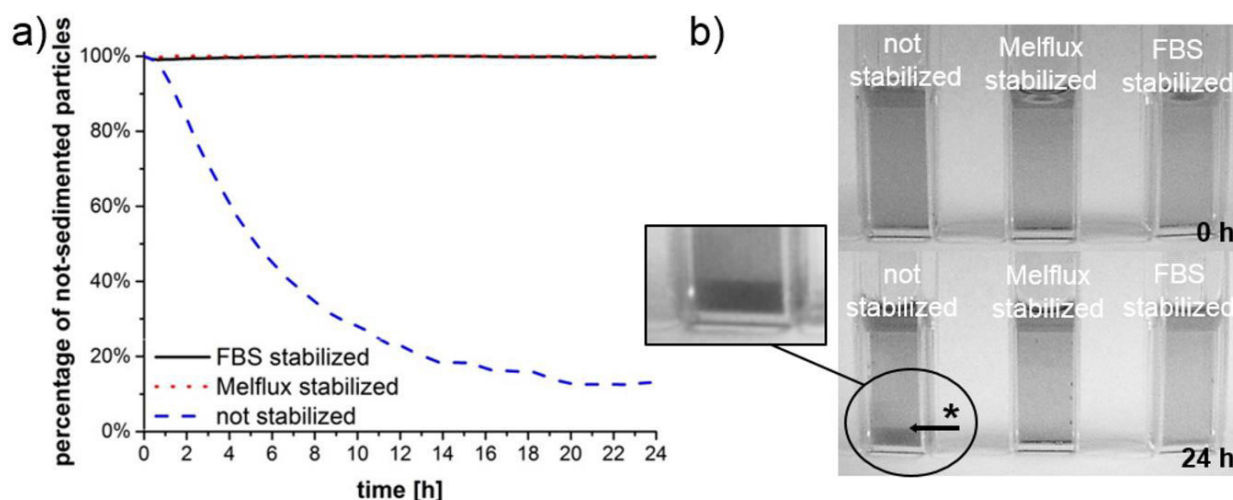


Figure IV - 5. Sedimentation study of AA-TiO₂ (0.5 mg/ml) in RPMI stabilised with FBS (1 mg NP:100 mg FBS) or Melflux (1 mg NP:0.4 mg Melflux) and not stabilised: a) percentage of not-sedimented particles determined via absorbance measurements and b) photograph of samples at 0 h and 24 h after addition of the stabiliser to the NP dispersion (*sedimented particles).

The pure NPs sedimented almost completely within one day while FBS- and Melflux-stabilised NPs did not show any sedimentation during this time range. Comparing both stabilisers it is worth noting that the amount of Melflux that is needed to stabilise the NPs is small. This indicates a very efficient stabilisation. For cell culture tests stabiliser concentrations as small as possible are desired in order to reduce potential influences regarding the particle toxicity and the uptake by the cells.

IV.2. Cytotoxicity of TiO₂ nanoparticles[†]

Prior to the cytotoxicity evaluation of stabilised and not-stabilised particles, the novel stabiliser Melflux had to prove its biocompatibility. This characteristic was assessed in cell culture studies; FaDu cells were treated with different Melflux concentrations for 24 h and examined via MTT assay. RPMI was chosen as cell culture medium for all viability tests as this medium was proved to be very suitable for PC tumour treatment experiments.³⁶ The viability of FaDu after incubation with Melflux is shown in Figure IV - 6. The stabiliser can be considered as non-toxic up to 500 µg/ml as the statistical analysis (Wilcoxon Test) showed no significant decrease in viability for all tested concentrations. For the cytotoxicity assay with TiO₂, nanoparticle concentrations up to 300 µg/ml were chosen and so the highest necessary Melflux concentration was 120 µg/ml. Therefore, with respect to the results of the MTT assay with Melflux alone, the stabiliser should not influence the toxicity of the particles.

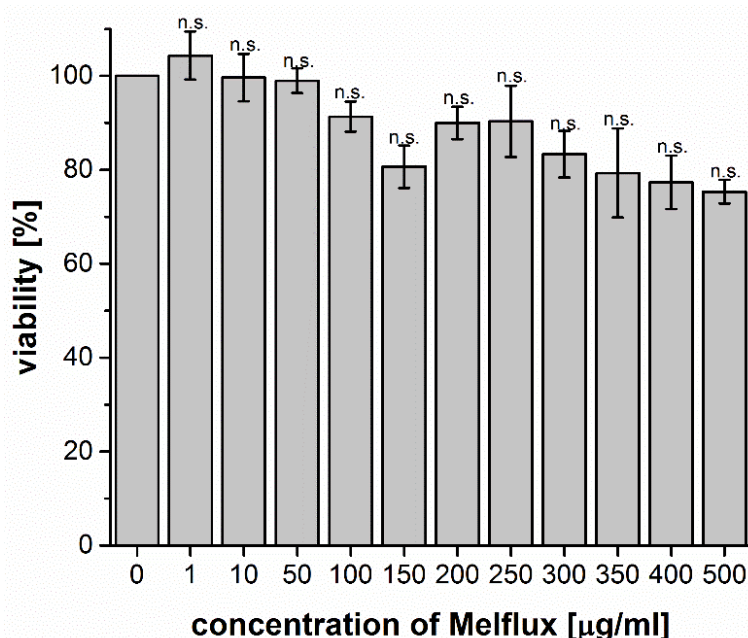


Figure IV - 6. Viability of FaDu cells treated with Melflux for 24 h compared to the viability of non-treated cells. No significance (n.s.) with $p < 0.05$ was found in all tested NP concentrations in comparison to the negative control.

After approval of Melflux as biocompatible stabilising agent, the cytotoxicity of AA-TiO₂ and MEEAA-TiO₂ with and without FBS or Melflux towards FaDu and stem cells was examined. The obtained viability results are shown in Figure IV - 7 and Figure IV - 8. Both particle systems were non-toxic up to 300 µg/ml for both stem cells and cancer cells: the not-stabilised particle agglomerates as well as the two differently stabilised agglomerates with diameters under 200

[†] Parts of this chapter have been published and are reused in this work by courtesy of Elsevier, original article: S. Koch et al., Colloids Surf., B, 2016, 143, 7–14.

nm. This indicates that both agglomerates as well as single particles are non-toxic towards malignant and non-malignant cells. Although cell viability of both cell types was decreased after exposure to high concentrations (such as 300 µg/ml) of AA-TiO₂, the results were not significant. Nevertheless, MEEAA-TiO₂ seems to be slightly more biocompatible in comparison to AA-TiO₂, which may be due to differences in the surface moieties of both particle systems: the MEEAA derivative has a polyethylene glycol-like structure and this polymer is known to be non-toxic and is therefore used for medical applications. As a result, MEEAA bearing MEEAA-TiO₂ may be slightly less toxic towards cells than AA-TiO₂. The addition of Melflux and FBS did not significantly influence the toxicity of the NPs. However, cell viability tended to increase in samples treated with MEEAA-TiO₂ and FBS (Figure IV - 7 b). A possible explanation for this is that with increasing NP concentration, the FBS concentration also increases, which may lead to enhanced cell viability. This is due to growth factors contained in FBS, which stimulate cell growth. The addition of FBS as a stabiliser can therefore significantly influence studies on particle toxicity. Furthermore in cell culture experiments addition of FBS varies the medium composition leading to less well-defined chemical conditions, notwithstanding any ethical implications.³⁷ For these reasons the use of Melflux as non-toxic stabiliser is a very promising alternative to commonly used stabilisers.

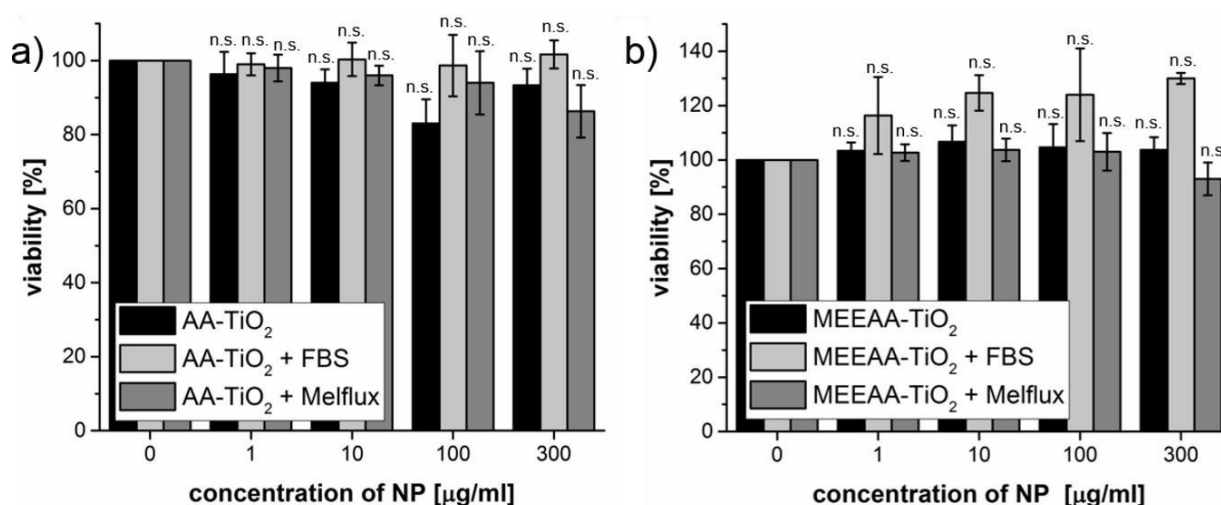


Figure IV - 7. Viability of tumour cells (FaDu) treated with a) AA-TiO₂ and b) MEEAA-TiO₂ without stabiliser and stabilised with FBS (1 mg NP:100 mg FBS) or Melflux (1 mg NP:0.4 mg Melflux). The values are normalised with respect to the vitality of no particle treated cells. No significance (n.s.) with $p < 0.05$ was found in all tested NP concentrations in comparison to the negative control.

IV. Cell culture examinations of synthesized TiO₂ particle systems

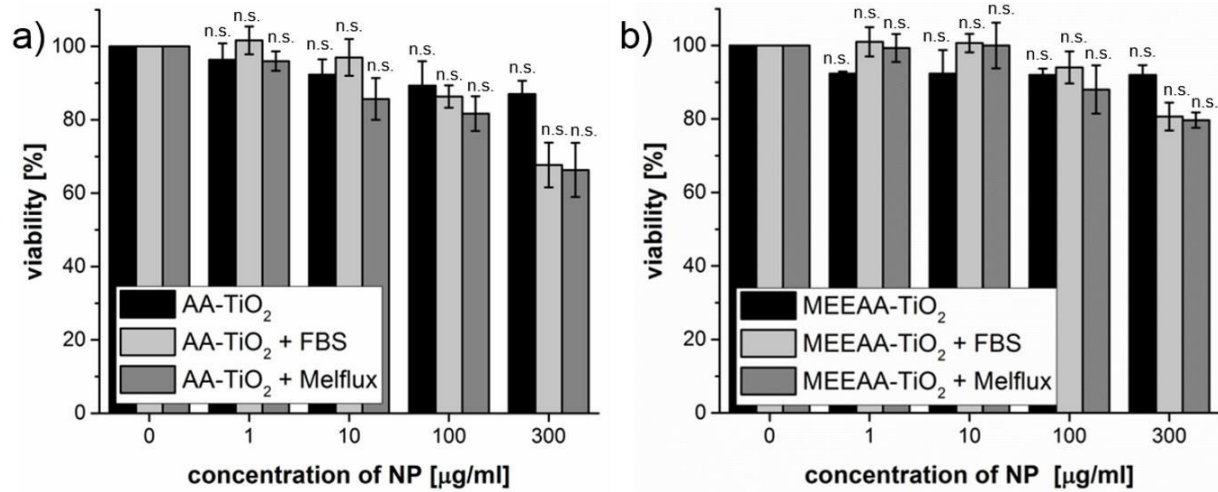


Figure IV - 8. Viability of stem cells (BMSC) treated with a) AA-TiO₂ and b) MEEAA-TiO₂ without stabiliser and stabilised with FBS (1 mg NP:100 mg FBS) or Melflux (1 mg NP:0.4 mg Melflux). The values are normalised with respect to the vitality of no particle treated cells. No significance (n.s.) with $p < 0.05$ was found in all tested NP concentrations in comparison to the negative control.

IV.3. Tumour treatment effect of MEEAA-TiO₂ particles

After successful stabilisation of the synthesized TiO₂ NPs in cell culture media and proof of their non-toxicity, the next logical step towards an application as PC anti-tumour agent is the assessment of their cytotoxicity after/during UVA-1 light application *in vitro*. The state of the art approach to determine the anti-tumour activity of PC NPs is shown in Figure IV - 9 a).³⁸⁻⁴³

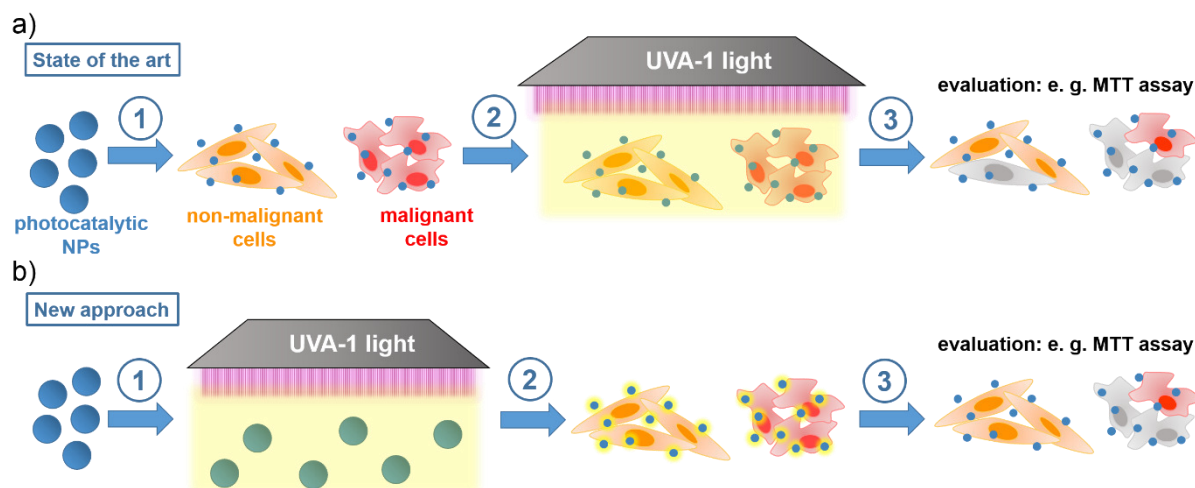


Figure IV - 9. a) State of the art photocatalytic tumour treatment including the direct UVA-1 light application onto cells after NP uptake compared to b) a new approach avoiding it.

For this examination, the NPs are exposed to the cells (Figure IV - 9 a), step 1) and incubated for 24 h to allow cellular uptake of the NPs before applying the UVA-1 (340-400 nm wavelength range) light (Figure IV - 9 a), step 2). During UVA-1 light application, the NPs are activated to do photocatalysis, which leads to cellular damages and apoptosis ((Figure IV - 9 a), step 3) as e. g. shown by a MTT assay. However, even if the NPs are exclusively taken up by malignant cells or their toxicity is specific towards malignant cells, the damage of non-malignant cells caused by UVA-1 light can never be avoided. Regarding our experimental approach, we tried to exclude direct UVA light application to cells and we found that MEEAA-TiO₂ (4 h, 160 °C) samples were anti-tumour active after a UVA (315-400 nm wavelength range) light pre-activation for 24 h (Figure IV - 9 b). Within this setting, the NPs were first pre-activated with UVA light (Figure IV - 9 b), step 1) for 24 h, then added to the cells and incubated for another 24 h (Figure IV - 9 b), step 2) before evaluating the cell viability (Figure IV - 9 b), step 3). This procedure was carried out with two malignant (FaDu, HLaC78) and two non-malignant (BMSC, fibroblasts) cell types and compared to the exposure of non-irradiated and therefore inactive MEEAA-TiO₂ samples to the cells. For all cell culture tests described in this chapter, NP samples without any stabilising agent were utilized to not further complicate the toxicity evaluations. The subsequent MTT test after incubation revealed that while the inactive NPs were as expected non-toxic to all cell types (Figure IV - 10 a), the pre-activated NPs showed

specific toxicity towards the cancer cells while affecting the non-malignant ones only at higher concentrations (Figure IV - 10 b).

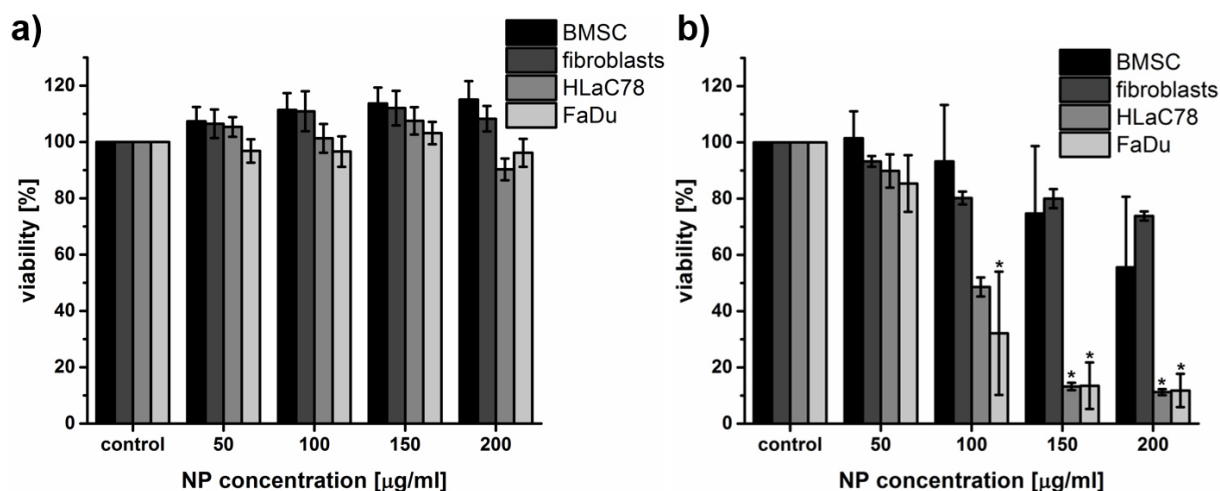


Figure IV - 10. Viability of non-malignant cells (BMSC, fibroblasts) and malignant cells (HLaC78, FaDu) treated with a) MEEAA-TiO₂ (160 °C, 4 h) without UVA light pre-activation and b) MEEAA-TiO₂ (160 °C, 4 h) pre-activated with UVA light for 24 h. The values are normalised with respect to the vitality of no particle treated cells. Significance compared to the control with a *P*-value < 0.05 is indicated by asterisks.

To further examine this result and to determine, which component of the samples may be responsible for the anti-tumour effect, four different samples were prepared and toxicologically evaluated (Figure IV - 11). The sample 1) was MEEAA as commercially obtained, which was UVA light pre-activated for 24 h and the sample 2) was pure TiO₂ as the present MEEAA was removed by washing steps with diluted HNO₃ and then UVA light pre-activated for 24 h. The sample 3) was MEEAA-TiO₂ as synthesized, which was first UVA light pre-activated for 24 h and then the NPs were removed via centrifugation and only the supernatant containing pre-activated MEEAA was utilized. The sample 4) consisted of MEEAA-TiO₂ as synthesized and was just treated with UVA light for 24 h exactly like the standard sample used before (Figure IV - 10). While sample 1) and 2) showed no anti-tumour activity, sample 3) was as toxic to cancer cells as the reference sample 4). These results lead to the conclusion that both components MEEAA and TiO₂ NPs are needed for the activation of the samples. The MEEAA is “activated” by the PC activity of the TiO₂ NPs and subsequently acts anti-tumour active even if no particles are present in the cell culture.

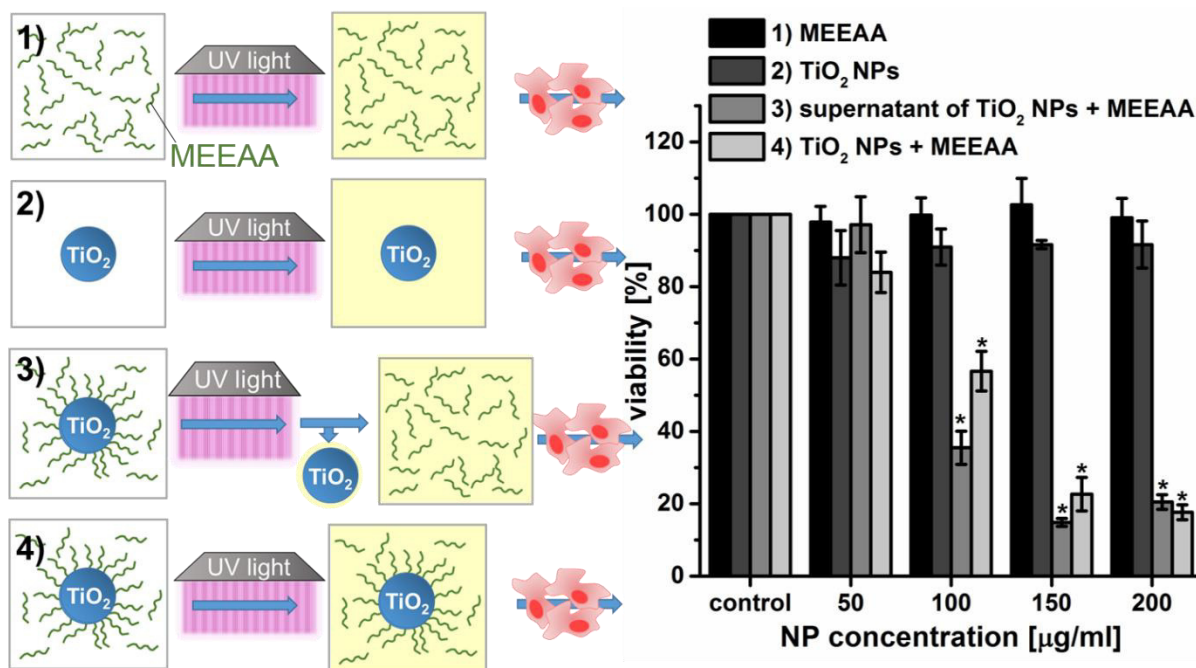


Figure IV - 11. Viability of tumour cells (FaDu) treated with UVA light (24 h) pre-activated samples: 1) pure MEEAA, 2) TiO₂ NPs (160 °C, 4 h) without MEEAA (realized with the help of washing steps), 3) MEEAA, which was separated from the TiO₂ NPs after pre-activation via centrifugation and 4) MEEAA-TiO₂ NPs (standard sample). The values are normalised with respect to the vitality of no particle treated cells. Significance compared to the control with a *P*-value < 0.05 is indicated by asterisks.

While reactive oxygen species ($\cdot\text{O}_2^-$, $\cdot\text{OH}$) generated by photocatalysis are short-lived entities (less than 70–200 ns),^{44,45} it is well-known that the photocatalysed degradation of an organic molecule usually does not result in instantaneous formation of carbon dioxide but long-lived intermediate species such as long-lived radicals are formed.^{46,47} Therefore, the long term activity of the samples were tested to investigate the possible creation of long-lived species, which could act toxic towards malignant cells either because of their properties or due to continuing degradation into carbon dioxide during cell culture incubation. If the photocatalysis by TiO₂ led to long-lasting but unstable intermediate species in the MEEAA sample, the probe would lose its anti-tumour activity during storage. As shown in Figure IV - 12 a), the samples do not change their toxic behaviour even after 5 days storage time and therefore, the acid must be irreversibly and long-term modified by the TiO₂ photocatalysis during UVA light treatment.

In order to study a possible degradation of the MEEAA during UVA light activation, HPLC and NMR analysis were planned to be carried out before and after UVA treatment. However, as the commercial MEEAA used for synthesis showed a low purity (70 %), the first analyses of the samples were not conclusive because of too high contamination by other unidentified organic compounds. Based on these findings, a purer commercial MEEAA sample (> 95 %) was purchased and compared to the standard compound. For this examination, the acids were intermixed with commercial P25 TiO₂ NPs as this procedure is less time consuming than the

hydrothermal synthesis approach for MEEAA-TiO₂ and gives the same results concerning PC UVA light activation of the MEEAA samples. The MTT tests depicted in Figure IV - 12 b) clearly show that the anti-tumour effect is caused by the impurities of the sample and not by the MEEAA as the purer commercial MEEAA does not induce any significant toxicity.

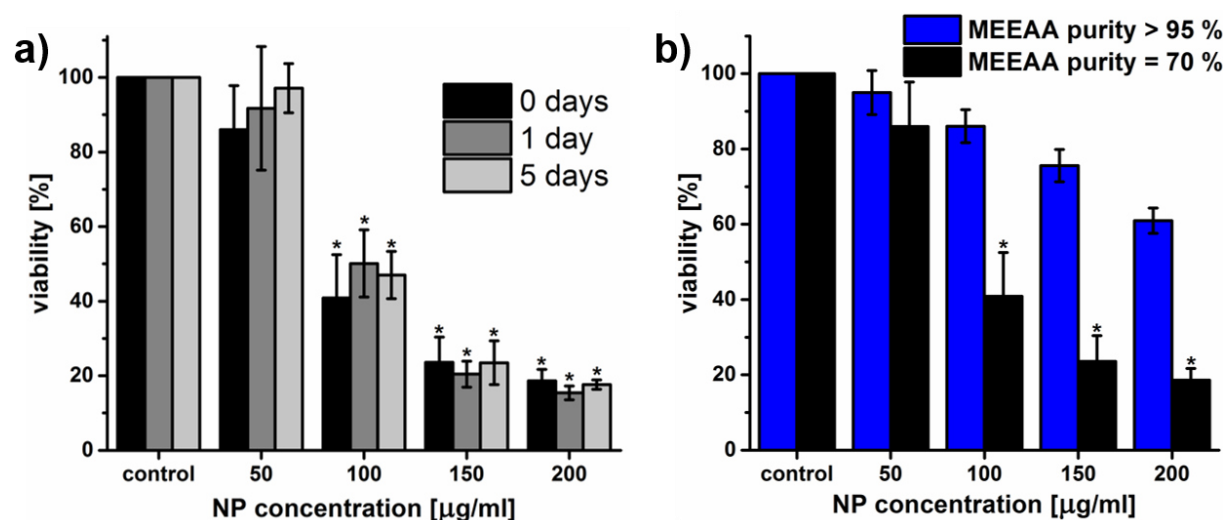


Figure IV - 12. Viability of tumour cells (FaDu) treated with UVA light (24 h) pre-activated samples: a) MEEAA-TiO₂ NPs (standard sample) after storage for 0, 1 or 5 days and b) P25 TiO₂ NP dispersions prepared with standard MEEAA (purity = 70 %) or MEEAA with a higher purity (> 95 %). The values are normalised with respect to the vitality of no particle treated cells. Significance compared to the control with a P-value < 0.05 is indicated by asterisks.

In order to further investigate, which is the compound responsible for the anti-tumour effect in the commercial MEEAA sample (70 %), it was divided into several fractions via distillation (heating up to 250 °C under dynamic vacuum – further information in the experimental part). The aim was to divide possible non-toxic from toxic components. After distillation, all samples were intermixed with P25 colloids, UVA light pre-activated and subsequently tested for their cytotoxicity towards cancer cells. The results are summarized in Figure IV - 13 and compared to the undistilled MEEAA. It is evident that fraction II did not show any significant anti-tumour effect up to 150 µg/ml NP concentration (included) while fraction IV exhibited the highest anti-tumour activity with significant toxicity already at a concentration of 100 µg/ml. This is why these two fractions were analysed in more detail; fraction II appeared to be the purified MEEAA (verified by NMR and MS), which explains the low cytotoxicity of this fraction. It is therefore also logical that the viability values of FaDu cells treated with this fraction II resemble the ones treated with commercial MEEAA with a higher purity (> 95 %, Figure IV - 12). Fraction IV could first not be identified as it was a mixture out of at least 2 compounds, which was mainly indicated by the detection of several molecular masses by MS and impossible integral ratios of the signals in the ¹H-NMR. This is why fraction IV was separated via column chromatography, obtaining two fractions, denoted as IV-a and IV-b. Fraction IV-a consists of

one single pure compound IV-a. This compound IV-a is the main component of fraction IV by weight (76 %) and its structure (Scheme IV - 2) was identified with the help of 2D NMR analysis and MS.

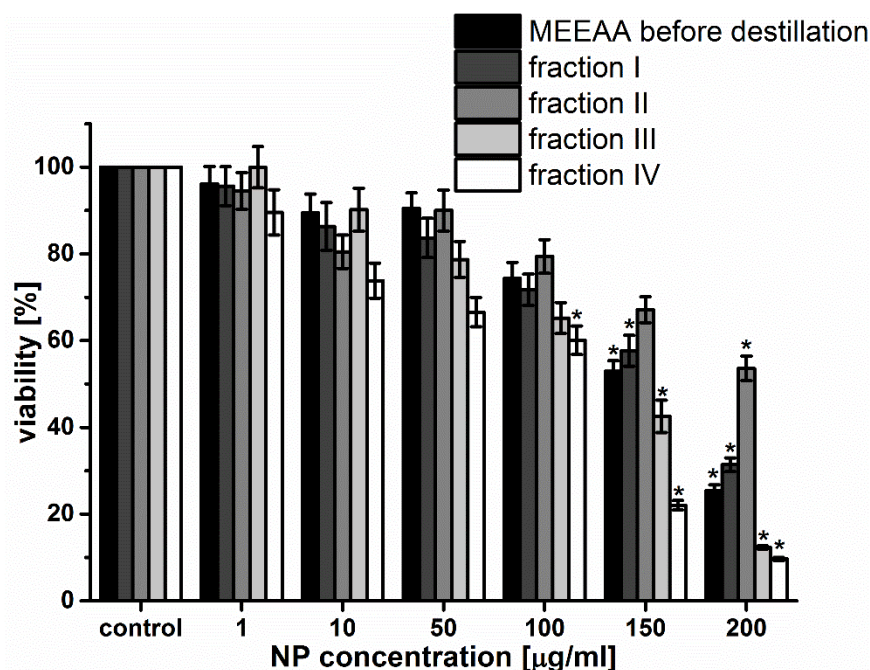
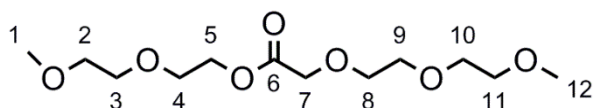


Figure IV - 13. Viability of tumour cells (FaDu) treated with UVA light (24 h) pre-activated P25 TiO₂ dispersions prepared with commercial MEEAA sample before distillation and fractions I to IV obtained during its distillation. Significance compared to the control with a *P*-value < 0.05 is indicated by asterisks.



Scheme IV - 2. Identified compound IV-a of fraction IV-a.

This compound IV-a did not show any anti-tumour activity after UVA light activation in presence of P25 TiO₂ NPs (Figure IV - 14) and also NMR analysis did not show any changes in molecular structure (such as signal shifts or changes in integral value). Thus, this compound seems to be not affected by the UVA light treatment and can be taken as internal standard for subsequent NMR analyses of the fraction IV.

In contrast to the fraction IV-a, the fraction IV-b is highly anti-tumour active after the pre-activation. The NMR measurements of this fraction showed pure spectra of MEEAA and also MS analysis indicated the presence of pure MEEAA. These results were rather surprising as it was shown before that the pure MEEAA does not possess any anti-tumour activity. This is why the presence of further undetectable impurities was expected. Organic impurities in the sample must be existent in concentrations lower than the detection limit of NMR while inorganic impurities such as salts can be present in higher concentrations as they are usually not

visualized by NMR or MS. This is why X-ray fluorescence spectroscopy (XRF) was carried out (Table – EP – 5, Experimental part) in order to detect all elements heavier than sodium. Ultimately, these measurements showed the presence of chloride as impurity.

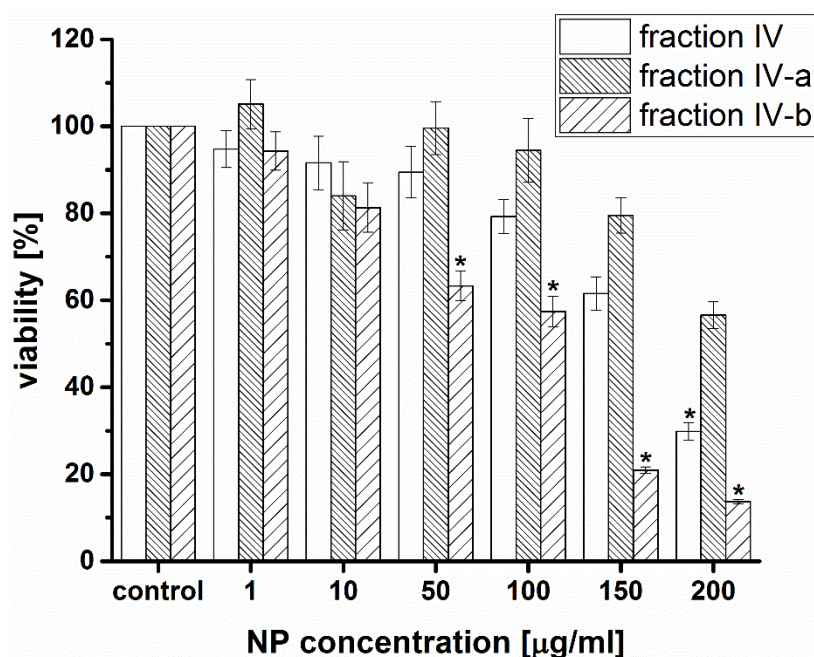


Figure IV - 14. Viability of tumour cells (FaDu) treated with UVA light (24 h) pre-activated P25 TiO₂ dispersions prepared with fractions IV obtained during distillation of the commercial MEEAA sample and with fraction IV-a and by IV-b obtained after column chromatography of fraction IV. Significance compared to the control with a *P*-value < 0.05 is indicated by asterisks.

The probability that the chloride substitutes a proton of the MEEAA (under formation of a covalent bond) is seen as quite low as this would result in shifts in the NMR spectra. The formation of a complex out of chloride and MEEAA also seems very unlikely given the acidic nature of both components (Cl⁻ and COO⁻). Thus, the detected chloride is possibly available as salt with elements that cannot be detected by XRF such as for example Li, Be or Na. The presence of this undetermined chloride compound could strongly influence the PC degradation of the MEEAA and result in an enhanced decomposition or in a modified degradation pathway resulting in molecular fragments different from those of pure MEEAA samples. It has already been shown in the current literature that the PC degradation of an organic molecule by TiO₂ can be significantly enhanced by the presence of other organic compounds or metal ions.^{48,49}

In order to further examine the processes caused by the UVA light activation, NMR analysis and high pressure liquid chromatography (HPLC) coupled to MS were carried out for the fraction IV before and after UVA light treatment. The ¹H-NMR spectra (Figure IV - 15) of fraction IV logically show signals caused by both MEEAA (fraction IV-b) and compound VI-a (fraction IV-a), which have been identified before thanks to their separation via column chromatography. No new signals were detected in the ¹³C- and ¹H-NMR spectra after UVA light treatment.

However, taking into account the integrals of the characteristic ¹H-NMR signals of compound IV-a as internal standards (marked in green) and comparing them to the signal, which is only caused by MEEAA (marked in red), it becomes evident that the integral of this signal is decreased (from 1.4 to 0.8) during UVA light treatment. Consequently, one can conclude that either only the CH₂ of the acetic acid moiety of MEEAA is removed during the pre-activation or the entire MEEAA is fragmented into small, highly volatile and therefore not measurable organic compounds such as CO₂. Furthermore, the degradation into smaller fragments in concentrations lower than the detection limit of NMR is conceivable. However, the possible decrease in the other MEEAA signals (C15-C19) cannot easily be determined by NMR as the signals lie in the same range as the ones caused by compound IV-a.

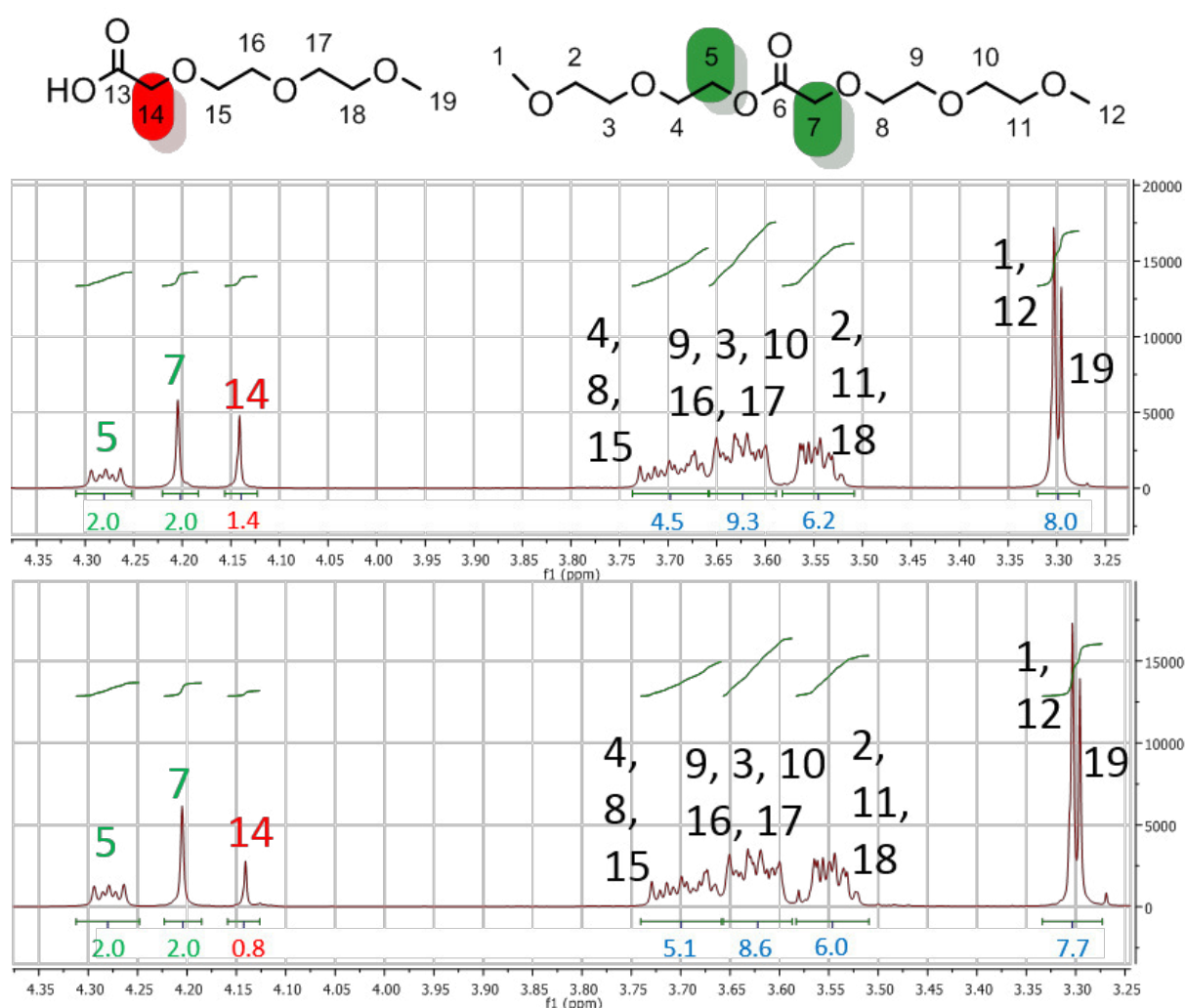
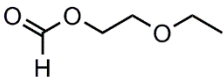
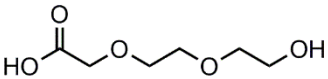


Figure IV - 15. ¹H-NMR spectra of fraction IV in D₂O before (on the top) and after 24 h UVA pre-activation (on the bottom). The carbon atoms of both the molecules are numbered and the numbers are related to the specific signals in the spectra.

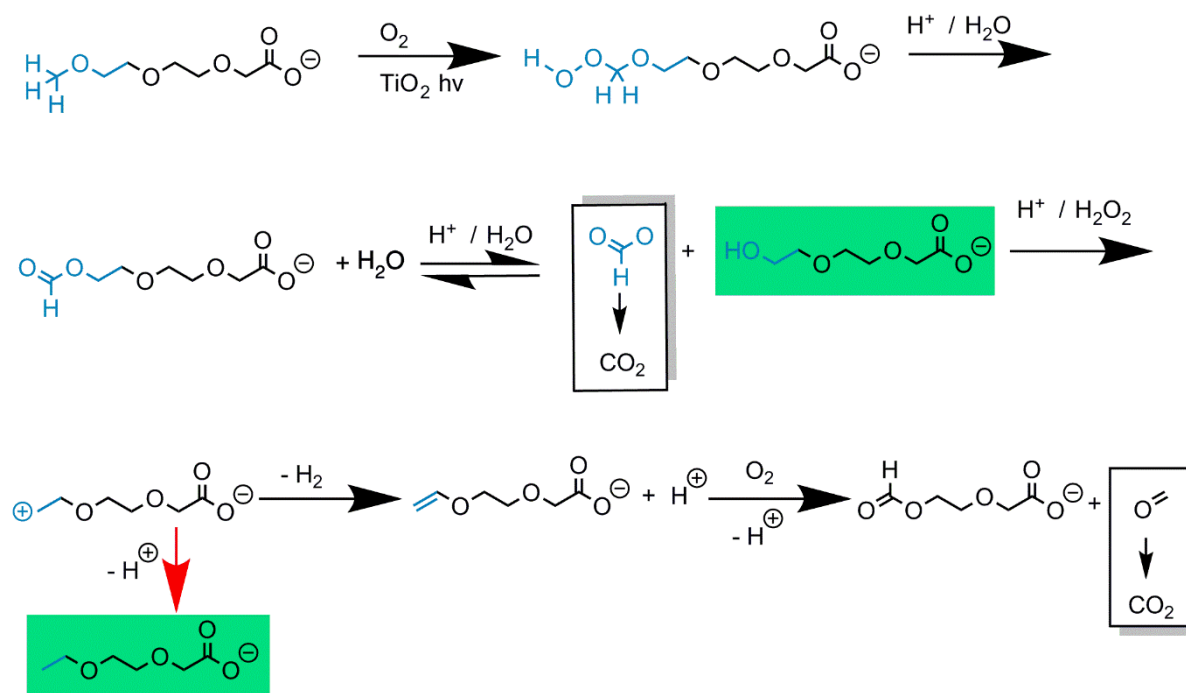
HPLC analysis indicated that the amount of MEEAA was lowered by 10 % during UVA light treatment and the appearance of two new mass fragments was detected. The measured m/z and probable structures with their calculated molecular masses are depicted in Table IV - 1.

The proposed structures were selected based on the reactant MEEAA and possible degradation pathways of the methyl ethers and carboxylic acids found in literature.^{48–53} However, it must be admitted that PC decomposition reactions are very complex and therefore, other possible structures may not have been identified. Also the proton abstractions of ethoxy groups could take place and lead to other degradation pathways not considered in this work. The degradation could occur similarly to the degradation of butanoic acid via the H abstraction from a methylene group.⁵⁴

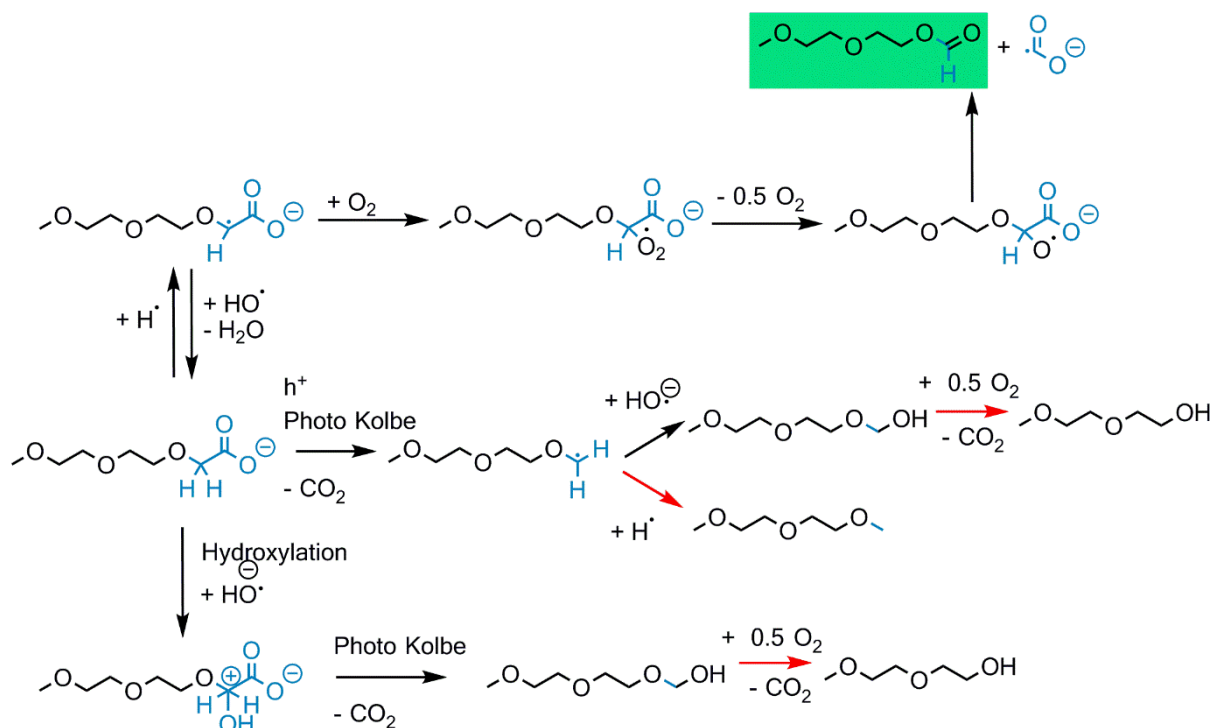
Table IV - 1. New fragments (m/z) after UVA light treatment detected by HPLC-MS and belonging possible molecular structures and their calculated m/z.

measured m/z, negative mode	probable structure, name	calculated m/z of [M-H] ⁻
117.07	 compound MS117	117.06
163.15	 compound MS163	163.06

The detected **compound MS163** is most probably obtained during the PC degradation of the methyl ether group (Scheme IV - 3, highlighted in green colour). The proposed possible degradation pathway of the methyl ether group of MEEAA was deduced from the PC decomposition of methyl-tert-butyl ether or methyl perfluoroalkyl ethers.^{52,53} The detected **compound MS117** must most probably be produced by both the removal of the methoxy group (Scheme IV - 3, highlighted in green colour) and the degradation of the carboxylic acid via the proton abstraction from the α -carbon by hydroxyl radicals and further reaction with the surrounding oxygen resulting in a formate ester. Possible degradation pathways of the carboxylic acid are depicted in Scheme IV - 4 deduced from the PC decompositions of carboxylic acids such as propanoic and octanoic acids.^{48–51} In both schemes the red arrows indicate reaction steps that are considered very probable but could not be confirmed by the literature.



Scheme IV - 3. Proposed possible degradation pathway of the methyl ether group of MEEAA deduced from the photocatalytic decomposition of methyl-tert-butyl ether or methyl perfluoroalkyl ethers.^{52,53} (red arrows: assumed reaction steps not confirmed by literature, green labelled compounds: possible degradation products detected by MS)



Scheme IV - 4. Proposed possible degradation pathway of the carboxyl group of MEEAA deduced from the photocatalytic decomposition of R-COOH (R= alkylchain).⁴⁸⁻⁵¹ (red arrows: assumed reaction steps not confirmed by literature, green labelled compound: possible degradation products detected by MS)

The potential cytotoxicity of the identified compounds has not been evaluated yet. While pure MEEAA (shown in this study) and (2-methoxyethoxy)acetic acid⁵⁵ are considered as non-toxic, the toxicity by alkoxyacetic acids has been proved to increase with decreasing chain length (e.g. in the case of testicular toxicity in rats).⁵⁶ Shorter alkoxyacetic acids such as methoxyacetic acid, ethoxyacetic acid or butoxyacetic acid have for example been confirmed to be embryotoxic.⁵⁷ They lead to an intracellular acidification of cells inhibiting their cell differentiation.⁵⁷ Studying the hematotoxicity of alkoxyacetic and -propionic acids, it was shown that the presence and location of the ether bond plays a determining role in the toxicity of the compound.⁵⁸ A cytotoxic behaviour of formates such as commercially available ethyl formate has not been reported.⁵⁹ Taking into account all the before mentioned insights, the cytotoxicity (e.g. towards malignant cells) of the two identified compounds seems probable and should therefore be studied in future.

IV.4. Conclusion

For the transfer of the samples into cell culture media, the synthesized unmodified AA- and MEEAA-TiO₂ NPs were stabilised to avoid agglomeration and sedimentation. Stabilising the NPs with BSA, FBS, Melpers® V4343 or Sika® ViscoCrete®-10110178 improved the NP dispersion in various cell culture media. Melflux® 4930 F appeared to be the most suitable stabilising agent in this study, stabilising the particles against agglomeration and subsequent sedimentation over 24 h in all three tested cell culture media. The stabilisation assures an accurate dosing of particles for cell culture tests and reliable concentration-dependent particle uptake studies as the particles do not sediment. In contrast to FBS, which is commonly used as a stabiliser in the literature, Melflux does not influence the cytotoxicity of the particles. Therefore, it is suitable as a stabilising agent of TiO₂ NPs and may be of special interest for studies on the toxicity or therapeutic potential of these NPs.

In addition and essential for this research work, the tested synthesized NP systems AA-TiO₂ and MEEAA-TiO₂ were both proved to be non-toxic towards both malignant and non-malignant cells in their inactive state, at least within the applied concentrations - both as well-stabilised single particles or not-stabilised agglomerates. This paves the way towards their application as tumour treatment agent as their non-toxicity may enable UVA light activated specific tumour treatment. Furthermore, these tests provide the basis for subsequent cytotoxicity tests of functionalized TiO₂ particles, enabling studies on the influence of modified surface properties on their toxicity.

The detected anti-tumour activity of 24 h UVA light pre-activated MEEAA-TiO₂ samples is most probably caused by the PC degradation of MEEAA into cytotoxic compounds enhanced by the presence of chloride impurities in the commercially obtained acid. This work on the one hand provided impressive results concerning a specific tumour treatment, on the other hand it stressed that the transfer of commercial and chemical compounds into biomedical applications can provoke unexpected obstacles concerning the toxicity of unidentified impurities. However, for the organically modified NPs synthesized in this work (Chapter III), this toxicity is of no relevance as the particles are purified during the functionalization procedure.

Future works should include the cytotoxicity assessment of the functionalized MEEAA-TiO₂ samples as well as the development of the state of the art PC tumour treatment via the UVA light application onto cells exposed to PC NPs (as shown in Figure IV - 9).

References:

- 1 A. L. Niles, R. A. Moravec and T. L. Riss, *Expert Opin. Drug Discov.*, 2008, **3**, 655–669.
- 2 S. Hackenberg, A. Scherzed, W. Harnisch, K. Froelich, C. Ginzkey, C. Koehler, R. Hagen and N. Kleinsasser, *J. Photochem. Photobiol. B*, 2012, **114**, 87–93.
- 3 M. Scanu, L. Mancuso and G. Cao, *Toxicol. In Vitro*, 2011, **25**, 1989–1995.
- 4 R. C. Stearns, J. D. Paulauskis and J. J. Godleski, *Am. J. Respir. Cell Mol. Biol.*, 2001, **24**, 108–115.
- 5 T. Mosmann, *J. Immunol. Methods*, 1983, **65**, 55–63.
- 6 P. R. Twentyman and M. Luscombe, *Br. J. Cancer*, 1987, **56**, 279–285.
- 7 A. Kroll, M. H. Pillukat, D. Hahn and J. Schnekenburger, *Eur. J. Pharm. Biopharm.*, 2009, **72**, 370–377.
- 8 M. C. Alley, D. A. Scudiero, A. Monks, M. L. Hursey, M. J. Czerwinski, D. L. Fine, B. J. Abbott, J. G. Mayo, R. H. Shoemaker and M. R. Boyd, *Cancer Res.*, 1988, **48**, 589–601.
- 9 J. M. Edmondson, L. S. Armstrong and A. O. Martinez, *J. Tissue Cult. Methods*, 1988, **11**, 15–17.
- 10 G. Ciapetti, E. Cenni, L. Pratelli and A. Pizzoferrato, *Biomaterials*, 1993, **14**, 359–364.
- 11 G. Fotakis and J. A. Timbrell, *Toxicol. Lett.*, 2006, **160**, 171–177.
- 12 D. A. Scudiero, R. H. Shoemaker, K. D. Paull, A. Monks, S. Tierney, T. H. Nofziger, M. J. Currens, D. Seniff and M. R. Boyd, *Cancer Res.*, 1988, **48**, 4827–4833.
- 13 Z. E. Allouni, M. R. Cimpan, P. J. HøI, T. Skodvin and N. R. Gjerdet, *Colloids Surf. B Biointerfaces*, 2009, **68**, 83–87.
- 14 Z. Ji, X. Jin, S. George, T. Xia, H. Meng, X. Wang, E. Suarez, H. Zhang, E. M. V. Hoek, H. Godwin, A. E. Nel and J. I. Zink, *Environ. Sci. Technol.*, 2010, **44**, 7309–7314.
- 15 P. Bihari, M. Vippola, S. Schultes, M. Praetner, A. G. Khandoga, C. A. Reichel, C. Coester, T. Tuomi, M. Rehberg and F. Krombach, *Part. Fibre Toxicol.*, 2008, **5**, 14.
- 16 N. Mandzy, E. Grulke and T. Druffel, *Powder Technol.*, 2005, **160**, 121–126.
- 17 A.-H. Lu, E. L. Salabas and F. Schüth, *Angew. Chem. Int. Ed.*, 2007, **46**, 1222–1244.
- 18 K. Mandel, F. Hutter, C. Gellermann and G. Sextl, *Colloids Surf. Physicochem. Eng. Asp.*, 2011, **390**, 173–178.
- 19 M. Robins and A. Fillery-Travis, *J. Chem. Technol. Biotechnol.*, 1992, **54**, 201–202.
- 20 C. Guiot and O. Spalla, *Environ. Sci. Technol.*, 2013, **47**, 1057–1064.
- 21 E. C. Cho, Q. Zhang and Y. Xia, *Nat. Nanotechnol.*, 2011, **6**, 385–391.
- 22 N. Lakshminarasimhan, W. Kim and W. Choi, *J. Phys. Chem. C*, 2008, **112**, 20451–20457.
- 23 A. Salvati, A. S. Pitek, M. P. Monopoli, K. Prapainop, F. B. Bombelli, D. R. Hristov, P. M. Kelly, C. Åberg, E. Mahon and K. A. Dawson, *Nat. Nanotechnol.*, 2013, **8**, 137–143.
- 24 L. Wang, J. Li, J. Pan, X. Jiang, Y. Ji, Y. Li, Y. Qu, Y. Zhao, X. Wu and C. Chen, *J. Am. Chem. Soc.*, 2013, **135**, 17359–17368.
- 25 S. Kawashima, J.-W. T. Seo, D. Corr, M. C. Hersam and S. P. Shah, *Mater. Struct.*, 2014, **47**, 1011–1023.
- 26 S. V. Samchenko, O. V. Zemskova and I. V. Kozlova, *Russ. J. Appl. Chem.*, 2014, **87**, 1872–1876.
- 27 L. Vaisman, H. D. Wagner and G. Marom, *Adv. Colloid Interface Sci.*, 2006, **128–130**, 37–46.
- 28 K. Rezwan, A. R. Studart, J. Vörös and L. J. Gauckler, *J. Phys. Chem. B*, 2005, **109**, 14469–14474.
- 29 S. Salgin, U. Salgin and S. Bahadır, *Int J Electrochem Sci*, 2012, **7**, 12404–12414.
- 30 T. Cedervall, I. Lynch, S. Lindman, T. Berggård, E. Thulin, H. Nilsson, K. A. Dawson and S. Linse, *Proc. Natl. Acad. Sci.*, 2007, **104**, 2050–2055.
- 31 J. Vidic, F. Haque, J. M. Guigner, A. Vidy, C. Chevalier and S. Stankic, *Langmuir*, 2014, **30**, 11366–11374.
- 32 A. L. Barrán-Berdón, D. Pozzi, G. Caracciolo, A. L. Capriotti, G. Caruso, C. Cavaliere, A. Riccioli, S. Palchetti and A. Laganà, *Langmuir*, 2013, **29**, 6485–6494.
- 33 O. Akhlaghi, O. Akbulut and Y. Z. Menceloglu, *Colloid Polym. Sci.*, 2015, **293**, 2867–2876.

- 34 D. H. Napper and A. Netschey, *J. Colloid Interface Sci.*, 1971, **37**, 528–535.
- 35 M. Horie, K. Nishio, K. Fujita, H. Kato, S. Endoh, M. Suzuki, A. Nakamura, A. Miyauchi, S. Kinugasa, K. Yamamoto, H. Iwahashi, H. Murayama, E. Niki and Y. Yoshida, *Toxicol. In Vitro*, 2010, **24**, 1629–1638.
- 36 C.-K. Yu, K.-H. Hu, S.-H. Wang, T. Hsu, H.-T. Tsai, C.-C. Chen, S.-M. Liu, T.-Y. Lin and C.-H. Chen, *Appl. Phys. A*, 2011, **102**, 271–274.
- 37 D. Brunner, *ALTEX*, 2010, 53–62.
- 38 I. Řehoř, V. Vilímová, P. Jendelová, V. Kubíček, D. Jiráček, V. Herynek, M. Kapcalová, J. Kotek, J. Černý, P. Hermann and I. Lukeš, *J. Med. Chem.*, 2011, **54**, 5185–5194.
- 39 K. T. Thurn, E. M. B. Brown, A. Wu, S. Vogt, B. Lai, J. Maser, T. Paunesku and G. E. Woloschak, *Nanoscale Res. Lett.*, 2007, **2**, 430–441.
- 40 J. Seo, H. Chung, M. Kim, J. Lee, I. Choi and J. Cheon, *Small*, 2007, **3**, 850–853.
- 41 S. Yamaguchi, H. Kobayashi, T. Narita, K. Kanehira, S. Sonezaki and Y. Kubota, *Photochem. Photobiol.*, 2010, **86**, 964–971.
- 42 X. Feng, S. Zhang and X. Lou, *Colloids Surf. B Biointerfaces*, 2013, **107**, 220–226.
- 43 J. Xu, Y. Sun, J. Huang, C. Chen, G. Liu, Y. Jiang, Y. Zhao and Z. Jiang, *Bioelectrochemistry*, 2007, **71**, 217–222.
- 44 H.-U. Simon, A. Haj-Yehia and F. Levi-Schaffer, *Apoptosis*, 2000, **5**, 415–418.
- 45 S. Koyama, S. Kodama, K. Suzuki, T. Matsumoto, T. Miyazaki and M. Watanabe, *Mutat. Res. Mol. Mech. Mutagen.*, 1998, **421**, 45–54.
- 46 I. K. Konstantinou and T. A. Albanis, *Appl. Catal. B Environ.*, 2004, **49**, 1–14.
- 47 A. Vidal, Z. Dinya, F. Mogyorodi Jr. and F. Mogyorodi, *Appl. Catal. B Environ.*, 1999, **21**, 259–267.
- 48 J. Araña, V. M. R. López, J. M. D. Rodríguez, J. A. H. Melián and J. P. Peña, *Catal. Today*, 2007, **129**, 185–193.
- 49 T. Sakata, T. Kawai and K. Hashimoto, *J. Phys. Chem.*, 1984, **88**, 2344–2350.
- 50 V. Gandhi, M. Mishra and P. A. Joshi, *Mater. Sci. Forum*, 2012, **712**, 175–189.
- 51 J. Schwitzgebel, J. G. Ekerdt, H. Gerischer and A. Heller, *J. Phys. Chem.*, 1995, **99**, 5633–5638.
- 52 R. D. Barreto, K. A. Gray and K. Anders, *Water Res.*, 1995, **29**, 1243–1248.
- 53 M. Toma, K. Takeuchi and T. Ibusuki, *Environ. Sci. Technol.*, 1999, **33**, 1071–1076.
- 54 C. Guillard, *J. Photochem. Photobiol. Chem.*, 2000, **135**, 65–75.
- 55 K. L. Cheever, D. E. Richards, W. W. Weigel, J. B. Lal, A. M. Dinsmore and F. B. Daniel, *Toxicol. Appl. Pharmacol.*, 1988, **94**, 150–159.
- 56 P. M. D. Foster, S. C. Lloyd and D. M. Blackburn, *Toxicology*, 1987, **43**, 17–30.
- 57 J. Louisse, Y. Bai, M. Verwei, J. J. M. van de Sandt, B. J. Blaauboer and I. M. C. M. Rietjens, *Toxicol. Appl. Pharmacol.*, 2010, **245**, 236–243.
- 58 B. I. Ghanayem, L. T. Burka and H. B. Matthews, *Chem. Biol. Interact.*, 1989, **70**, 339–352.
- 59 V. S. Haritos and G. Dojchinov, *Comp. Biochem. Physiol. Part C Toxicol. Pharmacol.*, 2003, **136**, 135–143.

General conclusion

Head and neck cancer is one of the ten most common cancers globally and typically shows difficult-to-treat field cancerization, which means that the tumour is not situated in a well-defined location but widely spread over the tissue. Usually these formations are a mixture of pre-malignant and malignant superficial manifestations with some regions having deeply invasive tumour fractions. This unclear extent of the tumour makes a surgical removal very difficult and also radiation or chemotherapy are often meeting their limits raising the desire for novel therapy strategies.

Photocatalytic nanoparticles (PC NPs), such as titanium dioxide, with their unique physical and chemical properties due to their dimensions below 100 nm have a great potential as photodynamic tumour treatment agent and could therefore enhance the current standard treatments. Additionally, these NPs combine their function as a therapeutic agent with surfaces that can be functionalized to mediate cellular uptake or carry molecules for diagnostic. Thus, the key points this research has sought to address were the synthesis of anatase NPs, their functionalization with dendritic and non-dendritic surface agents and the transfer of the developed NPs into cell culture studies.

The first part of this work was therefore dedicated to the synthesis and thorough characterization (XRD, TEM, zeta potential, DLS, TGA, nitrogen sorption, DRIFT and PC degradation) of two anatase NP systems AA-TiO₂ and MEEAA-TiO₂ mainly differing in their surface groups (acetate – AA plus para-toluene sulfonic acid and 2-[2-(2-methoxyethoxy)ethoxy]acetic acid - MEEAA) from the hydrothermal synthesis. The higher PC activity of the MEEAA-TiO₂ compared to the AA-TiO₂ was therefore mainly related to the different surface groups or more precisely the higher amount of organic groups on the AA-TiO₂. With increasing autoclaving time or temperature during the synthesis, the crystallite size of the synthesized systems was increased (from ~5 to ~8 nm) while the properties of the surface groups were not significantly influenced. Surprisingly, the photocatalytic performance of the samples augmented with increasing particle size, which is reverse to basic knowledge and was found to be caused by a change in crystal morphology at longer hydrothermal treatment times or higher temperatures. While small crystallites show the typical equilibrium state truncated tetragonal bipyramidal morphology, crystal growth leads to the formation of rod-like crystals with oxygen vacancies provoked by oriented attachment of single particles (XAFS, XRD and HR-TEM analyses). Both the more anisotropic crystal shape and the increase in oxygen vacancies improve the charge carrier separation and thus the photocatalytic activity of the samples.

For the next approach, the synthesized anatase NPs were prepared for cell culture examinations, which included their stabilisation in cell culture media. The polycarboxylate ether

Melflux® 4930 F, which has never been used for cell culture studies before, was shown to be the most suitable stabilising agent, stabilising the particles against agglomeration and subsequent sedimentation over 24 h in cell culture media. The non-toxicity of this stabiliser was demonstrated as well as its superiority (in stabiliser concentration and influence on the cytotoxicity) over foetal bovine serum, which is commonly used as a stabiliser in the literature. In addition both stabilised and not-stabilised NP systems AA-TiO₂ and MEEAA-TiO₂ were proved to be non-toxic towards both malignant and non-malignant cells in their inactive state, which paves the way towards their therapeutic application enabling ultraviolet (UV) light triggered specific tumour treatment.

With the help of commercial silanes ([3-(2-aminoethylamino)propyl]-trimethoxysilane, N¹-(3-trimethoxysilyl-propyl)diethylenetriamine) the feasibility of grafting onto the developed TiO₂ NPs was proved. The grafting procedure and the concentration of coupling agents for an efficient grafting of the NPs was optimized guaranteeing a strongly modified particle surface while maintaining the photocatalytic activity of the samples. These results were the basis for the functionalization of NPs with self-synthesized well-tailored and well-characterized surface agents. The synthesis routes for four either luminescent or non-luminescent dendritic or linear structures for the particle functionalization via silanization were planned, carried out and critically examined. Three of the synthesized coupling agents contained a rhodamine dye; while the first coupling agent was as linear molecule without terminal amine group, the second linear coupling agent combined the dye with a terminal functional group. The luminescent 1st generation dendritic molecule united the two terminal amine groups thanks to the dendritic branches with an off-centred dye. The last coupling agent also bore a dendritic structure with two terminal amine groups but no dye. Two of the mentioned coupling agents were grafted onto MEEAA-TiO₂ and the successful surface modification was shown via IR, DLS and zeta potential measurements. First studies on the PC activity of one of the modified samples were also carried out and indicated the surprising increase in its performance probably caused by the properties of the rhodamine dye-containing coupling agent that also resulted in a strong luminescence of the NPs.

This is why, one can state that the synthesis of luminescent NPs by grafting a dye-containing coupling agent was successfully carried out. Another approach to introduce luminescence properties into the TiO₂ particle systems via the synthesis of luminescent Rhodamine B doped TiO₂/SiO₂ core/shell NPs was shown to be feasible. However, this modification always resulted in a drastically reduced PC activity due to the silica shell that covers the photocatalytically active surface. Thus, the development of NPs consisting of a luminescent core and a photocatalytically active shell would be advantageous as it would ideally not influence the

photocatalytic performance of the sample while possessing luminescence properties. As a side effect, the synthesis of the coupling agents would be facilitated as there would be no more need for the integration of a dye into the molecule structure. While the feasibility to form a TiO₂ shell around inorganic NPs such as iron oxide NPs has been already shown in this work, future studies should search for a luminescent inorganic particle, which is sufficiently stable under the hydrothermal synthesis conditions of TiO₂.

Concerning the synthesis of luminescent, dendritic coupling agents, first synthesis routes have successfully been established. However, further research might well be conducted on these coupling agents in order to optimize the design and reaction pathway for example of the dye- and terminal amine-containing linear organosilane. Furthermore, the use of phthalimide as protecting group of the terminal amines and its cleavage after grafting should be rethought; either a more efficient cleavage procedure not affecting the Ti-O-Si bonds should be found or the phthalimide could be substituted by another protecting group, which can be cleaved under milder conditions.

Subsequently, future works should focus on the cytotoxicity assessment of the functionalized TiO₂ samples as well as the development of the state of the art PC tumour treatment via the UV light application onto cells exposed to PC NPs. Regarding the detected anti-tumour activity of 24 h UV light pre-activated MEEAA-TiO₂ samples, this work pointed out that the transfer of commercial and chemical compounds into biomedical applications can provoke unexpected obstacles concerning the toxicity of unidentified impurities. Nevertheless, the discovered specific anti-tumour activity is quite impressive and surely it would be interesting to evaluate it in more detail for the use of this compound as possible future tumour drug.

One unique characteristic of this research work has been the development of functionalized NP systems for biomedical applications, starting from the particle synthesis, proceeding the synthesis of organic coupling agents, as well as the grafting onto the particles and ending with the preparation of the samples for cell culture examinations and additional cytotoxicity studies. While most researches only focus on one step of the described pathway, the challenging option to carry out all steps in the same project allows the better understanding of the influences of each step on the others and the possibility to track back problems to their routes that occur in the later steps of the research.

The novel insights gained in the augmentation of PC performance of the synthesized anatase NPs due to a morphology change during crystal growth could benefit the perfection of the hydrothermal sol-gel synthesis of highly photocatalytically active TiO₂ NPs.

The stabilisation of these NPs in cell culture media with Melflux® 4930 F can surely be transferred to particles consisting of other materials and may therefore be of special interest for studies on the toxicity or therapeutic potential of NPs in general.

The proof of the feasibility to graft organo-silanes onto the synthesized TiO_2 particles paves the way for their utilization in a broad range of applications as well-determined, manipulable surface properties are the basis for this. They could possibly be used as additives for example in plastics or functional coatings, as drug carriers or in solar cells.

The development of novel luminescent dendritic coupling agents is not only of great importance for the functionalization of photocatalytic NPs used for tumour treatment, but also for the modification of for example drug-carrier particles consisting of other materials as they allow the combination of diagnostic with therapeutic applications and a monitoring of the applied substances. Also fundamental research concerning the particle uptake by cells could be facilitated by the functionalization of NPs with these luminescent coupling agents as they may allow their facile luminescence detection.

The photocatalytic TiO_2 NP systems in their functionalized or unmodified state, which were developed in this work, are of great interest for photodynamic tumour therapy. This therapy approach would consist of the particle application onto the tissue of interest and the cellular uptake of the NPs by cells. Subsequently, the UV light is supposed to be applied on the treated area to activate the NPs in order to photocatalytically destroy cellular components leading to cell apoptosis and tumour destruction. Due to the proved non-toxicity in their inactive state, areas that are not treated with UV light may not be damaged and TiO_2 photocatalysis is expected to specifically destroy tumour cells.

As well as photodynamic tumour treatment, the developed NP systems could also benefit photocatalytic water purification or the development of photonic and optoelectronic devices. In the case of water purification, the stably dispersed NP samples showing an excellent photocatalytic activity could be used to decompose organic contaminants in waste water such as pesticides or drugs. For the development of photonic and optoelectronic devices, the semiconductor properties of the anatase NPs providing a wide band-gap are ideal for the light energy conversion. The possibility to functionalize the surface gives the opportunity to couple sensitizers such as dyes on it in order to construct for example dye-sensitized solar cells.

Experimental part

Contents

Experimental part	- 175 -
1. Materials, equipment and experimental set-ups	- 175 -
1.1. Solvents, reagents and materials for cell culture experiments	- 175 -
1.2. Equipment and experimental set-ups	- 175 -
2. Inorganic nanoparticle synthesis protocols.....	- 179 -
2.1. Synthesis of TiO ₂ nanoparticles.....	- 179 -
2.2. Synthesis of luminescent TiO ₂ based core/shell nanoparticles	- 180 -
3. Organic coupling agent synthesis protocols	- 182 -
4. Grafting protocols.....	- 206 -
4.1. Optimization of grafting protocols with commercial silanes	- 206 -
4.2. Grafting of synthesized coupling agents onto MEEAA-TiO ₂ (200 °C, 4 h)	- 206 -
5. Cell culture tests	- 208 -

Experimental part*

1. Materials, equipment and experimental set-ups

1.1. Solvents, reagents and materials for cell culture experiments

Solvents and reagents for inorganic and organic syntheses

Solvents and starting materials were purchased from Acros, Alfa Aesar, Aldrich, Fisher Scientific, Lehmann & Voss & Co or Bachem. All chemical compounds were reagent-grade (but 2-[2-(2-methoxyethoxy)ethoxy]acetic acid which was technical grade) and used without further purification (but triethylamine and isocyanatopropyltriethoxysilane which were purified by distillation over CaH_2 or under dynamic vacuum). Water was deionised before use. All solvents for organic synthesis were anhydrous. DMF and dioxane were purchased, others were dried over dehydrating agents and distilled under inert atmosphere:

- CH_2Cl_2 : CaH_2 ;
- MeOH: CaH_2 ;
- EtOH: CaH_2 ;
- THF: Benzophenone, Na;
- pentane: Benzophenone, Na;

Solvents, media and cells for cell culture experiments

Stabilising agents for particles in cell culture media were purchased from Sigma–Aldrich, BASF and Sika. The cell culture media utilised for this research were bronchial epithelial cell growth medium (BEGM with 1 vol-% penicillin and streptomycin (10000 $\mu\text{g}/\text{ml}$, PenStrep) and supplement mix C-39165), Roswell Park Memorial Institute medium (RPMI with 1 vol-% FBS, 1 vol-% PenStrep, 1 vol-% non-essential amino acids and 1 vol-% sodium pyruvate) and Dulbecco's modified eagle medium (DMEM with 10 vol-% FBS and 1 vol% PenStrep). These substances were ordered from PromoCell GmbH, Sigma-Aldrich, Linaris, gibco^R life technologiesTM and Biochrom AG. 3-(4,5-dimethylthiazol-2-yl)-2,5-diphenyl tetrazolium bromide (MTT) was also ordered from Sigma-Aldrich.

The head and neck squamous cell carcinoma cell line FaDu was established from the lymph node metastasis of a hypopharyngeal squamous cell carcinoma. Primary human bone marrow-derived mesenchymal stem cells (BMSC) from human bone marrow were obtained from voluntary patients undergoing surgery in the Department of Orthopedics of the University Clinic Wuerzburg. The study was approved by the Ethics Committee of the Medical Faculty, University of Wuerzburg (12/06) and informed consent was obtained from all of the individuals included. Primary fibroblasts were obtained from voluntary patients undergoing surgery in the Department of Oto-Rhino-Laryngology, Plastic, Aesthetic and Reconstructive Head and Neck Surgery of the University Clinic Wuerzburg. The study was approved by the Ethics Committee of the Medical Faculty, University of Wuerzburg (16/06) and informed consent was obtained from all of the individuals included. The laryngeal squamous cell carcinoma cell line HLaC78 was generated at the Department of Oto-Rhino-Laryngology, Plastic, Aesthetic and Reconstructive Head and Neck Surgery of the University Clinic Wuerzburg.¹

1.2. Equipment and experimental set-ups

BET – Nitrogen sorption: Nitrogen sorption experiments were carried out on an automated volumetric analyser (Model Autosorb 3B). Prior to the measurement, the nanoparticle (NP) samples were dried at 110 °C for 16 h at reduced pressure. The specific surface area of the

* Parts of this chapter have been published and are reused in this work by courtesy of: The Royal Society of Chemistry, original article: S. Koch et al., J. Mater. Chem. C, 2015, 3, 12430-2435, Elsevier, original article: S. Koch et al., Colloids Surf., B, 2016, 143, 7–14.

powder samples was determined according to Brunauer, Emmet and Teller by using the adsorption data in the relative pressure range from 0.05 to 0.3 p/p_0 .

Elemental analysis (EA): The elemental compositions of the synthesized compounds were determined by elemental analysis, carried out on a THERMO FISHER FLASH 2000.

Fourier transform infrared analysis: Diffuse reflectance infrared Fourier transform (DRIFT) measurements were conducted on a Thermo Fisher Scientific Nicolet 6700 spectrometer equipped with a diffuse reflection unit. The spectra were recorded via 200 scans from 4000 to 400 cm^{-1} at a resolution of 4 cm^{-1} . All powder samples (at a concentration of 1 - 4 weight-%) were intermixed with dried KBr and finely ground. Attenuated total reflection (ATR) spectra were recorded on a Nicolet iS50 spectrometer with an integrated ATR unit using 200 scans from 4000 to 400 cm^{-1} at a resolution of 4 cm^{-1} .

High pressure liquid chromatography (HPLC): HPLC measurements were performed on a Shimadzu Nexera LC-30AD liquid chromatograph with a SIL-30AC autosampler and a column-thermostat with integrated column-switching valve. The system was coupled to a Shimadzu 8040 triple-quadrupole mass spectrometer with an electrospray ion source. Full scan mass spectra were taken from 50 to 400 m/z with a scan speed of 5000 u/sec in Q1 and 15000 u/sec in Q3 for 1.5 minutes. The mass spectrometer was used in the negative ion mode. The ESI source was operated with a capillary voltage of -3.5 kV. The temperature of the heat block and of the desolvation line in the ion source was set to 450°C and 200 °C, respectively. The nebulizing and drying gas flow was 3 and 10 l/min, respectively. An isocratic elution was performed with water and methanol in the ratio of 30 to 70, the flow rate was 0.2000 ml/min, and the column oven was set to 25°C.

Mass spectrometry (MS): Mass spectra were performed on a QStar Elite Mass Spectrometer equipped with an electrospray ionization (ESI) source (operated in a positive or negative ion mode) or on a Jeol Masse AccuToF Spectrometer with an electric ionization (EI) or field desorption (FD) source. All samples were dissolved in methanol for these measurements.

Nuclear magnetic resonance (NMR): NMR spectra were performed on the Bruker Avance 300 FT NMR spectrometer (^1H : 300 MHz, ^{13}C : 75 MHz), the Bruker DPX 400 FT NMR spectrometer (^1H : 400 MHz, ^{13}C : 101 MHz) and the Bruker DPX 600 FT NMR spectrometer (^1H : 600 MHz, ^{13}C : 151 MHz). Chemical shifts of ^1H NMR signals were calibrated according to the signals of deuterated solvents quoted to internal standard TMS ($\delta = 0.00$). All samples were dissolved in an appropriate deuterated solvent prior to the measurements. Following abbreviations are used for the analysis of NMR spectra: s = singlet, d = doublet, dd = doublet-doublet, t = triplet, q = quartet, p = pentet, m = multiplet, br = broad, J = J coupling constant.

Photocatalytic activity tests: The photocatalytic activity of the synthesized samples is measured by a dichloroacetic acid degradation with the set-up shown in Figure - EP - 1. The test is carried out in a double-jacket reactor that is cooled by water to 20 °C. In the center of the reactor a halogen lamp (Philips CLEO Compact 15W) with wavelengths of 300-400 nm is placed in a silica tube. Furthermore, a glass tube for bubbling compressed air into the testing solution, a temperature sensor, a chloride measuring electrode and its reference Ag/AgCl electrode were also placed into the vessel. For the photocatalytic activity test, 0.5 to 0.8 litre of solution (depending on the set-up) were filled into the reactor, consisting of water with 100 mg/l NPs and 1 g/l dichloroacetic acid. Magnetic stirring was used during the whole test to guarantee a homogeneous dispersion of the particles. Before starting the UV activated dichloroacetic acid decomposition, the aqueous solution was stirred for 20 min in darkness to ensure constant reaction conditions. Then the light was switched on and after 5 min the first chloride concentration was recorded as zero-point.

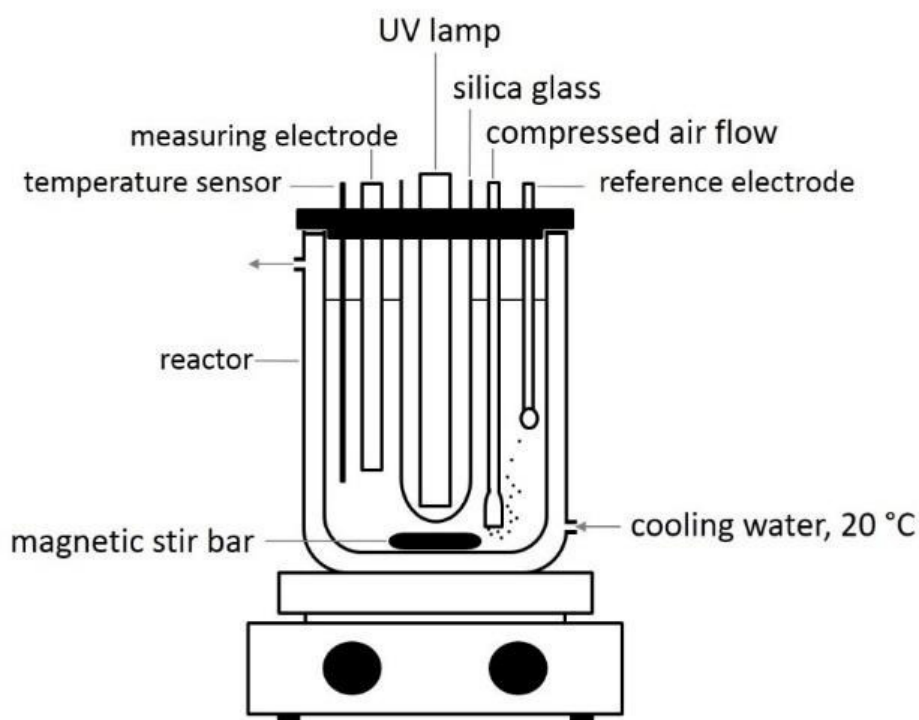


Figure - EP - 1. Photocatalytic activity test set-up.

Sedimentation studies: The sedimentation of AA-TiO₂ and MEEAA-TiO₂ NPs with or without chosen stabilising agents in cell culture media was examined by absorbance measurements; 6 ml of NPs in cell culture media (0.5 mg/ml) was transferred into a 15 ml vial and 0.2 ml of the upper 10 % of the dispersion was then taken immediately and at 24 h after NP transfer. The absorbance at 490 nm of the withdrawn aliquots was measured and as references the absorbance of the pure media with stabiliser was also measured at the two time points. The 24 h continuous sedimentation studies were carried out by monitoring the absorbance at 490 nm as a function of time. As a reference RPMI containing the appropriate amount of water and stabiliser without particles was simultaneously acquired. The percentage of non-sedimented particles was then calculated taking the first measurement as 100 % and the reference as 0 %.

Thermogravimetric (TG) measurements coupled with mass spectrometry: TG coupled with MS analyses were performed on Netzsch STA 409 Pyrolysor coupled to a Balzers Instruments Thermostar quadrupolar mass spectrometer. The mass loss of the dried samples (10–20 mg) was monitored under argon at temperatures from 30°C to 1000°C with a heating rate of 5 K/min.

Transmitted electron microscopy (TEM): TEM images were obtained on a HITACHI H7650, (100 kV, equipped with a GATAN 11 mPx camera) or on a JEOL JSM 2010 at an acceleration voltage of 200 kV. High resolution TEM micrographs were obtained on a FEI Titan operating at 300 keV. The samples were prepared onto carbon-coated copper grids and slowly dried on the grid under ambient conditions.

UV-Vis and photoluminescence analysis: UV-Vis measurements on sample solutions were carried out on a TECAN Multimode-Microplate-Reader Infinite® M1000 PRO, a Shimadzu UV-3100, a Titertek Multiskan PLUS MK II from Labsystems or a Shimadzu UV-1560 PC.

X-ray absorption fine structure (XAFS) analyses: The XAFS spectra were recorded at the K-edge of titanium (4966 eV) in transmission mode at the μ -Spot beamline, at the Bessy II light source, Berlin, Germany. The x-ray absorption near edge spectra (XANES) were measured

with a step of 0.5 eV at the absorption edge and with a 2 eV step above the edge. The extended x-ray absorption fine structure (EXAFS) range was scanned up to $k = 12 \text{ \AA}^{-1}$ with a constant step in k -space of 0.04 \AA^{-1} . The spectra underwent the standard data treatment procedure using the IFFEFIT software package.^{2,3} Cellulose pellets filled with dry powder sample with an absorption optimized thickness were produced for XAFS measurements.

X-ray diffraction (XRD): The phase composition of the prepared TiO_2 powder samples was analysed on a PANalytical Empyrean Series 2 or on a Bruker D2 PHASER employing $\text{Cu K}\alpha$ radiation.

X-ray fluorescence spectroscopy (XRF): The liquid samples were analysed on a PANalytical sequential spectrometer system AXIOS DY 1495 with an Rh-target x-ray spectrographic tube (60 kV, 4 kW).

X-ray photoelectron spectra (XPS): Electronic properties were investigated by the Darmstadt Integrated System for MATerial research (DAISY-MAT), which combines a Physical Electronics PHI 5700 multitechnique surface analysis system with several deposition chambers via an ultrahigh vacuum sample transfer. X-ray photoelectron spectra were recorded using monochromatic $\text{Al K}\alpha$ (1486.6 eV) radiation with an energy resolution of $\approx 0.4 \text{ eV}$ as determined from the broadening of the Fermi edge of a sputter-cleaned Ag sample. Binding energies of core levels and valence band maximum can be determined with an accuracy of 50 meV and 100 meV, respectively. Binding energies obtained by XPS were calibrated by the Fermi level energy of the sputter-cleaned Ag sample. Hence, all the binding energies are given respect to the calibrated Fermi level. TiO_2 powder samples were pressed onto the Indium foil as a conductive substrate to avoid a charging problem and transferred into the XPS chamber without any pre-treatments.

Zeta potential and dynamic light scattering (DLS): DLS and zeta potential analyses were carried out on the Malvern Instruments Zetasizer Nano ZS ZEN 3600 in combination with the Multi-Purpose Titrator MPT-2 or on Horiba Scientific NP analyzer SZ-100. The measurements were performed at 25°C for diluted aqueous particle dispersions. The isoelectric points were determined by zeta potential measurements during titration with the help of HCl and NaOH .

2. Inorganic nanoparticle synthesis protocols

2.1. Synthesis of TiO₂ nanoparticles

Synthesis of acetyl acetate (AA) coordinated TiO₂-NPs (AA-TiO₂)

100.12 g acetyl acetone (1 mol, 1 eq) was dropped into 342.17 g titanium (IV) ethoxide (1.5 mol, 1.5 eq) over 1.5 h under stirring. 90.08 g water (5 mol, 5 eq) was mixed with 9.51 g p-toluene sulfonic acid (0.05 mol, 0.05 eq). The water solution was added dropwise over 1 h to the titanium precursors and stirred overnight at room temperature. The solution was then concentrated by rotary evaporation resulting in an orange powder (TiO₂ content: 56.8 weight-%, determined by heating up to 800 °C). The powder was subsequently dissolved in water to obtain a 12 weight-% (dark red, clear) amorphous titanium sol. This dispersion was hydrothermally treated in an autoclave (with 250 ml teflon insert filled to 75 % volume) with one of the following settings:

- 1 h at 160 °C
- 4 h at 160 °C
- 16 h at 160 °C
- 4 h at 180 °C
- 4 h at 200 °C

The obtained orange to beige gel was dissolved in water (3 weight-% TiO₂ content) and subsequently pressure filtrated (0.8 µm membrane).

For analysis the samples were either washed with ethanol (for TEM and DRIFT) via centrifugation and redispersion (3 times at 30 000 rpm for 0.5 h), dried under vacuum if necessary (DRIFT) or washed via dialysis (10-20 kDa molecular cut-off) against water with up to 6 water changes (for photocatalytic activity test, TGA, XRD, zeta potential, DLS) and dried via freeze drying (TGA, XRD, XPS) or re-stabilised with the addition of 1 M HNO₃ (to obtain pH = 3, for DLS).

Synthesis of 2-[2-(2-methoxyethoxy)ethoxy]acetic acid (MEEAA) coordinated TiO₂-NPs (MEEAA-TiO₂)

204.19 g 2-[2-(2-methoxyethoxy)ethoxy]acetic acid (1.13 mol, 1.89 eq) was dropped into 342.17 g titanium(IV) butoxide (0.6 mol, 1 eq) over 1 h under stirring. 36.03 g water (2 mol, 3.33 eq) was added dropwise over 30 min to the titanium precursors and stirred overnight at room temperature. The solution was then concentrated by rotary evaporation resulting in an orange viscous liquid (TiO₂ content: 18.3 weight-%, determined by heating up to 800 °C). It was subsequently diluted with water to obtain a 12 weight-% orange, clear amorphous titanium sol. This dispersion was hydrothermally treated in an autoclave (with 250 ml Teflon insert filled to 75 % volume) with one of the following settings:

- 1 h at 160 °C
- 4 h at 160 °C
- 16 h at 160 °C
- 4 h at 180 °C
- 4 h at 200 °C

The obtained orange to beige gel was dissolved in water (3 weight-% TiO₂ content) and subsequently pressure filtrated (0.8 µm membrane).

For analysis the samples were either washed with ethanol (for TEM and DRIFT) via centrifugation and redispersion (3 times at 30 000 rpm for 0.5 h), dried under vacuum if necessary (DRIFT) or washed via dialysis (10-20 kDa molecular cut-off) against water with up to 6 water changes (for photocatalytic activity test, TGA, XRD, zeta potential, DLS) and dried via freeze drying (TGA, XRD, XPS, XAFS) or re-stabilised with the addition of 1 M HNO₃ (to obtain pH = 3, for DLS).

2.2. Synthesis of luminescent TiO₂ based core/shell nanoparticles

Synthesis of TiO₂/SiO₂ core/shell nanoparticles

For the coating of TiO₂ NPs with a SiO₂ shell 16.67 g TiO₂ NP dispersion (0.5 g titanium dioxide) was mixed with 2.7 ml ammonia aqueous solution (25 %) to obtain a pH of 10 and redispersed using ultrasonic treatment (Branson Sonifier 450, 4 min, duty cycle = 30 %, strength = 7). 60 ml of ethanol were immediately added and 0.38 g TEOS in 20 ml ethanol were dropwise added within 30 min under permanent stirring. After 2 h of stirring, the reaction mixtures were concentrated via rotary evaporation and subsequently washed three times with ethanol via centrifugation.

Synthesis of luminescent TiO₂/rhodamine-doped SiO₂ core/shell nanoparticles with varying shell thicknesses

Before the synthesis of the silica shell doped with RhBitc, the luminescent agent was conjugated to AMEO. Therefore, RhBitc (5.6 µg) was dissolved in DMF (2 ml) and a fivefold excess of AMEO was added to the dye solution under argon atmosphere. The reaction mixture was stirred overnight at room temperature in darkness. The modified luminescent agent is denoted as RhBitc-AMEO.

For the coating of TiO₂ NPs with a dye doped SiO₂ shell, 16.67 g TiO₂ NP dispersion (0.5 g TiO₂) was mixed with 2.7 ml ammonia aqueous solution (25 %) to obtain a pH of 10 and redispersed using ultrasonic treatment. 60 ml of ethanol were immediately added and 0.09 g, 0.18 g or 0.38 g TEOS with 49 µl, 106 µl or 212 µl RhBitc-AMEO in 20 ml ethanol were dropwise added within 30 min under permanent stirring. Due to this, 0.3 mol-% of Si-atoms added to the reaction belonged to AMEO or RhBitc-AMEO and the theoretic molar ratio Ti/Si/RhBitc was 1/0.07/4.11E-5, 1/0.14/8.8E-5 or 1/0.29/17.77E-5. After 2 h of stirring, the reaction mixtures were concentrated via rotary evaporation and subsequently washed with ethanol via centrifugation until a clear supernatant was obtained. The NPs were stored in ethanol or dried under vacuum for further characterization. The TiO₂/SiO₂ core/shell NPs are named as TiO₂/SiO₂_1 to TiO₂/SiO₂_3 (0.09 g to 0.38 g TEOS).

Synthesis of ZnO nanoparticles with LiOH as base

Zn(CH₃CO₂)₂ (37 mg, 0.2 mmol) was dissolved in ethanol (20 ml) in an ultrasonic bath. LiOH (36 mg, 1.5 mmol) was also ultrasonically dissolved in ethanol (20 ml). Then, both solutions were mixed together and stirred for 4 h at room temperature. The synthesis was carried out under three different conditions: firstly in a lid-covered flask, secondly in an open flask (which allowed for air exchange) and thirdly in a flask flooded with nitrogen.

Synthesis of ZnO nanoparticles with KOH as base

Zn(CH₃CO₂)₂ * H₂O (8.13 g, 37 mmol) was dissolved in ethanol (700 ml) with the help of continuous sonication using a Branson Sonifier II Model 450 for 15 min in an ice water bath. Also KOH (8.31 g, 148 mmol) was dissolved in ethanol (280 ml) in an ultrasonic bath. After combining both solutions, compressed air was continuously bubbled into the stirred reaction batch at a flow rate of 100 l/h. The compressed air was introduced into the reaction vessel via a glass frit with holes of a diameter of 200 µm. The reaction was performed for 6 h at room temperature.

Synthesis of ZnO nanoparticles with varying LiOH ratios

Zn(CH₃CO₂)₂ (37 mg, 0.2 mmol) was dissolved in ethanol (3.08 ml) in an ultrasonic bath. LiOH (in appropriate concentration – see Table - EP - 1) was also ultrasonically dissolved in ethanol. Then, both solutions were mixed together and stirred for 24 h in an open flask at room temperature.

Table - EP - 1. Variation of reactant ratios for ZnO synthesis.

concentration ZnOAc:LiOH [mol]:[mol]	mass [g] (quantity [mmol])	amount of ethanol as solvent [ml]
1:1.15	0.0055 (0.23)	0.55
1:2	0.0096 (0.4)	0.96
1:3	0.0144 (0.6)	1.44
1:7.5	0.0360 (1.5)	3.6

Synthesis of Fe₂O₃/TiO₂ core/shell nanoparticles

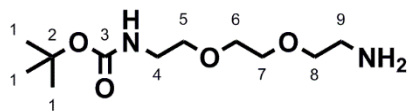
First the synthesis of 3.9 g Fe₂O₃ NPs was carried out by a precipitation method. For this, Fe(II)Cl₂ * 4 H₂O (1 eq., 8 mmol, 1.59 g) and Fe(III)Cl₃ * 6 H₂O (2 eq., 16 mmol, 4.325 g) were dissolved in 200 ml water under strong stirring. 12 ml of 25 % ammonium hydroxide in water was quickly added. The obtained particles were washed twice with water and twice with ethanol by magnetic separation and redispersion. The ethanol was removed before the transfer of the particle pellet into the titanium precursor batch.

For the shell synthesis, 33.56 g 2-[2-(2-methoxyethoxy)ethoxy]acetic acid (0.1883 mol, 1.883 eq) was dropped into 34.03 g titanium(IV) butoxide (0.1 mol, 1 eq) over 1 h under stirring. This batch was added to the Fe₂O₃ particle pellet (3.9 g) under stirring. Then 6.01 g water (0.33 mol, 3.33 eq) was added dropwise over 30 min to the titanium precursors and stirred overnight at room temperature. The solution was then concentrated by rotary evaporation resulting in a black viscous liquid (Fe₂O₃/TiO₂ content: 25.2 weight-%, determined by heating up to 800 °C). It was subsequently diluted with water to obtain sol with 12 weight-% inorganic core/shell precursor. This dispersion was hydrothermally treated in an autoclave (with 100 ml Teflon insert filled to 75 % volume) at 160 °C for 4 h. The finally obtained brown to black gel was diluted with water, destabilised with NaOH (pH = 10), 5 times washed with water via magnetic separation and redispersion and finally stabilised with HNO₃ (pH = 3-4).

3. Organic coupling agent synthesis protocols

All reactions described below were carried out under argon atmosphere. Exceptions were the reactions for **compound 9**, **compound 10**, **compound 15**, **compound 19**, **compound 21** and **compound 24**.

Compound 1:



Chemical formula: $C_{11}H_{24}N_2O_4$

Molecular weight: 248.32 g/mol

Di-tert-butyl dicarbonate (1 eq., 0.05 mmol, 10.91 g) was dissolved in 100 ml CH_2Cl_2 and dropwise added to 2,2-(ethylenedioxy)bis(ethylamine) (10 eq., 0.5 mmol, 74.10 g) under strong stirring at 0 °C over 8 h. The reaction batch was then stirred for 16 h at room temperature. 300 ml water was added and the product was extracted with 3 x 50 ml CH_2Cl_2 . The combined organic phases were washed with 3 x 150 ml water. The organic phase was dried over $MgSO_4$, filtrated and concentrated under vacuum to yield **compound 1** (97 %) as clear and pale yellow oil.

1H NMR (300 MHz, DMSO, δ [ppm]):

5.77 (s, 1H, 3-NH-4), 3.51-3.49 (m, 4H, **7**, **6**), 3.41-3.37 (m, 4H, **8**, **5**), 3.07 (dd, $J = 5.97$ Hz, 2H, **4**), 2.80 (s, 2H, 9-NH₂), 2.68 (t, $J = 5.73$ Hz, 2H, **9**), 1.38 (s, 9H, **1**).

^{13}C NMR (75 MHz, DMSO, δ [ppm]):

156.03 (1C, **3**), 78.02 (1C, **2**), 72.85 (2C, **8**, **5**), 70.01/69.94 (2C, **7**, **6**), 41.51 (1C, **9**), ~ 40.12 (1C, **4** in solvent signal), 29.57 (3C, **1**).

MS (ESI, m/z)

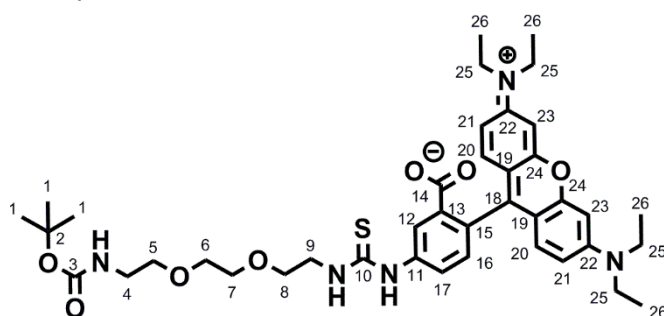
$[M+H]^+$ calculated: 249.18, found: 249.20

EA[†]

calculated: C, 53.21; H, 9.74; N, 11.28; O, 25.77

found: C, 50.72; H, 9.03; N, 10.26

Compound 2:



Chemical formula: $C_{40}H_{53}N_5O_7S$

Molecular weight: 747.95 g/mol

Compound 1 (1.2 eq., 0.48 mmol, 0.119 g) was dissolved in 3 ml CH_2Cl_2 , triethylamine (TEA – 1.5 eq., 0.6 mmol, 83.74 μ l) was then added and stirred for 10 min. Rhodamine B isothiocyanate (RhBic – 1 eq., 0.4 mmol, 0.214 g) was dissolved in 3 ml DMF and added to the reaction batch. The reaction was carried out for 16 h under stirring at room temperature in darkness. The crude compound as powder was obtained by complete removal of all volatile compounds under vacuum. It was extensively washed with diethyl ether with the aid of

[†] The difference between calculated and found percentage of the elements is caused by traces of di-Boc protected compound.

ultrasonic treatment. The product was dissolved in 5 ml CH₂Cl₂ and 1 ml 1 M KOH solution was added. The organic solvent and liberated TEA were removed under vacuum and the product was extracted from the water phase with 3 x 20 ml and 3 x 10 ml CH₂Cl₂. The combined organic phases were dried over MgSO₄, filtrated and concentrated under vacuum to yield **compound 2** (94 %) as dark violet solid.

¹H NMR (300 MHz, DMSO, δ [ppm]):

8.33-6.11 (m, 9H, **12, 16, 17, 20, 21, 23**), 5.72 (s, 1H, 3-NH-4), 3.51 (s, 4H, **6, 7**), 3.41-3.35 (m, 12H, **5, 8, 25**), 3.07 (dd, J = 5.55 Hz / 10.95 Hz, 2H, **4**), 2.74-2.71 (m, 2H, **9**), 1.39 (s, 9H, **1**), 1.25-1.08 (m, 12H, **26**).

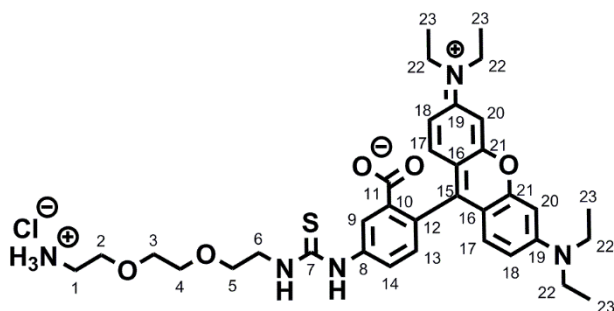
¹³C NMR (75 MHz, DMSO, δ [ppm])[‡]:

169.70 (1C, **10**), 156.08 (2 C, **3, 14**), 153.20/152.73/149.67/149.27 (6C, **15, 18, 22, 24**), 139.66 (1C, **11**), 129.07 (2C, **20**), 125.36 (3C, **12, 16, 17**), 123.22 (1C, **13**), 108.58 (2C, **21**), 106.74 (2C, **19**), 97.35 (2C, **23**), 78.11 (1C, **2**), 69.91 (4C, **5-8**), 44.26 (1C, **9**), ~ 40.12 (1C, **4** in solvent signal), 34.82 (4C, **25**), 30.87 ([4-x-y]C, **26**), 28.66 (3C, **1**), 21.48 (xC, **26**), 12.79 (yC, **26**) [x,y < 4].

MS (ESI, m/z)

[M+H]⁺ calculated: 478.37, found: 478.40

Compound 3:



Chemical formula: C₃₅H₄₆N₅O₅S⁺Cl⁻

Molecular weight: 683.29 g/mol

Compound 2 (0.45 g) was dissolved in 25 ml CH₂Cl₂ and gaseous HCl was bubbled through the solution during 15 min. At the end of the reaction the solvent was evaporated under vacuum to yield the precipitated **compound 3** (quantitative) in salt form as a dark violet solid.

¹H NMR (300 MHz, CDCl₃ + TEA·HCl[§], δ [ppm]):

8.00-6.12 (m, 9 H, **9, 13, 14, 17, 18, 20**), 3.55 – 3.18 (br/m, 20 H, **1, 2-5, 6, 22**), 1.18-1.07 (m, 12 H, **23**).

¹³C NMR (75 MHz, CDCl₃ + TEA·HCl^{**}, δ [ppm]):

169.95 (1C, **7**), 155.80 (1 C, **11**), 154.23/153.24/152.44/149.49 (6 C, **12, 15, 19, 21**), 131.04 (2C, **17**), 129.19 (3C, **9, 13, 14**), 129.14 (1C, **8**), 127.86 (1C, **10**), 108.00 (2C, **18**), 106.64 (2C, **16**), 97.35 (2C, **20**), 69.91 (4C, **2-5**), 44.94 (2C, **1,6**), 44.49 ([4-x]C, **22**), 29.65 (xC, **22**), 12.69 (4C, **23**) [x < 4].

MS (ESI, m/z)

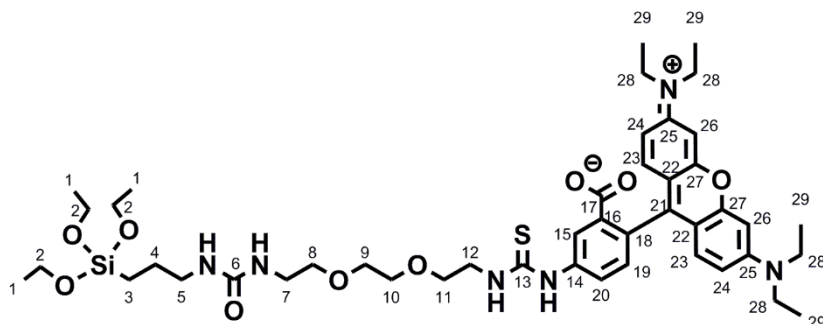
[M+H]⁺ calculated: 648.84, found: 648.3

[‡] resolution of signals of aromatic carbons of rhodamine was very low

[§] addition of TEA to obtain better solubility of the compound as free amine

^{**} addition of TEA to obtain better solubility of the compound as free amine

Compound 4:



Chemical formula:

$C_{45}H_{66}N_6O_9SSi$

Molecular weight:

895.20 g/mol

Compound 3 (1 eq., 0.208 mmol, 0.15 g) was dispersed in 6 ml CH_2Cl_2 , TEA (15 eq., 3.12 mmol, 435 μ l) was added and stirred until **compound 3** was solubilized. Isocyanatopropyltriethoxysilane (1.2 eq., 0.250 mmol, 61.8 μ l) was added and the reaction proceeded at room temperature for 16 h. Afterwards the solvent and excess TEA were evaporated. The obtained product was washed with pentane (3 x 30 ml). Then, all traces of the solvent were evaporated to yield **compound 4** as purple solid (~ 90 %).

1H NMR (300 MHz, $CDCl_3$ + TEA·HCl^{††}, δ [ppm]):

8.03-6.32 (m, 9H, **15, 19, 20, 23, 24, 26**), 5.73/5.36/5.12 (br s/s/s, 2H/1H/1H, 4x**NH**), 3.79-3.72 (m, 6H, **2**), 3.64 (dd, $J = 7.05$ Hz / 13.95 Hz, 8H, **28**), 3.54 (s, 4H, **9, 10**), 3.44 (t, $J = 5.10$ Hz, 4H, **8, 11**), 3.42-3.37 (m, 2H, **12**), 3.29 (t, $J = 5.36$ Hz, 2H, **7**), 3.05 (covered by TEA·HCl, 2H, **5**), 1.59-1.54 (m, 2H, **4**), 1.19-1.14 (m, 21H, **1, 29**), 0.60-0.55 (m, 2H, **3**).

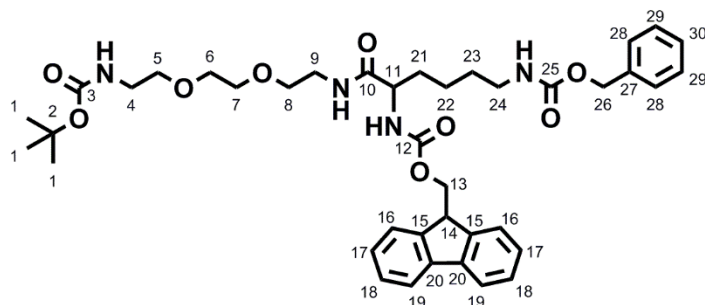
^{13}C NMR (75 MHz, $CDCl_3$ + TEA·HCl^{††}, δ [ppm])^{§§}:

169.95 (1C, **13**), 157.68 (1C, **6**), 155.28 (1C, **17**), 154.23/153.24/152.44/149.49 (6C, **18, 21, 25, 27**), 131.04 (2C, **23**), 129.19 (3C, **15, 19, 20**), 129.14 (1C, **14**), 127.86 (1C, **16**), 108.00 (2C, **24**), 106.64 (2C, **22**), 97.35 (2C, **26**), 70.71/ 70.28 (4C, **8-11**), 58.33 (4C, **28**), 57.99 (3C, **2**), 44.92 (1C, **12**), 42.85 (1C, **5**), 40.08 (1C, **7**), 23.63 (1C, **4**), 18.33 (3C, **1**), 12.52 (4C, **29**), 7.56 (1C, **3**).

MS (ESI, m/z)

[M+H]⁺ calculated: 895.44, found: 895.4

Compound 5:



Chemical formula: $C_{40}H_{52}N_4O_9$

Molecular weight: 732.88 g/mol

Fmoc-lysine-Z-OH (1 eq., 8.725 mmol, 4.385 g) was dissolved in 175 ml CH_2Cl_2 and cooled down to 0 °C. N-hydroxysuccinimide (1.2 eq., 10.47 mmol, 1.205 g) and N,N'-dicyclohexylcarbodiimide (1.2 eq., 10.47 mmol, 2.160 g) were added and stirred for 6 h (30

^{††} side product due to reaction of Cl⁻ and TEA

^{††} side product due to reaction of Cl⁻ and TEA

^{§§} resolution of signals of aromatic carbons of rhodamine was very low

min at 0 °C and then at room temperature). The reaction mixture was filtered and rinsed with CH₂Cl₂. The filtrate was mixed with compound **1** (1.2 eq., 10.47 mmol, 2.60 g) and stirred for 16 h at room temperature. The reaction batch was washed with 3 x 100 ml 10 vol-% acetic acid, 3 x 100 ml saturated NaHCO₃ and 3 x 100 ml water. The organic phase was evaporated to obtain a highly concentrated solution and filtrated. The organic solvent of the filtrate was evaporated and the obtained powder was washed with 1 x 80 ml and 3 x 40 ml diethyl ether. The crude powder was then again dissolved in 10 ml CH₂Cl₂ per g powder and was purified by column chromatography on 25 g silica gel per g powder with 100% EtOAc as eluent to yield the pure **compound 5** (61 %) as white powder.

¹H NMR (300 MHz, DMSO, δ [ppm]):

7.91-7.89 (m, 3H, **19**, 9-NH-10), 7.73 (d, J = 7.03 Hz, 2H, **16**), 7.42-7.16 (m, 11H, **28-30**, **17**, **18**, 11-NH-12, 24-NH-25), 6.76 (t, J = 4.88 Hz, 1 H, 3-NH-4), 5.01 (s, 2H, **26**), 4.31-4.22 (m, 3H, **14**, **13**), 3.97-3.89 (m, 1H, **11**), 3.49 (s, 4H, **6**, **7**), 3.39-3.33 (m, 4H, **5**, **8**), 3.24-3.16 (m, 2H, **9**), 3.08 (dd, J = 6.15 Hz / 11.85 Hz, 2H, **4**), 2.98 (dd, J = 6.52 Hz / 12.75 Hz, 2H, **24**), 1.61-1.49 (br/m, 2H, **21**), 1.37 (s, 9H, **1**), 1.37-1.24 (br/m, 4H, **23**, **22**).

¹³C NMR (75 MHz, DMSO, δ [ppm]):

172.50 (1C, **10**), 156.53 (1C, **25**), 156.38 (1C, **12**), 156.04 (1C, **3**), 144.35 (2C, **15**), 141.17 (2C, **20**), 137.72 (1C, **27**), 128.80-127.52 (9C, **17**, **18**, **28-30**), 125.81 (2C, **16**), 120.57 (2C, **19**), 78.05 (1C, **2**), 69.99/69.91/69.45 (4C, **5-8**), 66.25/65.57 (2C, **13**, **26**), 55.06 (1C, **11**), 47.13 (1C, **14**), ~ 40 (3C, **4**, **9**, **24** in solvent signal), 32.18 (1C, **21**), 29.57 (1C, **23**), 28.68 (3C, **1**), 23.27 (1C, **22**).

MS (ESI, m/z)

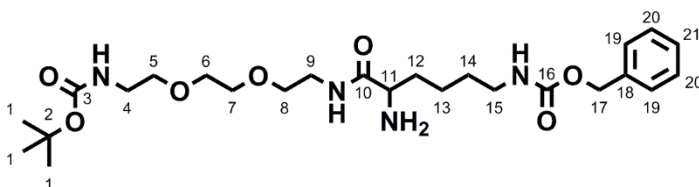
[M+Na]⁺ calculated: 755.87, found 755.4

EA

calculated: C, 65.56; H, 7.15; N, 7.64; O, 19.65

found: C, 64.72; H, 6.89 ; N, 7.13

Compound 6:



Chemical formula: C₂₅H₄₂N₄O₇

Molecular weight: 510.63 g/mol

Compound 5 (1 eq., 4.09 mmol, 3.00 g) was dissolved in 30 ml THF and Et₂NH (38 eq., 155.42 mmol, 16.24 ml) was added. The reaction batch was stirred for 16 h at room temperature. The product was concentrated under vacuum, then dissolved in 10 ml acetonitrile and 90 ml of water was added. The water phase was washed with 3 x 100 ml pentane. To the water phase 10 ml of 0.5 M NaOH were added and the product was finally extracted with 3 x 100 ml CH₂Cl₂. The combined organic phases were dried over MgSO₄, filtrated and concentrated under vacuum to yield **compound 6** (98 %) as slightly yellow, highly viscous, clear oil.

¹H NMR (300 MHz, DMSO, δ [ppm]):

7.87 (t, J = 5.79 Hz, 1H, 9-NH-10), 7.41-7.32 (m, 5H, **19-21**), 7.20 (t, J = 5.76 Hz, 1H, 15-NH-16), 6.75 (t, J = 5.63 Hz, 1H, 3-NH-4), 5.01 (s, 2H, **17**), 3.50 (s, 4H, **6**, **7**), 3.44-3.32 (m, 4H, **5**, **8**), 3.24-3.15 (m, 2H, **9**), 3.13-2.90 (m, 3H, **4,11**), 2.96 (dd, J = 6.52 Hz / 12.75 Hz, 2H, **15**), 1.72 (s, 2H, 11-NH₂), 1.57-1.48 (br/m, 2H, **12**), 1.37 (s, 9H, **1**), 1.33-1.25 (br/m, 4H, **14**, **13**).

¹³C NMR (75 MHz, DMSO, δ [ppm]):

172.46 (1C, **10**), 156.52 (1C, **16**), 156.05 (1C, **3**), 137.76 (1C, **18**), 128.80/128.19 (5C, **19-21**), 78.36 (s, 1C, **2**), 69.99/69.58 (4C, **5-8**), 65.54 (1C, **17**), 55.05 (1C, **11**), ~ 40 (2C, **4, 9** in solvent signal), 38.70 (1C, **15**), 33.30 (1C, **12**), 29.82 (1C, **14**), 28.69 (3C, **1**), 23.04 (1C, **13**).

MS (ESI, m/z)

[M+H]⁺ calculated: 511.63, found: 511.3

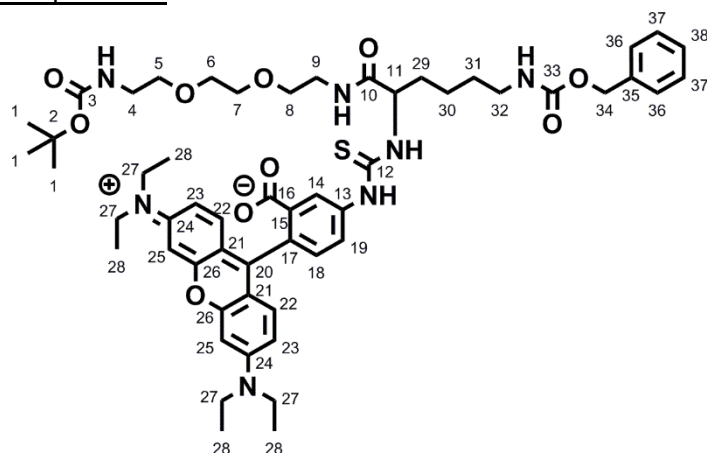
[M+Na]⁺ calculated: 533.62, found: 533.3

EA

calculated: C, 58.80; H, 8.29; N, 10.97; O, 21.93

found: C, 57.38 ; H, 8.44 ; N, 10.25

Compound 7:



Chemical formula: C₅₄H₇₁N₇O₁₀S

Molecular weight: 1010.26 g/mol

Compound 6 (1.2 eq., 0.448 mmol, 0.229 g) was dissolved in 4 ml CH₂Cl₂, TEA (1.5 eq., 0.560 mmol, 77.98 μl) was added and stirred for 10 min. Rhodamine B isothiocyanate (RhBic – 1 eq., 0.373 mmol, 0.2 g) was dissolved in 2 ml DMF and added to the reaction batch. The reaction was carried out for 16 h under stirring at room temperature in darkness. The crude compound as powder was obtained by complete removal of all volatile compounds under vacuum. It was extensively washed with diethyl ether with the aid of ultrasonic treatment. This crude product was dissolved in 5 ml CH₂Cl₂ and 1 ml 1 M KOH solution was added. The organic solvent and liberated TEA were removed under vacuum and the product was extracted from the water phase with 3 x 20 ml and 3 x 10 ml CH₂Cl₂. The combined organic phases were dried over MgSO₄, filtrated and concentrated under vacuum to yield **compound 7** (91 %) as dark violet solid.

¹H NMR (300 MHz, DMSO, δ [ppm]):

8.5-6.0 (m, "9 H", **14, 18, 19, 22, 23, 25**), 7.91 (t, J = 5.25 Hz, 1H, 9-NH-10), 7.39-7.30 (m, 7H, **36-38**, 11-NH-12-NH-13), 7.22 (t, J = 4.95 Hz, 1H, 32-NH-33), 6.78 (t, 1H, 3-NH-4), 5.01 (s, 2H, **34**), 3.50 (s, 4H, **6, 7**), 3.38-3.34 (m, 12H, **5, 8, 27**), 3.24-3.20 (m, 2H, **9**), 3.12-3.03 (m, 3H, **4, 11**), 2.96 (dd, J = 6.00 Hz / 11.70 Hz, 2H, **32**), 1.71 (br/m, 2H, **29**), 1.37 (s, 9H, **1**), 1.29 (br/m, 4H, **30, 31**), 1.10 (t, 12 H, **28**).

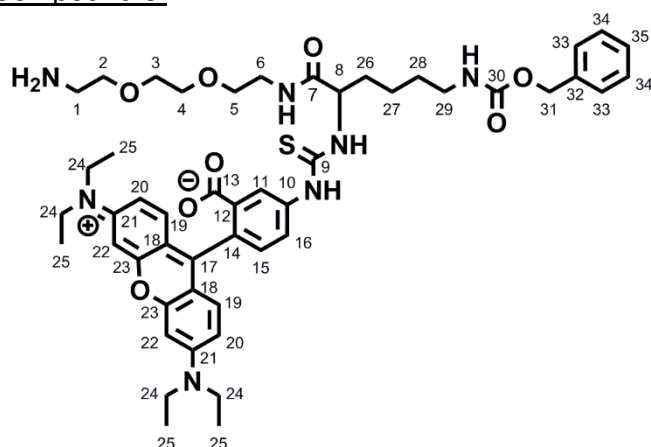
¹³C NMR (75 MHz, DMSO, δ [ppm]):

184.69 (1C, **12**), 175.37(1C, **10**), 156.53 (1C, **33**), 156.05 (2C, **3, 16**), 153.15/152.70/149.37 (6C, **17, 20, 24, 26**), 137.76 (2C, **35, 13**), 129.09 (2C, **22**), 128.80/128.18 (5C, **36-38**), 123.20 (4C, **14, 15, 18, 19**), 108.58 (2C, **23**), 106.76 (1C, **21**), 97.32 (1C, **25**), 78.06 (1C, **2**), 69.99-69.56 (4C, **5-8**), 65.55 (1C, **34**), 55.37 (1C, **11**), 44.26 (4C, **27**), ~ 40 (2C, **4, 9** in solvent signal), 38.74 (1C, **32**), 35.08 (1C, **29**), 29.80 (1C, **31**), 28.69 (3C, **1**), 22.98 (1C, **30**), 12.82 (4C, **28**).

MS (ESI, m/z)

[M+Na]⁺ calculated: 1032.5, found: 1032.5

Compound 8:



Chemical formula: C₄₉H₆₄ClN₇O₈S

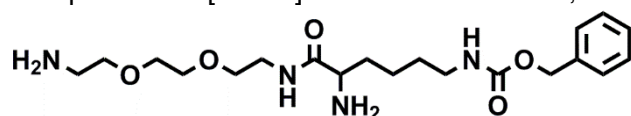
Molecular weight: 946.6 g/mol

First attempt:

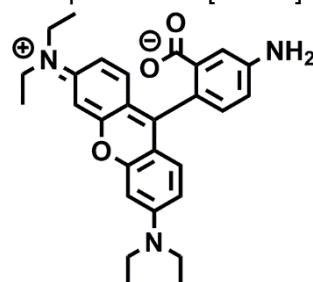
Compound 7 (0.3 g) was dissolved in 17 ml CH₂Cl₂ and gaseous HCl was bubbled through the solution during 4 min. At the end of the reaction the solvent and all volatile side products were evaporated under vacuum. **Compound 8** was not obtained due to fragmentation of the **compound 7** and/or **8** during the reaction.

MS (ESI, m/z) – detected fragments:

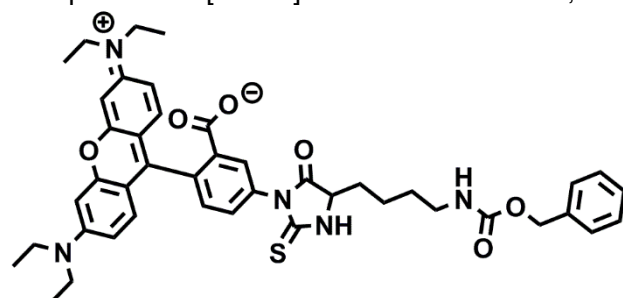
Compound 8a: [M + H]⁺: calculated: 411.25, found: 411.3



Compound 8b: [M + H]⁺: calculated: 458.24, found: 458.2



Compound 8c: [M + H]⁺: calculated: 762.32, found: 762.3



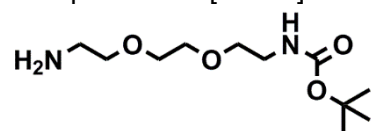
Second attempt:

Compound 7 (1 eq., 0.265 mmol, 0.268 g) was dissolved in 15 ml CH₂Cl₂ and trifluoroacetic acid (15 eq., 3.975 mmol, 0.304 µl) was dropwise added under stirring. The reaction was stirred for 16 h. To eliminate all free TFA, a coevaporation with 3 x 20 ml toluene was subsequently carried out. **Compound 8** was not obtained due to fragmentation of the **compound 7** and/or **8** during the reaction.

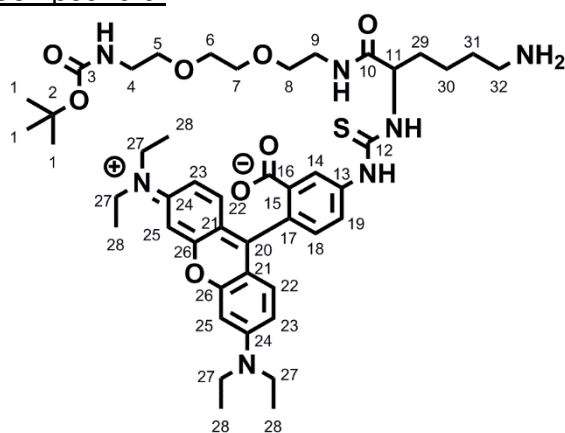
MS (ESI, m/z) – detected fragments:

Compound 8c: [M + H]⁺: calculated: 762.32, found: 762.3

Compound 8d: [M + H]⁺: calculated: 248.17, found: 249.2



Compound 9:



Chemical formula: C₄₆H₆₅N₇O₈S

Molecular weight: 876.13 g/mol

Compound 7 (1 eq., 0.148 mmol, 0.150 g) was dissolved in 4 ml methanol and 100 µl acetic acid in 0.9 ml water was added under stirring. The catalyst Pd on C with 10 weight-% loading (0.015 g) was added and the flask was set under H₂ atmosphere by setting the sample 3 times under vacuum and subsequently flooding it with H₂. The reaction was stirred for 24 h, the Pd/C was filtered off over celite and the solvent was evaporated. **Compound 9** was not obtained due to fragmentation of the **compound 7** during the reaction.

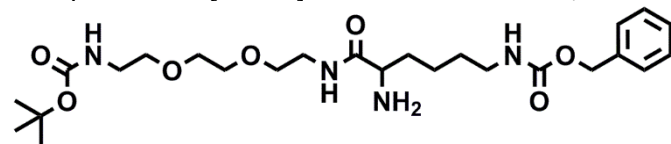
MS (ESI, m/z) – detected fragments:

Compound 8b: [M + H]⁺: calculated: 458.24, found: 458.2

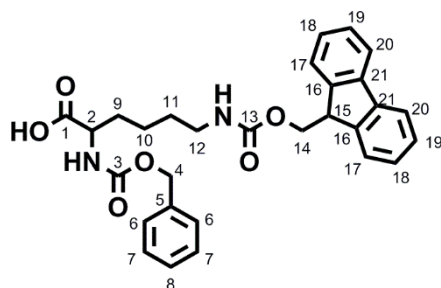
Compound 8c: [M + H]⁺: calculated: 762.32, found: 762.3

Compound 8d: [M + H]⁺: calculated: 248.17, found: 249.2

Compound 8e: [M + H]⁺: calculated: 511.31, found: 511.3



Compound 10:



Chemical formula: $C_{29}H_{30}N_2O_6$

Molecular weight: 502.57 g/mol

First attempt:

Sodiumbicarbonate (2.5 eq., 25 mmol, 2.10 g) was dissolved in 25 ml water, added to Na-Z-lysine (1 eq., 10 mmol, 2.80 g) and stirred for 15 min at 0 °C to yield a turbid solution. 15 ml of THF was added. To this batch, 9-Fluorenylmethoxycarbonyl chloride (1 eq., 10 mmol, 2.59 g) was stepwise added with a spatula. The reaction was complete after stirring for 3 h at 0 °C and 1 h at room temperature. 200 ml 0.5 M and 40 ml 1 M potassium hydrogensulfate solution were added under stirring. The precipitate was filtered and washed with 3 x 50 ml water, followed by excessive washing with toluene (9 x 20 ml). Finally the precipitate was washed with diethyl ether (3 x 100 ml). The ether phases were combined and concentrated to yield **compound 10** (30 %) as white powder.

Second attempt:

The same protocol was followed as in the first attempt but dioxane instead of THF was used as solvent. After purification, **compound 10** with a yield of 11 % was obtained.

Third attempt:

The same protocol was followed as in the first attempt but DMF instead of THF was used as solvent. After purification, **compound 10** with a yield of 68 % was obtained.

¹H NMR (300 MHz, DMSO, δ [ppm]):

12.59 (s, 1H, **HO-1**), 7.90 (d, $J = 7.36$ Hz, 2H, **20**), 7.69 (d, $J = 7.38$ Hz, 2H, **17**), 7.58 (d, $J = 7.89$ Hz, 1H, **12-NH-13**), 7.45-7.30 (m, 10H, **18, 19, 6-8, 2-NH-3**), 5.04 (s, 2H, **14**), 4.30 (d, $J = 6.76$ Hz, 2H, **4**), 4.21 (t, $J = 6.68$ Hz, 1H, **15**), 3.96-3.89 (m, 1H, **2**), 2.96 (dd, $J = 6.00$ Hz / 12.00 Hz, 2H, **12**), 1.68-57 (br/m, 2H, **9**), 1.39-1.31 (br/m, 4H, **11, 10**).

¹³C NMR (75 MHz, DMSO, δ [ppm]):

174.4 (1C, **1**), 156.65 (2C, **3, 13**), 144.40 (1C, **16**), 141.20 (1C, **21**), 137.46 (1C, **5**), 128.80-128.05 (10C, **18, 19, 6-8**), 125.60 (2C, **17**), 120.58 (2C, **20**), 65.86 (1C, **4**), 65.62 (1C, **14**), 54.32 (1C, **2**), 47.24 (1C, **15**), ~ 40 (2C, **12** in solvent signal), 30.91 (1C, **9**), 29.39 (1C, **11**), 23.35 (1C, **10**).

MS (ESI, m/z)

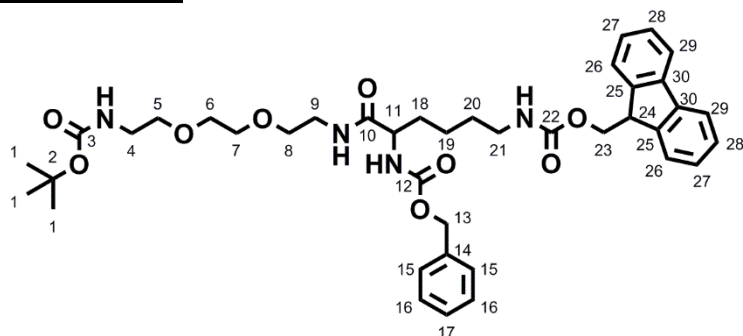
[M+Na]⁺ calculated: 525.56, found: 525.2

[M+K]⁺ calculated: 541.67, found: 541.2

EA

calculated: C, 69.31; H, 6.02; N, 5.57; O, 19.10

found: C, 68.79; H, 4.67; N, 5.42

Compound 11:Chemical formula: $C_{40}H_{52}N_4O_9$

Molecular weight: 732.88 g/mol

Compound 10 (1 eq., 5.717 mmol, 2.873 g) was dissolved in 115 ml CH_2Cl_2 and cooled down to 0 °C. N-hydroxysuccinimide (1.2 eq., 6.860 mmol, 0.790 g) and then N,N'-dicyclohexylcarbodiimide (1.2 eq., 6.860 mmol, 1.415 g) were added and stirred for 6 h (30 min at 0 °C and then at room temperature). The reaction mixture was filtered and rinsed with CH_2Cl_2 . The filtrate was mixed with compound **1** (1.2 eq., 6.680 mmol, 1.703 g) and stirred for 16 h at room temperature. The reaction batch was washed with 3 x 100 ml 10 vol-% acetic acid, 3 x 100 ml saturated $NaHCO_3$ and 3 x 100 ml water. The organic phase was evaporated to obtain a highly concentrated solution and filtrated. The organic solvent of the filtrate was evaporated and the obtained powder was washed with 1 x 80 ml and 3 x 40 ml diethyl ether. The crude powder was then again dissolved in 10 ml CH_2Cl_2 per g powder and was purified by column chromatography on 25 g silica gel per g powder with 100% EtOAc as eluent to yield the pure **compound 11** (80 %) as white powder.

1H NMR (300 MHz, DMSO, δ [ppm]):

7.91-7.89 (m, 5H, **29, 26, 9-NH-10**), 7.78-7.68 (m, 2H, **27**), 7.42-7.27 (m, 9H, **15-17, 28, 11-NH-12, 21-NH-22**), 6.78 (t, $J = 6.20$ Hz, 1H, **3-NH-4**), 5.02 (s, 2H, **13**), 4.31-4.21 (m, 3H, **24, 23**), 3.95-3.90 (m, 1H, **11**), 3.49 (s, 4H, **6, 7**), 3.40-3.35 (m, 4H, **5, 8**), 3.25-3.17 (m, 2H, **9**), 3.06 (dd, $J = 5.70$ Hz / 11.70 Hz, 2H, **4**), 2.97 (dd, $J = 6.90$ Hz / 12.90 Hz, 2H, **21**), 1.61-1.53 (br/m, 2H, **18**), 1.38 (s, 9H, **1**), 1.27-1.19 (br/m, 4H, **20, 19**).

^{13}C NMR (75 MHz, DMSO, δ [ppm]):

172.51 (1C, **10**), 156.65 (2C, **22, 12**), 156.05 (1C, **3**), 144.40 (2C, **25**), 144.20 (2C, **30**), 137.54 (1C, **14**), 128.80-128.14 (9C, **27, 28, 15-17**), 125.60 (2C, **26**), 120.50 (2C, **29**), 78.05 (1C, **2**), 70.00-69.43 (4C, **5-8**), 65.81/65.62 (2C, **23, 13**), 55.14 (1C, **11**), 47.24 (1C, **24**), ~ 40 (3C, **4, 9, 21** in solvent signal), 33.20 (1C, **18**), 29.79 (1C, **20**), 28.69 (3C, **1**), 23.29 (1C, **19**).

MS (ESI, m/z)

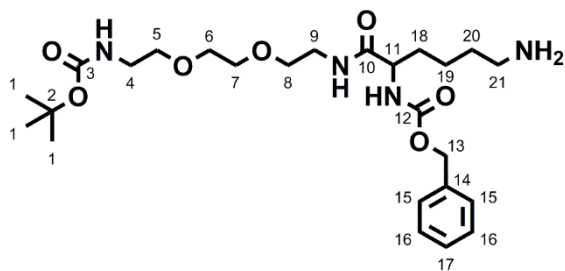
$[M+Na]^+$ calculated: 755.87, found 755.4

EA

calculated: C, 65.56; H, 7.15; N, 7.64; O, 19.65

found: C, 64.91; H, 6.77; N, 6.78

Compound 12:



Chemical formula: $C_{25}H_{42}N_4O_7$

Molecular weight: 510.63 g/mol

Compound 11 (1 eq., 3.14 mmol, 2.30 g) was dissolved in 23 ml THF and diethylamine (38 eq., 119.26 mmol, 12.5 ml) was added. The reaction batch was stirred for 16 h at room temperature. The product was concentrated under vacuum, then dissolved in 10 ml acetonitrile and 90 ml of water was added. The water phase was washed with 4 x 100 ml pentane. To the water phase 10 ml of 0.5 M NaOH were added and the product was finally extracted with 3 x 100 ml CH_2Cl_2 . The combined organic phases were dried over $MgSO_4$, filtrated and concentrated under vacuum to yield **compound 12** (93 %) as slightly yellow, highly viscous, clear oil.

1H NMR (300 MHz, DMSO, δ [ppm]):

7.92 (t, J = 5.55 Hz, 1H, 9-NH-10), 7.40-7.30 (m, 6H, **15-17**, 11-NH-12), 6.79 (t, J = 5.74 Hz, 1H, 3-NH-4), 5.02 (s, 2H, **13**), 3.98-3.89 (m, 1H, **11**) 3.49 (s, 4H, **6, 7**), 3.42-3.35 (m, 6H, **5, 8, 21**), 3.25-3.12 (m, 2H, **9**), 3.06 (dd, J = 6.00 Hz / 12.00 Hz, 2H, **4**), 1.61-1.51 (br/m, 4H, **18, 20**), 1.37 (s, 9H, **1**), 1.28-1.19 (br/m, 2H, **19**).

^{13}C NMR (75 MHz, DMSO, δ [ppm]):

172.51 (1C, **10**), 156.35 (1C, **12**), 156.05 (1C, **3**), 137.54 (1C, **14**), 128.78/128.14 (5C, **15-17**), 78.36 (1C, **2**), 69.99/69.64/69.44 (5C, **5-8, 21**), 65.58 (1C, **13**), 55.17 (1C, **11**), 41.88/~40 (2C, **4, 9** in solvent signal), 33.35 (1C, **18**), 32.40 (1C, **20**), 28.69 (3C, **1**), 23.29 (1C, **19**).

MS (ESI, m/z)

$[M+H]^+$ calculated: 511.31, found: 511.3

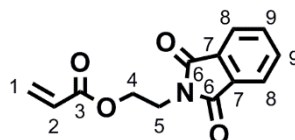
$[M+Na]^+$ calculated: 533.32, found: 533.3

EA

calculated: C, 58.80; H, 8.29; N, 10.97; O, 21.93

found: C, 56.65; H, 7.97; N, 10.37

Compound 13:



Chemical formula: $C_{13}H_{11}NO_4$

Molecular weight: 245.33 g/mol

N-(2-Hydroxyethyl)phthalimide (1 eq., 35 mmol, 6.69 g) was dissolved in 100 ml CH_2Cl_2 and TEA (1.1 eq., 38.5 mmol, 5.34 ml) was added. The reaction batch was cooled down to 0°C, acryloylchloride (1.1 eq., 38.5 mmol, 3.17 ml) was added dropwise over an hour under agitation and then the reaction was stirred for 16 h at room temperature. The batch was filtered and the residue (TEA·HCl) was rinsed with CH_2Cl_2 . The filtrate was washed with 1 x 100 ml water and 3 x 100 ml 0.5 M NaOH. The organic phase was dried over $MgSO_4$, filtrated and concentrated under vacuum to yield **compound 13** (59 %) as white to slightly yellow powder.

¹H NMR (300 MHz, DMSO, δ [ppm]):

7.92-7.82 (m, 4H, **8**, **9**), 6.25 (dd, $J = 1.81$ Hz / 17.16 Hz, 1H, **1**), 6.07 (dd, $J = 10.26$ Hz / 17.16 Hz, 1H, **2**), 5.86 (dd, $J = 1.81$ Hz / 10.26 Hz, 1H, **1**), 4.33 (t, $J = 5.34$ Hz, 2H, **4**), 4.03 (t, $J = 5.34$ Hz, 2H, **5**).

¹³C NMR (75 MHz, DMSO, δ [ppm]):

168.03 (2C, **6**), 165.80 (1C, **3**), 134.08 (2C, **9**), 131.98 (2C, **7**), 131.43 (1C, **1**), 127.91 (1C, **2**), 123.39 (2C, **8**), 61.70 (1C, **4**), 36.96 (1C, **5**).

MS (ESI, m/z)

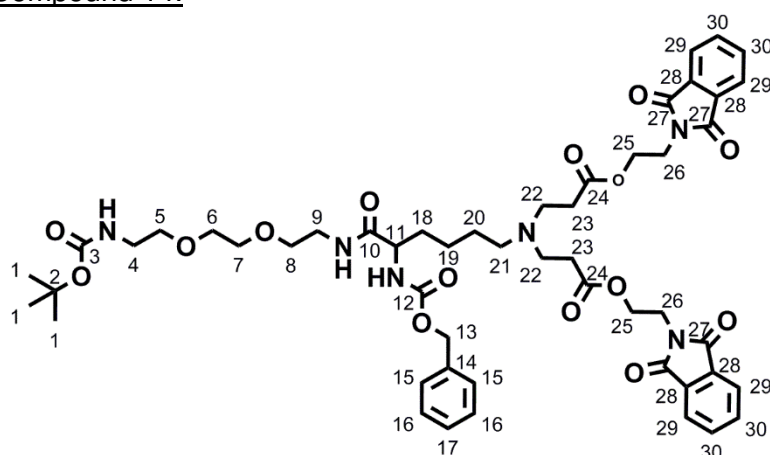
$[M+Na]^+$ calculated: 268.32, found: 268.1

EA

calculated: C, 63.67; H, 4.52; N, 5.71; O, 26.1;

found: C, 63.62; H, 4.4 ; N, 5.5

Compound 14:



Chemical formula:

$C_{51}H_{64}N_6O_{15}$

Molecular weight:

1001.10 g/mol

Compound 12 (1 eq., 0.930 mmol, 0.500 g) was dissolved in 20 ml THF and **compound 13** (5 eq., 4.896 mmol, 1.201 g) was added. The reaction batch was stirred for 6 days at 65 °C. The solvent was evaporated and the crude product was dissolved in CH_2Cl_2 . Over a short column (10 g silica per g crude product), the excess acrylate was removed with 100 % CH_2Cl_2 . To obtain the product, 10 % methanol in CH_2Cl_2 was used. The solvent was evaporated to obtain the pure **compound 14** (91 %) as orange, clear, highly viscous liquid.

¹H NMR (300 MHz, DMSO, δ [ppm]):

7.93-7.80 (m, 9H, 9-NH-10, **29**, **30**), 7.34-7.29 (m, 6H, **15-17**, 11-NH-12), 6.76 (t, $J = 5.49$ Hz, 1H, 3-NH-4), 5.01 (s, 2H, **13**), 4.21 (t, $J = 5.29$ Hz, 4H, **25**), 3.91 (dd, $J = 8.21$ Hz / 13.66 Hz, 1H, **11**), 3.81 (t, $J = 5.29$ Hz, 4H, **26**), 3.44 (s, 4H, **6**, **7**), 3.39-3.36 (m, 4H, **5**, **8**), 3.25-3.16 (m, 2H, **9**), 3.05 (dd, $J = 5.85$ Hz / 11.85 Hz, 2H, **4**), ~2.5 (4H, **23** in solvent signal), 2.26 (t, $J = 6.98$ Hz, 4H, **22**), 2.16 (t, $J = 5.55$ Hz, 2H, **21**), 1.61-1.43 (br/m, 2H, **18**), 1.37 (s, 9H, **1**), 1.28-1.16 (br/m, 4H, **20**, **19**).

¹³C NMR (75 MHz, DMSO, δ [ppm]):

172.33 (3C, **10**, **24**), 169.03 (4C, **27**), 156.32 (1C, **12**), 156.02 (1C, **3**), 137.51 (1C, **14**), 134.91 (4C, **30**), 131.94 (4C, **28**), 128.76/128.14 (5C, **15-17**), 123.53 (4C, **29**), 78.04 (1C, **2**), 69.99/69.91/69.63/69.44 (4C, **5-8**), 65.79 (1C, **13**), 61.39 (2C, **25**), 55.17 (1C, **11**), 53.13 (1C, **21**), 48.66 (2C, **22**), ~40 (2C, **4**, **9** in solvent signal), 37.14 (2C, **23**), 32.54 (1C, **18**), 32.08 (2C, **26**), 28.67 (3C, **1**), 26.48 (1C, **20**), 23.67 (1C, **19**).

MS (ESI, m/z)

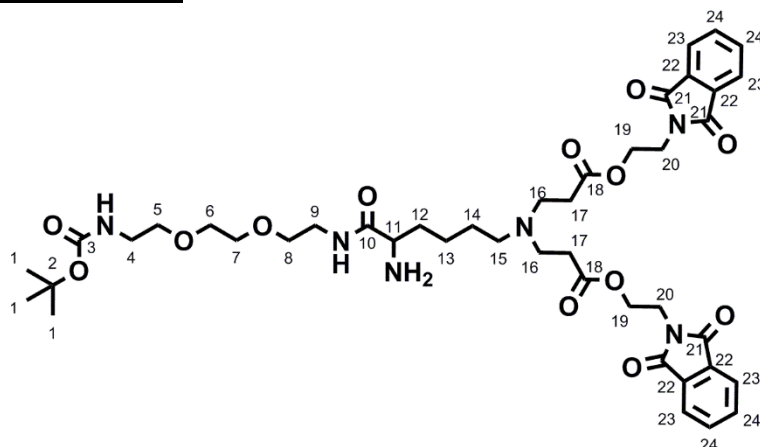
$[M+Na]^+$ calculated: 1023.44, found: 1023.4

EA

calculated: C, 61.19; H, 6.44; N, 8.39; O, 23.97

found: C, 60.51; H, 6.27; N, 8.22

Compound 15:



Chemical formula:

$C_{43}H_{58}N_6O_{13}$

Molecular weight:

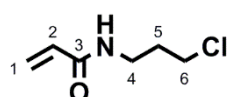
866.97 g/mol

Compound 14 (1 eq., 0.100 mmol, 0.100 g) was dissolved in 2 ml methanol and 100 μ l 1 M HCl was added under stirring. The catalyst Pd on C with 10 weight-% loading (0.030 g) was added and the flask was set under H_2 atmosphere by setting the sample 3 times under vacuum and subsequently flooding it with H_2 . The reaction was stirred for 24 h, the Pd/C was filtered off over celite and the solvent was evaporated. During this synthesis, the ester moieties of the molecule have react with the present methanol via transesterification so **compound 15** was not obtained. To examine the stability of **compound 14**, various synthesis conditions have been tested (Table - EP - 2).

Table - EP - 2. Stability tests of **compound 14** under different synthesis conditions.

starting material	0.020 g compound 14					
solvent	0.4 ml MeOH	0.4 ml MeOH	0.5 ml MeOH	0.5 ml THF	0.4 ml THF	1.6 ml EtOH 345 μ l H_2O
catalyst	20 μ l 1 M HCl	20 μ l 1 M KOH	4 mg Pd/C, H_2	4 mg Pd/C, H_2	20 μ l 1 M KOH	50 μ l NH_3 (28 % in water)
duration	stirring for 24 h at room temperature					16 h

Compound 16:



Chemical formula: C_3H_7ClNO

Molecular weight: 147.60 g/mol

2-Chloropropylamine hydrochloride (1 eq., 100 mmol, 11.002 g) was dissolved in 50 ml CH_2Cl_2 . Acryloylchloride (1.2 eq, 120 mmol, 9.874 ml) was dissolved in 50 ml CH_2Cl_2 and quickly added under agitation to the 2-chloropropylamine hydrochloride solution at 0 $^{\circ}C$. Then TEA (2.2 eq., 220 mmol, 30.496 ml) was also diluted with 50 ml CH_2Cl_2 and dropwise added to the reaction at 0 $^{\circ}C$ under agitation over 1 h. The reaction was finally stirred for 3.5 h at room temperature. The batch was filtered and the residue (TEAxHCl) was rinsed with CH_2Cl_2 . To the filtrate, 8 g NaOH in 30 ml water was added. The phases were separated and the water phase was extracted with 2 x 30 ml CH_2Cl_2 . The combined organic phases were dried over $MgSO_4$, filtrated and concentrated under vacuum to yield **compound 16** (88 %) as orange to brown oil.

¹H NMR (300 MHz, CDCl₃, δ [ppm]):

6.53 (br/s, 1H, 3-NH-4), 6.29 (dd, J = 1.66 Hz / 16.97 Hz, 1H, **1**), 6.16 (dd, J = 10.08 Hz / 16.97 Hz, 1H, **2**), 5.69 (dd, J = 1.66 Hz / 10.08 Hz, 1H, **1**), 3.65 (t, J = 6.33 Hz, 2H, **6**), 3.54 (q, J = 6.48 Hz, 2H, **4**), 2.09 (p, J = 6.52 Hz, 2H, **5**).

¹³C NMR (75 MHz, CDCl₃, δ [ppm]):

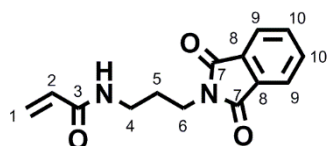
166.02 (1C, **3**), 130.81 (1C, **2**), 126.42 (1C, **1**), 42.55 (1C, **6**), 37.03 (1C, **4**), 32.05 (1C, **5**).

EA

calculated: C, 48.82; H, 6.83; Cl, 24.02; N, 9.49; O, 10.84

found: C, 47.92; H, 6.74; N, 9.08

Compound 17:



Chemical formula: C₁₄H₁₄N₂O₃

Molecular weight: 258.28 g/mol

Potassium phthalimide (1 eq., 46 mmol, 8.52 g) was dissolved in 24 ml DMF. N-Acryloyl-3-chloropropylamine (1 eq, 46 mmol, 6.79 g) was dissolved in 25 ml DMF and quickly added under agitation to the potassium phthalimide solution. Then the reaction was stirred for 15 h at 75 °C. The batch was filtered and the residue (KCl) was rinsed with DMF. The solvent of the filtrate was evaporated and the crude solid was dissolved in 50 ml CH₂Cl₂. The organic phase was washed with 3 x 30 ml brine, dried over MgSO₄, filtrated and concentrated under vacuum. The obtained orange to brown crude product was then again dissolved in 10 ml CH₂Cl₂ per g powder and was purified by column chromatography on 50 g silica gel per g powder with 50 % ethyl acetate in CH₂Cl₂ to yield the pure **compound 17** (55 %) as white powder.

¹H NMR (300 MHz, CDCl₃, δ [ppm]):

7.93-7.86 (m, 2H, **9**), 7.84-7.74 (m, 2H, **10**), 6.49 (br/s, 1H, 3-NH-4), 6.30 (dd, J = 1.73 Hz / 17.04 Hz, 1H, **1**), 6.17 (dd, J = 10.00 Hz / 17.04 Hz, 1H, **2**), 5.66 (dd, J = 1.73 Hz / 10.00 Hz, 1H, **1**), 3.80 (t, J = 6.30 Hz, 2H, **6**), 3.37 (q, J = 6.28 Hz, 2H, **4**), 1.94 (p, J = 6.23 Hz, 2H, **5**).

¹³C NMR (75 MHz, CDCl₃, δ [ppm]):

168.79 (2C, **7**), 165.73 (1C, **3**), 134.77 (2C, **10**), 131.92 (2C, **8**), 131.01 (1C, **1**), 126.33 (1C, **2**), 123.39 (2C, **9**), 36.06 (1C, **4**), 34.92 (1C, **6**), 28.21 (1C, **5**).

MS (EI, m/z)

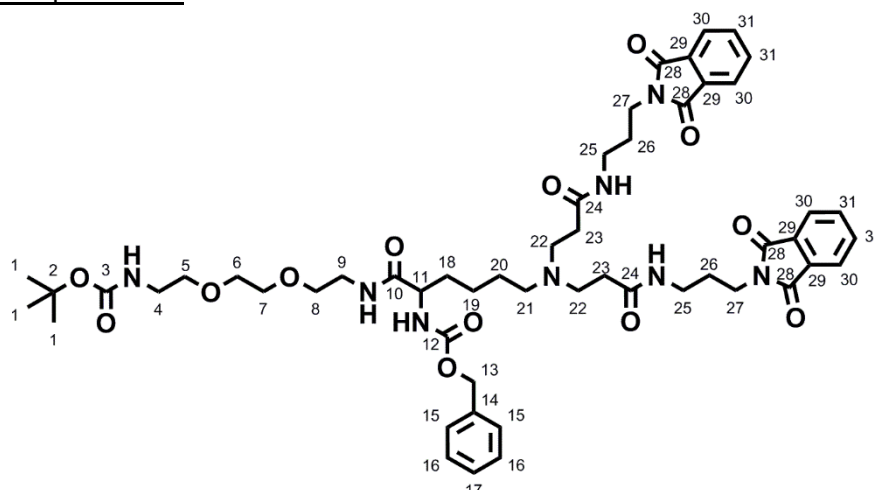
[M] calculated: 258.10, found: 258.10

EA

calculated: C, 65.11; H, 5.46; N, 10.85; O, 18.58

found: C, 64.45; H, 5.39; N, 10.45

Compound 18:



Chemical formula:
C₅₃H₇₀N₈O₁₃

Molecular weight:
1027.19 g/mol

Compound 12 (1 eq., 2.651 mmol, 1.354 g) was dissolved in 35 ml methanol and **compound 17** (5 eq., 13.258 mmol, 3.424 g) was added. The reaction batch was stirred for 7 days at 75 °C. The solvent was evaporated and the crude product was dissolved in CH₂Cl₂. Excess acrylamide (**compound 17**) was removed over a column (25 g silica per g crude product) with 5 % methanol in CH₂Cl₂. To obtain the product (**compound 18**), the polarity of the eluent was increased (10 % methanol in CH₂Cl₂). The solvent was evaporated to obtain the pure **compound 18** (57 %) as orange, clear, highly viscous liquid.

¹H NMR (300 MHz, DMSO, δ [ppm]):

7.92 (t, J = 5.40 Hz, 2H, 24-NH-25), 7.88-7.81 (m, 9H, 9-NH-10, **30**, **31**), 7.36-7.31 (m, 6H, **15-17**, 11-NH-12), 6.78 (t, J = 5.73 Hz, 1H, 3-NH-4), 5.01 (s, 2H, **13**), 3.95-3.88 (m, 1H, **11**), 3.57 (t, J = 7.14 Hz, 4H, **27**), 3.49 (s, 4H, **6**, **7**), 3.39-3.33 (m, 4H, **5**, **8**), 3.20-3.16 (m, 2H, **9**), 3.07-3.01 (m, 6H, **4**, **25**), 2.59 (t, J = 6.74 Hz, 4H, **22**), 2.31 (t, J = 6.00 Hz, 2 H, **21**), 2.18 (t, J = 6.75 Hz, 4 H, **23**), 1.74 (p, J = 7.06 Hz, 4 H, **26**), 1.59-1.48 (br/m, 2H, **18**), 1.37 (s, 9H, **1**), 1.28-1.15 (br/m, 4H, **20**, **19**).

¹³C NMR (75 MHz, DMSO, δ [ppm]):

172.45 (1C, **10**), 171.73 (2C, **24**), 168.32 (4C, **28**), 156.34 (1C, **12**), 156.03 (1C, **3**), 137.49 (1C, **14**), 134.77 (4C, **31**), 132.09 (4C, **29**), 128.75/128.12 (5C, **15-17**), 123.42 (4C, **30**), 78.03 (1C, **2**), 69.99/69.91/69.63/69.43 (4C, **5-8**), 65.80 (1C, **13**), 55.14 (1C, **11**), 53.00 (1C, **21**), 49.83 (2C, **22**), ~40 +38.98 (2C, **4**, **9** in solvent signal), 36.57 (2C, **25**), 35.95 (2C, **27**), 33.50 (2C, **23**), 32.47 (1C, **18**), 28.68 (5C, **1**, **26**), 26.58 (1C, **20**), 23.83 (1C, **19**).

MS (FD)

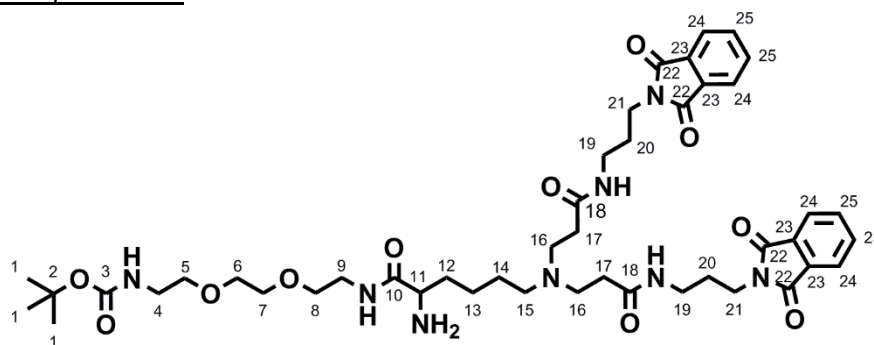
[M+H]⁺ calculated: 1027.51, found: 1027.52

EA

calculated: C, 61.97; H, 6.87; N, 10.91; O, 20.25

found: C, 62.27; H, 7.04; N, 11.37

Compound 19:



Chemical formula:
C₄₅H₆₄N₈O₁₁

Molecular weight:
893.05 g/mol

Compound 18 (1 eq., 0.574 mmol, 0.590 g) was dissolved in 4 ml methanol and 1 ml water. Acetic acid (4 eq, 2.298 mmol, 131.5 μ l) is added under stirring. The catalyst Pd on C with 10 weight-% loading (0.059 g) was added and the flask was set under H₂ atmosphere by setting the sample 3 times under vacuum and subsequently flooding it with H₂. The reaction was stirred for 24 h under H₂ atmosphere, the Pd/C was filtered off over celite and the solvent was evaporated. The crude product was dissolved in 10 ml water and washed with 3 times 10 ml CH₂Cl₂ to remove unreacted **compound 18**. The water phase was then neutralized with saturated NaHCO₃ and extracted with 3 times 10 ml CH₂Cl₂. The combined organic phases were dried over MgSO₄, filtrated and concentrated under vacuum to yield **compound 19** (54 %) as transparent solid.

¹H NMR (300 MHz, DMSO, δ [ppm]):

7.92 (m, 2H, 18-NH-19), 7.88-7.80 (m, 9H, 9-NH-10, **24**, **25**), 6.75 (t, J = 5.47 Hz, 1H, 3-NH-4), 3.56 (t, J = 7.16 Hz, 4H, **21**), 3.49 (s, 4H, **6**, **7**), 3.43-3.29 (m, 4H, **5**, **8**), 3.27-3.13 (m, 2H, **9**), 3.10-2.99 (m, 7H, **4**, **19**, **11**), 2.59 (t, J = 7.10 Hz, 4H, **16**), 2.32 (t, J = 6.95 Hz, 2 H, **15**), 2.15 (t, J = 7.06 Hz, 4 H, **17**), 1.71 (p, J = 7.03 Hz, 4 H, **20**), 1.59-1.48 (br/m, 2H, **12**), 1.36 (s, 9H, **1**), 1.28-1.15 (br/m, 4H, **14**, **13**).

¹³C NMR (75 MHz, DMSO, δ [ppm]):

175.41 (1C, **10**), 171.76 (2C, **18**), 168.33 (4C, **22**), 156.02 (1C, **3**), 134.78 (4C, **25**), 132.09 (4C, **23**), 123.42 (4C, **24**), 78.04 (1C, **2**), 69.91-69.56 (4C, **5-8**), 54.98 (1C, **11**), 53.12 (1C, **15**), 49.90 (2C, **16**), ~40 +38.98 (2C, **4**, **9** in solvent signal), 36.68 (2C, **19**), 35.96 (2C, **21**), 35.34 (1C, **12**), 33.56 (2C, **17**), 28.65 (5C, **1**, **20**), 26.86 (1C, **14**), 23.61 (1C, **13**).

MS (EI, m/z)

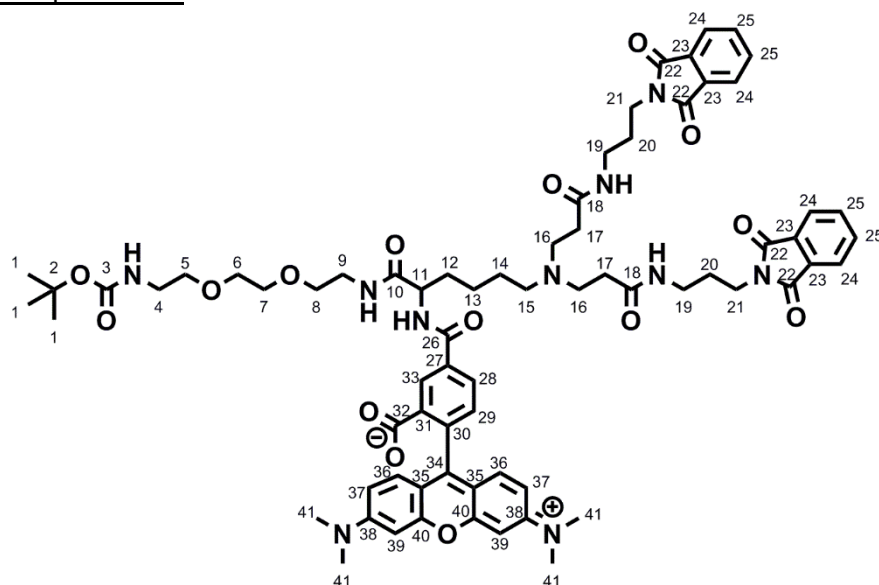
[M+H]⁺ calculated: 893.47; found: 893.5

[M+Na]⁺ calculated: 915.47; found: 915.5

EA

calculated: C, 60.52; H, 7.22; N, 12.55; O, 19.71

found: C, 58.66; H, 7.17; N, 11.42

Compound 20:

Chemical Formula:
C₇₀H₈₄N₁₀O₁₅

Molecular Weight:
1305.50 g/mol

Compound 19 (1.2 eq., 0.056 mmol, 0.050 g) was dissolved in 0.25 ml DMF, TEA (2 eq., 0.093 mmol, 13.00 µl) was added and stirred for 10 min. NHS-Rhodamine (5-/6-carboxytetramethylrhodamine, succinimidyl ester, 1 eq., 0.047 mmol, 0.025 g) was dissolved in 0.3 ml DMF and added to the reaction batch. The reaction was carried out for 16 h under stirring at room temperature in darkness. All volatile compounds were evaporated and the crude product was dissolved in 5 ml CH₂Cl₂. The organic phase was washed with 3 x 5 ml saturated NaHCO₃ and 3 x 1 ml 10 vol-% acetic acid in water. The organic phase was subsequently dried over MgSO₄, filtrated and concentrated under vacuum to yield **compound 20** (85 %) as pink highly viscous liquid.

¹H NMR (300 MHz, CDCl₃, δ [ppm]):

8.66 (s, 1H, **33**), 8.25 / 8.14 (d / d, J = 8.02 / 9.43 Hz, 1H, **27/28** 5/6-isomere), 7.78-7.76 (m, 5H, **24**, 9-NH-10), 7.68-7.64 (m, 6H, **25**, 18-NH-19), 7.20 (d, J = 7.97 Hz, 1H, **29**), 6.90-6.87 (m, 2H, **36**), 6.62-6.59 (m, 6H, **37**, **39**, 3-NH-4, 11-NH-26), 4.73 (m, 1H, **11**), 3.68 (t, J = 6.90 Hz, 4H, **21**), 3.57-3.46 (m, 10H, **5-8**, **9**), 3.26-3.20 (m, 10H, **4**, **16**, **19**), 3.11 (s, 12H, **41**), 2.89 (br/s, 2H, **15**), 2.69 (t, J = 6.67 Hz, 4H, **17**), 1.86-1.75 (m, 8H, **20**, **12**, **14**), 1.42-39 (m, 11H, **1**, **13**).

¹³C NMR (151 MHz, CDCl₃, δ [ppm]):

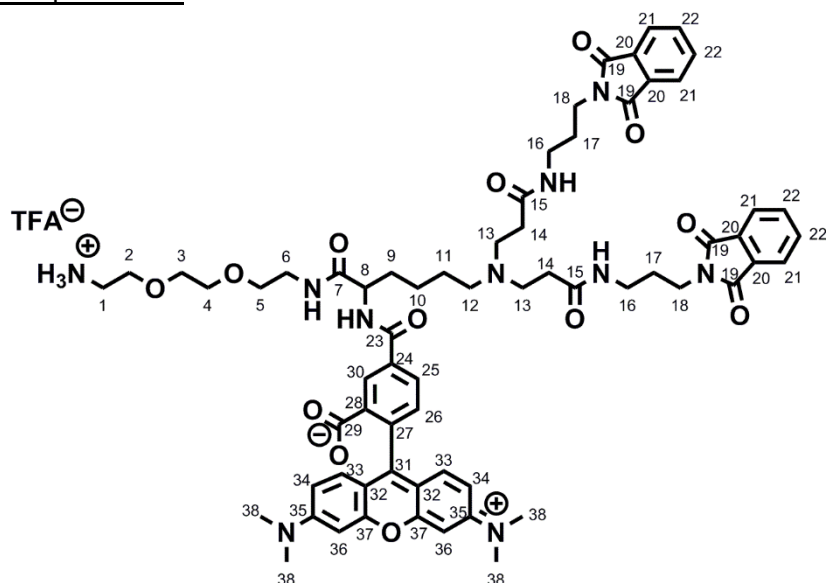
172.18 (1C, **10**), 170.98 (2C, **18**), 168.98 (1C, **26**), 168.33 (4C, **22**), 166.29 (1C, **32**), 162.75 (1C, **34**), 156.07 (1C, **3**), 154.41 (2C, **40**), 153.79 (2C, **38**), 135.35 (1C, **27/28** 5/6-isomere), 133.93/133.89 (5C, **25**, **30**), 132.30 (1C, **27/28** 5/6-isomere), 131.88 (4C, **23**), 129.68 (2C, **36**), 126.04 (1C, **33**), 125.68 (1C, **31**), 123.14 (5C, **24**, **29**), 110.47 (2C, **37**), 108.76 (2C, **35**), 97.61 (2C, **39**), 79.11 (1C, **2**), 70.07/69.47 (4C, **5-8**), 53.45 (1C, **11**), 52.52 (1C, **15**), 49.34 (2C, **16**), 40.27/39.31 (6C, **4**, **9**, **41**), 36.64 (2C, **19**), 35.33 (2C, **21**), 31.72 (2C, **17**), 29.58 (1C, **12**), 28.31/28.17 (5C, **1**, **20**), 23.57 (1C, **14**), 22.95 (1C, **13**).

MS (ESI, m/z)

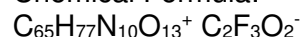
[M+H]⁺ calculated: 1305.61, found: 1305.6

[M+Na]⁺ calculated: 1327.60, found: 1327.6

Compound 21:



Chemical Formula:



Molecular Weight:

1206.39 g/mol

+ 113.02 g/mol

Compound 20 (1 eq., 0.038 mmol, 0.050 g) was dissolved in 3 ml CH_2Cl_2 and trifluoroacetic acid (15 eq., 0.575 mmol, 44 μl) was dropwise added under stirring. The reaction was stirred for 16 h at room temperature. At the end of the reaction the solvent and all volatile side products were evaporated under vacuum. To eliminate all free TFA, a coevaporation with 3 x 5 ml toluene was carried out to yield the pure **compound 21** (quantitative) as pink solid in TFA-salt form.

^1H NMR (600 MHz, MeOD, δ [ppm]):

8.79 (d, $J = 1.86$ Hz, 1H, **30**), 8.42 (dd, $J = 1.88 / 7.87$ Hz, 1H, **24/25** 5/6-isomere), 7.76 (s, 8H, **21, 22**), 7.56 (d, $J = 7.89$ Hz, 1H, **26**), 7.08 (dd, $J = 6.02 / 9.48$ Hz, 2H, **33**), 7.01 (dd, $J = 2.42 / 9.48$ Hz, 2H, **34**), 6.85 (dd, $J = 2.42 / 10.90$ Hz, 2H, **36**), 4.63-4.58 (m, 1H, **8**), 3.77-3.72 (m, 2H, **2**), 3.69 (s, 6H, **3-5**), 3.65-3.54 (m, 8H, **18, 13**), 3.53-3.41 (m, 4H, **12, 6**), 3.26 (s, 12H, **38**), 3.42-3.12 (m, 6H, **16, 1**), 2.81 (br/s, 4H, **14**), 2.06-1.95 (m, 2H, **9**), 1.95-1.89 (m, 2H, **11**), 1.80 (br/s, 4H, **17**), 1.65-1.58 (m, 2H, **10**).

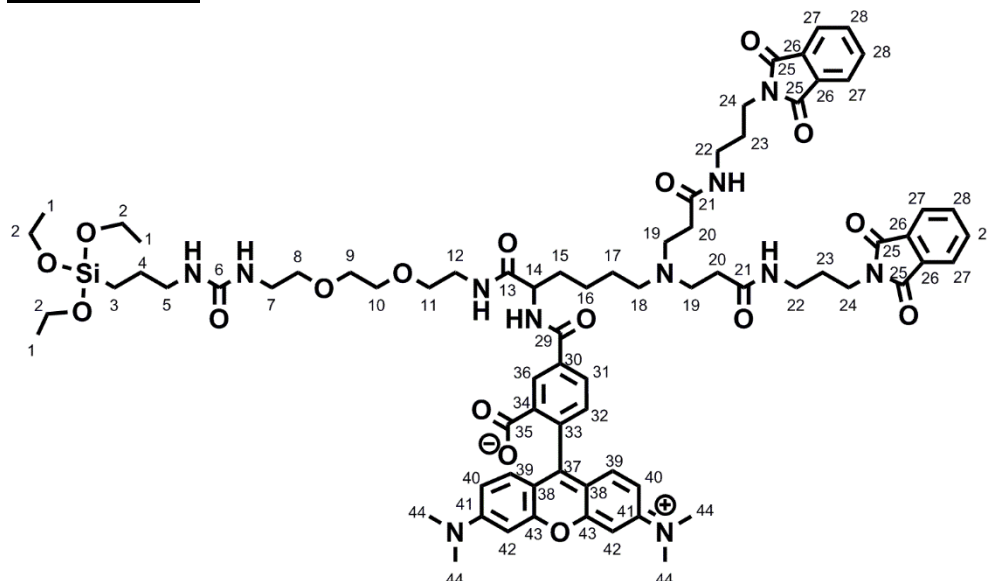
^{13}C NMR (151 MHz, MeOD, δ [ppm]):

173.04 (1C, **7**), 171.07 (2C, **15**), 168.75 (4C, **19**), 167.10 (1C, **23**), 165.94 (1C, **29**), 159.09 (1C, **31**), 157.53/157.43 (4C, **35, 37**), 136.84 (1C, **24/25** 5/6-isomere), 135.85 (1C, **27**), 134.02 (4C, **22**), 131.79 (4C, **20**), 131.53 (1C, **28**), 131.17 (3C, **24/25** 5/6-isomere, **30**), 130.43 (3C, **26, 33**), 122.72 (4C, **21**), 114.12 (2C, **34**), 113.27 (2C, **32**), 96.06 (2C, **36**), 69.97/69.13/66.52 (4C, **2-5**), 54.30 (1C, **8**), 52.92 (1C, **12**), 50.08 (2C, **13**), 39.53 (4C, **38**), 39.33/39.00 (3C, **6, 16**), 36.64 (1C, **1**), 35.03 (2C, **18**), 30.94 (1C, **9**), 27.75 (4C, **17, 14**), 23.19 (1C, **11**), 22.60 (1C, **10**).

MS (ESI, m/z)

$[\text{M}+\text{H}]^{+}$ calculated: 1205.57, found: 1305.5

$[\text{M}+\text{Na}]^{+}$ calculated: 1227.58, found: 1227.2

Compound 22:Chemical Formula: C₇₅H₉₇N₁₁O₁₇Si

Molecular Weight: 1452.75 g/mol

Compound 21 (1.05 eq., 0.0288 mmol, 0.038 g) was dispersed in 6 ml CH₂Cl₂, TEA (8.4 eq., 0.2304 mmol, 32.11 µl) was added and stirred until **compound 21** was solubilized. Isocyanatopropyltriethoxysilane (1.0 eq., 0.0274 mmol, 6.78 µl) was added and the reaction proceeded at room temperature for 16 h. Afterwards the solvent and excess TEA were evaporated to yield **compound 22** as purple solid (quantitative).

¹H NMR (600 MHz, CDCl₃, δ [ppm]):

8.50 (s, 1H, **36**), 8.13 (d, J = 8.74 Hz, 1H, **30/31** 6/5-isomere), 7.77-7.74 (m, 5H, **27**, 12-NH-13), 7.68-7.64 (m, 5H, **28**, 14-NH-29), 7.58 (br/s, 2H, 21-NH-22), 7.20 (d, J = 7.93 Hz, 1H, **32**), 6.64 (br/s, 2H, **39**), 6.50 (s, 2H, **40**), 6.45-6.43 (m, 2H, **42**), 5.59-5.53 (br/m, 2H, 5-NH-6-NH-7), 4.71-4.64 (m, 1H, **14**), 3.80-3.76 (m, 6H, **2**), 3.70-3.63 (m, 4H, **24**), 3.55-3.14 (m, 18H, **7-12**, **5**, **22**), 3.01 (s, 12H, **44**), 2.85-2.83 (m, 4H, **19**), 2.53 (br/s, 2H, **18**), 2.42 (br/s, 4H, **20**), 2.02-1.95 (m, 2H, **15**), 1.86-1.79 (m, 6H, **23**, **17**), 1.60-1.53 (m, 4H, **4**, **16**), 1.21-1.15 (m, 9H, **1**), 0.60-0.57 (m, 2H, **3**).

¹³C NMR (151 MHz, CDCl₃, δ [ppm]):

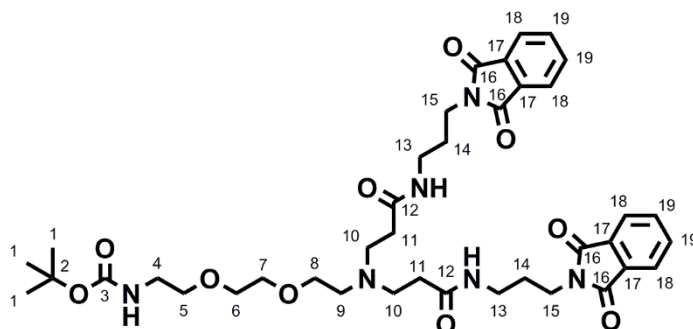
172.13 (1C, **13**), 169.02 (2C, **21**), 168.48 (4C, **25**), 168.33 (1C, **29**), 166.13 (1C, **35**), 162.01 (1C, **37**), 158.95 (1C, **6**), 153.59 (2C, **43**), 152.85 (2C, **41**), 135.72 (2C, **33**, **30/31** 6/5-isomere), 133.99 (4C, **28**), 131.98 (4C, **26**), 131.88 (3C, **30/31** 5/6-isomere, **23**), 129.09 (2C, **39**), 126.81 (1C, **36**), 123.21 (4C, **27**), 119.75 (1C, **32**), 109.50 (2C, **40**), 107.18 (2C, **38**), 98.12 (2C, **42**), 70.62/70.30/69.60 (4C, **8-11**), 58.34 (3C, **2**), 54.07 (1C, **14**), 53.44 (1C, **18**), 49.98 (2C, **19**), 42.95 (1C, **5**), 40.29/40.20 (5C, **44**, **7**), 39.55 (1C, **12**), 36.48 (2C, **22**), 35.48 (2C, **24**), 28.54/28.41 (4C, **20**, **23**), 23.74/23.63/23.38 (3C, **4**, **17**, **16**), 18.30 (3C, **1**), 7.62 (1C, **3**).

MS (ESI, m/z)[M+H]⁺ calculated: 1452.68, found: 1452.7[M+Na]⁺ calculated: 1474.69, found: 1474.7

Compound 23:

Chemical formula: $C_{39}H_{52}N_6O_{10}$

Molecular weight: 764.88 g/mol



Compound 1 (1 eq., 3.020 mmol, 0.750 g) and **compound 17** (5 eq., 15.101 mmol, 3.901 g) were dissolved in a total volume of 30 ml methanol and the reaction mixture was stirred at 75 °C for 7 days. The solvent was evaporated and the crude product was dissolved in CH_2Cl_2 . Over a column (25 g silica per g crude product), the excess acrylamide (**compound 17**) was removed with 2 % methanol in CH_2Cl_2 . To obtain the product, the polarity of the eluent was increased (6 % methanol and in CH_2Cl_2). The solvent was evaporated to obtain the pure **compound 23** (46 %) as slightly yellow, clear, highly viscous liquid.

1H NMR (300 MHz, $CDCl_3$, δ [ppm]):

7.81-7.79 (m, 4H, **18**), 7.71-7.68 (m, 4H, **19**), 7.31 (br/s, 2H, 12-NH-13), 5.13 (br/s, 1H, 3-NH-4), 3.73 (t, $J = 6.90$ Hz, 4H, **15**), 3.61-3.57 (m, 6H, **5-7**), 3.54-3.47 (m, 2H, **8**), 3.29-3.25 (m, 6H, **4,13**), 2.85 (t, $J = 6.53$ Hz, 4H, **10**), 2.74 (t, $J = 5.58$ Hz, 2 H, **9**), 2.43 (t, $J = 6.47$ Hz, 4 H, **11**), 1.87 (p, $J = 6.77$ Hz, 4 H, **14**), 1.42 (s, 9H, **1**)

^{13}C NMR (75 MHz, DMSO, δ [ppm]):

171.73 (2C, **12**), 171.73 (4C, **16**), 156.01 (1C, **3**), 134.78 (4C, **19**), 132.07 (4C, **17**), 123.41 (4C, **18**), 78.02 (1C, **2**), 70.00/69.91/69.63 (4C, **5-8**), 52.70 (1C, **9**), 50.39 (2C, **10**), ~40.00 (1C, **4**), 36.69 (2C, **13**), 35.94 (2C, **15**), 33.72 (2C, **11**), 28.67 (5C, **1, 14**)

MS (ESI, m/z)

$[M+H]^+$ calculated: 765.37, found: 765.4

$[M+Na]^+$ calculated: 787.36, found: 787.4

EA

calculated: C, 61.24; H, 6.85; N, 10.99; O, 20.92

found: C, 59.82; H, 6.69; N, 10.84

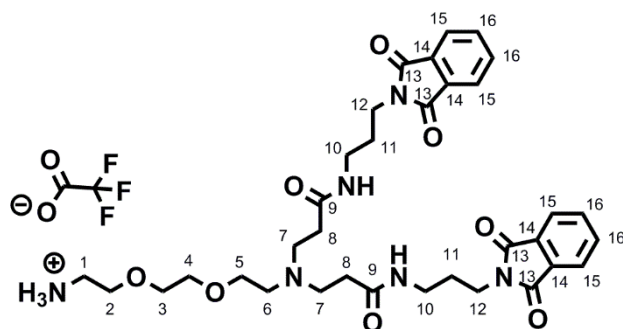
Compound 24:

Chemical formula:

$C_{34}H_{45}N_6O_8^+ C_2F_3O_2^-$

Molecular weight:

664.76 g/mol + 113.02 g/mol



Compound 23 (1 eq., 0.870 mmol, 0.650 g) was dissolved in 40 ml CH_2Cl_2 and trifluoroacetic acid (15 eq., 13.054 mmol, 999 μ l) was dropwise added under stirring. The reaction was stirred for 16 h at room temperature. At the end of the reaction the solvent and all volatile side products

were evaporated under vacuum. To eliminate all free TFA, a coevaporation with 3 x 20 ml toluene was carried out to yield the pure **compound 24** (quantitative) as yellowish, clear, highly viscous liquid in TFA-salt form.

¹H NMR (300 MHz, CDCl₃, δ [ppm]):

8.11 (s, 3H, **H₃N⁺-1**), 7.78-7.76 (m, 4H, **15**), 7.73-7.68 (m, 6H, **16**, 9-NH-10), 3.85-3.83 (m, 2H, **5**), 3.75-3.67 (m, 6H, **2**, **12**), 3.64 (s, 4H, **3**, **4**), 3.57-3.56 (m, 4H, **7**), 3.45-3.43 (m, 2H, **6**), 3.28-3.19 (m, 6H, **1**, **10**), 2.84 (t, J = 5.97, 4H, **8**), 1.86 (p, J = 6.58 Hz, 4H, **11**)

¹³C NMR (75 MHz, CDCl₃, δ [ppm]): (signals of TFA are not attributed)

170.12 (2C, **9**), 168.24 (4C, **13**), 133.83 (4C, **16**), 131.59 (4C, **14**), 122.95 (4C, **15**), 69.82 (2C, **3**, **4**), 66.06 (1C, **2**), 64.00 (1C, **5**), 53.16 (1C, **6**), 50.53 (2C, **7**), 39.52 (1C, **1**), 36.65 (2C, **10**), 34.86 (2C, **12**), 28.95 (2C, **8**), 27.58 (2C, **11**)

MS (ESI, m/z)

[M-TFA+H]⁺ calculated: 665.32 found: 665.3

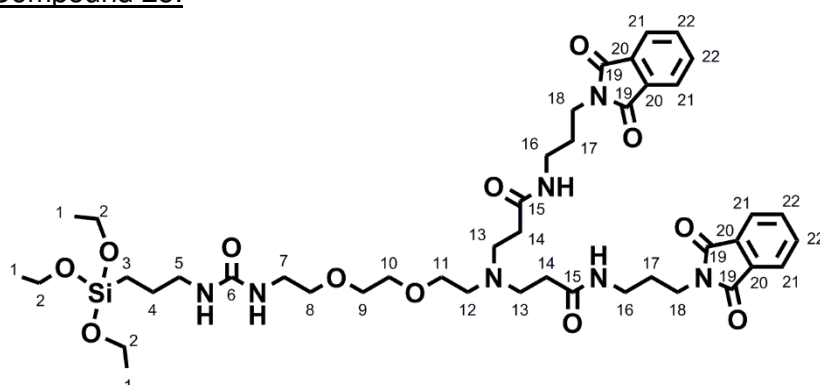
[M-TFA+Na]⁺ calculated: 687.31 found: 687.3

EA

calculated: C, 61.43; H, 6.67; N, 12.64; O, 19.25

found: C, 59.4; H, 6.57; N, 10.71

Compound 25:



Chemical formula:

C₄₄H₆₅N₇O₁₂Si

Molecular weight:

912.13 g/mol

Compound 24 (1.05 eq., 0.210 mmol, 0.163 g) was dissolved in 6 ml CH₂Cl₂ and TEA (8.4 eq., 1.68 mmol, 234.2 μl) was added. Subsequently isocyanatopropyltriethoxysilane (1 eq., 0.200 mmol, 49.5 μl) was added under stirring and the reaction proceeded at room temperature for 16 h. Then the solvent and excess TEA were evaporated to yield **compound 25** as yellow highly viscous liquid (quantitative).

¹H NMR (300 MHz, CDCl₃, δ [ppm]): (signals of TFA-TEA are not attributed)

7.83-7.72 (m, 4H, **22**), 7.72-7.64 (m, 4H, **21**), 7.48 (br/s, 2H, 15-NH-16), 5.58/5.47 (2*br/s, 2H, 5-NH-6, 6-NH-7), 3.82-3.68 (m, 10H, **2**, **18**), 3.62-3.46 (m, 10H, **8-12**), 3.34-3.22 (m, 8H, **7**, **16**, **5**), ~3.12 (m, 4H, **13**), 1.85 (p, J = 6.70 Hz, 4 H, **17**), 1.55 (p, J = 7.71, 2H, **4**), 1.25-1.16 (m, 13H, **14**, **1**), 0.61-0.58 (m, 2H, **3**).

¹³C NMR (75 MHz, CDCl₃, δ [ppm]): (signals of TFA-TEA are not attributed)

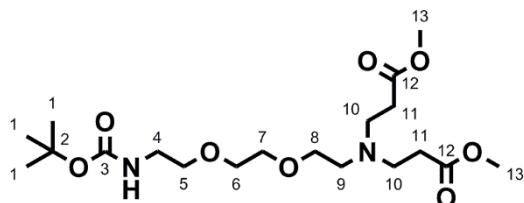
168.80 (4C, **19**), 162.61 (2C, **15**), 159.17 (1C, **6**), 134.39 (4C, **22**), 132.27 (4C, **20**), 123.55 (4C, **21**), 71.39/70.76/70.68 (4C, **8-11**), 58.78 (3C, **2**), 53.42 (1C, **12**), 51.06 (2C, **13**), 43.19 (1C, **5**), 40.45 (1C, **7**), 36.76 (2C, **16**), 35.70 (2C, **18**), 30.00 (2C, **14**), 28.76 (2C, **17**), 24.13 (1C, **4**), 18.61 (3C, **1**), 8.00 (1C, **3**).

MS (ESI, m/z)

[M+H]⁺ calculated: 912.45, found: 912.4

[M+Na]⁺ calculated: 934.44, found: 934.4

Compound 26:^{***}



Chemical formula: C₁₉H₃₆N₂O₈

Molecular weight: 420.50 g/mol

Compound 1 (1 eq., 24.16 mmol, 6.00 g) was dissolved in 100 ml methanol and methylacrylate (10 eq., 241.6 mmol, 20.8 g) was added. The reaction mixture was stirred at 50 °C for 3 days. The solvent and the excess methyl acrylate were evaporated to obtain the pure **compound 26** (quantitative) as slightly yellow oil.

¹H NMR (300 MHz, CDCl₃, δ [ppm]):

5.09 (s, 1H, 3-NH-4), 3.66 (s, 6H, **13**), 3.58 (s, 4H, **7, 6**), 3.52 (t, J = 5.4 Hz, 4H, **8, 5**), 3.31 (dd, J = 10.4 Hz, 2H, **4**), 2.83 (t, J = 7.1 Hz, 4H, **10**), 2.67 (t, J = 6.1 Hz, 2H, **9**), 2.46 (t, J = 7.1 Hz, 4H, **11**), 1.38 (s, 9H, **1**).

¹³C NMR (75 MHz, CDCl₃, δ [ppm]):

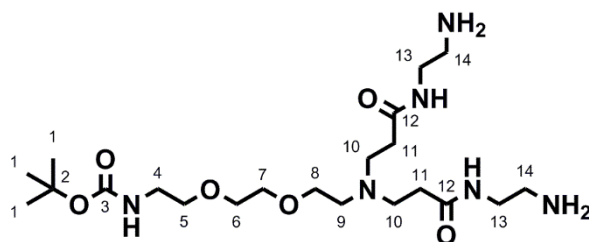
172.92 (2C, **12**), 156.01 (1C, **3**), 79.16 (1C, **2**), 70.39/70.28 (4C, **5-8**), 53.23 (1C, **9**), 51.58 (2C, **13**), 49.91 (2C, **10**), 40.38 (1C, **4**), 32.52 (2C, **11**), 29.57 (3C, **1**).

MS (ESI, m/z)

[M+H]⁺ calculated: 421.25, found: 421.2

[M+Na]⁺ calculated: 443.24, found: 443.2

Compound 27:^{†††}



Chemical formula: C₂₁H₄₄N₆O₆

Molecular weight: 467.62 g/mol

Compound 26 (1 eq., 22.8 mmol, 9.57 g) was dissolved in 100 ml methanol and ethylenediamine (80 eq., 1824 mmol, 109.4 g) was added. The reaction mixture was stirred at 25 °C for 5 days. The solvent and the excess diamine were evaporated. The compound was then washed with 3 x 20 ml diethyl ether to remove di-boc protected 2,2-(ethylenedioxy)bis(ethylamine) which was a side product of **compound 1**. This compound was soluble in diethylether while the desired product was not and thus sedimented. The pure **compound 27** (92 %) was obtained as yellow oil.

¹H NMR (300 MHz, CDCl₃, δ [ppm]):

7.40 (s, 2H, 12-NH-13), 5.69 (s, 1H, 3-NH-4), 3.57 (s, 4H, **7, 6**), 3.52 (m, 4H, **8, 5**), 3.27 (dd,

^{***} This synthesis route was not completed; the reaction is therefore not discussed in Chapter III

^{†††} This synthesis route was not completed; the reaction is therefore not discussed in Chapter III

$J = 11.7$, 6H, **4**, **13**), 2.81-2.73 (m, 8H, **10**, **14**), 2.65 (t, $J = 5.3$ Hz, 2H, **9**), 2.35 (t, $J = 6.2$ Hz, 4H, **11**), 1.57 (s, 4H, 14-NH₂), 1.42 (s, 9H, **1**).

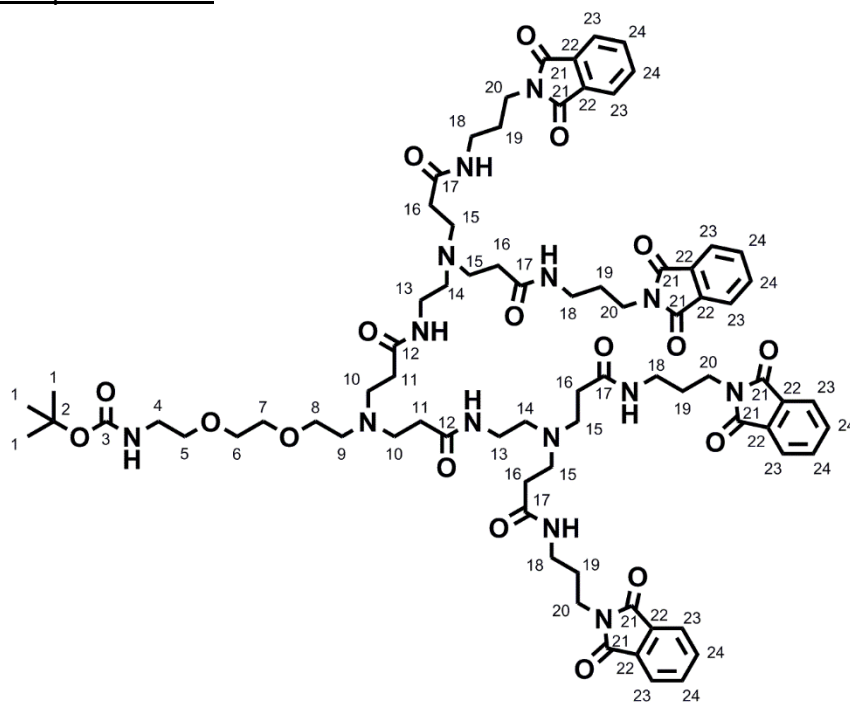
¹³C NMR (75 MHz, CDCl₃, δ [ppm]):

172.88 (2C, **12**), 156.26 (1C, **3**), 79.23 (1C, **2**), 70.39 (2C, **6**, **7**), 69.39 (2C, **5**, **8**), 53.81 (1C, **9**), 51.07 (2C, **10**), 42.24 (2C, **13**), 41.56 (2C, **14**), 40.38 (1C, **4**), 34.42 (2C, **11**), 28.55 (3C, **1**).

MS (ESI, m/z) – exact mass

[M+Na]⁺ calculated: 499.3214, found: 499.3199

Compound 28:†††



Chemical formula:

C₇₇H₁₀₀N₁₄O₁₈

Molecular weight:

1509.73 g/mol

Compound 27 (1 eq., 1.621 mmol, 0.758 g) and **compound 17** (8 eq., 12.970 mmol, 3.350 g) were dissolved in a total volume of 30 ml methanol and the reaction mixture was stirred at 75 °C for 14 days. The solvent was evaporated and the crude product was dissolved in CH₂Cl₂. Over a column (25 g silica per g crude product), the excess of reactant (**compound 17**) and side products were removed with 1 % methanol and 2 % TEA in CH₂Cl₂. To obtain the product (**compound 28**), the polarity of the eluent was slightly increased (2 % methanol and 2 % TEA in CH₂Cl₂). The solvent was evaporated to obtain the pure **compound 28** (21 %) as yellow, highly viscous liquid.

¹H NMR (300 MHz, CDCl₃, δ [ppm]):

7.79-7.76 (m, 8H, **23**), 7.69-7.66 (m, 8H, **24**), 7.48 (t, $J = 5.42$, 2H, 12-NH-13), 7.23 (br/s, 4H, 17-NH-18), 5.25 (br/s, 1H, 3-NH-4), 3.81-3.67 (m, 8H, **20**), 3.55-3.44 (m, 8H, **5-8**), 3.29-3.18 (m, 14H, **4**, **13**, **18**), 2.78-2.74 (m, 12H, **10**, **15**), 2.68-2.65 (m, 4H, **14**), 2.54 (t, $J = 5.89$ Hz, 2H, **9**), 2.36 (t, $J = 6.15$ Hz, 8H, **16**), 2.27 (t, $J = 6.06$ Hz, 4H, **11**), 1.87 (p, $J = 6.63$ Hz, 8H, **19**), 1.39 (s, 9H, **1**).

¹³C NMR (75 MHz, CDCl₃, δ [ppm]):

172.71 (2C, **12**), 172.28-171.97 (4C, **17**), 168.13 (8C, **21**), 155.75 (1C, **3**), 133.72 (8C, **24**), 131.68 (8C, **22**), 122.92 (8C, **23**), 79.23 (1C, **2**), 69.91/69.79.39 (2C, **6**, **7**), 68.51 (2C, **5**, **8**),

††† This synthesis route was not completed; the reaction is therefore not discussed in Chapter III

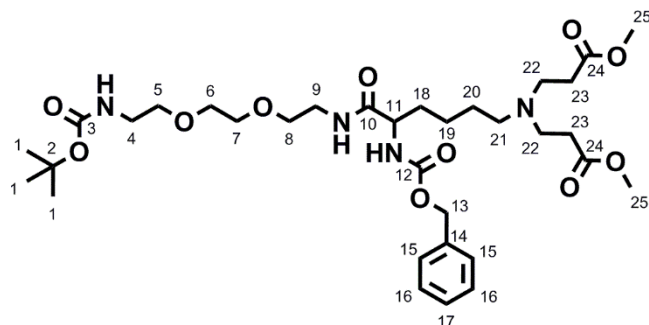
52.69/52.39 (3C, **9**, **14**), 49.95/49.68 (6C, **10**, **15**), 37.63/37.56 (5C, **4**, **18**), 36.12 (2C, **13**), 36.12 (4C, **20**), 35.09 (2C, **11**), 33.96 (4C, **16**), 28.23/28.10 (7C, **1**, **19**).

MS (ESI, m/z)

[M+H]⁺ calculated: 1509.73, found: 1509.7

[M+Na]⁺ calculated: 1531.72, found: 1531.7

Compound 29:§§§



Chemical formula:

C₃₃H₅₄N₄O₁₁

Molecular weight:

682.81 g/mol

Compound 12 (1 eq., 0.257 mmol, 0.131 g) was dissolved in 2.1 ml methanol and methyl acrylate (10 eq., 2.565 mmol, 0.231 ml) was added. The reaction batch was stirred for 3 days at 30 °C. The excess methyl acrylate and solvent were evaporated to obtain the pure **compound 29** (quantitative) as yellow, clear liquid.

¹H NMR (300 MHz, DMSO, δ [ppm]):

7.92 (t, J = 5.55 Hz, 1H, 9-NH-10), 7.38-7.30 (m, 6H, **15-17**, 11-NH-12), 6.77 (br/s, 1H, 3-NH-4), 5.02 (s, 2H, **13**), 3.99-3.91 (m, 1H, **11**), 3.59 (s, 6H, **25**), 3.50 (s, 4H, **6**, **7**), 3.41-3.34 (m, 4H, **5**, **8**), 3.24-3.18 (m, 2H, **9**), 3.08 (appears q, J = 5.97, 2H, **4**), 2.72-2.60 (m, 4H, **22**), 2.44-2.27 (m, 6H, **23**, **21**), 1.61-1.46 (br/m, 2H, **18**), 1.38 (s, 9H, **1**), 1.28-1.16 (br/m, 4H, **20**, **19**)

¹³C NMR (75 MHz, DMSO, δ [ppm]):

172.86 (2C, **24**), 172.46 (1C, **10**), 156.34 (1C, **12**), 156.04 (1C, **3**), 137.53 (1C, **14**), 128.76/128.14 (5C, **15-17**), 78.04 (1C, **2**), 70.00/69.64/69.44 (4C, **5-8**), 65.80 (1C, **13**), 55.10 (1C, **11**), 53.23 (1C, **21**), 51.63 (2C, **25**), 49.08 (2C, **22**), ~40 (2C, **4**, **9** in solvent signal), 32.42 (2C, **23**), 32.40 (1C, **18**), 29.65 (1C, **20**), 28.68 (3C, **1**), 23.60 (1C, **19**)

MS (ESI, m/z)

[M+Na]⁺ calculated: 705.38, found: 705.4

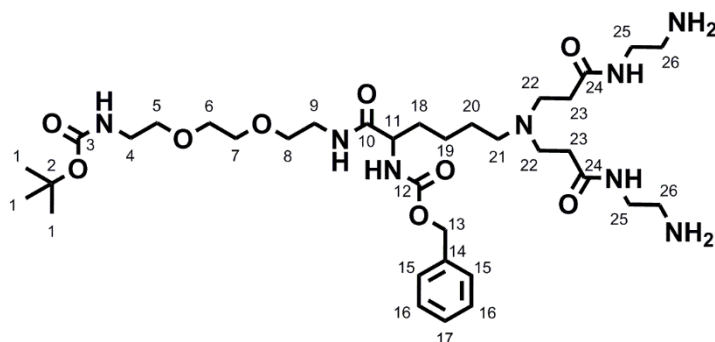
[M+H]⁺ calculated: 683.38, found: 683.4

EA

calc: C, 58.05; H, 7.97; N, 8.21; O, 25.77

found: C, 58.91; H, 7.82; N, 7.16

§§§ This synthesis route was not completed; the reaction is therefore not discussed in Chapter III

Compound 30:****

Chemical formula:

 $C_{35}H_{62}N_8O_9$

Molecular weight:

738.93 g/mol

Compound 29 (1 eq., 0.158 mmol, 0.108 g) was dissolved in 2.1 ml methanol and ethylene diamine (80 eq., 12.64 mmol, 0.846 ml) was added. The reaction batch was stirred for 5 days at 25 °C. The excess ethylene diamine and solvent were evaporated to obtain the pure **compound 30** (quantitative) as yellow, clear and viscous liquid.

^1H NMR (300 MHz, DMSO, δ [ppm]):

8.03-7.91 (m, 1H, 9-**NH**-10), 7.37-7.30 (m, 8H, 24-**NH**-25, **15-17**, 11-**NH**-12), 6.78 (br/s, 1H, 3-**NH**-4), 5.02 (s, 2H, **13**), 4.06 (br/s, 4H, 26-**NH**₂), 4.11-3.90 (m, 1H, **11**), 3.50 (s, 4H, **6, 7**), 3.39-3.45 (m, 4H, **5, 8**), 3.22-3.16 (m, 2H, **9**), 3.10-3.06 (m, 6H, **4, 25**), 2.70-2.60 (m, 8H, **22, 26**), 2.37-2.25 (m, 2H, **21**), 2.20 (t, $J = 6.79$, 4H, **23**), 1.59-1.49 (br/m, 2H, **18**), 1.38 (s, 9H, **1**), 1.28-1.16 (br/m, 4H, **20, 19**)

^{13}C NMR (75 MHz, DMSO, δ [ppm]):

172.50 (2C, **10**), 171.96 (1C, **24**), 156.37 (1C, **12**), 156.05 (1C, **3**), 137.51 (1C, **14**), 128.78/128.22 (5C, **15-17**), 78.06 (1C, **2**), 69.99/69.63/69.44 (4C, **5-8**), 65.82 (1C, **13**), 55.18 (1C, **11**), 53.14 (1C, **21**), 49.93 (2C, **22**), ~40 (2C, **4, 9, 25, 26** in solvent signal), 33.64 (2C, **23**), 32.48 (1C, **18**), 29.65 (1C, **20**), 28.68 (3C, **1**), 23.83 (1C, **19**)

MS (FD)

$[\text{M}+\text{H}]^+$ calculated: 739.46, found: 739.47

**** This synthesis route was not completed; the reaction is therefore not discussed in Chapter III

4. Grafting protocols

4.1. Optimization of grafting protocols with commercial silanes

Grafting of 3-(2-aminoethyl-amino)propyl-trimethoxy-silane onto AA-TiO₂ under acidic conditions, adding the base after silane addition

200 mg AA-TiO₂ NPs as synthesized in water (30 mg/ml) were mixed with 24 ml ethanol and 100 µl of 1 M nitric acid. 3-(2-aminoethyl-amino)propyl-trimethoxy-silane (50, 10, 5, 1 and 0.5 µmol/mg particles) was mixed with 8 ml anhydrous ethanol and added to the particle solution in 50 addition steps under agitation over 2.5 h (every 3 min) at 50 °C. The reaction was then stirred for 1 h at 50 °C and subsequently the pH was changed to 9.5 to 10 via addition of 28-30 % ammonium hydroxide in water solution. Afterwards the reaction batch was heated up to 70 °C for one hour.

Grafting of 3-(2-aminoethyl-amino)propyl-trimethoxy-silane onto AA-TiO₂ under basic conditions

200 mg AA-TiO₂ NPs as synthesized in water (30 mg/ml) were mixed with 24 ml ethanol and 1 ml of 28-30 % ammonium hydroxide in water solution. 3-(2-aminoethyl-amino)propyl-trimethoxy-silane (50, 10, 5, 1 and 0.5 µmol/mg particles) was mixed with 8 ml anhydrous ethanol and added in 50 addition steps to the particle solution under agitation over 2.5 h (every 3 min at room temperature). Then the reaction batch was heated up to 40 °C for one hour.

Grafting of (3-Trimethoxysilylpropyl)-diethylenetriamine onto AA-TiO₂ under basic conditions

The grafting protocol as described above (Grafting of 3-(2-aminoethyl-amino)propyl-trimethoxy-silane onto AA-TiO₂ under basic conditions) was carried out with the following change: as organo-silane (3-Trimethoxysilylpropyl)-diethylenetriamine in concentrations from 1, 0.5, 0.1 and 0.05 µmol/mg particles was used.

Grafting of (3-Trimethoxysilylpropyl)-diethylenetriamine onto MEEAA-TiO₂ (200 °C, 4 h) under basic conditions

The grafting protocol as described above (Grafting of 3-(2-aminoethyl-amino)propyl-trimethoxy-silane onto AA-TiO₂ under basic conditions) was carried out with the following changes: as organo-silane (3-Trimethoxysilylpropyl)-diethylenetriamine in concentrations from 4, 2, 1 and 0.5 µmol/mg particles was utilized and as particle samples MEEAA-TiO₂ (200 °C, 4 h) was chosen.

Purification of the obtained functionalized particle samples

After reaction, the samples were centrifuged at 10.000 rpm for 1 h and redispersed in 10 ml water. For zeta potential titrations and photocatalysis tests, 75 % of each sample was dialysed against water (including 3 water changes). For DLS and DRIFT examinations, the rest of each sample was washed with ethanol via centrifugation (3 times at 30000 rpm for 1 h and subsequent redispersion) and dried under vacuum if necessary (DRIFT).

4.2. Grafting of synthesized coupling agents onto MEEAA-TiO₂ (200 °C, 4 h)

Grafting of coupling agent I onto MEEAA-TiO₂ (200 °C, 4 h) under basic conditions

100 mg MEEAA-TiO₂ NPs as synthesized in water (30 mg/ml) were mixed with 12 ml ethanol and 0.5 ml of 28 % ammonium hydroxide in water solution. Coupling agent I (2 µmol/mg particles) was mixed with 4 ml freshly distilled ethanol and added in 50 addition steps to the particle solution under agitation over 2.5 h (every 3 min at room temperature). Then the reaction batch was heated up to 40 °C for one hour.

Grafting of coupling agent IV onto MEEAA-TiO₂ (200 °C, 4 h) under basic conditions

100 mg MEEAA-TiO₂ NPs as synthesized in water (30 mg/ml) were mixed with 12 ml ethanol and 0.5 ml of 28 % ammonium hydroxide in water solution. Coupling agent IV (2 µmol/mg particles) was mixed with 4 ml freshly distilled ethanol and added in 50 addition steps to the

particle solution under agitation over 2.5 h (every 3 min at room temperature). Then the reaction batch was heated up to 40 °C for one hour.

Washing of the obtained functionalized particle samples

After reaction, the samples were centrifuged at 8.000 rpm for 1 h and redispersed in 10 ml water. The samples were subsequently dialysed against water (including 5 water changes) and dried under vacuum if necessary (DRIFT).

Phthalimide cleavage attempt of coupling agent IV grafted onto MEEAA-TiO₂ (200 °C, 4 h)

The dispersion of coupling agent IV-MEEAA-TiO₂ (5 mg NPs, 10 µmol coupling agent IV) in water in a concentration of 3 mg/ml was transferred into an Eppendorf cap and the desired amount of base was added (Table - EP - 3). The reaction mixture was stirred for 16 h at room temperature. Then, each batch was transferred into a dialysis bag and dialysed against 1 l of water including 3 water changes (after 3 h, 8 h and 24 h) and dried under vacuum if necessary (DRIFT).

Table - EP - 3. Amount of base used for the phthalimide deprotection procedure.

ratio of primary amine (from base) to phthalimide group of the grafted coupling agent IV (on MEEAA-TiO ₂ NP)	methylamine 40 w%		hydrazine monohydrate 65 %	
3:1	60 µmol	5.194 µl	30 µmol	1.433 µl
10:1	200 µmol	17.31 µl	100 µmol	4.778 µl
100:1	2 000 µmol	173.13 µl	1 000 µmol	47.778 µl
1000:1	20 000 µmol	1731.33 µl	10 000 µmol	477.787 µl
unmodified MEEAA-TiO ₂ as reference	20 000 µmol	1731.33 µl	10 000 µmol	477.787 µl

5. Cell culture tests

Stabilisation of particles in cell culture media

The as synthesized samples AA-TiO₂ (160 °C, 4 h) and MEEAA-TiO₂ (160 °C, 4 h) in a concentration of 3 mg/ml in water were ultrasonically treated (Branson Sonifier 450, 4 min, duty cycle 30 %, strength 7); if a stabilisation of the particles was chosen, the selected stabiliser was added at this time point under magnetic stirring. Finally the pH was adjusted to 7 adding 1 M sodium hydroxide solution and the stabilised dispersion was transferred into the selected cell culture media (DMEM, RPMI and BEGM) resulting in NP concentrations of 0.5 mg/ml. From this standard dilution, the required particle concentrations for cytotoxicity tests were generated by dilution with cell culture medium.

Cytotoxicity tests

From the standard dilution (0.5 mg/ml NPs in cell culture medium), the required particle concentrations for cell culture tests were generated by dilution with cell culture medium, respectively. For cytotoxicity assessment cells were seeded into 96 well round bottom culture plates (1x10⁴ cells per well). Cells were allowed to attach and proliferate for 24 h. The particle dispersions were added at working concentrations on the second day and incubated with the cells for 24 h. After that, the exposure medium was removed by suction and the cells were then washed three times with PBS in order to remove residual NPs. Then, the MTT colorimetric staining method was applied to study cell viability. All plates were incubated with cell culture medium containing 1 mg/ml of MTT-solution for 4 h. The MTT solution from each well was replaced by isopropanol after 4 h of inoculation at 37 °C with 5 % CO₂. Isopropanol was used to solubilise the resulting formazan crystals overnight at 37 °C with 5 % CO₂. The colour conversion of the blue formazan dye was measured by a spectrophotometer at a wavelength of 570 nm. All cytotoxicity studies were carried out on 8 technical and 3 biological replicates. Positive control samples (non-cellular controls) were carried out and confirmed that there are no interferences between the tested nanomaterials and the biochemical assay reagents. Statistical analysis of the results was performed using Graph Pad Prism software 4. The Wilcoxon test was used to evaluate statistical significance of the mean viability values compared to the untreated control, which was defined to be 100%. Differences were considered statistically significant when the P-value was less than 0.05.

24 h UV light pre-activation of particles

The as synthesized MEEAA-TiO₂ (160 °C, 4 h) samples in a concentration of 3 mg/ml in water were neutralized with 1 M NaOH (when necessary). Then they were transferred into a glass petri dish and covered with a fused silica lid. UV-light (0.3-0.5 mW/cm², 366 nm) was applied on its top for 24 h. The samples were then diluted with the selected cell culture medium (in general RPMI) to obtain a stock solution with a NP concentration of 0.5 mg/ml. From this standard dilution, the required particle concentrations for cytotoxicity tests were generated by dilution with cell culture medium.

For further studies on the 24 h UV light pre-activation of particles and the resulting anti-tumour effect (described in Chapter IV.3.), following protocols were carried out:

- "pure MEEAA": MEEAA as commercially obtained was diluted in water to a concentration of 12.6 mg/ml which is the same concentration present in a 3 mg/ml MEEAA-TiO₂ (160°C, 4) NP sample. The sample was neutralized, pre-activated, diluted with cell culture medium and tested for cytotoxicity as described before.

- "TiO₂ NPs": MEEAA-TiO₂ (160°C, 4) were washed with HNO₃ water (pH = 3) via repeated centrifugation and redispersion. The sample was neutralized, pre-activated, diluted with cell culture medium and tested for cytotoxicity as described before.

- "MEEAA separated from the TiO₂ NPs after pre-activation": The sample was neutralized and pre-activated as described before. Then, the particles were sedimented via centrifugation and

only the supernatant containing the MEEAA was diluted with cell culture medium and tested for cytotoxicity as described before.

- “pre-activated samples stored for 1 or 5 days”: The samples were neutralized and pre-activated as described before. Then, the samples were stored at room temperature in a closed flask for 1 or 5 days. They were diluted with cell culture medium and tested for cytotoxicity as described before.

- comparison of MEEAAs with different purity grades: For cell culture tests, the commercially obtained MEEAA compounds (12.6 mg/ml) with either 70 % purity which is the standard sample used or 95 % purity were intermixed with commercial P25 TiO₂ NPs (3 mg/ml) in water and ultrasonically treated (ultrasound bath, 1 h). The samples were then neutralized, pre-activated, diluted with cell culture medium and tested for cytotoxicity as described before.

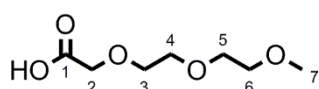
- NMR analysis of UV light activated compounds: 3 mg/ml P25 NPs, 12.6 mg/ml MEEAA compound (or other compounds to be examined) were intermixed in D₂O. One part of this solution was transferred into a UV light transparent cuvette, air-sealed and 24 h UV light treated while the other part was stored as reference. Both sample parts were then centrifuged at 13 000 rpm for 1 h in order to remove the P25 NPs and the supernatants were transferred into NMR tubes for analysis.

- distillation of MEEAA: MEEAA was distilled under dynamic vacuum (~9 mbar), increasing the heating temperature up to 250 °C, the heating temperature, appearance, name of the fraction and the amount of each distilled fraction is shown in the following Table - EP - 4. The most interesting fractions were chosen based on the cytotoxicity results, analytically analysed and are presented in the following section. For cell culture tests, all obtained fractions (12.6 mg/ml) were intermixed with commercial P25 TiO₂ NPs (3 mg/ml) in water and ultrasonically treated (ultrasound bath, 1 h). The samples were then neutralized, pre-activated, diluted with cell culture medium and tested for cytotoxicity as described before.

Table - EP - 4. MEEAA fractions obtained at different distillation temperatures; their appearance, name and obtained amount.

T	appearance	name of fraction	amount
	starting material, slightly yellow	MEEAA before distillation	151 g
< 194 °C	yellow	fraction I	57 g
194 °C	slightly yellow	fraction II	54 g
194 °C – 204 °C	slightly yellow	fraction III	20 g
204 °C – 250 °C	slightly yellow	fraction IV	15 g
residue in the flask	dark brown	residue (discarded)	4 g

Analysis of fraction II:



Chemical formula: C₇H₁₄O₅

Molecular weight: 178.18 g/mol

Compound name: 2-[2-(2-methoxyethoxy)ethoxy]acetic acid

¹H NMR (300 MHz, CDCl₃, δ [ppm]):

7.96 (br/s, 1H, **HO-1**), 4.19 (s, 2H, **2**), 3.79-3.77 (m, 2H, **3**), 3.73-3.69 (m, 4H, **4, 5**), 3.60-3.57 (m, 2H, **6**), 3.40 (s, 3H, **7**).

¹³C NMR (75 MHz, CDCl₃, δ [ppm]):

173.31 (1C, **1**), 71.69 (1C, **6**), 71.12 (1C, **5**), 70.46 (1C, **4**), 70.27 (1C, **3**), 68.51 (1C, **2**), 58.95 (1C, **7**).

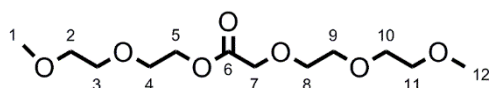
MS (ESI, m/z)

[M+Na]⁺ calculated: 201.09, found: 201.1

Analysis of fraction IV:

A column chromatography of fraction IV was carried out over 50 g silica per g product, starting with 2 % MeOH in CH₂Cl₂ as eluent and then increasing to 5 % MeOH in CH₂Cl₂. Fraction IV-a and IV-b were obtained and analysed.

Fraction IV-a:



Chemical formula: C₁₂H₂₄O₇

Molecular weight: 280.32 g/mol

Yield: 76 %

¹H NMR (300 MHz, D₂O, δ [ppm]):

4.39-4.36 (m, 2H, **5**), 4.30 (s, 2H, **7**), 3.82-3.77 (m, 4H, **4, 8**), 3.75-3.69 (m, 6H, **9, 3, 10**), 3.66-3.59 (m, 4H, **2, 11**), 3.40 (s, 3H, **1**), 3.39 (s, 3H, **12**).

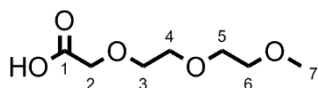
¹³C NMR (75 MHz, D₂O, δ [ppm]):

172.22 (1C, **6**), 70.96/70.91 (2C, **2, 11**), 70.21 (1C, **8**), 69.49/69.43/69.40 (3C, **9, 3, 10**), 68.28 (1C, **4**), 67.75 (1C, **7**), 64.13 (1C, **5**), 58.03 (2C, **1, 12**).

MS (ESI, m/z) – exact mass

[M+Na]⁺ calculated: 303.1414, found: 303.1419

Fraction IV-b:



Chemical formula: C₇H₁₄O₅

Molecular weight: 178.18 g/mol

Yield: 8 %

Compound name: 2-[2-(2-methoxyethoxy)ethoxy]acetic acid

¹H NMR (300 MHz, D₂O, δ [ppm]):

4.23 (s, 2H, **2**), 3.76-3.74 (m, 2H, **3**), 3.73-3.67 (m, 4H, **4, 5**), 3.64-3.62 (m, 2H, **6**), 3.38 (s, 3H, **7**).

^{13}C NMR (75 MHz, D_2O , δ [ppm]):

174.29 (1C, **1**), 70.94 (1C, **6**), 70.07 (1C, **5**), 69.51 (1C, **4**), 69.38 (1C, **3**), 67.58 (1C, **2**), 58.01 (1C, **7**).

MS (ESI, m/z) – exact mass

$[\text{M}+\text{Na}+\text{Na}]^+$ calculated: 223.0552, found: 223.0560

X-ray fluorescence spectroscopy

Table - EP - 5. X-ray fluorescence spectroscopy of fraction IV, compared to the MEEAA before distillation and pure MEEAA. Due to the small concentration of the detected elements, the obtained results cannot be taken as quantitative values.

element	MEEAA purity = 70% [weight-%]	distilled fraction IV [weight-%]	MEEAA purity > 95% [weight-%]
Al	-	0.001	0.002
Br	0.006	-	-
Cl	0.117	0.014	-
Fe	0.003	-	-
Si	0.004	0.002	0.002

Bibliography:

- 1 H. P. Zenner, W. Lehner and I. F. Herrmann, *Arch. Otorhinolaryngol.*, 1979, **225**, 269–277.
- 2 M. Newville, *J. Synchrotron Radiat.*, 2001, **8**, 322–324.
- 3 B. Ravel and M. Newville, *J. Synchrotron Radiat.*, 2005, **12**, 537–541.

Appendices

Appendix I: Influence of hydrothermal processing parameters on AA-TiO₂ particle

Table A I - 1. Particle (XRD, TEM) and agglomerate sizes (DLS) as well as experimental (BET) compared to theoretic specific surface area of AA-TiO₂ samples treated with varied autoclaving parameters. Additionally, pHs at IEP of AA-TiO₂ determined by zeta potential titrations.

sample: treatment time / temperature	crystallite size [nm] (XRD)	NP size [nm] (TEM)	hydrodynamic diameter [nm] / PDI [-] pH 2-3, US-treated (DLS)	specific surface area [m ² /g] (BET, N ₂ sorption)	theoretic specific surface area [m ² /g]	pH at IEP [-]
1 h / 160 °C	4.9	5.2 ± 1.0	13.0 ± 0.1 / 0.3	249.9	314.0	6.2
4 h / 160 °C (standard sample)	5.6	6.3 ± 1.5	22.5 ± 0.8 / 0.2	207.5	274.7	6.9
16 h / 160 °C	6.7	7.2 ± 1.3	22.7 ± 0.3 / 0.2	176.3	229.6	6.3
4 h / 180 °C	6.1	6.3 ± 1.3	22.2 ± 0.4 / 0.2	186.5	254.3	6.8
4 h / 200 °C	6.8	6.6 ± 1.3	25.9 ± 0.6 / 0.2	168.7	226.2	6.9

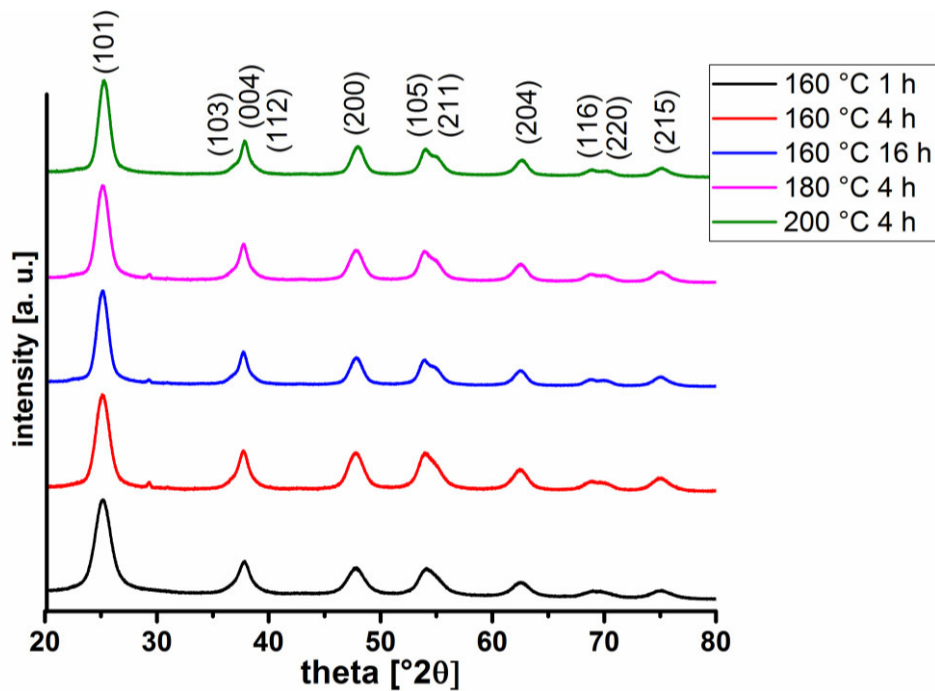


Figure A I - 1. Powder X-ray diffraction (XRD) patterns of AA-TiO₂ samples treated with varied autoclaving parameters.

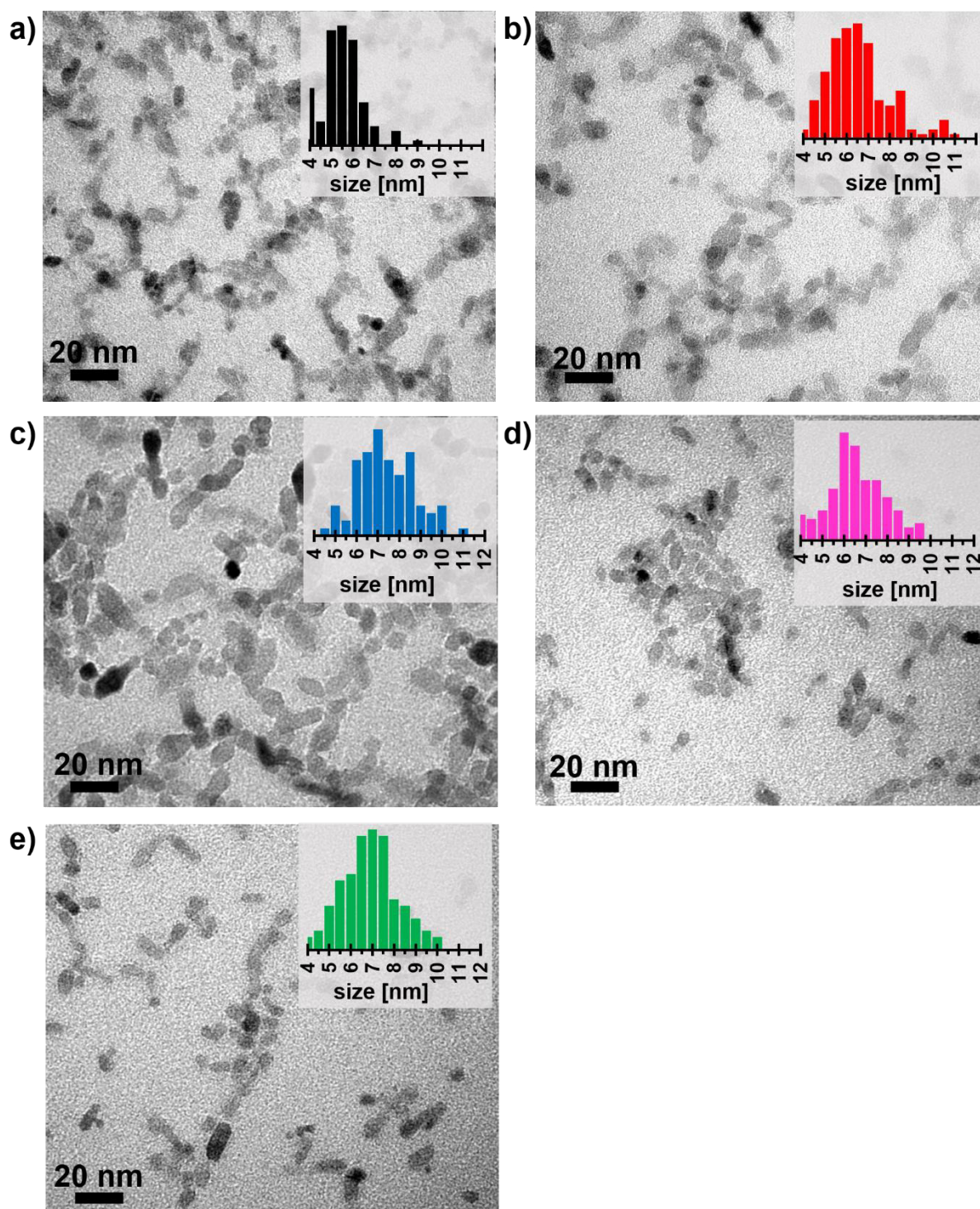


Figure A I - 2. Transmission electron microscopy (TEM) of AA-TiO₂ samples treated with varied hydrothermal processing parameters and their size distributions, obtained from counting at least 100 particles per sample: a) 1 h, 160 °C; b) 4 h, 160 °C; c) 16 h, 160 °C; d) 4 h, 180 °C; e) 4 h, 200 °C.

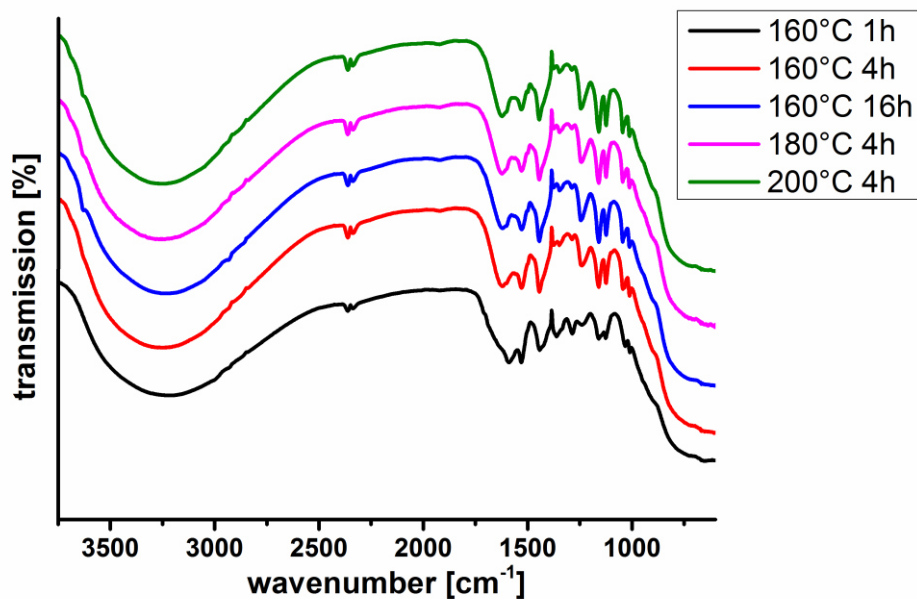


Figure A I - 3. IR (DRIFT) spectra of AA-TiO₂ samples synthesized with varied hydrothermal treatment parameters. [the attribution of vibration band can be found in II.1.2. Figure II – 4.]

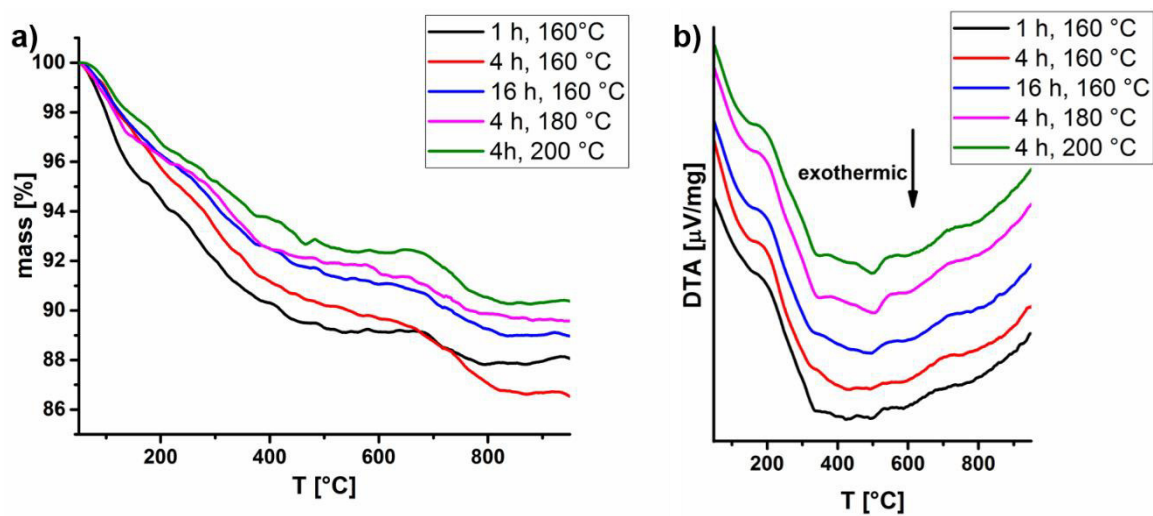


Figure A I - 4. a) Simultaneous thermogravimetric (TGA) and b) differential thermal analysis (DTA) performed on dried AA-TiO₂ particle samples synthesized with varied hydrothermal processing parameters.

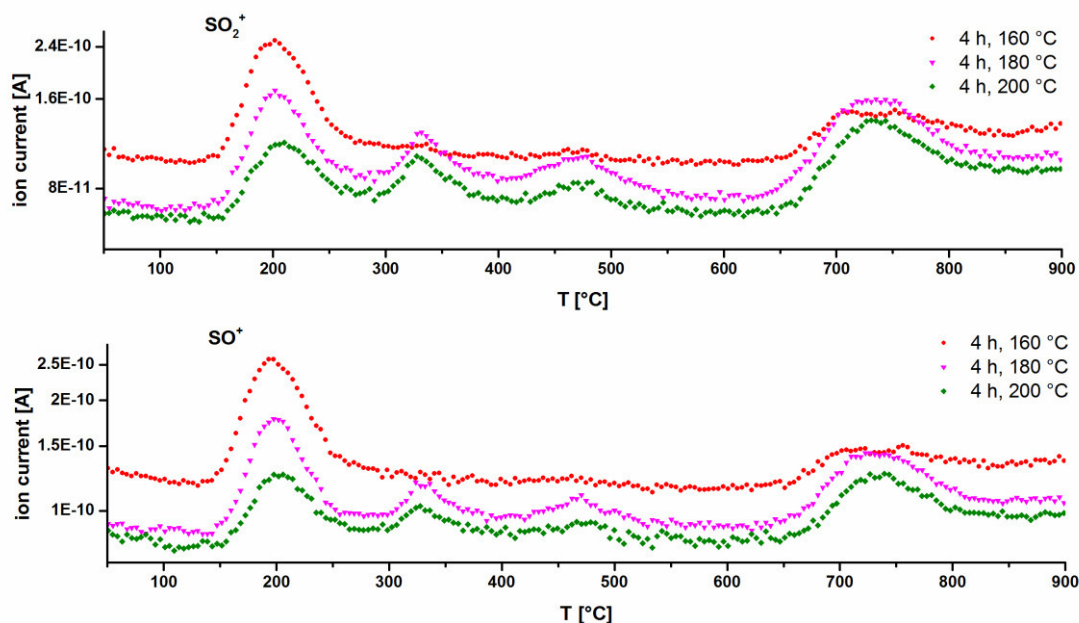


Figure A I - 5. Evolved gas analysis by mass spectrometry during TGA/DTA experiments on dried AA- TiO_2 particle samples synthesized with varied hydrothermal processing parameters (only the most interesting spectra shown).

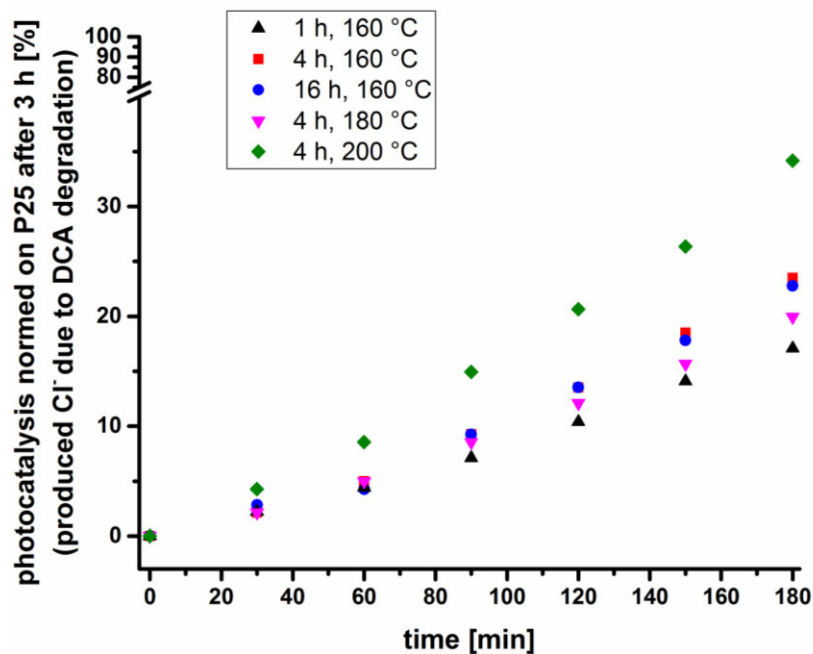


Figure A I - 6. Photocatalytic activity of AA- TiO_2 samples synthesized with varied processing parameters normed on the commercial standard TiO_2 NP (P25); determined by measurement of produced Cl^- during the degradation of dichloroacetic acid (DCA). The values are normed on the amount of degraded DCA (produced Cl^-) by P25 after 3 h photocatalysis test (= 100%).

Appendix II: Cleavage of the phthalimide protecting group of the coupling agent IV grafted onto MEEAA-TiO₂ (200 °C, 4 h)

*Table A II - 2. IEP (zeta potential) and agglomerate size (DLS) of MEEAA-TiO₂ functionalized with **coupling agent IV** and treated with either methylamine or hydrazine.*

	amount of amine (from base) per phthalimide group of the grafted coupling agent IV (on MEEAA-TiO ₂ NP)	pH(IEP) determined by zeta potential titration	Agglomerate size [nm] (PDI [-]) in water pH = 3
methylamine	3	5.8	319.1 ± 30.2 (0.6)
	10	5.9	283.0 ± 6.0 (0.4)
	100	6.0	288.9 ± 17.2 (0.4)
	1000	6.1	544.3 ± 113.5 (0.9)
hydrazine	3	5.8	285.1 ± 7.0 (0.4)
	10	5.8	406.5 ± 47.4 (0.7)
	100	6.0	198.5 ± 2.0 (0.3)
	1000	6.1	1059.2 ± 105.1 (0.7)

Appendix III: Stabilization of MEEAA-TiO₂ in cell culture media with FBS, BSA, Melflux, Melpers or Sika ViscoCrete

Table A III - 3. MEEAA-TiO₂ (0.5 mg/ml) in different cell culture media (DMEM, BEGM, RPMI) stabilized with 1 mg, 10 mg, 50 mg or 100 mg BSA, FBS, Melflux, Melpers or Sika ViscoCrete per 1 mg NP. a) Percentage of particles still stably dispersed after 24 h with decreasing dispersion stability from A: 100% (dark green) to E: <25 % (dark red). b) Agglomerate size (Z-average) with increasing hydrodynamic diameter from a: <100 nm (dark green) to f: >700 nm (dark red).

a)

Percentage of NP, still stably dispersed after 24 h

A: 100%

B: >74 %

C: 50-74 %

D: 25-49 %

E: <25 %

MEEAA-TiO ₂ (0.5 mg/ml)	DMEM				BEGM				RPMI			
1 mg NP : x mg	1	10	50	100	1	10	50	100	1	10	50	100
BSA	E	B	C	B	E	E	E	E	E	E	E	E
FBS	-	E	C	B	-	E	E	E	-	E	A	A
Melflux	A	E	D	-	A	D	C	-	A	E	B	-
Melpers	A	A	E	E	-	E	D	A	-	E	E	E
Sika ViscoCrete	-	B	A	B	-	E	A	B	-	D	D	B

b)

Z-Av d in [nm]

a: <100

b: 101-200

c: 201-300

d: 301-500

e: 501-700

f: > 700

MEEAA-TiO ₂ (0.5 mg/ml)	DMEM				BEGM				RPMI			
1 mg NP : x mg	1	10	50	100	1	10	50	100	1	10	50	100
BSA	d	c	d	c	-	f	f	f	f	f	f	f
FBS	-	c	b	b	-	f	f	f	-	f	d	b
Melflux	a	c	d	-	a	b	d	-	a	c	d	-
Melpers	c	c	e	f	-	f	f	f	-	f	f	f
Sika ViscoCrete	-	e	c	e	-	f	d	e	-	f	e	e

List of appreviations

List of abbreviations

AA	acetyl acetone
AMEO	<i>aminopropyltriethoxy silane</i>
ATR	attenuated total reflection
BEGM	bronchial epithelial cell growth medium
BET	Brunauer-Emmett-Teller
BMSC	bone marrow-derived mesenchymal stem cells
Boc	<i>tert</i> -butyloxycarbonyl
BSA	bovine serum albumin
DAISY-MAT	Darmstadt Integrated System for MATerial research
DCA	dichloroacetic acid
DCC	<i>N,N'</i> -dicyclohexylcarbodiimide
DCU	dicyclohexylurea
DLS	dynamic light scattering
DLVO	Derjaguin-Landau-Verwey-Overbeek
DMEM	Dulbecco's modified eagle medium
DMF	dimethylformamide
DRIFT	diffuse reflectance infrared Fourier transformed (spectroscopy)
DTA	differential thermal analysis
EA	elemental analysis
EXAFS	extended X-ray absorption fine structure
FBS	fetal bovine serum
FFT	fast Fourier transformation
Fmoc	Fluorenylmethoxycarbonyl
FTIR	Fourier transformed infrared (spectroscopy)
IARC	International Agency for Research on Cancer
HNSCC	head and neck squamous cell carcinoma
HPLC	high pressure liquid chromatography
IR	infrared
JECFA	Joint FAO/WHO Expert Committee on Food Additives
MEEAA	2-[2-(2-methoxyethoxy)ethoxy]acetic acid
MS	mass spectrometry
MTT	3-(4,5-dimethylthiazol-2-yl)-2,5-diphenyl tetrazolium bromide
NHS	<i>N</i> -hydroxysuccinimide
NHS-Rhodamine	5-/6-carboxytetramethylrhodamine, succinimidyl ester
NMR	nuclear magnetic resonance (spectroscopy)
NP	nanoparticle
PAMAM	polyamidoamine
PEG	polyethylene glycol
PC	photocatalytic
PDI	polydispersity index
PL	photoluminescence
PTSA	para-toluene sulfonic acid
P25	commercial Degussa P25 TiO ₂ nanoparticles
RhBic	Rhodamine B isothiocyanate
ROS	reactive oxidizing species
RPMI	Roswell Park Memorial Institute medium
rt	room temperature
TEA	triethylamine
TEM	transmission electron microscopy
TFA	trifluoroacetic acid
TGA	thermogravimetric analysis
TG	thermogravimetric
THF	tetrahydrofuran
TiO ₂	titanium dioxide

List of abbreviations

TLC	thin layer chromatography
US	ultrasonic
UV	ultraviolet
XAFS	X-ray absorption fine structure
XANES	X-ray absorption near edge structure
XPS	X-ray photoelectron spectroscopy
XRD	X-ray diffraction
XRF	X-ray fluorescence spectroscopy
Z	benzyloxycarbonyl

Functional coupling agents

S. Koch: Dendritic surface modification of photocatalytic nanoparticles for tumour therapy

